frontiers | Research Topics

Vascular involvement in eye diseases

Edited by
Doina Gherghel and Leopold Schmetterer

Published in
Frontiers in Medicine
Frontiers in Physiology

ISSN 1664-8714
ISBN 978-2-8325-4283-5
DOI 10.3389/978-2-8325-4283-5

About Frontiers

Frontiers is more than just an open access publisher of scholarly articles: it is a pioneering approach to the world of academia, radically improving the way scholarly research is managed. The grand vision of Frontiers is a world where all people have an equal opportunity to seek, share and generate knowledge. Frontiers provides immediate and permanent online open access to all its publications, but this alone is not enough to realize our grand goals.

Frontiers journal series

The Frontiers journal series is a multi-tier and interdisciplinary set of open-access, online journals, promising a paradigm shift from the current review, selection and dissemination processes in academic publishing. All Frontiers journals are driven by researchers for researchers; therefore, they constitute a service to the scholarly community. At the same time, the *Frontiers journal series* operates on a revolutionary invention, the tiered publishing system, initially addressing specific communities of scholars, and gradually climbing up to broader public understanding, thus serving the interests of the lay society, too.

Dedication to quality

Each Frontiers article is a landmark of the highest quality, thanks to genuinely collaborative interactions between authors and review editors, who include some of the world's best academicians. Research must be certified by peers before entering a stream of knowledge that may eventually reach the public - and shape society; therefore, Frontiers only applies the most rigorous and unbiased reviews. Frontiers revolutionizes research publishing by freely delivering the most outstanding research, evaluated with no bias from both the academic and social point of view. By applying the most advanced information technologies, Frontiers is catapulting scholarly publishing into a new generation.

What are Frontiers Research Topics?

Frontiers Research Topics are very popular trademarks of the *Frontiers journals series*: they are collections of at least ten articles, all centered on a particular subject. With their unique mix of varied contributions from Original Research to Review Articles, Frontiers Research Topics unify the most influential researchers, the latest key findings and historical advances in a hot research area.

Find out more on how to host your own Frontiers Research Topic or contribute to one as an author by contacting the Frontiers editorial office: frontiersin.org/about/contact

Vascular involvement in eye diseases

Topic editors

Doina Gherghel — Aston University, United Kingdom

Leopold Schmetterer — Medical University of Vienna, Austria

Citation

Gherghel, D., Schmetterer, L., eds. (2024). *Vascular involvement in eye diseases*. Lausanne: Frontiers Media SA. doi: 10.3389/978-2-8325-4283-5

Table of contents

frontiers | Frontiers in Medicine

TYPE Editorial
PUBLISHED 04 January 2024
DOI 10.3389/fmed.2023.1301145

OPEN ACCESS

EDITED AND REVIEWED BY
Sofia Zaira Otin Mallada,
University of Zaragoza, Spain

*CORRESPONDENCE
Leopold Schmetterer
✉ leopold.schmetterer@meduniwien.ac.at

RECEIVED 24 September 2023
ACCEPTED 28 November 2023
PUBLISHED 04 January 2024

CITATION
Schmetterer L and Gherghel D (2024) Editorial: Vascular involvement in eye diseases.
Front. Med. 10:1301145.
doi: 10.3389/fmed.2023.1301145

Editorial: Vascular involvement in eye diseases

Leopold Schmetterer[1,2,3,4,5,6,7]* and Doina Gherghel[8]

[1]Singapore Eye Research Institute, Singapore National Eye Centre, Singapore, Singapore, [2]SERI-NTU Advanced Ocular Engineering (STANCE), Singapore, Singapore, [3]Academic Clinical Program, Duke-NUS Medical School, Singapore, Singapore, [4]School of Chemistry, Chemical Engineering and Biotechnology, Nanyang Technological University, Singapore, Singapore, [5]Department of Clinical Pharmacology, Medical University of Vienna, Vienna, Austria, [6]Center for Medical Physics and Biomedical Engineering, Medical University of Vienna, Vienna, Austria, [7]Institute of Molecular and Clinical Ophthalmology Basel, Basel, Switzerland, [8]Department of Life & Health Sciences, Aston University, Birmingham, United Kingdom

KEYWORDS

retinal blood flow, choroidal blood flow, OCT angiography, vascular changes, ocular blood flow

Editorial on the Research Topic
Vascular involvement in eye diseases

A variety of common eye diseases, including age-related macular degeneration (AMD), diabetic retinopathy (DR), retinal vascular occlusions, glaucoma, and pathological myopia, have a detrimental effect on the ocular blood vessels at many levels, from the anterior to the posterior segment of the eye. As a well-organized ocular vascular system is essential to ensure normal visual function, any damage to these structures may result in loss of vision. Although the current knowledge of the underlying mechanisms for vascular damage in various ocular diseases is quite advanced, more research is necessary to fine-tune our understanding, with the final goal of bringing to our patients better therapies that address this cause of visual morbidities. None of the above would be possible, however, without proper imaging techniques. As such, in parallel with various other studies, more advanced techniques, such as optical coherence tomography angiography (OCTA), have become recently commercially available. This type of technique allows for the visualization of the ocular vasculature *in vivo* with unprecedented resolution, and, as a result, ensures better and earlier diagnosis of ocular vascular disease.

This Research Topic entitled "*Vascular involvement in eye diseases*" brings together 14 articles of various formats, from reviews and original articles, to study protocols and case reports. They highlight various aspects of this field of research, from pathological mechanisms to the use of imaging techniques in the diagnosis of various ocular pathologies. A summary of these articles is presented as follows.

As described above, the OCTA represents an advanced technique for the visualization of the ocular vessels. Although this method allows for the quantification of parameters such as vessel density and foveal avascular zone, no information on volumetric blood flow can be obtained as yet. In their article, Chen R. et al. investigate the OCTA precision in assessing retinal vasculature in children and report moderate-to-good repeatability and reproducibility for papillary and peripapillary perfusion measurement.

In their review article, Tan et al. highlight the importance of ultra-widefield fluorescein angiography and OCTA in the management of retinal vein occlusion, an important sight-threatening vascular disease of the eye. They conclude that the clinical use of these techniques can improve risk stratification and prognostication for neovascularization and cystoid macular edema.

In diabetes, a wide variety of studies has shown that OCTA is capable of identifying microvascular retinal changes before the onset of any clinical features of DR. Li et al. report systemic factors associated with the microvascular alterations including apolipoprotein B and platelets. Hommer et al. investigate retinal neurovascular coupling using Doppler OCT and heart rate variability in patients with type II diabetes. Both parameters were reduced in the patient group as compared to controls but there was no correlation between them.

Idiopathic epiretinal membranes are avascular proliferations between the posterior vitreous cortex and the internal limiting membrane that cause visual impairment including distortion and scotoma. Wang et al. show that choroidal and retinal vascular parameters are associated with both inner and outer retinal morphologic biomarkers in eyes with idiopathic epiretinal membranes.

OCTA is also an invaluable technique to assess the effects of various therapeutic interventions. In a systematic review, Chen X. et al. give an overview of the importance of OCTA in assessing retinal microcirculation in patients who underwent surgery for rhegmatogenous retinal detachment. Even in cases where the retina is fully reattached through primary surgery, the foveal avascular zone area in the deep capillary plexuses was enlarged and vascular density in the foveal deep capillary plexus was reduced. On the same theme, Jiang et al. present a case report that focuses on a pediatric patient with aplastic anemia showing retinal hemorrhages and serous retinal detachment in both eyes and subsequent retinal changes after pars plana vitrectomy.

Another therapeutic intervention in the case of many ocular vascular diseases that result in neovascularisation, is represented by the use of anti-VEGF intravitreal injections. OCTA is, yet again, useful in following up disease evolution in these patients. Türksever et al. showed that age-related macular degeneration subjects treated with anti-VEGF intravitreal injections have reduced OCTA parameters in the retinal vasculature as compared to control subjects, which are, however, not related to the frequency of injections. This confirms that VEGF has vasodilator properties and inhibition of the angiogenic factors induces vasoconstriction.

Glaucoma represents another sight-threatening disease with vascular involvement. Whereas retinal and optic nerve head microvasculature changes have been unequivocally shown in glaucoma, choroidal vascular changes are controversial. Lun et al. did not find any alterations of choriocapillaris microvasculature in patients with primary open-angle glaucoma using optical coherence tomography angiography, which may be expected since the outer retina is largely unaffected in this condition. Differences between retinal vascular parameters were, however, reported in a study by Van Eijgen et al. between primary open-angle glaucoma patients, normal tension glaucoma patients, and healthy controls. This study has also shown that OCTA may not represent a good clinical tool to study vascular dysregulation, because no changes in vascular parameters were observed during provocation tests, such as handgripping.

In addition to the focus on OCTA and related techniques, this Research Topic also presents knowledge on other aspects of vascular involvement in eye disease. Loo et al. review the involvement of the cell surface protein caveolin-1, in vascular abnormalities in glaucoma. The authors emphasize that caveolin-1 is involved in IOP-dependent and independent Mechanisms involving vascular dysregulation. Popa Cherecheanu et al. present two cases with Ehlers–Danlos Syndromes that present with severe vision loss and vascular abnormalities.

Two articles by the group of Benavente-Perez highlight the role of perfusion abnormalities in myopia. A mini-review emphasizes that myopia represents a risk factor for choroidal neovascularisations and glaucoma and indicates the presence of gross, cellular, and molecular alterations at the level of the ocular microvasculature. The same group provides an additional original article that demonstrates how aging interacts with the retinal microvascular changes due to myopia in the marmoset retina.

Author contributions

LS: Conceptualization, Writing – original draft. DG: Conceptualization, Writing – original draft, Writing – review & editing.

Conflict of interest

The authors declare that the research was conducted in the absence of any commercial or financial relationships that could be construed as a potential conflict of interest.

Publisher's note

frontiers | Frontiers in Medicine

TYPE Original Research
PUBLISHED 21 September 2022
DOI 10.3389/fmed.2022.999167

OPEN ACCESS

EDITED BY
Huaizhou Wang,
Capital Medical University, China

REVIEWED BY
Eduardo Normando,
Imperial College London,
United Kingdom
Pasquale Viggiano,
University of Bari Aldo Moro, Italy

*CORRESPONDENCE
Jacqueline Chua
jacqueline.chua.y.m@seri.com.sg

SPECIALTY SECTION
This article was submitted to Ophthalmology, a section of the journal Frontiers in Medicine

RECEIVED 20 July 2022
ACCEPTED 05 September 2022
PUBLISHED 21 September 2022

CITATION
Lun K, Sim YC, Chong R, Wong D, Tan B, Husain R, Aung T, Sng CCA, Schmetterer L and Chua J (2022) Investigating the macular choriocapillaris in early primary open-angle glaucoma using swept-source optical coherence tomography angiography. *Front. Med.* 9:999167. doi: 10.3389/fmed.2022.999167

Investigating the macular choriocapillaris in early primary open-angle glaucoma using swept-source optical coherence tomography angiography

Katherine Lun[1,2], Yin Ci Sim[3], Rachel Chong[3,4], Damon Wong[3,5,6,7], Bingyao Tan[3,5,6], Rahat Husain[3], Tin Aung[2,3,4], Chelvin C. A. Sng[2,3], Leopold Schmetterer[3,4,5,6,7,8,9] and Jacqueline Chua[3,4]*

[1]Department of Ophthalmology, National University Health System, Singapore, Singapore, [2]Yong Loo Lin School of Medicine, National University of Singapore, Singapore, Singapore, [3]Singapore National Eye Centre, Singapore Eye Research Institute, Singapore, Singapore, [4]Ophthalmology & Visual Sciences Academic Clinical Program, Duke-NUS Medical School, Singapore, Singapore, [5]SERI-NTU Advanced Ocular Engineering (STANCE), Singapore, Singapore, [6]School of Chemical and Biomedical Engineering, Nanyang Technological University, Singapore, Singapore, [7]Institute of Molecular and Clinical Ophthalmology, Basel, Switzerland, [8]Department of Clinical Pharmacology, Medical University Vienna, Vienna, Austria, [9]Center for Medical Physics and Biomedical Engineering, Medical University Vienna, Vienna, Austria

Introduction: There has been a growing interest in the role of vascular factors in glaucoma. Studies have looked at the characteristics of macular choriocapillaris in patients with glaucoma but with conflicting results. Our study aims to use swept-source optical coherence tomography angiography (SS-OCTA) to evaluate macular choriocapillaris metrics in normal participants and compare them with patients with early primary open-angle glaucoma (POAG) (mean deviation better than −6dB).

Methods: In this prospective, observational, cross-sectional study, 104 normal controls (157 eyes) and 100 patients with POAG (144 eyes) underwent 3 mm × 3mm imaging of the macula using the Plex Elite 9000 (Zeiss Meditec, Dublin, CA, USA). Choriocapillaris OCTA images were extracted from the device's built-in review software and were subsequently evaluated for the density and size of choriocapillaris flow deficits.

Results: After adjusting for confounding factors, the density of flow deficits was independently higher in those aged 53 years and above ($P \leq 0.024$) whereas the average flow deficit size was significantly larger in those aged 69 years and above (95% CI = 12.39 to 72.91; $P = 0.006$) in both normal and POAG patients. There were no significant differences in the density of flow deficits ($P = 0.453$) and average flow deficit size ($P = 0.637$) between normal and POAG participants.

Conclusion: Our study found that macular choriocapillaris microvasculature on SS-OCTA is unaltered by subjects with POAG. This suggests that OCTA macular choriocapillaris may not be potentially helpful in differentiating early glaucoma from healthy eyes.

KEYWORDS

primary open-angle glaucoma, choroid, choriocapillaris, swept-source optical coherence tomography angiography, glaucoma

Introduction

Glaucoma is an optic neuropathy associated with progressive loss of retinal ganglion cells and their axons, with resultant structural changes at the optic nerve head (ONH) (1). The ONH is believed to be the primary site of damage in glaucoma and disruption of its blood flow and the surrounding peripapillary retina is believed to play a role in its pathogenesis (2, 3). Deeper structures of the ONH, such as the lamina cribrosa, and the choroid, share the same blood supply (posterior ciliary artery) (4, 5), and various studies have reported abnormal choroidal blood flow parameters in patients with glaucoma (6–10). Evaluation of choroidal hemodynamics was challenging with previous imaging modalities such as fluorescein angiography (11), indocyanine green angiography (12), and laser doppler flowmetry (9). This was due to the invasive nature of tests (6), an inability to differentiate choroidal vascular layers (6, 9, 13), and the inability to have reproducible, quantitative measurements (13). Fortunately, with the arrival of optical coherence tomography angiography (OCTA) (14–16), a non-invasive imaging modality that allows the quantitative assessment of the microcirculation of the choroid, vascular layers of the choroid can be better examined and it has become possible to assess macular choriocapillaris circulation in patients with glaucoma. In addition, in cases where evaluation of the ONH is challenging due to anatomical features of the optic disc, OCTA may serve as an additional diagnostic tool to detect early glaucoma by assessing the disruptions of macular choriocapillaris in these patients.

Studies examining the macular choroidal circulation using OCTA are, unfortunately, limited with conflicting results in subjects with glaucoma (17–20). Chao et al. used spectral domain optical coherence tomography angiography (SD-OCTA; Angiovue, Optovue Inc., Bayview, CA, USA) to evaluate macular circulation in patients with glaucoma [18 eyes with open angle glaucoma, 14 with normal tension glaucoma (NTG), ocular hypertension (OHT) (18 eyes)] and healthy subjects and did not find any difference in choriocapillaris perfusion between groups (17). Similarly, Milani et al. examined healthy individuals and patients with POAG (39 eyes) and OHT (43 eyes) using SD-OCTA (XR Avanti device with the AngioVue imaging system) and did not find any significant differences in macular choriocapillaris flow perfusion area between groups (18). On the other hand, Yip et al. carried out a cross-sectional study on healthy subjects and glaucoma subjects (15 eyes with POAG, 14 with NTG, 1 Juvenile open angle glaucoma, and 2 eyes with angle closure glaucoma) using SD-OCTA (XR Avanti with Angiovue imaging system and novel in-house developed software to determine vessel density) and found a reduction in microvascular density of the macula and optic disc in glaucoma patients compared with healthy controls (20). Lastly, Tepelus et al. used swept source (SS)-OCTA (Plex Elite 9000, Zeiss Meditec, Dublin, CA, USA) and reported lower choriocapillaris perfusion density in NTG patients (49 eyes) when compared to normal subjects (40 eyes) (19). It is not clear whether the variations seen in these studies were due to imaging modality differences (SS-OCTA vs. SD-OCTA) or the discrepancies in study design (small sample size of < 35 subjects), pathological subgroup (i.e., POAG, NTG, OHT), and analytical method (frequency matching by age or statistical adjustments of confounding factors such as age, glaucoma severity, and signal strength), thus making direct comparisons between normal and glaucoma eyes challenging.

Therefore, we evaluated the macular choriocapillaris metrics using SS-OCTA Plex Elite 9000 in healthy participants and individuals having early primary open-angle glaucoma (POAG). Clinically, there is an interest to detect glaucoma in the earlier stages to enable timely treatment and to minimize the risk of irreversible visual field loss. Hence OCTA may act as an additional diagnostic tool that can assess damage to the macular choriocapillaris vasculature in glaucoma patients.

Abbreviations: ANOVA, analysis of variance; DBP, diastolic blood pressure; GEE, generalized estimating equations; NTG, normal tension glaucoma; OCTA, optical coherence tomography angiography; ONH, optic nerve head; POAG, primary open-angle glaucoma; RPE, retinal pigment epithelium; SD-OCTA, spectral domain optical coherence tomography angiography; SBP, Systolic blood pressure; SS-OCTA, swept-source optical coherence tomography angiography.

Materials and methods

Participants

In this prospective cross-sectional study, participants aged 21 years and older (21–99 years old) were consecutively recruited from the Singapore National Eye Centre, a tertiary eye care institution in Singapore, between July 2018 to May 2021. This study was approved by the SingHealth Centralized Institutional Review Board, Singapore (protocol number R1500/83/2017) and conducted in accordance with the Declaration of Helsinki, with written informed consent obtained from all participants.

Patients with early primary open-angle glaucoma (POAG) patients were defined by the following criteria during an ophthalmic examination: presence of glaucomatous optic neuropathy (defined as loss of neuroretinal rim with a vertical cup: disc ratio of $>$ 0.7 or an inter-eye asymmetry of $>$ 0.2 and/or notching attributable to glaucoma) with compatible and reproducible visual fields in standard automated perimetry (glaucoma hemifield test outside normal limits) with mean deviation (MD) better than -6dB (21), open angles on gonioscopy, and absence of secondary causes of glaucomatous optic neuropathy (22, 23). Normal controls were individuals who did not have clinically relevant eye conditions, such as glaucoma, age-related macular degeneration, diabetic retinopathy, and ocular vascular occlusive disorders, diabetes and other causes of neuro-ophthalmic disease (24). POAG patients were on the following intra-ocular pressure lowing eye drops: prostaglandin analogs (latanoprost, bimatoprost, travoprost, tafluprost), beta blockers (timolol), alpha-2 adrenergic agonists (brimonidine), and carbonic anhydrase inhibitors (brinzolamide).

Ocular examinations

Participants underwent auto-refraction-keratometry (Canon RK-5 Autorefractor Keratometer; Canon Inc., Tokyo, Japan) and intra-ocular pressure measurement using airpuff tonometer at the Singapore Eye Research Institute. Spherical equivalent was calculated as the spherical value plus half of the negative cylinder value. Central corneal thickness was measured using an ultrasound pachymeter (Advent; Mentor O & O Inc., Norwell, MA, USA); the mean of the five measurements were used for analysis (25).

Demographic data, medical history (e.g., diabetes and systemic hypertension), ocular history (e.g., eye diseases) and medication use were collected from all participants using a detailed interviewer-administered questionnaire. A digital automatic blood pressure monitor (Dinamap model Pro Series DP110X-RW, 100V2; GE Medical Systems Information Technologies, Inc., Milwaukee, WI, USA) was used to measure systolic and diastolic blood pressures (SBP, DBP) after subjects were seated for at least 5 min (26). Blood pressure was measured twice, 5 min apart. If the previous 2 SBP readings differed by more than 10 mmHg or the DBP by more than 5 mmHg, a third measurement was then taken.

Imaging acquisition

During the same visit, participants underwent 3 mm $\times$ 3mm macular-centered imaging using SS-OCTA (Plex Elite 9000; Version 1.7; Carl Zeiss Meditec). Both eyes of each participant were imaged after pharmacological dilation (Tropicamide 1%). To ensure high quality images were taken, all images were obtained by a trained ophthalmic photographer (HQ) and acquisitions were repeated multiple times. Each scan consisted of four repeated volumes of 300 cross-sectional images, and each image consisted of 300 A-scans (27).

Imaging analysis

Quality of OCTA scans were reviewed by one trained grader who was masked to the participant's characteristics. Poor quality scans were defined as having any of the following characteristics: (i) poor signal strength (index $<$ 6), (ii) poor clarity (i.e., blurred vessels), (iii) significant motion artifacts visible as irregular vessel patterns on the en-face angiogram, (iv) segmentation error, or (v) local weak signal caused by artifacts such as floaters (28). Both eyes were included in the study only if both met the eligibility criteria.

Choriocapillaris OCTA images, spanning from 31 μm below the retinal pigment epithelium (RPE) to 40 μm below the RPE, were extracted from the built-in review software (Carl Zeiss Meditec, Inc., Dublin, CA, USA) (29). These OCTA images were subsequently loaded into a customized MATLAB (The MathWorks Inc., Natick, MA, USA) algorithm that evaluates the density of flow deficits in the choriocapillaris automatically (30). The algorithm comprises of the following steps (**Figure 1**): (i) binarization of flow deficits in the choriocapillaris OCTA image by setting a threshold that is 1.5 standard deviation below the mean intensity of the image; (ii) dilation of the foveal avascular zone (FAZ; segmented *via* a trained U-Net prior to analysis) in the superficial retinal plexus by 800 μm to generate a mask that indicates the region to be analyzed; (iii) application of the mask on the binarized flow deficit image; (iv) computation of choriocapillaris flow deficit density as the percentage of flow deficit area per total imaged area in the region of interest, and

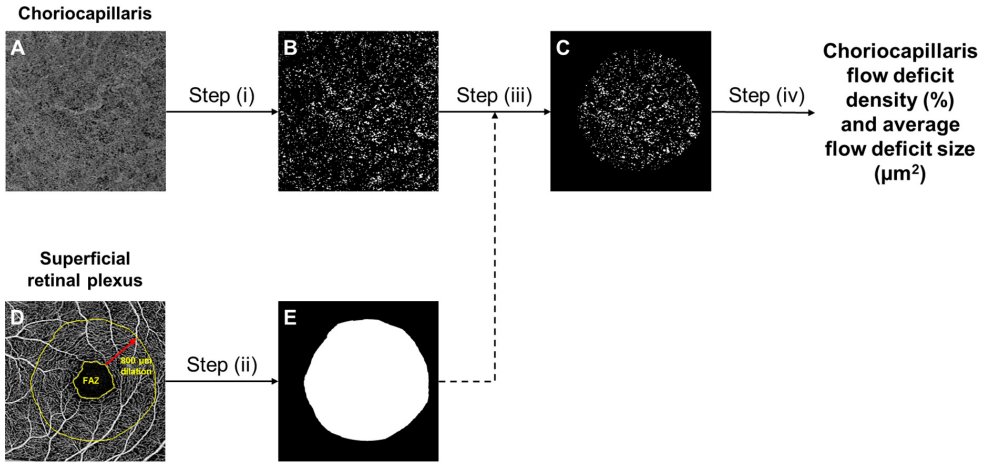

FIGURE 1
The framework of choriocapillaris OCTA image processing. Raw choriocapillaris OCTA image extracted from the OCTA machine **(A)** was binarized with a threshold of 1.5 standard deviation below the mean intensity of the image to segment flow deficits **(B)**. Foveal avascular zone (FAZ) segmented from the raw superficial retinal plexus OCTA image was dilated by 800 μm **(D)** to generate a mask **(E)** that indicates the region to be analysed. The mask **(E)** was applied to the segmented flow deficits **(B)** to generate the final flow deficit image **(C)** where the density and size of flow deficits were computed.

flow deficit size (μm^2) as the total flow deficit area divided by the total number of flow deficits in the region of interest.

Statistical analyses

Primary outcome was the density and size of choriocapillaris flow deficits. Shapiro–Wilk test was used to assess the normality of the distribution of the continuous variables. We compared the variables between groups using one-way analysis of variance (ANOVA) for normally distributed continuous variables or Kruskal–Wallis equality-of-populations rank test for non-normally distributed continuous variables and with Chi-square tests or Fisher's exact tests for categorical variables. We determined the strength of the correlation between choriocapillaris flow deficits and blood pressure using Pearson correlation coefficient, where r value less than 0.3, between 0.3 and 0.5, and greater than 0.50 indicate small, moderate, and strong correlation, respectively (31). To analyze correlated eye data, multivariable linear regression analysis with generalized estimating equations (GEE) was performed to assess the effect of age (performed only in normal controls) and eye diseases (independent variables) on density or size of the choriocapillaris flow deficit (dependent variable), adjusting for potential confounders such as diabetes, hypertension, intraocular pressure, axial length, and signal strength of scans. Since the recruited patients come from an ongoing, existing study consisting of glaucoma patients and normal controls, we did a *post hoc* power calculation to evaluate the statistical power of the existing study (n = 100 glaucoma cases vs. 104 controls) using the means and standard deviations derived from the current study. For choriocapillaris density (9.06 ± 0.14% vs. 8.90 ± 0.13%), using an alpha error of 5%, we would have a *post hoc* power of 100%. For size, using 283 ± 5 μm^2 vs. 287 ± 7 μm^2, we would have a *post hoc* power of 100%.[1] P-value < 0.05 was considered statistically significant. Data were analyzed with statistical software (STATA, version 16; StataCorp LP).

Results

Of the 235 participants recruited for the study, 31 (13.2%) were excluded because of poor quality OCTA images. This left 104 normal controls and 100 glaucoma subjects for analysis. The median (interquartile range) age was 59.0 (11.5) years for normal controls and 62.0 (12.0) years for glaucoma patients. Patients with glaucoma had significantly lower intraocular pressure, longer axial length, and scans of lower signal strength (**Table 1**). Glaucoma patients were also more likely to have diabetes and hypertension than normal controls ($P < 0.001$).

There was marginal positive correlation between choriocapillaris characteristics and systolic blood pressure (density: r = 0.050, P = 0.411; size: r = 0.007, P = 0.898). Among the POAG patients, 12% (12 patients) were not on any form of glaucoma medications (five were post-cataract and trabeculectomy surgery, two were patients with stable NTG and not on treatment, two had poor adherence to medications and were not using medications at point of recruitment, and

1 https://clincalc.com/stats/Power.aspx

TABLE 1 Comparison of demographics, systemic, and ocular characteristics between normal control and primary open angle glaucoma patients.

	Normal control	Early POAG	*P-value
Number of participants	104	100	
Age, years	59.0 (11.5)	62.0 (12.0)	0.134
Gender, Male	51 (49.0)	53 (53.0)	0.572
Ethnicity, Chinese	91 (87.5)	87 (87.0)	0.287
Diabetes	0 (0)	24 (24.0)	< **0.001**
Hypertension	2 (1.9)	40 (40.0)	< **0.001**
Systolic blood pressure, mmHg	136.3 (18.6)	129.9 (25.7)	0.093
Diastolic blood pressure, mmHg	76.5 (14.6)	74.8 (14.8)	0.339
Number of eyes	157	144	
Intraocular pressure, mmHg	17 (5)	14 (4)	< **0.001**
Axial length, mm	24.11 (1.71)	24.81 (2.17)	< **0.001**
Visual field mean deviation (MD), dB	–	−2.40 (1.66)	–
Signal strength of scans†	9.15 ± 0.64	8.85 ± 0.93	**0.004**

Data are number (%), mean ± standard deviation (SD), or median (interquartile range), as appropriate.
*Test for differences between groups, based on one-way analysis of variance (ANOVA) for normally distributed continuous variables or Kruskal–Wallis equality-of-populations rank test for non-normally distributed continuous variables and with Chi-square tests or Fisher's exact tests for categorical variables.
†1 represents poor scan quality while 10 represents high scan quality. dB, decibels; POAG, primary open angle glaucoma. Bold values denote statistical significance at the $P < 0.05$ level.

three were not started on medications yet). For the remaining 88%, 57% were on one medication, and 31% were on two or more types. Amongst the patients using glaucoma medications, 75% were using prostaglandin analogues, 25% beta blockers, 18% alpha-2 adrenergic agonists, and 7% carbonic anhydrase inhibitors. Neither number of glaucoma medications nor types of glaucoma medications were associated with choriocapillaris characteristics ($P \geq 0.05$).

The multivariable linear regression modeling of associations of choriocapillaris density and size with normal aging and glaucoma, while controlling for diabetes, hypertension, intraocular pressure, axial length, and signal strength of scans are as shown in **Table 2**. Persons who were in the older age groups (53–82 years old) tended to have more flow deficits as compared to those in the youngest age group ($P \leq 0.24$). In terms of the average flow deficit size, it was significantly larger in the oldest age group ($P < 0.001$) whereas it appeared similar for those aged 53–68 years old ($P \geq 0.237$) when compared to the youngest group (42–52 years old). Specifically, the oldest group (69–82 years old) had 1% higher density of flow deficits in the choriocapillaris (95% CI = 0.34 to 1.65; $P = 0.003$) that were also 42.65 μm^2 larger in size (95% CI = 12.39 to 72.91; $P = 0.006$) than those in the youngest age group. In contrast, the density ($P = 0.453$) and size ($P = 0.637$) of flow deficits in the choriocapillaris were similar between POAG and normal participants. **Figure 2** shows representative OCTA images taken from normal controls of different age groups and glaucoma patients and illustrates the above findings, highlighting the increasing size of choriocapillaris flow deficit density with age. There were no differences in the density and size of choriocapillaris flow deficit between POAG patients and normal controls. **Figure 3** is a graphical representation of the general increment of choriocapillaris flow deficits in terms of its density and size with age in both glaucoma patients and normal controls. There was a statistically significant difference in choriocapillaris flow deficit density in patients aged 53 years and older compared to the reference age group (all $P \leq 0.024$). When comparing the average flow deficit size, the average flow deficit size was significantly larger only in those aged 69 years and above ($P = 0.006$) in both normal controls and glaucoma patients.

Discussion

In our study, we used SS-OCTA to examine macular choriocapillaris in normal and early POAG participants. After adjusting for relevant confounding factors such as diabetes, hypertension, intraocular pressure, axial length, and signal strength of scans, we found that older patients were more likely to have less perfused choriocapillaris (e.g., larger sized flow deficits) as compared to younger patients. In contrast, we did not find any significant differences in macular choriocapillaris features between normal and early POAG participants.

Ours is the largest study to date demonstrating that flow patterns in the macular choriocapillaris is not altered in early glaucoma. The current study had a statistical power of 100% to detect a minimal difference of 0.17% for density and −4.56 μm^2 for size, between glaucoma cases and normal controls. Previous smaller studies (with ≤ 35 subjects in each group) either found a difference (20) in choriocapillaris in glaucoma subjects, or none (17, 18). When small sample size is used, the study may have low statistical power and hence carry a risk that observations occur due to chance. Our

TABLE 2 Multivariable linear regression modeling of the association between normal aging, primary open angle glaucoma and choriocapillaris flow deficits.

Characteristic	Flow deficit density (%)			Average flow deficit size (μ m^2)		
	β	95% CI	*P-value	β	95% CI	*P-value
Normal aging						
Age quintile, years						
42–52 (n = 35 eyes of 22 patients)		Reference			Reference	
53–57 (n = 36 eyes of 23 patients)	0.81	0.13 to 1.49	**0.019**	15.52	−13.30 to 44.33	0.291
58–61 (n = 32 eyes of 19 patients)	0.71	0.16 to 1.27	**0.012**	16.66	−10.93 to 44.25	0.237
62–68 (n = 31 eyes of 20 patients)	0.71	0.09 to 1.32	**0.024**	15.45	−12.59 to 44.47	0.280
69–82 (n = 23 eyes of 20 patients)	1.00	0.34 to 1.65	**0.003**	42.65	12.39 to 72.91	**0.006**
Eye diseases						
Normal (n = 157 eyes of 104 patients)		Reference			Reference	
Early POAG (n = 144 of 100 patients)	0.17	−0.27 to 0.60	0.453	−4.56	−23.60 to 14.44	0.637

*Adjusted for diabetes, hypertension, intraocular pressure, axial length, and signal strength of scans. Bold values denote statistical significance at the $P < 0.05$ level. β, beta coefficient; CI, confidence interval; NA, not applicable; POAG, primary open angle glaucoma. Bold values denote statistical significance at the $P < 0.05$ level.

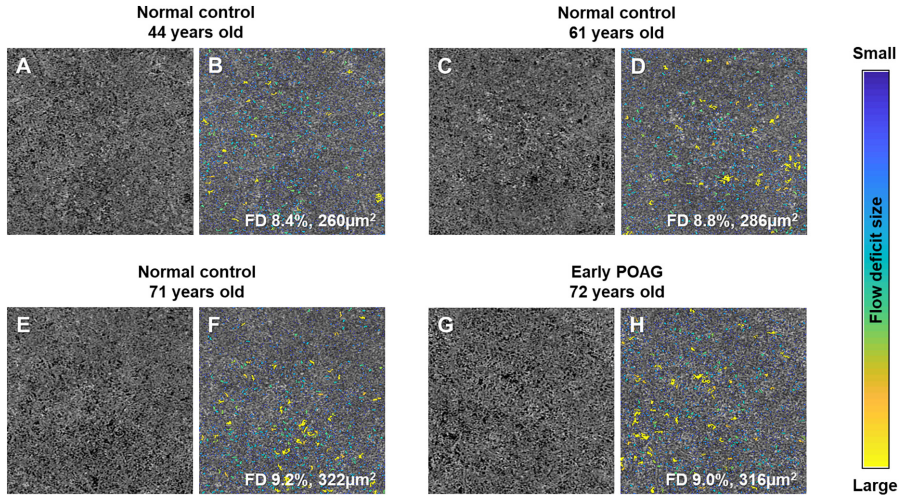

FIGURE 2
Representative choriocapillaris OCTA 3 × 3 mm2 images **(A,C,E,G)** and their corresponding color-coded maps **(B,D,F,H)**. The density and average size of choriocapillaris flow deficits (FD) in normal controls increases with age, where it is 8.4% and 260 μm^2 in the 44-year-old subject **(A,B)**, followed by 8.8% and 286 μm^2 in the 61-year-old subject **(C,D)**, and highest at 9.2% and 322 μm^2 in the 71-year-old **(E,F)**. Similar density and average size of choriocapillaris FD can be seen in a 72-year-old patient with mild primary open angle glaucoma (POAG; visual field mean deviation of −2.85 dB; G and H; 9.0% and 316 μm^2) and a 71-year-old normal control **(E,F**; 9.2% and 322 μm^2**)**.

study is adequately powered with 104 normal controls and 100 glaucoma patients. There was a tendency for a difference between glaucoma patients and normal controls at all ages (Figure 3). It is likely that this difference could become significant as OCTA technology advances and higher quality images can be obtained. On the other hand, while larger studies detect tiny or small associations, these findings may not be clinically important or relevant in improving the detection of early glaucoma.

Apart from the small sample size, earlier studies did not account for relevant confounding factors (32), such as axial length (17) and signal strength of scans (17, 18, 20) which are well-known to affect OCTA metrics. Another potential discrepancy is the severity of glaucoma as the differences in choriocapillaris flow deficits may be more prominent in more advanced glaucoma. In the paper by Yip et al. (20) the mean deviation of glaucoma subjects was −11.07 (±8.25) dB, suggesting that the study may have had patients with more moderate-severe glaucoma, whereas our POAG participants had early glaucoma (visual field mean deviation score of −2.40 (± −1.66) dB.

By allowing in-depth assessment of the choroidal circulation in a non-invasive manner, SS-OCTA has improved our understanding of ocular circulation and its role in the

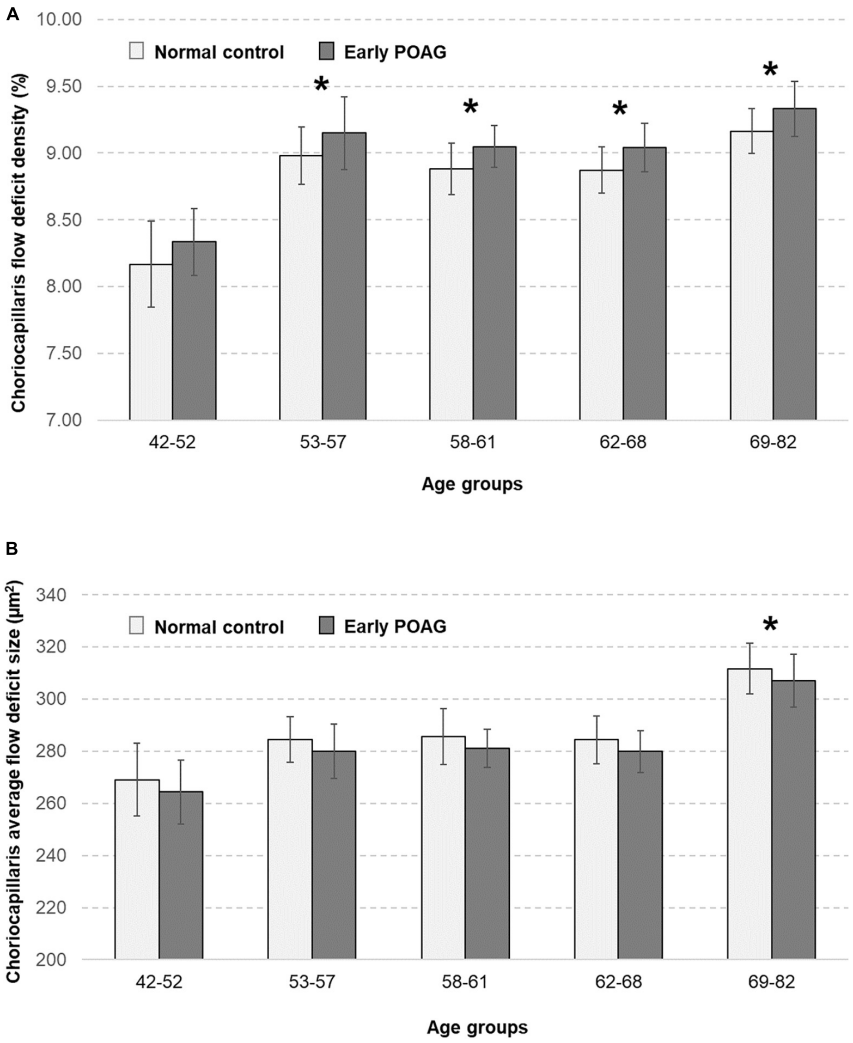

FIGURE 3
Relationship between the choriocapillaris **(A)** flow deficit density (%) and **(B)** average flow deficit size (μm^2) in normal controls (light grey bars) and patients with early primary open angle glaucoma (POAG; dark grey bars), stratified by age groups. Choriocapillaris flow deficit density was evidently higher in those aged 53 years and above (all $P \leq 0.024$) whereas the average flow deficit size was significantly larger in those aged 69 years and above ($P = 0.006$) in both normal and glaucoma patients. There were no differences in the choriocapillaris characteristics between normal and glaucoma patients. Asterisks mark significant differences in reference to the youngest age group according to multivariable linear regression analysis with generalized estimating equations (GEE) adjusted for diabetes, hypertension, intraocular pressure, axial length, and signal strength of scans.

pathogenesis of eye diseases, including glaucoma (14, 15, 33). The use of SS-OCTA to study choriocapillaris hemodynamics seems to be more advantageous compared to the use of SD-OCTA in previous studies (17, 18, 20). Compared to SD-OCTA, SS-OCTA uses a longer wavelength (1050 nm) which allows deeper penetration and enhanced imaging of choroidal structures (33). For a given acquisition time, the faster image acquisition of SS-OCTA also enables scan patterns to be denser and of a larger area compared with SD-OCT scans (34, 35). One possible explanation as to why the macular choriocapillaris is unaffected in early POAG is that glaucoma is characterized by the progressive loss of retinal ganglion cells (RGCs), and these cells receive their blood supply from the superficial vascular complex (36) whereas the choriocapillaris supplies the outer retina. On the other hand, in the SS-OCTA study by Tepelus et al. (19) involving 22 NTG patients, eyes with NTG demonstrated lower macular choriocapillaris flow deficit density compared to normal eyes. Unlike POAG, where IOP is the main risk factor, progression of NTG is multifactorial and not solely IOP dependent (37). The vascular theory behind NTG offers a possible explanation for this difference in findings between the two groups. Vascular factors have been hypothesized to contribute to the development and progression of glaucoma (2). It is believed that these factors are especially significant in NTG

patients, where optic nerve damage is believed to be a result of vascular dysregulation and poor blood supply (16, 38–40).

Our finding on the impact of normal aging on the macular choriocapillaris is in line with previous studies (41–45). Cheng et al. (41) found that a higher density of choriocapillaris flow deficits was associated with older age among 830 healthy Chinese individuals who were imaged using SS-OCTA. This was also reported by Zheng et al. (42) where the density increased with age, with greatest increase seen in the central 1 mm region of the macula. Similarly, Fujiwara et al. (43) reported a significant negative relationship between vascular density of the choroid and subjects' age in 163 healthy volunteers. These findings are also consistent with histopathological studies by Ramrattan et al. (46) who showed decreased choriocapillaris density with age. The reason for these age-dependent changes of the choriocapillaris, however, is still not clear. The age-related loss of choriocapillaris flow deficit features should be carefully considered when estimating disease-related choriocapillaris changes.

Strengths and limitations

The strengths of our study include sufficient study sample size of normal and early POAG participants, use of the SS-OCTA device, and accounting of a comprehensive list of potential confounding factors. Conversely, we recognize the limitations of our study. Our study did not include other glaucoma subtypes. It will be useful to study macular choriocapillaris differences between NTG and POAG patients, especially given the role of vascular factors in NTG pathogenesis as discussed above. Also, our study did not include moderate-severe glaucoma given our intention was to assess whether the OCTA-based vascular metrics of the macular choriocapillaris may offer an additional diagnostic tool to discriminate early glaucoma from normal controls.

Conclusion

In conclusion, the macular choriocapillaris density with SS-OCTA is affected by normal aging but unaffected by early POAG. Our findings suggest that the macular choriocapillaris perfusion appear to be unaffected by POAG mechanism and may not be a helpful OCTA diagnostic option for early glaucoma.

Data availability statement

The raw data supporting the conclusions of this article will be made available by the authors, without undue reservation.

Ethics statement

The studies involving human participants were reviewed and approved by the SingHealth Centralized Institutional Review Board, Singapore (protocol number: R1500/83/2017). The patients/participants provided their written informed consent to participate in this study.

Author contributions

JC, KL, and LS conceived and designed the study and wrote the main manuscript text. JC, KL, YS, RC, DW, BT, RH, TA, CS, and LS analyzed and interpreted the data. All authors reviewed the manuscript.

Funding

This work was funded by grants from the National Medical Research Council (CG/C010A/2017_SERI; OFLCG/004c/2018-00; MOH-000249-00; MOH-000647-00; MOH-001001-00; MOH-001015-00; MOH-000500-00; and MOH-000707-00), National Research Foundation Singapore (NRF2019-THE002-0006 and NRF-CRP24-2020-0001), A*STAR (A20H4b0141), Singapore Eye Research Institute, Nanyang Technological University [SERI-NTU Advanced Ocular Engineering (STANCE) Program], and SERI-Lee Foundation (LF1019-1) Singapore.

Acknowledgments

We would like to acknowledge Ms. Hu Qinglan for the capturing of scans.

Conflict of interest

The authors declare that the research was conducted in the absence of any commercial or financial relationships that could be construed as a potential conflict of interest.

Publisher's note

References

1. Weinreb RN, Aung T, Medeiros FA. The pathophysiology and treatment of glaucoma: a review. *JAMA.* (2014) 311:1901–11. doi: 10.1001/jama.2014.3192

2. Flammer J, Orgul S, Costa VP, Orzalesi N, Krieglstein GK, Serra LM, et al. The impact of ocular blood flow in glaucoma. *Prog Retin Eye Res.* (2002) 21:359–93. doi: 10.1016/S1350-9462(02)00008-3

3. Cherecheanu AP, Garhofer G, Schmidl D, Werkmeister R, Schmetterer L. Ocular perfusion pressure and ocular blood flow in glaucoma. *Curr Opin pharmacol.* (2013) 13:36–42. doi: 10.1016/j.coph.2012.09.003

4. Hayreh SS. Blood supply of the optic nerve head. *Ophthalmologica.* (1996) 210:285–95. doi: 10.1159/000310727

5. Lejoyeux R, Benillouche J, Ong J, Errera MH, Rossi EA, Singh SR, et al. Choriocapillaris: Fundamentals and advancements. *Prog Retin Eye Res.* (2022) 87:100997. doi: 10.1016/j.preteyeres.2021.100997

6. Duijm HF, van den Berg TJ, Greve EL. Choroidal haemodynamics in glaucoma. *Br J Ophthalmol.* (1997) 81:735–42. doi: 10.1136/bjo.81.9.735

7. Garhofer G, Fuchsjager-Mayrl G, Vass C, Pemp B, Hommer A, Schmetterer L. Retrobulbar blood flow velocities in open angle glaucoma and their association with mean arterial blood pressure. *Invest Ophthalmol Vis Sci.* (2010) 51:6652–7. doi: 10.1167/iovs.10-5490

8. Portmann N, Gugleta K, Kochkorov A, Polunina A, Flammer J, Orgul S. Choroidal blood flow response to isometric exercise in glaucoma patients and patients with ocular hypertension. *Invest Ophthalmol Vis Sci.* (2011) 52:7068–73. doi: 10.1167/iovs.11-7758

9. Marangoni D, Falsini B, Colotto A, Salgarello T, Anselmi G, Fadda A, et al. Subfoveal choroidal blood flow and central retinal function in early glaucoma. *Acta Ophthalmol.* (2012) 90:e288–94. doi: 10.1111/j.1755-3768.2011.02340.x

10. Shin DY, Hong KE, Lee NY, Park CK, Park HYL. Association of choroidal blood flow with autonomic dysfunction in patients with normal tension glaucoma. *Sci Rep.* (2022) 12:5136. doi: 10.1038/s41598-022-09162-4

11. Yamazaki S, Inoue Y, Yoshikawa K. Peripapillary fluorescein angiographic findings in primary open angle glaucoma. *Br J Ophthalmol.* (1996) 80:812–7. doi: 10.1136/bjo.80.9.812

12. O'Brart DP, de Souza Lima M, Bartsch DU, Freeman W, Weinreb RN. Indocyanine green angiography of the peripapillary region in glaucomatous eyes by confocal scanning laser ophthalmoscopy. *Am J Ophthalmol.* (1997) 123:657–66. doi: 10.1016/S0002-9394(14)71078-5

13. Kim K, Yang J, Feuer W, Gregori G, Kim ES, Rosenfeld PJ, et al. A comparison study of polypoidal choroidal vasculopathy imaged with indocyanine green angiography and swept-source optical coherence tomography angiography. *Am J Ophthalmol.* (2020) 217:240–51. doi: 10.1016/j.ajo.2020.05.017

14. Spaide RF, Fujimoto JG, Waheed NK, Sadda SR, Staurenghi G. Optical coherence tomography angiography. *Prog Retin Eye Res.* (2018) 64:1–55. doi: 10.1016/j.preteyeres.2017.11.003

15. Van Melkebeke L, Barbosa-Breda J, Huygens M, Stalmans I. Optical coherence tomography angiography in glaucoma: A review. *Ophthalmic Res.* (2018) 60:1–13. doi: 10.1159/000488495

16. Chua J, Tan B, Ang M, Nongpiur ME, Tan AC, Najjar RP, et al. Future clinical applicability of optical coherence tomography angiography. *Clin Exp Optom.* (2019) 102:260–9. doi: 10.1111/cxo.12854

17. Chao SC, Yang SJ, Chen HC, Sun CC, Liu CH, Lee CY. Early macular angiography among patients with glaucoma, ocular hypertension, and normal subjects. *J Ophthalmol.* (2019) 2019:7419470. doi: 10.1155/2019/7419470

18. Milani P, Urbini LE, Bulone E, Nava U, Visintin D, Cremonesi G, et al. The macular choriocapillaris flow in glaucoma and within-day fluctuations: an optical coherence tomography angiography study. *Invest Ophthalmol Vis Sci.* (2021) 62:22. doi: 10.1167/iovs.62.1.22

19. Tepelus TC, Song S, Borrelli E, Nittala MG, Baghdasaryan E, Sadda SR, et al. Quantitative analysis of retinal and choroidal vascular parameters in patients with low tension glaucoma. *J Glaucoma.* (2019) 28:557–62. doi: 10.1097/IJG.0000000000001242

20. Yip VCH, Wong HT, Yong VKY, Lim BA, Hee OK, Cheng J, et al. Optical coherence tomography angiography of optic disc and macula vessel density in glaucoma and healthy eyes. *J Glaucoma.* (2019) 28:80–7. doi: 10.1097/IJG.0000000000001125

21. Chua J, Baskaran M, Ong PG, Zheng Y, Wong TY, Aung T, et al. Prevalence, risk factors, and visual features of undiagnosed glaucoma: the singapore epidemiology of eye diseases study. *JAMA Ophthalmol.* (2015) 133:938–46. doi: 10.1001/jamaophthalmol.2015.1478

22. Chua J, Tan B, Ke M, Schwarzhans F, Vass C, Wong D, et al. Diagnostic ability of individual macular layers by spectral-domain oct in different stages of glaucoma. *Ophthalmol Glaucoma.* (2020) 3:314–26. doi: 10.1016/j.ogla.2020.04.003

23. Chua J, Schwarzhans F, Wong D, Li C, Husain R, Crowston JG, et al. Multivariate normative comparison, a novel method for improved use of retinal nerve fiber layer thickness to detect early glaucoma. *Ophthalmol Glaucoma.* (2021) 5:359–68. doi: 10.1016/j.ogla.2021.10.013

24. Chua J, Tham YC, Tan B, Devarajan K, Schwarzhans F, Gan A, et al. Age-related changes of individual macular retinal layers among Asians. *Sci Rep.* (2019) 9:20352. doi: 10.1038/s41598-019-56996-6

25. Chua J, Tham YC, Liao J, Zheng Y, Aung T, Wong TY, et al. Ethnic differences of intraocular pressure and central corneal thickness: the Singapore Epidemiology of Eye Diseases study. *Ophthalmology.* (2014) 121:2013–22. doi: 10.1016/j.ophtha.2014.04.041

26. Chua J, Le TT, Tan B, Ke M, Li C, Wong DWK, et al. Choriocapillaris microvasculature dysfunction in systemic hypertension. *Sci Rep.* (2021) 11:4603. doi: 10.1038/s41598-021-84136-6

27. Borrelli E, Toto L, Viggiano P, Evangelista F, Palmieri M, Mastropasqua R. Widefield topographical analysis of the retinal perfusion and neuroretinal thickness in healthy eyes: a pilot study. *Eye (Lond).* (2020) 34:2264–70. doi: 10.1038/s41433-020-0804-5

28. Hong J, Tan B, Quang ND, Gupta P, Lin E, Wong D, et al. Intra-session repeatability of quantitative metrics using widefield optical coherence tomography angiography (OCTA) in elderly subjects. *Acta Ophthalmol.* (2019) 98:570–8. doi: 10.1111/aos.14327

29. Lin E, Ke M, Tan B, Yao X, Wong D, Ong L, et al. Are choriocapillaris flow void features robust to diurnal variations? A swept-source optical coherence tomography angiography (OCTA) study. *Sci Rep.* (2020) 10:11249. doi: 10.1038/s41598-020-68204-x

30. Zhang Q, Zheng F, Motulsky EH, Gregori G, Chu Z, Chen CL, et al. A Novel Strategy for Quantifying Choriocapillaris Flow Voids Using Swept-Source OCT Angiography. *Invest Ophthalmol Vis Sci.* (2018) 59:203–11. doi: 10.1167/iovs.17-22953

31. Cohen J. Set Correlation and Contingency Tables. *Appl Psychol Meas.* (1988) 12:425–34. doi: 10.1177/014662168801200410

32. Chua J, Sim R, Tan B, Wong D, Yao X, Liu X, et al. Optical coherence tomography angiography in diabetes and diabetic retinopathy. *J Clin Med.* (2020) 9:1723. doi: 10.3390/jcm9061723

33. Lains I, Wang JC, Cui Y, Katz R, Vingopoulos F, Staurenghi G, et al. Retinal applications of swept source optical coherence tomography (OCT) and optical coherence tomography angiography (OCTA). *Prog Retin Eye Res.* (2021) 84:100951. doi: 10.1016/j.preteyeres.2021.100951

34. Novais EA, Adhi M, Moult EM, Louzada RN, Cole ED, Husvogt L, et al. Choroidal neovascularization analyzed on ultrahigh-speed swept-source optical coherence tomography angiography compared to spectral-domain optical coherence tomography angiography. *Am J Ophthalmol.* (2016) 164:80–8. doi: 10.1016/j.ajo.2016.01.011

35. Miller AR, Roisman L, Zhang Q, Zheng F, Rafael de Oliveira Dias J, Yehoshua Z, et al. Comparison between spectral-domain and swept-source optical coherence tomography angiographic imaging of choroidal neovascularization. *Invest Ophthalmol Vis Sci.* (2017) 58:1499–505. doi: 10.1167/iovs.16-20969

36. Penteado RC, Zangwill LM, Daga FB, Saunders LJ, Manalastas PIC, Shoji T, et al. Optical coherence tomography angiography macular vascular density measurements and the central 10-2 visual field in glaucoma. *J Glaucoma.* (2018) 27:481–9. doi: 10.1097/IJG.0000000000000964

37. Anderson DR. Normal tension glaucoma s. collaborative normal tension glaucoma study. *Curr Opin Ophthalmol.* (2003) 14:86–90. doi: 10.1097/00055735-200304000-00006

38. Nakazawa T. Ocular blood flow and influencing factors for glaucoma. *Asia Pac J Ophthalmol (Phila).* (2016) 5:38–44. doi: 10.1097/APO.0000000000000183

39. Schmidl D, Garhofer G, Schmetterer L. The complex interaction between ocular perfusion pressure and ocular blood flow - relevance for glaucoma. *Exp Eye Res.* (2011) 93:141–55. doi: 10.1016/j.exer.2010.09.002

40. Kiyota N, Shiga Y, Takahashi N, Yasuda M, Omodaka K, Tsuda S, et al. Progression in open-angle glaucoma with myopic disc and blood flow in the optic nerve head and peripapillary chorioretinal atrophy zone. *Ophthalmology Glaucoma.* (2020) 3:202–9. doi: 10.1016/j.ogla.2020.03.005

41. Cheng W, Song Y, Lin F, Jin L, Wang Z, Jonas JB, et al. Choriocapillaris flow deficits in normal chinese imaged by swept-source optical coherence tomographic angiography. *Am J Ophthalmol.* (2022) 235:143–53. doi: 10.1016/j.ajo.2021.09.018

42. Zheng F, Zhang Q, Shi Y, Russell JF, Motulsky EH, Banta JT, et al. Age-dependent changes in the macular choriocapillaris of normal eyes imaged with swept-source optical coherence tomography angiography. *Am J Ophthalmol.* (2019) 200:110–22. doi: 10.1016/j.ajo.2018.12.025

43. Fujiwara A, Morizane Y, Hosokawa M, Kimura S, Kumase F, Shiode Y, et al. Factors affecting choroidal vascular density in normal eyes: quantification using en face swept-source optical coherence tomography. *Am J Ophthalmol.* (2016) 170:1–9. doi: 10.1016/j.ajo.2016.07.006

44. Park SH, Cho H, Hwang SJ, Jeon B, Seong M, Yeom H, et al. Changes in the retinal microvasculature measured using optical coherence tomography angiography according to age. *J Clin Med.* (2020) 9:883. doi: 10.3390/jcm9030883

45. Uji A, Balasubramanian S, Lei J, Baghdasaryan E, Al-Sheikh M, Sadda SR. Choriocapillaris imaging using multiple en face optical coherence tomography angiography image averaging. *JAMA Ophthalmol.* (2017) 135:1197–204. doi: 10.1001/jamaophthalmol.2017.3904

46. Ramrattan RS, van der Schaft TL, Mooy CM, de Bruijn WC, Mulder PG, de Jong PT. Morphometric analysis of Bruch's membrane, the choriocapillaris, and the choroid in aging. *Invest Ophthalmol Vis Sci.* (1994) 35:2857–64.

frontiers | Frontiers in Medicine

TYPE Original Research
PUBLISHED 10 November 2022
DOI 10.3389/fmed.2022.1025853

OPEN ACCESS

EDITED BY
Ovidiu Constantin Baltatu,
Anhembi Morumbi University, Brazil

REVIEWED BY
Rebekka Heitmar,
University of Huddersfield,
United Kingdom
Doina Gherghel,
The University of Manchester,
United Kingdom

*CORRESPONDENCE
Gerhard Garhöfer
gerhard.garhoefer@meduniwien.ac.at

SPECIALTY SECTION
This article was submitted to Ophthalmology, a section of the journal Frontiers in Medicine

RECEIVED 23 August 2022
ACCEPTED 26 October 2022
PUBLISHED 10 November 2022

CITATION
Hommer N, Kallab M, Schlatter A, Janku P, Werkmeister RM, Howorka K, Schmidl D, Schmetterer L and Garhöfer G (2022) Neuro-vascular coupling and heart rate variability in patients with type II diabetes at different stages of diabetic retinopathy.
Front. Med. 9:1025853.
doi: 10.3389/fmed.2022.1025853

Neuro-vascular coupling and heart rate variability in patients with type II diabetes at different stages of diabetic retinopathy

Nikolaus Hommer[1], Martin Kallab[1], Andreas Schlatter[1,2,3], Patrick Janku[1], René M. Werkmeister[4], Kinga Howorka[5], Doreen Schmidl[1], Leopold Schmetterer[1,4,6,7,8,9] and Gerhard Garhöfer[1]*

[1]Department of Clinical Pharmacology, Medical University of Vienna, Vienna, Austria, [2]Hanusch Hospital, Karl Landsteiner Institute, Vienna, Austria, [3]Hanusch Hospital, Vienna Institute for Research in Ocular Surgery, Vienna, Austria, [4]Center for Medical Physics and Biomedical Engineering, Medical University of Vienna, Vienna, Austria, [5]Metabolic Competence Center, Medical University of Vienna, Vienna, Austria, [6]Singapore National Eye Centre, Singapore Eye Research Institute, Singapore, Singapore, [7]Ophthalmology and Visual Sciences Academic Clinical Program, Duke-NUS Medical School, Singapore, Singapore, [8]School of Chemical and Biomedical Engineering, Nanyang Technological University, Singapore, Singapore, [9]Institute of Clinical and Experimental Ophthalmology, Basel, Switzerland

Aims/Hypothesis: There is evidence that diabetes is accompanied by a breakdown of functional hyperemia, an intrinsic mechanism of neural tissues to adapt blood flow to changing metabolic demands. However, to what extent functional hyperemia is altered in different stages of diabetic retinopathy (DR) in patients with type II diabetes is largely unknown. The current study set out to investigate flicker-induced retinal blood flow changes in patients with type II diabetes at different stages of DR.

Materials and methods: A total of 76 subjects were included in the present parallel-group study, of which 56 had diabetes with either no DR or different stages of non-proliferative DR (n = 29 no DR, 12 mild DR, 15 moderate to severe DR). In addition, 20 healthy subjects were included as controls. Retinal blood flow was assessed before and during visual stimulation using a combined measurement of retinal vessel calibers and blood velocity by the means of Doppler optical coherence tomography (OCT). To measure systemic autonomic nervous system function, heart rate variability (HRV) was assessed using a short-term orthostatic challenge test.

Results: In healthy controls, retinal blood flow increased by 40.4 ± 27.2% during flicker stimulation. Flicker responses in patients with DR were significantly decreased depending on the stage of the disease (no DR 37.7 ± 26.0%, mild DR 26.2 ± 28.2%, moderate to severe DR 22.3 ± 13.9%; p = 0.035, ANOVA). When assessing systemic autonomous neural function using HRV, normalized low frequency (LF) spectral power showed a significantly different response to the orthostatic maneuver in diabetic patients compared to healthy controls ($p < 0.001$).

Conclusion/Interpretation: Our study indicates that flicker induced hyperemia is reduced in patients with DR compared to healthy subjects. Further, this impairment is more pronounced with increasing severity of DR. Further studies are needed to elucidate mechanisms behind the reduced hyperemic response in patients with type II diabetes.

Clinical trial registration: [https://clinicaltrials.gov/], identifier [NCT03 552562].

KEYWORDS

diabetes type II, diabetic retinopathy, functional hyperemia, neuro-vascular coupling, retinal blood flow, heart rate variability

Introduction

The incidence and prevalence of type II diabetes and its associated co-morbidities is constantly rising (1–3). Traditionally, diabetic complications are classified as macrovascular – leading to cardiovascular and peripheral vascular disease – and microvascular complications, the latter being characterized by the triade of nephropathy, neuropathy, and diabetic retinopathy (DR) (4). Although microvascular damage usually occurs early in the disease process, changes can be clinically silent for a long time before a symptomatic manifestation occurs. Thus, biomarkers of disease progress reflecting microvascular complications are still warranted to identify high-risk patients (5).

The eye has the unique advantage that the microvasculature can be assessed directly and non-invasively without the need for an injection of contrast agents or radiation exposure. As such, microvascular changes such as microaneurysms, hemorrhages, or hard exudates are well known clinical signs of DR that can easily be graded on the slit lamp or using fundus photography. Further, recently developed imaging devices such as optical coherence tomography (OCT) angiography show rarefication of retinal vessels (6–10) indicative for changes in retinal perfusion (11–15).

However, there is evidence that functional alterations may proceed structural changes in patients with diabetes. As such, it has been consistently shown in the brain as well as in the retina that functional hyperemia, a term describing the ability of the tissue to adapt blood flow to different metabolic demands is impaired in patients with diabetes. However, whereas this hyperemic response, also known as neuro-vascular coupling is difficult to investigate in the brain and requires costly investigations such as Positron emission tomography (PET) or functional magnetic resonance imaging (fMRI) (16–18), neuro-vascular coupling can be easily and none-invasively assessed at the level of the retina by visual stimulation with flickering light. As such, most (19–26) but not all (27) human studies indicate a breakdown of neuro-vascular coupling in patients with diabetes. However, previous studies on this topic were limited by the fact that only information regarding vessel diameter not volumetric blood flow was assessed. Thus, the retinal blood flow response to flicker stimulation in patients with type II diabetes is largely unknown (24).

The present study set out to extend our knowledge on neuro-vascular coupling in patients with type two diabetes and different stages of DR. To assess retinal blood flow under visual stimulation, a recently developed, custom-built Doppler OCT system was used. Based on the measurement of retinal vessel diameters and blood flow velocity our approach allows us to expand our knowledge and assess volumetric blood flow during visual stimulation (28, 29). In addition, the current study included a test for measuring autonomic nervous system function. This test assesses heart rate variability (HRV) (30–32) and allows to investigate whether alterations in the autonomic nervous system may correlate with the severity of DR.

Materials and methods

Subjects

The study protocol was approved by the Ethics Committee of the Medical University of Vienna, the national competent authorities and was conducted in compliance with the Declaration of Helsinki and Good Clinical Practice (GCP) guidelines of the European Union. All subjects, selected by the Department of Clinical Pharmacology, provided written informed consent before any study-related procedures were performed. All subjects passed a prestudy screening in the 4 weeks before the first study day including the following examinations: medical history, pregnancy test in women of childbearing potential, blood pressure and heart rate measurement, laboratory testing for HbA1c, blood glucose levels and hemoglobin, assessment of visual acuity, slit lamp biomicroscopy, indirect funduscopy, 7-standard field color fundus photography for grading of DR (33), and measurement

of intraocular pressure (IOP) with Goldmann applanation tonometry. Subjects were not included, if any clinically significant medical condition (except diabetes type II in the patient group) was found as part of the screening examination. Exclusion criteria were ametropia of more than six diopters, smoking and history, or family history of epilepsy.

Study design

The current study was a prospective parallel group study with observer blinded analysis.

On the screening day and on the study day all subjects arrived in the morning after 7–8 h of sleep and abstained from alcohol and stimulating beverages containing xanthine derivates like tea, coffee, or cola-like drinks 12 h before the study day. At the beginning of the study day, a pregnancy test was performed in females of childbearing potential. Then, one drop of mydriaticum (Mydriaticum "Agepha," Agepha, Vienna, Austria) was administered into the chosen study eye and a resting period of at least 20 min was scheduled before measurements were started to allow pupil dilatation and ensure constant hemodynamic conditions. Capillary blood glucose level measurements were performed using a glucose meter and a blood draw for laboratory testing for HbA1c was done. Then, retinal vessel diameters were measured at baseline and during flicker stimulation using the dynamic vessel analyzer (DVA) and retinal venous blood flow using DOCT was assessed. Blood pressure, heart rate, and IOP were measured before and after these measurements. Assessment of HRV was done as final study day investigation. Blood flow measurements were performed under light-adapted conditions.

Measurement of retinal vessel diameters

Measurement with the DVA allows the real time determination of retinal vessel diameters *in vivo*. This commercially available system (IMEDOS, Jena, Germany) combines a fundus camera (FF 450; Carl Zeiss Meditec, Jena, Germany), a video camera, a real time monitor and a personal computer with an analyzing software to measure retinal and venous diameters (34). The device allows the evaluation of the diameters of one temporal retinal artery and vein between 1 and 2 disk diameters from the margin of the optic disk by analyzing digital pictures from a continuous video of the respective vessels (35).

Before flicker stimulation, a baseline recording for 60 s was performed. After the baseline recording, flicker was applied for another period of 60 s. For flicker stimulation, the white light spectrum of a halogen lamp was filtered using a 550 nm low pass cut-off-filter, ensuring that the yellow and red spectral part are filtered and only wavelengths below 550 nm were used for stimulation. Flicker was applied at a frequency of 12.5 Hz.

Measurement of retinal venous blood flow

A previously described system allows quantification of retinal venous blood flow *in vivo* (13, 28, 29, 36–38). This custom-built dual-beam Doppler Fourier Domain-OCT (DOCT), coupled to a fundus camera, which ensures simultaneous view for selection of the region of interest, used a specific rectangular scanning pattern around the optic nerve head (ONH) to gain measurements from retinal veins with a diameter of at least 40 μm. To obtain averaged blood velocity values, this scanning pattern was applied on each vessel for several pulse periods. For quantification of mean absolute blood velocity (V_{abs}), phase shifts in the two probe beams and channels, respectively, were calculated. Venous blood flow (Q_{abs}) was calculated using vessel diameters *(d),* which were extracted from the DVA and V_{abs} as $Q_{abs} = V_{abs}\ d_2\ \pi/4$ for each vessel. DVA and DOCT measurements were performed simultaneously at the same vessel location. The detailed description of the setup has been published previously (28).

Measurement of heart rate variability

Measurement of HRV is a standardized, non-invasive method for quantification of autonomic sympathetic and parasympathetic control and therefore used for evaluation of cardiovascular autonomic neuropathy in diabetes (39–41). This assessment is based on analysis of HRV in frequency-domain, using a short-term modified orthostatic load (42). Using VariaCardio® (Vario Cardio TF5; Advanced Medical Diagnostic Group, Leeds, UK), this short-term spectral analysis of HRV is obtained from recordings consisting of 256 s of artifact-free records in three positions (supine1-standing-supine2). The recorded high-resolution one-channel echocardiogram (ECG) is transferred to a receiver connected to a personal computer and displayed on-line. Then R–R intervals are identified with a sampling rate of 1,000 Hz. Artifacts are identified and labeled and a specific algorithm inserts beat-to-beat intervals throughout an artifact period to preserve the timing relationships of the adjacent, uncorrupted heart rate data. The final results are immediately displayed on the monitor as three-dimensional running spectra. Parameters of frequency-domain HRV are measured within the low-frequency (LF) band (0.05–0.15 Hz) and high-frequency (HF) band (0.15–0.50 Hz). A reduced LF and HF spectral power at rest, a reduced increase of normalized LF spectral power during orthostasis and a reduced normalization after an orthostatic challenge are known to be a sensitive sign of a limited autonomic cardiovascular control (42, 43).

Statistical analysis

Statistical analysis was performed using IBM SPSS Statistics (Version 26, IBM, Armonk, NY, USA). All values are presented as means ± SD. Normal distribution for all outcome variables was confirmed using the Shapiro–Wilk test. Extreme outliers [according to the 3 (IQR) rule], were removed, these were two data points for the flicker response in arterial diameter in the "no DR" group. Descriptive statistics are reported for all values obtained. Flicker response was calculated as percent change from baseline in vessel diameter and retinal blood flow. A Welch ANOVA was carried out for all parameters to assess overall differences between groups. Planned contrasts between groups were used to assess differences between two groups (in particular between healthy subjects, patients with no DR, patients with mild DR, and patients with moderate to severe DR). To assess differences in HRV during the orthostatic maneuver, a repeated measures ANOVA model was calculated. A p-value < 0.05 was considered as the level of significance.

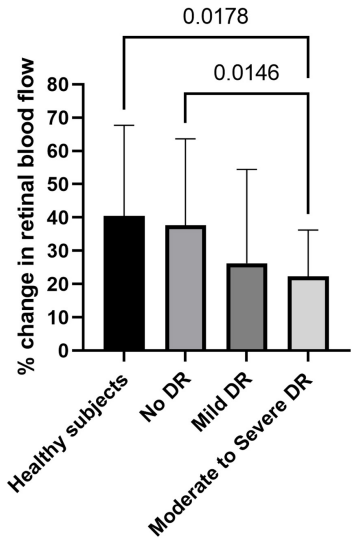

FIGURE 1
Flicker response of retinal blood flow in healthy subjects, patients with no diabetic retinopathy (no DR), mild diabetic retinopathy (mild DR), and moderate to severe diabetic retinopathy (moderate to severe DR). Data are presented as mean ± SD. Planned comparisons were used to calculate p-values between groups.

Results

A total of 76 subjects were included in the present study, of which 56 had diabetes with no DR or different stages of non-proliferative DR. Among these, twenty-nine (29) had no DR, 12 had mild DR, and 15 had moderate to severe DR. In addition, 20 ages matched healthy subjects were included as controls. The demographics and baseline characteristics of the four study groups are shown in Table 1.

A significantly different response to flicker stimulation was observed between the four groups in regards to retinal venous blood flow (Figure 1). While in healthy subjects, retinal venous blood flow increased by 40.4 ± 27.2% and in patients with no DR by 37.7 ± 26.0%, it only increased by 26.2 ± 28.2% in patients with mild DR, and by 22.3 ± 13.9% in patients with moderate to severe DR ($p = 0.035$).

The hyperemic response in retinal arterial diameter was 2.5 ± 2.4% in healthy subjects, 1.7 ± 1.6% in patients with no DR, 1.2 ± 2.3% in patients with mild DR, and 1.0 ± 1.3% in patients with moderate to severe DR, respectively. Although there was a tendency toward a decreased response in arterial diameters with increasing stage of DR, this effect failed to

TABLE 1 Baseline characteristics of the four study groups.

	Healthy subjects ($n = 20$)	No DR ($n = 29$)	Mild DR ($n = 12$)	Moderate to severe DR ($n = 15$)
Age (years)	59 ± 9	61 ± 10	64 ± 9	63 ± 7
Body mass index (kg/m^2)	26 ± 6	28 ± 5	30 ± 3	30 ± 5
Diabetes duration (years)	N/A	14 ± 10	15 ± 10	11 ± 7
HbA1c (%)	N/A	6.6 ± 0.7	6.9 ± 0.8	7.3 ± 1.0
Plasma glucose level (mg/dL)	N/A	184 ± 58	186 ± 63	221 ± 52
Systolic blood pressure (mmHg)	128 ± 13	135 ± 13	130 ± 15	138 ± 11
Diastolic blood pressure (mmHg)	77 ± 10	80 ± 11	76 ± 14	77 ± 10
Heart rate (bpm)	69 ± 8	71 ± 12	72 ± 10	71 ± 10
Mean arterial pressure (mmHg)	100 ± 12	104 ± 11	100 ± 13	106 ± 9
Intraocular pressure (mmHg)	14 ± 2	15 ± 3	15 ± 2	15 ± 2
Ocular perfusion pressure (mmHg)	52 ± 7	55 ± 8	52 ± 8	55 ± 7
Retinal venous blood flow obtained in one single vessel (µl/min)	15.7 ± 6.3	15.0 ± 9.4	17.8 ± 4.0	13.5 ± 6.2

Values are presented as mean ± SD.

reach significance ($p = 0.109$, Figure 2A). Planned comparisons revealed that there was a significant difference in arterial diameter response between healthy subjects and patients with moderate to severe DR.

As for retinal veins, the response of venous diameters to flicker light was significantly different between the four groups ($p < 0.001$, Welch ANOVA, Figure 2B). Flicker induced vasodilation was 4.1 ± 1.5% in healthy subjects, 3.5 ± 2.2% in patients with no DR, 2.8 ± 2.1% in patients with mild DR, and lowest in patients with moderate to severe DR (1.4 ± 0.9%). When comparing individual groups, the response was significantly different between patients with moderate to severe DR and healthy subjects or patients with no DR.

When looking at HRV, normalized LF spectral power showed a significantly different response to the orthostatic maneuver in diabetic patients compared to healthy controls ($p < 0.001$). As shown in Figure 3A, the response was more blunted with increasing severity of DR. Data showed a significant difference between healthy subjects and patients with no DR ($p = 0.004$), healthy subjects and patients with mild DR ($p < 0.001$) and healthy subjects and moderate to severe DR ($p < 0.001$).

The time course of HF spectral power during the orthostatic maneuver was not altered in diabetic patients compared to healthy controls ($p = 0.270$, Figure 3B). However, HF spectral power was generally lower at all assessments in patients with diabetes compared to healthy subjects. No correlation between the flicker response in retinal blood flow, retinal arterial diameter, retinal venous diameter, and the HRV parameters normalized LF and HF spectral power was found ($p > 0.30$ each).

Discussion

The results of the present study indicate that the blood flow response to visual stimulation with flicker light is reduced with increasing severity of DR in patients with type II diabetes. This effect was paralleled by an altered HRV in patients with diabetes, again associated with disease severity. In summary, our data support the concept of a strong neuro-vascular component in the pathogenesis of DR in patients with type II diabetes.

Several lines of evidence indicate that in the brain, as well as in the retina, a breakdown of neuro-vascular coupling may be a pathogenic factor in the development of diabetic complications. Studies in the brain using blood oxygenation level–dependent functional magnetic resonance imaging (BOLD fMRI) to assess functional hyperemia have shown reduced functional hyperemia in patients with diabetes (44, 45). As for the retina, there is compelling evidence that flicker induced vasodilatation is reduced in patients with type I and type II diabetes (20, 23, 46–48). However, the latter studies do not give a full picture of functional hyperemia in human diabetic subjects: First, previous studies report only data regarding flicker induced retinal vasodilatation in large retinal vessels, but not blood flow *per se*. Given that the microcirculation is the major determinant of vascular resistance and therefore blood flow, caliber changes in large vessel do not necessarily fully predict changes in blood flow. Secondly, studies assessing neuro-vascular coupling in different clinical stages of DR are sparse. Mandecka et al. (46) have reported reduced retinal vasodilatation, an effect that was more pronounced in more severe patients. As the latter study has included patients with both type I and type II diabetes, it remains unclear whether type I and type II diabetics share the same characteristics in neuro-vascular coupling.

Our data expands our knowledge in patients with type II diabetes and indicates that flicker-induced hyperemia is reduced in patients with moderate to severe DR compared to healthy subjects. Indeed, the results show that in patients with moderate to severe non-proliferative DR, blood flow response is approximately only 50% of the response observed in the healthy control group. Further, the reduction in flicker induced hyperemia was also significantly more pronounced in patients with moderate to severe DR compared to patients with no or mild DR indicating that neuro-vascular coupling is reduced depending on the severity of DR. Thus, our data supports the hypothesis of a break-down in neuro-vascular coupling early in the disease processes, which may aggravate with the progression of the disease. They also extend our previous findings in patients with type I diabetes, showing that the blood flow response to flicker stimulation is significantly reduced (22). However, since in this previous study only patients with no DR were included, no conclusion can be made on a potential difference between different grades of severity.

The reason for the diminished hyperemic response in patients with type II diabetes is still not fully elucidated. It has been suggested that the uncoupling between neural function and blood flow in diabetes may be related to endothelial dysfunction (23, 46). Following this hypothesis, the impaired hyperemic response is related to an impaired dilatory response of the microvasculature. Indeed, an impaired endothelial-dependent vasodilatation has been demonstrated in other vascular beds such as the brachial artery (49). Further, it has been reported that conditions associated with endothelial dysfunction such as smoking or systemic hypertension are also characterized by diminished flicker induced vasodilatation (47, 50). On the other hand, it has been shown that the vasodilatory response of retinal vessels to exogenous nitric oxide is preserved in patients with diabetes, indicating that the impaired flicker response is not caused by a generally reduced retinal vascular reactivity of retinal vessels (51). Thus, the question whether reduced flicker response can mainly be attributed to endothelial dysfunction is not entirely clear.

Alternatively, it has been hypothesized that impaired neural activity may be responsible for the observed uncoupling of visual stimulation and blood flow (52). Along this line of

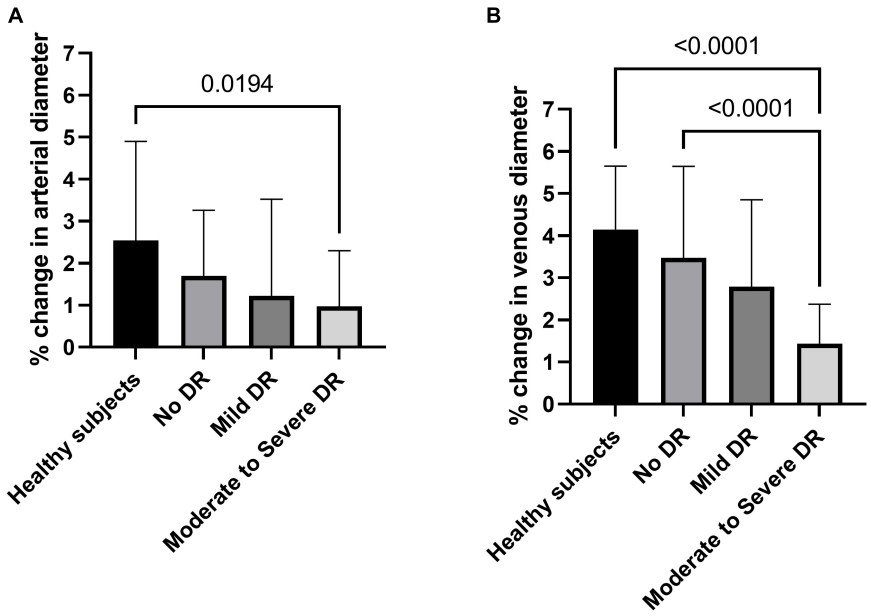

FIGURE 2
Flicker response of retinal arterial **(A)** and venous **(B)** diameter in healthy subjects, patients with no diabetic retinopathy (no DR), mild diabetic retinopathy (mild DR), and moderate to severe diabetic retinopathy (moderate to severe DR). Data are presented as mean ± SD. Planned comparisons were used to calculate *p*-values between groups.

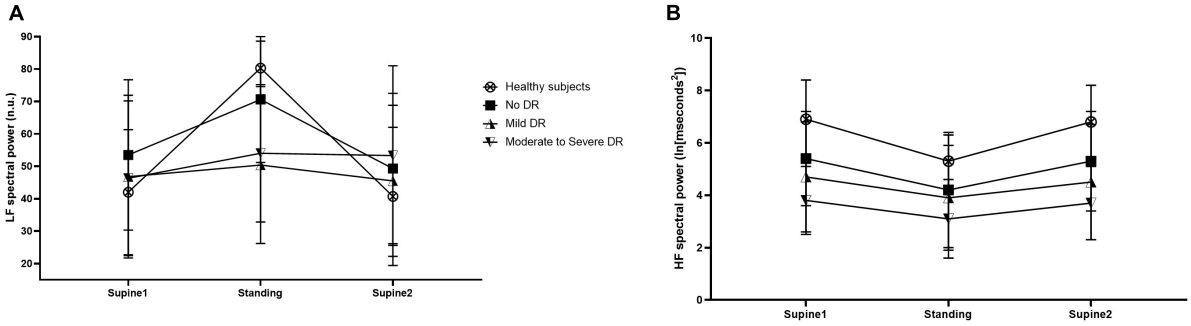

FIGURE 3
Normalized low-frequency (LF) spectral power of heart rate variability (HRV) in normalized units (nu) **(A)** and high-frequency (HF) spectral power **(B)** in healthy controls (open circles), patients with no diabetic retinopathy (no DR) (black squares), patients with mild diabetic retinopathy (mild DR) (upward triangles), and patients with moderate to severe diabetic retinopathy (moderate to severe DR) (downward triangles) before, during and after the orthostatic challenge. Data are presented as mean ± SD.

thought it has consistently been demonstrated that both the retinal nerve fiber layer as well as the ganglion cell layer are considerably thinner in patients with diabetes and no DR as compared to healthy controls (53, 54). This observed retinal thinning is associated with HbA1c, duration of diabetes and the severity of DR, indicating that neural degeneration plays an important role in the pathogenesis of the disease (55, 56). Whether these neurodegenerative changes observed in patients with diabetes occur prior to vascular manifestations or develop independently from them is yet to be investigated (52). Finally, longitudinal trials are warranted to clarify whether neural dysfunction plays a causative role in the observed breakdown of neuro-vascular coupling.

Impairment of neural function is also reflected in the data of the current study. In particular, differences between the four groups were also found for HRV, a marker for the autonomic nervous system (31, 32). While HF spectral power reflects vagal activity, the LF component is interpreted as a marker for sympathetic modulation (31). LF spectral power showed a statistically significant different response to the orthostatic maneuver in all patients with diabetes compared to healthy subjects and the difference became more pronounced with

increasing disease severity. This all points toward dysfunction of the autonomic system in patients with type II diabetes. Along this line of thought, several studies report disturbed function of the autonomic nervous system as a risk factor for cardiovascular disease (57, 58), which also has a higher prevalence in diabetic patients (59, 60). Interestingly, there also seems to be a link between the autonomic nervous system and the vascular endothelium in that sense that both act in opposition in order to regulate vascular tone (61). However, as the retinal blood supply is not under direct autonomic nerve control, a potential effect of the observed dysfunction of the autonomic system in patients with type II diabetes on ocular blood flow needs to be further investigated.

Some strengths and limitations of the present study need to be addressed. The strength of the current study is that by using the Doppler OCT technique, retinal vessel diameter and blood flow could be measured concomitantly, which allows for the exact determination of volumetric blood flow. We have recently shown that this system provides excellent repeatability and reproducibility in detecting even subtle changes in retinal blood flow (29). However, as a disadvantage of the used approach, the measurements during visual stimulation are challenging for the subjects and require excellent target fixation. Thus, blood flow measurement data have only been obtained from one vessel and no information on total retinal blood flow is available from the current study. In this context, it needs to be noted that there is still no general agreement in the literature on blood flow changes in patients with diabetes. Whereas some studies found decreased retinal perfusion in patients with diabetes (11, 12, 62, 63), others have reported an increase, especially in early stages (13–15, 64). Thus, further studies are needed to clarify this issue. Further, it also needs to be mentioned that some of the patients were under systemic antihypertensive medication and we cannot fully exclude that this may have influenced ocular perfusion parameters. However, as the outcome of the study was flicker induced hyperemia not absolute blood flow and systemic hemodynamic procedures were comparable between the study days, we deem that this does not interfere with our conclusions.

An additional limitation of the current study is the cross-sectional design, which allows only for conclusions regarding one certain time point, but does not finally clarify whether impaired neuro-vascular coupling is causative for the development of retinal vascular complications of diabetes type II. Longitudinal studies are required to further investigate this issue.

Conclusion

In conclusion, the results of the present study show that retinal neurovascular coupling and HRV are both impaired in patients with type II diabetes. These impairments seem to be more pronounced in later stages of DR. Further studies are required to assess whether the break-down of flicker induced hyperemia may be used as a predictive marker for the individual risk assessment of DR.

Data availability statement

The raw data supporting the conclusions of this article will be made available by the authors, without undue reservation.

Ethics statement

The studies involving human participants were reviewed and approved by the Ethics Committee of the Medical University of Vienna. The patients/participants provided their written informed consent to participate in this study.

Author contributions

NH, KH, DS, LS, and GG: conceptualization. NH, RW, LS, and GG: methodology. RW: software. NH, DS, and GG: validation, formal analysis, and visualization. NH, MK, AS, PJ, and GG: investigation. KH and GG: resources. DS and GG: data curation. NH and GG: writing – original draft preparation and project administration. MK, AS, PJ, RW, KH, DS, and LS: writing – review and editing. RW and GG: supervision. GG: funding acquisition. All authors contributed to the article and approved the submitted version.

Funding

Financial support from the Austrian Science Foundation FWF Projects Grant numbers: KLI529 and KLI721 are gratefully acknowledged.

Conflict of interest

The authors declare that the research was conducted in the absence of any commercial or financial relationships that could be construed as a potential conflict of interest.

Publisher's note

References

1. Andreadi A, Bellia A, Di Daniele N, Meloni M, Lauro R, Della-Morte D, et al. The molecular link between oxidative stress, insulin resistance, and type 2 diabetes: a target for new therapies against cardiovascular diseases. *Curr Opin Pharmacol.* (2021) 62:85–96. doi: 10.1016/j.coph.2021.11.010

2. Liggi S, Griffin JL. Metabolomics applied to diabetes-lessons from human population studies. *Int J Biochem Cell Biol.* (2017) 93:136–47. doi: 10.1016/j.biocel.2017.10.011

3. Ali MK, Pearson-Stuttard J, Selvin E, Gregg EW. Interpreting global trends in type 2 diabetes complications and mortality. *Diabetologia.* (2022) 65:3–13. doi: 10.1007/s00125-021-05585-2

4. Cole JB, Florez JC. Genetics of diabetes mellitus and diabetes complications. *Nat Rev Nephrol.* (2020) 16:377–90. doi: 10.1038/s41581-020-0278-5

5. Marcovecchio ML. Importance of identifying novel biomarkers of microvascular damage in type 1 diabetes. *Mol Diagn Ther.* (2020) 24:507–15. doi: 10.1007/s40291-020-00483-6

6. Veiby N, Simeunovic A, Heier M, Brunborg C, Saddique N, Moe MC, et al. Associations between macular oct angiography and nonproliferative diabetic retinopathy in young patients with type 1 diabetes mellitus. *J Diabetes Res.* (2020) 2020:8849116. doi: 10.1155/2020/8849116

7. Koçer AM, Şekeroğlu MA. Evaluation of the neuronal and microvascular components of the macula in patients with diabetic retinopathy. *Doc Ophthalmol.* (2021) 143:193–205. doi: 10.1007/s10633-021-09834-y

8. Frizziero L, Parrozzani R, Londei D, Pilotto E, Midena E. Quantification of vascular and neuronal changes in the peripapillary retinal area secondary to diabetic retinopathy. *Br J Ophthalmol.* (2021) 105:1577–83. doi: 10.1136/bjophthalmol-2020-316468

9. Tan B, Chua J, Lin E, Cheng J, Gan A, Yao X, et al. Quantitative microvascular analysis with wide-field optical coherence tomography angiography in eyes with diabetic retinopathy. *JAMA Netw Open.* (2020) 3:e1919469. doi: 10.1001/jamanetworkopen.2019.19469

10. Tey KY, Teo K, Tan ACS, Devarajan K, Tan B, Tan J, et al. Optical coherence tomography angiography in diabetic retinopathy: a review of current applications. *Eye Vis.* (2019) 6:37. doi: 10.1186/s40662-019-0160-3

11. Pechauer AD, Hwang TS, Hagag AM, Liu L, Tan O, Zhang X, et al. Assessing total retinal blood flow in diabetic retinopathy using multiplane en face doppler optical coherence tomography. *Br J Ophthalmol.* (2018) 102:126–30. doi: 10.1136/bjophthalmol-2016-310042

12. Srinivas S, Tan O, Nittala MG, Wu JL, Fawzi AA, Huang D, et al. Assessment of retinal blood flow in diabetic retinopathy using doppler fourier-domain optical coherence tomography. *Retina.* (2017) 37:2001–7. doi: 10.1097/iae.0000000000001479

13. Fondi K, Wozniak PA, Howorka K, Bata AM, Aschinger GC, Popa-Cherecheanu A, et al. Retinal oxygen extraction in individuals with type 1 diabetes with no or mild diabetic retinopathy. *Diabetologia.* (2017) 60:1534–40. doi: 10.1007/s00125-017-4309-0

14. Patel V, Rassam S, Newsom R, Wiek J, Kohner E. Retinal blood flow in diabetic retinopathy. *BMJ.* (1992) 305:678–83. doi: 10.1136/bmj.305.6855.678

15. Grunwald JE, DuPont J, Riva CE. Retinal haemodynamics in patients with early diabetes mellitus. *Br J Ophthalmol.* (1996) 80:327–31. doi: 10.1136/bjo.80.4.327

16. Sander CY, Hooker JM, Catana C, Normandin MD, Alpert NM, Knudsen GM, et al. Neurovascular coupling to D2/D3 dopamine receptor occupancy using simultaneous pet/functional mri. *Proc Natl Acad Sci U.S.A.* (2013) 110:11169–74. doi: 10.1073/pnas.1220512110

17. Tournier N, Comtat C, Lebon V, Gennisson JL. Challenges and perspectives of the hybridization of pet with functional mri or ultrasound for neuroimaging. *Neuroscience.* (2021) 474:80–93. doi: 10.1016/j.neuroscience.2020.10.015

18. Abraham T, Feng J. Evolution of brain imaging instrumentation. *Semin Nucl Med.* (2011) 41:202–19. doi: 10.1053/j.semnuclmed.2010.12.001

19. Lott ME, Slocomb JE, Shivkumar V, Smith B, Gabbay RA, Quillen D, et al. Comparison of retinal vasodilator and constrictor responses in type 2 diabetes. *Acta Ophthalmol.* (2012) 90:e434–41. doi: 10.1111/j.1755-3768.2012.02445.x

20. Garhöfer G, Zawinka C, Resch H, Kothy P, Schmetterer L, Dorner GT. Reduced response of retinal vessel diameters to flicker stimulation in patients with diabetes. *Br J Ophthalmol.* (2004) 88:887–91. doi: 10.1136/bjo.2003.033548

21. Lott ME, Slocomb JE, Shivkumar V, Smith B, Quillen D, Gabbay RA, et al. Impaired retinal vasodilator responses in prediabetes and type 2 diabetes. *Acta Ophthalmol.* (2013) 91:e462–9. doi: 10.1111/aos.12129

22. Lasta M, Pemp B, Schmidl D, Boltz A, Kaya S, Palkovits S, et al. Neurovascular dysfunction precedes neural dysfunction in the retina of patients with type 1 diabetes. *Invest Ophthalmol Vis Sci.* (2013) 54:842–7. doi: 10.1167/iovs.12-10873

23. Nguyen TT, Kawasaki R, Wang JJ, Kreis AJ, Shaw J, Vilser W, et al. Flicker light-induced retinal vasodilation in diabetes and diabetic retinopathy. *Diabetes Care.* (2009) 32:2075–80. doi: 10.2337/dc09-0075

24. Garhöfer G, Chua J, Tan B, Wong D, Schmidl D, Schmetterer L. Retinal neurovascular coupling in diabetes. *J Clin Med.* (2020) 9:2829. doi: 10.3390/jcm9092829

25. Streese L, Kotliar K, Deiseroth A, Infanger D, Vilser W, Hanssen H. Retinal endothelial function, physical fitness and cardiovascular risk: a diagnostic challenge. *Front Physiol.* (2019) 10:831. doi: 10.3389/fphys.2019.00831

26. Sörensen BM, Houben AJ, Berendschot TT, Schouten JS, Kroon AA, van der Kallen CJ, et al. Prediabetes and type 2 diabetes are associated with generalized microvascular dysfunction: the maastricht study. *Circulation.* (2016) 134:1339–52. doi: 10.1161/circulationaha.116.023446

27. Baier JM, Funck KL, Petersen L, Vernstrøm L, Knudsen ST, Bek T, et al. Retinal vessel reactivity is not attenuated in patients with type 2 diabetes compared with matched controls and is associated with peripheral endothelial function in controls. *J Diabetes Complications.* (2019) 33:641–7. doi: 10.1016/j.jdiacomp.2019.05.024

28. Doblhoff-Dier V, Schmetterer L, Vilser W, Garhöfer G, Gröschl M, Leitgeb RA, et al. Measurement of the total retinal blood flow using dual beam fourier-domain doppler optical coherence tomography with orthogonal detection planes. *Biomed Opt Express.* (2014) 5:630–42. doi: 10.1364/boe.5.000630

29. Szegedi S, Hommer N, Kallab M, Puchner S, Schmidl D, Werkmeister RM, et al. Repeatability and reproducibility of total retinal blood flow measurements using bi-directional doppler Oct. *Transl Vis Sci Technol.* (2020) 9:34. doi: 10.1167/tvst.9.7.34

30. McCraty R, Shaffer F. . Heart rate variability: new perspectives on physiological mechanisms, assessment of self-regulatory capacity, and health risk. *Glob Adv Health Med.* (2015) 4:46–61. doi: 10.7453/gahmj.2014.073

31. Horsten M, Ericson M, Perski A, Wamala SP, Schenck-Gustafsson K, Orth-Gomér K. Psychosocial factors and heart rate variability in healthy women. *Psychosom Med.* (1999) 61:49–57. doi: 10.1097/00006842-199901000-00009

32. Hjortskov N, Rissén D, Blangsted AK, Fallentin N, Lundberg U, Søgaard K. The effect of mental stress on heart rate variability and blood pressure during computer work. *Eur J Appl Physiol.* (2004) 92:84–9. doi: 10.1007/s00421-004-1055-z

33. Wilkinson CP, Ferris FL III, Klein RE, Lee PP, Agardh CD, Davis M, et al. Proposed international clinical diabetic retinopathy and diabetic macular edema disease severity scales. *Ophthalmology.* (2003) 110:1677–82. doi: 10.1016/s0161-6420(03)00475-5

34. Blum M, Bachmann K, Wintzer D, Riemer T, Vilser W, Strobel J. Noninvasive measurement of the bayliss effect in retinal autoregulation. *Graefes Arch Clin Exp Ophthalmol.* (1999) 237:296–300. doi: 10.1007/s004170050236

35. Garhofer G, Bek T, Boehm AG, Gherghel D, Grunwald J, Jeppesen P, et al. Use of the retinal vessel analyzer in ocular blood flow research. *Acta Ophthalmol.* (2010) 88:717–22. doi: 10.1111/j.1755-3768.2009.01587.x

36. Werkmeister RM, Dragostinoff N, Palkovits S, Told R, Boltz A, Leitgeb RA, et al. Measurement of absolute blood flow velocity and blood flow in the human retina by dual-beam bidirectional doppler fourier-domain optical coherence tomography. *Invest Ophthalmol Vis Sci.* (2012) 53:6062–71. doi: 10.1167/iovs.12-9514

37. Werkmeister RM, Palkovits S, Told R, Groschl M, Leitgeb RA, Garhofer G, et al. Response of retinal blood flow to systemic hyperoxia as measured with dual-beam bidirectional doppler fourier-domain optical coherence tomography. *PLoS One* (2012) 7:e45876. doi: 10.1371/journal.pone.0045876

38. Werkmeister RM, Schmidl D, Aschinger G, Doblhoff-Dier V, Palkovits S, Wirth M, et al. Retinal oxygen extraction in humans. *Sci Rep.* (2015) 5:15763. doi: 10.1038/srep15763

39. Ewing DJ, Martyn CN, Young RJ, Clarke BF. The value of cardiovascular autonomic function tests: 10 years experience in diabetes. *Diabetes Care.* (1985) 8:491–8. doi: 10.2337/diacare.8.5.491

40. Howorka K, Pumprla J, Schabmann A. Optimal parameters of short-term heart rate spectrogram for routine evaluation of diabetic cardiovascular autonomic neuropathy. *J Auton Nerv Syst.* (1998) 69:164–72. doi: 10.1016/s0165-1838(98)00015-0

41. Pumprla J, Howorka K, Groves D, Chester M, Nolan J. Functional assessment of heart rate variability: physiological basis and practical applications. *Int J Cardiol.* (2002) 84:1–14.

42. Howorka K, Pumprla J, Jirkovska A, Lacigova S, Nolan J. Modified orthostatic load for spectral analysis of short-term heart rate variability improves the sensitivity of autonomic dysfunction assessment. *J Diabetes Complications.* (2010) 24:48–54. doi: 10.1016/j.jdiacomp.2008.10.003

43. Bellavere F, Balzani I, De Masi G, Carraro M, Carenza P, Cobelli C, et al. Power spectral analysis of heart-rate variations improves assessment of diabetic cardiac autonomic neuropathy. *Diabetes.* (1992) 41:633–40. doi: 10.2337/diab.41.5.633

44. Hu B, Yan LF, Sun Q, Yu Y, Zhang J, Dai YJ, et al. Disturbed neurovascular coupling in type 2 diabetes mellitus patients: evidence from a comprehensive fmri analysis. *Neuroimage Clin.* (2019) 22:101802. doi: 10.1016/j.nicl.2019.101802

45. Duarte JV, Pereira JM, Quendera B, Raimundo M, Moreno C, Gomes L, et al. Early disrupted neurovascular coupling and changed event level hemodynamic response function in type 2 diabetes: an fmri study. *J Cereb Blood Flow Metab* (2015) 35:1671–80. doi: 10.1038/jcbfm.2015.106

46. Mandecka A, Dawczynski J, Blum M, Müller N, Kloos C, Wolf G, et al. Influence of flickering light on the retinal vessels in diabetic patients. *Diabetes Care* (2007) 30:3048–52. doi: 10.2337/dc07-0927

47. Pemp B, Weigert G, Karl K, Petzl U, Wolzt M, Schmetterer L, et al. Correlation of flicker-induced and flow-mediated vasodilatation in patients with endothelial dysfunction and healthy volunteers. *Diabetes Care.* (2009) 32:1536–41. doi: 10.2337/dc08-2130

48. Bek T, Hajari J, Jeppesen P. Interaction between flicker-induced vasodilatation and pressure autoregulation in early retinopathy of type 2 diabetes. *Graefes Arch Clin Exp Ophthalmol.* (2008) 246:763–9. doi: 10.1007/s00417-008-0766-y

49. McVeigh GE, Brennan GM, Johnston GD, McDermott BJ, McGrath LT, Henry WR, et al. Impaired endothelium-dependent and independent vasodilation in patients with type 2 (non-insulin-dependent) diabetes mellitus. *Diabetologia.* (1992) 35:771–6. doi: 10.1007/bf00429099

50. Garhöfer G, Resch H, Sacu S, Weigert G, Schmidl D, Lasta M, et al. Effect of regular smoking on flicker induced retinal vasodilatation in healthy subjects. *Microvasc Res.* (2011) 82:351–5. doi: 10.1016/j.mvr.2011.07.001

51. Pemp B, Garhofer G, Weigert G, Karl K, Resch H, Wolzt M, et al. Reduced retinal vessel response to flicker stimulation but not to exogenous nitric oxide in type 1 diabetes. *Invest Ophthalmol Vis Sci.* (2009) 50:4029–32. doi: 10.1167/iovs.08-3260

52. Sachdeva MM. Retinal neurodegeneration in diabetes: an emerging concept in diabetic retinopathy. *Curr Diab Rep.* (2021) 21:65. doi: 10.1007/s11892-021-01428-x

53. Carpineto P, Toto L, Aloia R, Ciciarelli V, Borrelli E, Vitacolonna E, et al. Neuroretinal alterations in the early stages of diabetic retinopathy in patients with type 2 diabetes mellitus. *Eye.* (2016) 30:673–9. doi: 10.1038/eye.2016.13

54. van Dijk HW, Verbraak FD, Kok PH, Garvin MK, Sonka M, Lee K, et al. Decreased retinal ganglion cell layer thickness in patients with type 1 diabetes. *Invest Ophthalmol Vis Sci.* (2010) 51:3660–5. doi: 10.1167/iovs.09-5041

55. Garcia-Martin E, Cipres M, Melchor I, Gil-Arribas L, Vilades E, Polo V, et al. Neurodegeneration in patients with type 2 diabetes mellitus without diabetic retinopathy. *J Ophthalmol.* (2019) 2019:1825819. doi: 10.1155/2019/1825819

56. Chatziralli I, Karamaounas A, Dimitriou E, Kazantzis D, Theodossiadis G, Kozobolis V, et al. Peripapillary retinal nerve fiber layer changes in patients with diabetes mellitus: a case-control study. *Semin Ophthalmol.* (2020) 35:257–60. doi: 10.1080/08820538.2020.1810289

57. Souza HCD, Philbois SV, Veiga AC, Aguilar BA. Heart rate variability and cardiovascular fitness: what we know so far. *Vasc Health Risk Manag.* (2021) 17:701–11. doi: 10.2147/vhrm.S279322

58. Scott-Solomon E, Boehm E, Kuruvilla R. The sympathetic nervous system in development and disease. *Nat Rev Neurosci.* (2021) 22:685–702. doi: 10.1038/s41583-021-00523-y

59. Nørgaard CH, Starkopf L, Gerds TA, Malmborg M, Bonde AN, Zareini B, et al. Temporal changes in risk of cardiovascular events in people with newly diagnosed type 2 diabetes with and without cardiovascular disease. *J Diabetes Complications* (2022) 36:108126. doi: 10.1016/j.jdiacomp.2022.108126

60. Sattar N, Rawshani A, Franzén S, Rawshani A, Svensson AM, Rosengren A, et al. Age at diagnosis of type 2 diabetes mellitus and associations with cardiovascular and mortality risks. *Circulation.* (2019) 139:2228–37. doi: 10.1161/circulationaha.118.037885

61. Harris KF, Matthews KA. Interactions between autonomic nervous system activity and endothelial function: a model for the development of cardiovascular disease. *Psychosom Med.* (2004) 66:153–64. doi: 10.1097/01.psy.0000116719.95524.e2

62. Nagaoka T, Sato E, Takahashi A, Yokota H, Sogawa K, Yoshida A. Impaired retinal circulation in patients with type 2 diabetes mellitus: retinal laser doppler velocimetry study. *Invest Ophthalmol Vis Sci.* (2010) 51:6729–34. doi: 10.1167/iovs.10-5364

63. Dimitrova G, Chihara E, Takahashi H, Amano H, Okazaki K. Quantitative retinal optical coherence tomography angiography in patients with diabetes without diabetic retinopathy. *Invest Ophthalmol Vis Sci.* (2017) 58:190–6. doi: 10.1167/iovs.16-20531

64. Hommer, N, Kallab M, Schlatter A, Howorka K, Werkmeister RM, Schmidl D, et al. Retinal oxygen metabolism in patients with type ii diabetes and different stages of diabetic retinopathy. *Diabetes.* (2022) db220219. doi: 10.2337/db22-0219 [Epub ahead of print].

frontiers | Frontiers in Physiology

TYPE Systematic Review
PUBLISHED 14 December 2022
DOI 10.3389/fphys.2022.995353

OPEN ACCESS

EDITED BY
Leopold Schmetterer,
Medical University of Vienna, Austria

REVIEWED BY
Mehmet Cem Sabaner,
Kutahya Evliya Celebi Training and Research Hospital, Turkey
Jacqueline Chua,
Singapore Eye Research Institute (SERI), Singapore

*CORRESPONDENCE
Tiecheng Liu,
ltc301@sina.com

SPECIALTY SECTION
This article was submitted to Vascular Physiology, a section of the journal Frontiers in Physiology

RECEIVED 15 July 2022
ACCEPTED 24 November 2022
PUBLISHED 14 December 2022

CITATION
Chen X, Li W, Jin X, Zhang Y, Li R and Liu T (2022), Macular microcirculation changes after repair of rhegmatogenous retinal detachment assessed with optical coherence tomography angiography: A systematic review and meta-analysis.
Front. Physiol. 13:995353.
doi: 10.3389/fphys.2022.995353

Macular microcirculation changes after repair of rhegmatogenous retinal detachment assessed with optical coherence tomography angiography: A systematic review and meta-analysis

Xiaofei Chen, Wanyue Li, Xin Jin, Ying Zhang, Runpu Li and Tiecheng Liu*

Senior Department of Ophthalmology, The Third Medical Center of Chinese PLA General Hospital, Beijing, China

Purpose: The aim of the study was to investigate microcirculation changes in the macula evaluated by optical coherence tomography angiography (OCTA)in patients receiving anatomical repair after surgery for rhegmatogenous retinal detachment (RRD).

Methods: A literature search was conducted in PubMed, EMBASE, Web of Science and the Cochrane Library. Studies including patients with macula-on or macula-off RRD and repaired successfully through primary surgery were selected. Foveal avascular zone (FAZ) area and macular vascular density (VD) in both the superficial capillary plexus (SCP) and deep capillary plexus (DCP) were analyzed using RevMan 5.4 software.

Results: Twelve studies including 430 RRD eyes and 430 control eyes were selected. In eyes with macula-on RRD, FAZ area, VD in the foveal SCP and DCP, and VD in the parafoveal SCP and DCP were not altered compared with control eyes, after the retina was reattached. In eyes with macula-off RRD that was repaired successfully through surgery, FAZ area in the DCP (0.13 mm^2, 95% CI: 0.02 to 0.25, p = 0.02) remained enlarged compared with control eyes. Meanwhile, VD in the foveal DCP was also significantly reduced (–3.12%, 95% CI: –6.15 to –0.09%, p = 0.04), even though retinal reattachment was achieved by surgery in eyes with macula-off RRD.

Conclusion: In patients with macula-off rhegmatogenous retinal detachment, foveal avascular zone area in the deep capillary plexuses was enlarged and vascular density in the foveal deep capillary plexus was reduced, even after the retina was successfully reattached through a primary surgery.

KEYWORDS

rhegmatogenous retinal detachment, macular microcirculation, foveal avascular zone, optical coherence tomography angiography, meta analysis

Introduction

Rhegmatogenous retinal detachment is a vision-threatening disease that affects visual activity in people of working age. Although it has been reported that the retina is reattached successfully after surgery in approximately 90% of patients (Shlomit et al., 2011), the recovery of visual function is limited, especially in patients with macula-off retinal detachment. The limitation of visual recovery has been demonstrated to be related with microstructural changes of the retina in macular region, such as the disruption of ellipsoid zone and reduction of photoreceptor outer segment length (Schocket et al., 2006; Shimoda et al., 2010; Park et al., 2018).

In recent years, optical coherence tomography angiography (OCTA) has been utilized to investigate detailed changes in microcirculation in the macular area and peripapillary area in various diseases, such as diabetic retinopathy, macular degeneration and glaucoma (Kuehlewein et al., 2015; Yarmohammadi et al., 2016; Greig et al., 2020; Zhang et al., 2020). In patients with diabetic retinopathy, an increased foveal avascular zone (FAZ) area, intraretinal microvascular abnormalities, and a decrease in vascular density (VD) in macular and peripapillary areas, as detected *via* OCTA, have been found correlated with progression of diabetic retinopathy and diabetic macular edema (Sun et al., 2019; Greig et al., 2020).

In patients with macula-off rhegmatogenous retinal detachment, FAZ area and VD in the macular area evaluated by OCTA have also been investigated. Several studies have reported that FAZ area and VD in the macular area remain different from those of healthy fellow eyes after the retina was successfully reattached through surgery (Woo et al., 2018; Agarwal et al., 2019; Tsen et al., 2019). Enlarged FAZ and decreased VD have also been showed to be associated with postoperative visual activity in eyes with successful anatomical repair (Woo et al., 2018; McKay et al., 2020; Ng et al., 2020). However, in other studies, VD in the macular area of eyes receiving surgery for retinal detachment has not changed significantly (Wang et al., 2019).

This study was to investigate and meta-analyze macular microcirculation changes assessed with OCTA after successful repair for rhegmatogenous retinal detachment with or without macular involvement.

Materials and methods

This meta-analysis was conducted in accordance with the guidelines presented by the Meta-Analysis of Observational Studies statements (Stroup et al., 2000).

Search strategy

The databases PubMed, EMBASE, Web of Science and the Cochrane Library were searched using the terms "retinal detachment" and "Optical Coherence Tomography Angiography", "OCT Angiography" or "OCTA" up to 07 July 2022. The detailed search query for PubMed was showed in Supplementary Table S1. Language was restricted to English.

Study selection

Studies included should meet all of the following inclusion criteria: 1) the affected eyes had primary rhegmatogenous retinal detachment; 2) the contralateral healthy eyes or eyes of healthy people were used as controls; 3) the retina was successfully reattached after single surgery; and 4) optical coherence tomography angiography was applied to evaluate macular microcirculation. Exclusion criteria were as follows: 1) the affected eyes had any preexisting macular impairing disease, such as diabetic retinopathy, retinal vein occlusion, macular degeneration, uveitis and high myopia (axial length>26 mm); 2) the affected eyes had previous retinal surgery; 3) retinal detachment was complicated by macular hole, epi-macular membrane, submacular membrane/subfoveal fibrous band, macular scar or choroidal detachment; 4) retina was reattached after two or more surgeries; 5) internal limiting membrane was peeled in the surgery; 6) eyes with silicone oil tamponade were included and data of eyes with gas or air tamponade could not be extracted for analysis; 7) the affected eyes had any of postoperative complications including epi-macular membrane, macular edema, macular cyst and submacular fluid; 8) normal control eyes were not included; 9) children were included. The search results were reviewed by two investigators.

Data extraction

Data from each selected study were extracted by two investigators, including first author, year of publication, location, study design, number and mean age of patients, gender, time between initial symptoms and surgery, type of surgery, time of OCTA measurement, type of OCTA device, FAZ area, VD in the foveal area, and VD in the parafoveal area. If OCTA measurements were taken at different times after surgery, data containing sufficient information at the last time of follow up were collected. FAZ area was defined as the area inside the central border of the capillary network. VD was defined as the

TABLE 1 The characteristics of included studies.

Study	Location	Design	RRD eyes	Control eyes	Age (years)	Gender (F/M)	Status of macula		Duration between symptoms and surgery		Surgery		Time of OCTA	Device	Quality
							On	Off	On	Off	SB	PPV(T)			
Agarwal 2018	India	prospective	19	19*	40.21 ± 16.81	4/15	0	19	N	52.8 ± 85.2d	8	11 (C3F8)	3 m	Optovue	6
Woo 2018	Korea	retrospective	34	34	55.4 ± 11.1	14/20	15	19	NA	3.21 ± 2.25d	0	34 (C3F8)	<2 m	Topcon	7
Bonfiglio 2019	Italy	retrospective	93	93	62 ± 8	41/52	56	37	2.2 ± 1.1d	3.6 ± 1.3d	0	93 (SF6)	17.2 ± 5.6 m	Optovue	7
Wang 2019	China	retrospective	14	14	56.0 (42–73)	6/8	0	14	N	4.21 (3–7) d	0	14 (Air)	12 w	Optovue	7
Barca 2020	Italy	prospective	33	33	60.26 ± 11.52	13/20	15	18	1.48 ± 0.67 d		15	18 (Air)	6 m	Optovue	8
Hong 2020	Korea	retrospective	31	31	53.3 ± 14.4	8/23	11	20	6.4 ± 5.5d	7.7 ± 6.5d	0	31 (C3F8)	6 m	Topcon	8
McKay 2020	United States	retrospective	17	17	57 ± 11	6/11	0	17	N	3 ± 2d	0	17 (Gas)	4 ± 4 m	Optovue	7
Ng 2020	Netherlands	prospective	47	47	60 ± 9	11/36	0	47	N	5 (3–7)d	4	43 (C3F8 or SF6)	12 m	Heidelberg	7
Christou 2021	Greece	retrospective	23	23	62.7 ± 8.18	5/18	0	23	N	11.3 ± 8.4d	0	23 (C2F6)	12 w	Zeiss	8
Liu 2021	China	retrospective	16	16	55.5 ± 9.68	12/4	16	0	18.2 ± 15.9d	N	0	16 (C3F8)	36.3 ± 3.7 m	Optovue	8
Chatziralli 2022	Greece	prospective	89	89	67.9 ± 5.7	36/53	0	89	N	≤15d	0	89 (C3F8 or SF6)	5 w	Optovue	8
D'Aloisio 2022	Italy	prospective	14	14	52.6 ± 15.2	6/8	14	0	<24 h	N	0	14 (C3F8 or SF6)	3 m	Canon	8

*Eyes of healthy subjects were used as control in this study while the fellow eyes used as control in other studies. RRD, rhegmatogenous retinal detachment; SB, scleral buckling; PPV, pars plana vitrectomy, m, months, d, days, h, hours, NA, not available N none.

10.3389/fphys.2022.995353

percentage of area occupied by vessels in a defined region. FAZ area and VD both in the superficial capillary plexus (SCP) and in the deep capillary plexus (DCP) were extracted. In studies in which the layer for measurement was not mentioned, the data were analyzed as in the SCP group in our study. Discrepancies were addressed through discussion.

Quality assessment

Method quality of the selected studies was evaluated according to the Newcastle-Ottawa Scale (NOS) (Stang, 2010). Scores ranging from 1 to 9 were applied to assess the selection criteria of subjects, comparability between controls and cases, and measurement values of each study. This procedure was completed by two reviewers and disagreements were discussed to achieve consensus. Publication bias was evaluated by Egger's test and Begg's test.

Statistical analysis

Data analysis was performed with Cochrane Collaboration's Review Manager Software (RevMan 5.4, Cochrane Collaboration, Oxford, United Kingdom). Means and standard deviations of the area of foveal avascular zone and vessel density were calculated as continuous variables to obtain the weighted mean difference. Heterogeneity among the selected studies was tested by Chi-square test and Higgins I^2 test. If the heterogeneity was not significant ($p > 0.10$, $I^2<50\%$), the fixed-effect analysis model was used. Otherwise, the random-effect model was applied. A p value < 0.05 was considered significant for all data analysis.

Results

Characteristics and quality assessments

Twelve studies including 430 RRD eyes and 430 control eyes were selected in this study (Agarwal et al., 2019; Woo et al., 2018; McKay et al., 2020; Ng et al., 2020; Wang et al., 2019; Hong et al., 2020; Bonfiglio et al., 2020; Barca et al., 2020; Christou et al., 2021; Liu et al., 2021; D'Aloisio et al., 2022; Chatziralli et al., 2022), as indicated in Table 1. The search strategy for Pubmed is showed in Supplementary Table S1. The selection process is showed in Figure 1. As showed in Table 1, two studies selected macular-on RRD, six studies collected macula-off RRD, and the remaining four studies included both macula-on and macula-off RRD. In the study by D'Aloisio et al., part of the macula was detached before surgery in 6 RRD patients who received treatment within 24 h of onset (D'Aloisio et al., 2022). This group of eyes was considered as macular-on RRD for analysis in our study. Data were collected and analyzed separately in macula-on retinal detachment and macula-off retinal detachment. Patients with RRD received pars plana vitrectomy (PPV) with gas or air tamponade or scleral buckling (SB) in selected studies. One study was exclude since patients with RRD were treated with pneumatic retinopexy (Kaderli et al., 2021). Since silicone oil tamponade has been reported to be related to changes of macular microcirculation (Ma et al., 2020; Lee and Park, 2021), eyes with silicone oil tamponade were exclude in this study. The duration between symptoms and surgery was less than 14 days in most studies. However, in one study (Agarwal et al., 2019), the duration time was 1.76 ± 2.84 months (10 days–6 months), which was converted to the day unit in Table 1. The time that from surgery to OCTA measurement was at least 1 month in all studies, as showed in Table 1. As indicated in the selected studies, the foveal area was defined as a central circular region within a diameter of 1–1.5 mm, and the parafoveal area was defined as a circular annulus region between 1 and 2.5–3 mm in diameter. VD in the foveal area and the parafoveal area were analyzed separately. In the study of McKay et al. (McKay et al., 2020), VD was evaluated in a central area of 3 × 3 mm, which was not included for analysis in our study. The NOS score of each selected study is also showed in Table 1, and detailed information is showed in Supplementary Table S2.

Foveal avascular zone area

Seven studies were included for analyzing FAZ area of macula-on RRD. As showed in Figure 2, FAZ area in the SCP and in the DCP of macula-on RRD was not different from that of control eyes after surgery (−0.01 mm^2, 95% CI: −0.03 to 0.01, p = 0.40; 0.03 mm^2, 95% CI: −0.04 to 0.09, p = 0.43). Nine studies collecting 289 eyes with RRD and 304 control eyes were selected for analyzing FAZ area in the SCP of macula-off RRD. FAZ area in the SCP was not changed after treatment (0.05 mm^2, 95% CI: −0.01 to 0.10, p = 0.08). To calculate FAZ area in the DCP of macula-off RRD, five studies including 191 eyes in the RRD group and 206 eyes in the control group were collected. As indicated in Figure 3, FAZ area in the DCP was significantly increased even after the retina was reattached successfully through surgery in macula-off RRD eyes compared with that of control eyes (0.13 mm^2, 95% CI: 0.02 to 0.25, p = 0.02).

Vascular density in the foveal area

In macula-on RRD, VD in the SCP and in the DCP of the foveal area was not changed compared with that of control eyes after surgery (1.04%, 95% CI: −0.80%–2.89%, p = 0.27; −0.30%, 95% CI: −1.67%–2.26%, p = 0.77, Figure 4). A total of 183 eyes with RRD and 183 control eyes in five studies were analyzed for

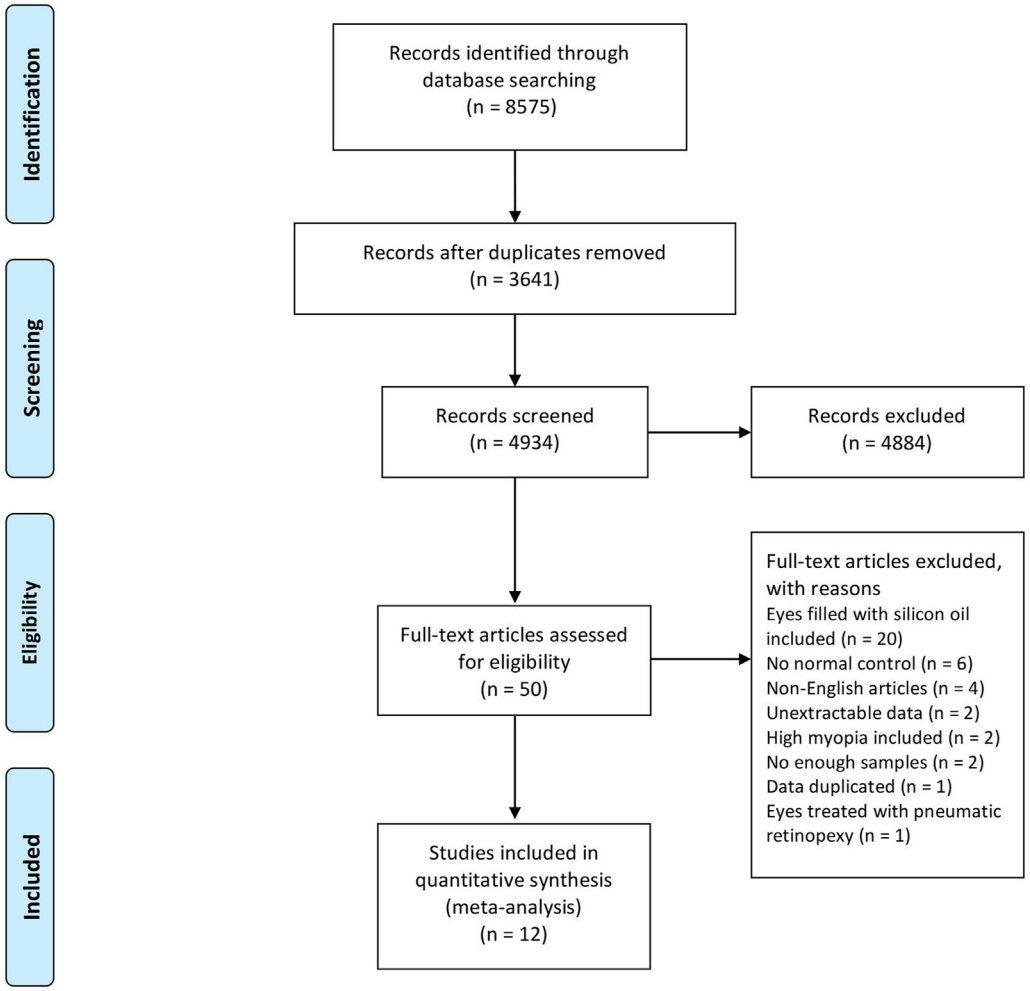

FIGURE 1
Flow chart of studies selection.

VD changes in the foveal area of macula-off RRD. As demonstrated in Figure 5, no change in VD in the SCP was observed when compared with that of controls (−0.95%, 95% CI: −4.56 to 2.67%, $p = 0.61$). However, VD in the DCP of the foveal area was significantly reduced in macula-off RRD (−3.12%, 95% CI: −6.15% to −0.09%, $p = 0.04$), even though retinal detachment was repaired successfully after surgery.

Vascular density in the parafoveal area

VD in the parafoveal area was also analyzed in patients with RRD. No difference was detected in VD in the SCP or the DCP between eyes with macula-on RRD and control eyes (−0.76%, 95% CI: −1.84 to 0.31%, $p = 0.16$; −1.01%, 95% CI: −2.51 to −0.48%, $p = 0.18$, Figure 6). In patients with macula-off RRD, 225 eyes in the RRD group and 225 eyes in the control group from six studies were summarized for calculation. As showed in Figure 7 VD in the SCP and the DCP was not changed after retina was reattached (−2.00%, 95% CI: −5.99 to 2.00%, $p = 0.33$; −2.54%, 95% CI: −6.58% to 1.49%, $p = 0.22$).

Vascular density of the choriocapillaris

VD of the choriocapillaris was evaluated in four studies. Three studies were selected for meta-analysis, because VD of the choriocapillaris was measured in an area of 8 mm × 8 mm while the measurement was performed within an area of 3 mm × 3 mm in other studies. VD of the choriocpillaris in eyes with macula-off RRD was analyzed. As showed in Figure 8, VD of the choriocpillaris was not altered after retinal reattachment (−0.73%, 95% CI: −1.64% to 0.17%, $p = 0.11$).

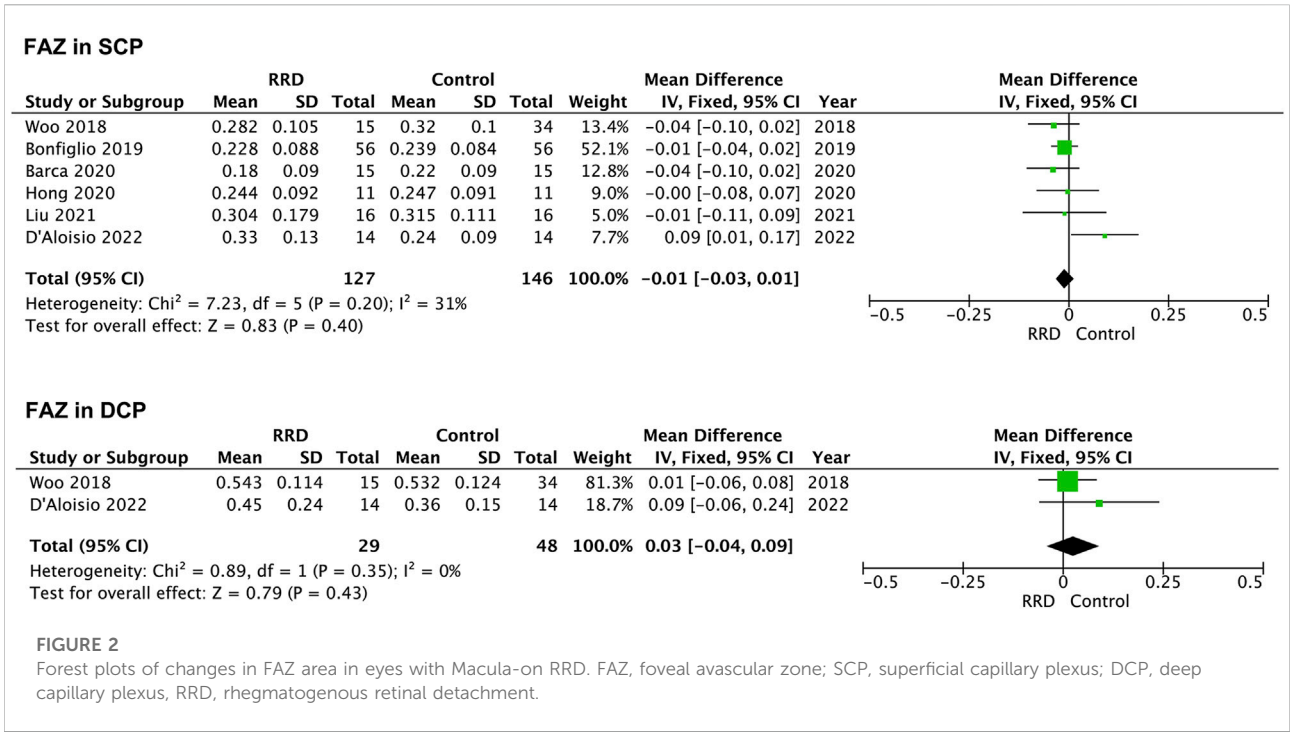

FIGURE 2
Forest plots of changes in FAZ area in eyes with Macula-on RRD. FAZ, foveal avascular zone; SCP, superficial capillary plexus; DCP, deep capillary plexus, RRD, rhegmatogenous retinal detachment.

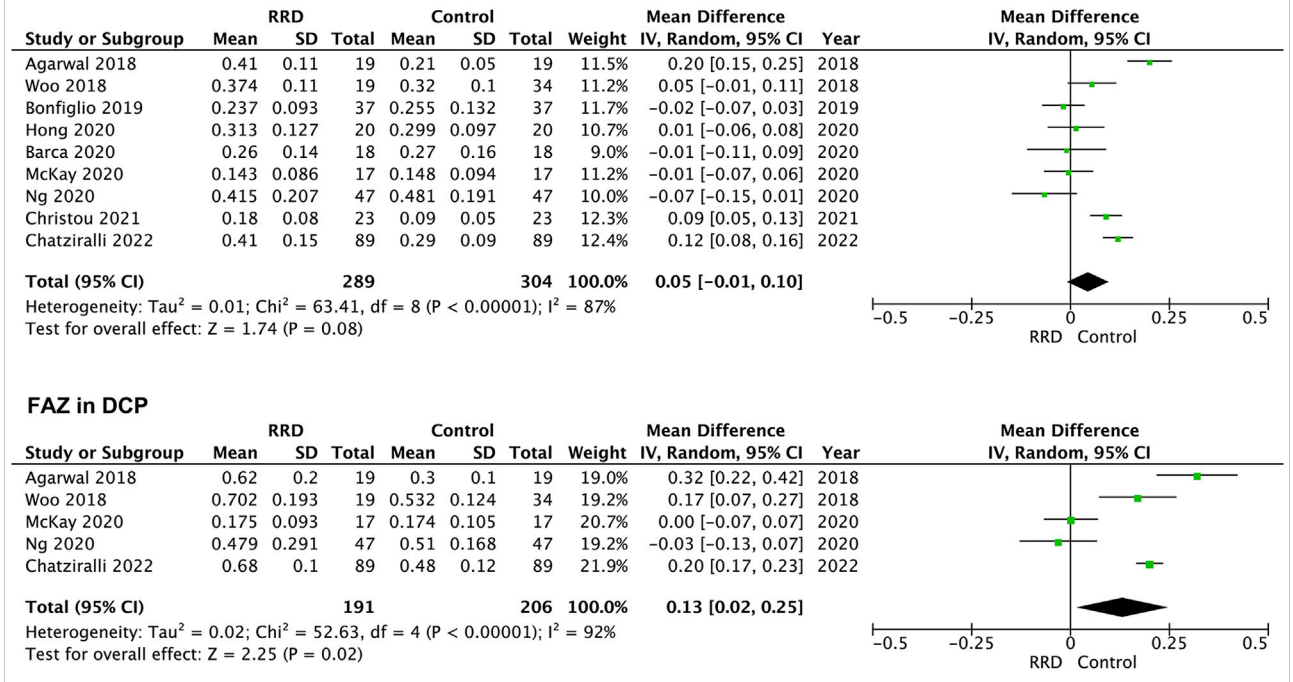

FIGURE 3
Forest plots of changes in FAZ area in eyes with Macula-off RRD. FAZ, foveal avascular zone; SCP, superficial capillary plexus; DCP, deep capillary plexus, RRD, rhegmatogenous retinal detachment.

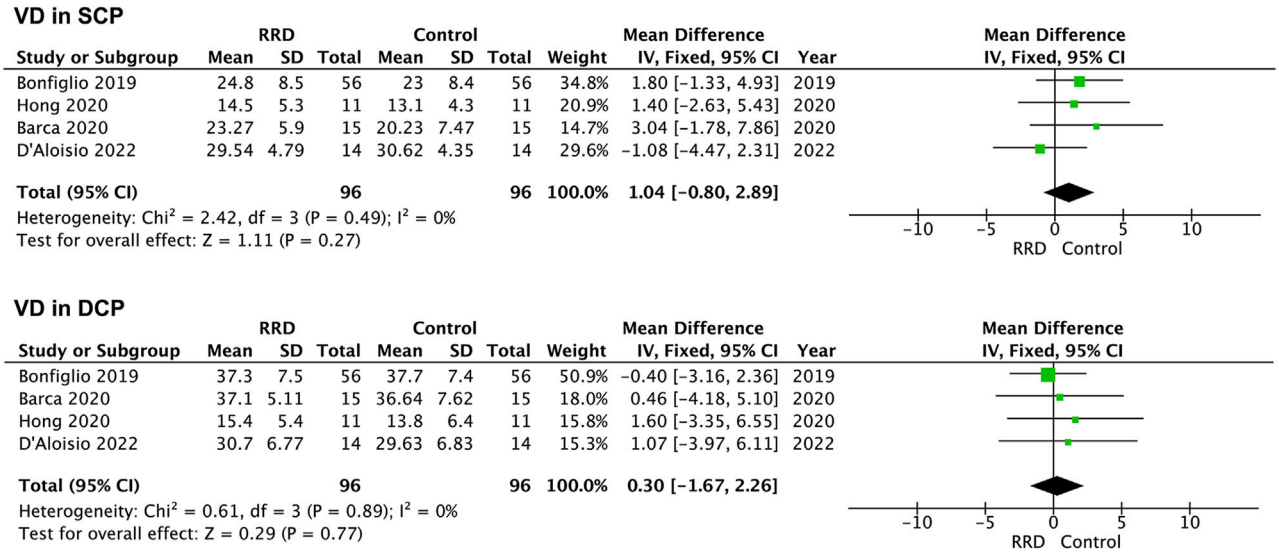

FIGURE 4
Forest plots of changes in foveal VD in eyes with Macula-on RRD. VD, vascular density, SCP, superficial capillary plexus; DCP, deep capillary plexus, RRD, rhegmatogenous retinal detachment.

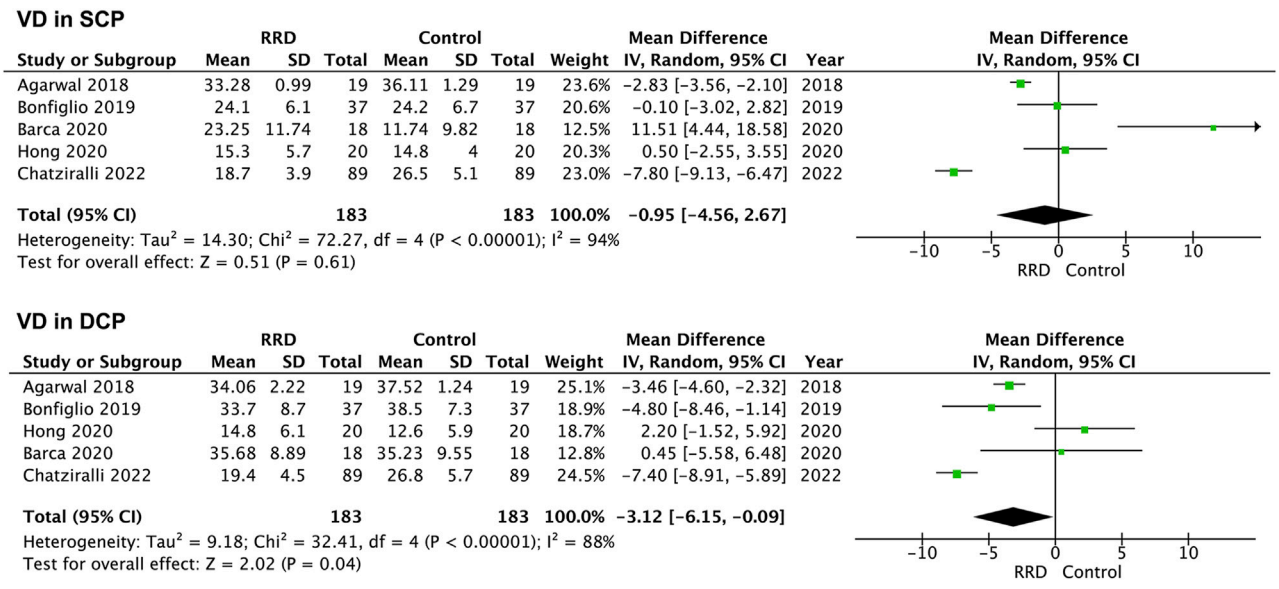

FIGURE 5
Forest plots of changes in foveal VD in eyes with Macula-off RRD. VD, vascular density, SCP, superficial capillary plexus; DCP, deep capillary plexus, RRD, rhegmatogenous retinal detachment.

Publication bias

Publication bias was assessed by Egger's test and Begg's test. No publication bias was revealed in FAZ area, VD in the foveal and the parafoveal areas of eyes with macular-off RRD. However, publication bias was found in VD in the DCP of the foveal area in eyes with macular-on RRD by Egger's test ($p = 0.04$) but not by Begg's test. No significant publication bias was observed in other measurements in eyes with macular-on RRD. Funnel plots of studies are showed in Supplementary Figure S1.

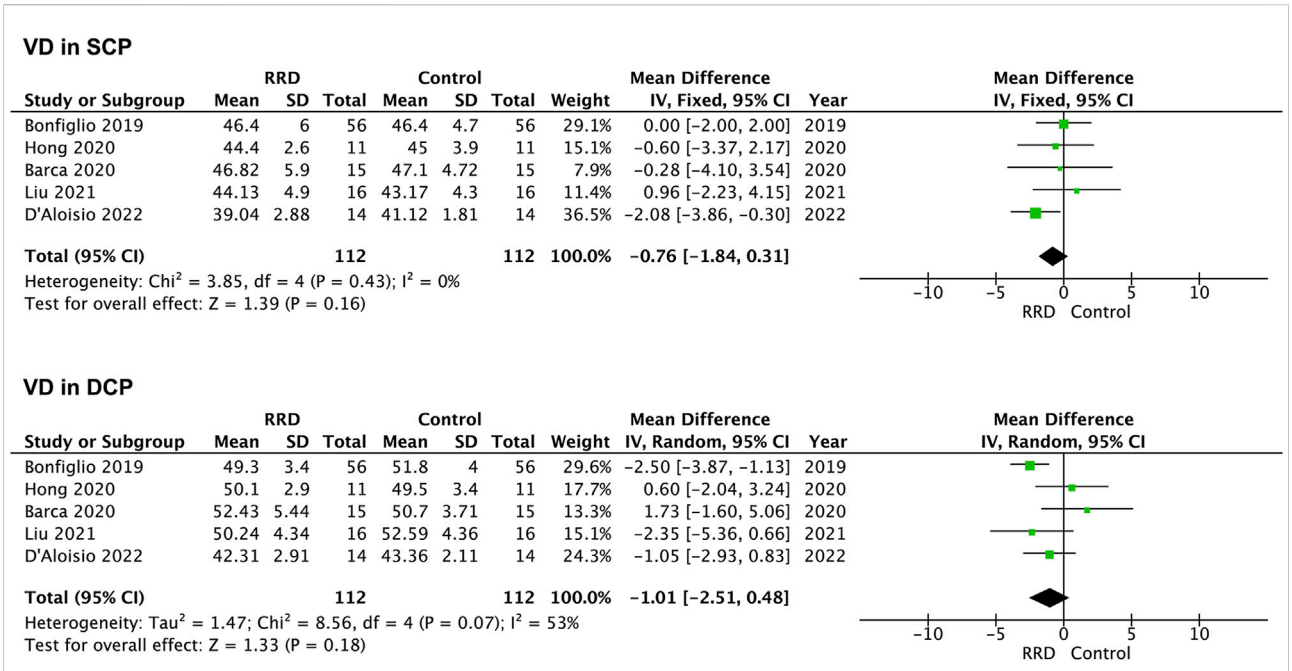

FIGURE 6
Forest plots of changes in parafoveal VD in eyes with Macula-on RRD. VD, vascular density, SCP, superficial capillary plexus; DCP, deep capillary plexus, RRD, rhegmatogenous retinal detachment.

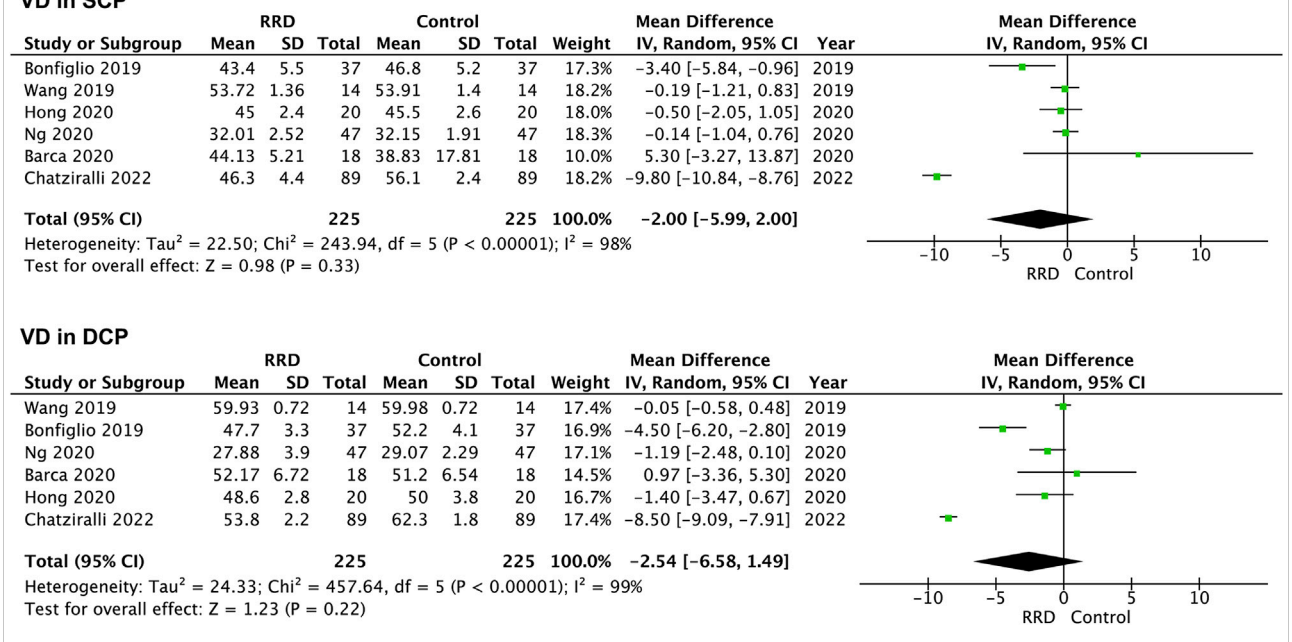

FIGURE 7
Forest plots of changes in parafoveal VD in eyes with Macula-off RRD. VD, vascular density, SCP, superficial capillary plexus; DCP, deep capillary plexus, RRD, rhegmatogenous retinal detachment.

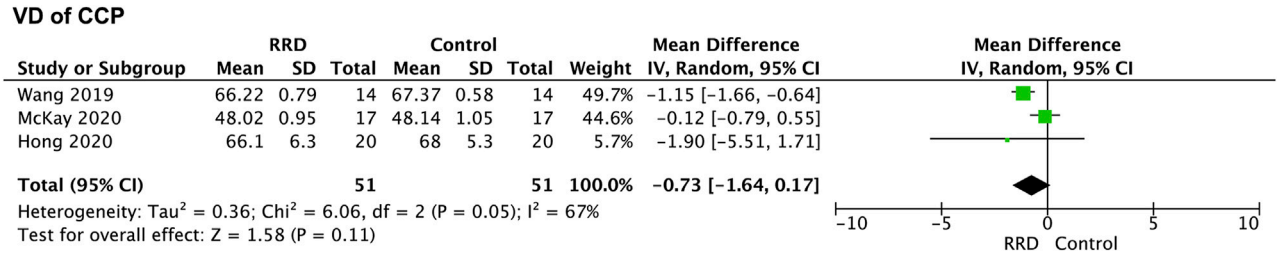

FIGURE 8
Forest plots of changes in VD of the choriocpillaris in eyes with macula-off RRD. VD, vascular density; RRD, rhegmatogenous retinal detachment.

Discussion

This study indicated that FAZ area in the DCP of eyes with macula-off RRD remained enlarged when the retina was reattached successfully after a single surgery, as compared with control eyes. Meanwhile, VD in the DCP of the foveal area in eyes with macula-off RRD also remained diminished after anatomical repair.

It has been reported that blood flow in the macular area was not different between eyes that received SB and those that received PPV and gas tamponade for retinal detachment (Sato et al., 2007). Other studies indicated that macular microcirculation was changed after silicone oil tamponade, including narrowing of arterioles and reduced blood flow (Agnieszka et al., 2011; Roohipoor et al., 2020). Accordingly, patients who received SB or PPV with gas tamponade, but not silicone oil tamponade, were selected in this study.

It has been found that capillaries in the DCP are more vulnerable to retinal and systemic diseases, such as retinal vein occlusion, diabetic macular edema, hypertension and systemic lupus erythematosus (Adhi et al., 2016; Lee et al., 2016; Chua et al., 2019; Arfeen et al., 2020). The mechanism is not clear. In the SCP of normal eyes, capillaries were located between arterioles and venules, forming an interconnected plexus. In the DCP, capillaries were arranged as polygonal units and were speculated to drain into the superficial venules (Bonnin et al., 2015). Moreover, as a single monolayer of the capillary plexus, VD in the DCP has been found to be lower than that in SCP (Lavia et al., 2019). The difference in structural pattern may be associated with unbalanced vulnerability to ischemia between the SCP and the DCP.

Decreased visual activity has been reported to be related to capillary loss in the DCP in type 1 diabetes without macular edema (Dupas et al., 2018). Furthermore, nonperfusion in the DCP has been proved to be correlated with photoreceptor disruption, which suggests that blood flow in the DCP is critical to the survival and function of photoreceptors (Scarinci et al., 2016).

In patients with macula-off retinal detachment, Woo et al. have reported that FAZ area in the SCP and the DCP are negatively associated with postoperative best-corrected visual acuity (BCVA) (Woo et al., 2018). In the study by Bonfiglio et al., BCVA has been proved to be related not only to FAZ area but also to VD in the foveal SCP and the parafoveal DCP (Bonfiglio et al., 2020). In McKay's investigation, VD in the DCP, but not VD in the SCP and FAZ area, was found to be changed and correlated with BCVA (McKay et al., 2020). Ng et al. observed that a smaller FAZ area in the DCP was associated with better postoperative BCVA (Ng et al., 2020).

The pathogenetic mechanism is not clear. Deep capillaries are located in the inner nuclear layer. The avascular outer retinal layers are supplied by diffusion of oxygen and nourishment from the choriocapillaris (Tasman and Jaeger, 1991). However, it has also been found that 10%–15% of oxygen supplied to photoreceptors comes from retinal circulation (Birol et al., 2007), which indicates capillaries in the DCP may play an important role. In addition, capillaries in the DCP have also been considered important to provide oxygen and nutrition to synapses formed between photoreceptors and bipolar cells (Provis, 2001; Masland, 2012), which are therefore important for visual signal transmission. Usui et al. have speculated that vasculature, glia and neurons within retinal neurovascular units are highly interdependent and that their interactions are vital to maintain normal metabolism. Loss of either or both retinal interneurons and vasculature may lead to photoreceptor dysfunction (Usui et al., 2015). Inflammatory cytokines, such as tumor necrosis factor α (TNF-α) and monocyte chemotactic protein-1 (MCP-1), may take part in the process (Nakazawa et al., 2006; Nakazawa et al., 2011).

Some limitations should be mentioned in this meta-analysis. First, the sample size of most selected studies was small. Second, the duration between symptoms and surgery, type of surgery, time and device of OCTA examination were different among the included studies, which contributed to the heterogeneity. The consistency of measurements among different OCTA devices has been investigated. It has been reported that FAZ area and VD in the SCP show good repeatability, while VD in the DCP dose not (Anegondi et al., 2018). In another study, FAZ area

measurements were consistent across different devices, while differences in VD measurements were observed (Lu et al., 2021). Subgroup analysis could be performed when more studies are collected. Third, variations in software, layer segmentation and area selection during OCTA measurement also added to the heterogeneity. The SCP and the DCP were segmented automatically in most studies. The SCP was located from 3 μm under the internal limiting membrane (ILM) to 15 μm under the inner plexiform layer (IPL), and the DCP extended from 15 to 70 μm below the IPL. In the study by Liu et al., however, SCP was located between the ILM and 10 μm above the IPL and the inner nuclear layer (IPL-INL) junction, while the DCP was located between 10 μm above the IPL-INL junction and 10 μm below the outer plexiform layer and outer nuclear layer junction. Finally, the correlation between visual activity and FAZ or VD were not analyzed because of insufficient data in the selected studies.

In conclusion, in eyes with macula-off rhegmatogenous retinal detachment, FAZ area in the DCP was enlarged and VD in foveal DCP was reduced as compared with normal control eyes, even after successful anatomical repair through primary surgery. Multicenter studies with larger sample sizes are needed to evaluate changes in macular microcirculation in rhegmatogenous retinal detachment and its association with vision recovery after surgery.

Data availability statement

The original contributions presented in the study are included in the article/Supplementary Material, further inquiries can be directed to the corresponding author.

Author contributions

TL and XC conceived and designed the study. XC and WL searched literature. RL and XC extracted data and performed data analysis. XJ and TL conducted the quality assessment. XC drafted the manuscript. TL and YZ reviewed and revised the manuscript. All authors have read and approved the final manuscript.

Conflict of interest

The authors declare that the research was conducted in the absence of any commercial or financial relationships that could be construed as a potential conflict of interest.

Publisher's note

Supplementary material

The Supplementary Material for this article can be found online at: https://www.frontiersin.org/articles/10.3389/fphys.2022.995353/full#supplementary-material

SUPPLEMENTARY FIGURE S1
Funnel plots of studies. **(A)** , FAZ area in SCP of eyes with Macula-on RRD; **(B)**, FAZ area in DCP of eyes with Macula-on RRD; **(C)**, FAZ area in SCP of eyes with Macula-off RRD; **(D)**, FAZ area in DCP of eyes with Macula-off RRD; **(E)**, Foveal VD in SCP of eyes with Macula-on RRD; **(F)**, Foveal VD in DCP of eyes with Macula-on RRD; **(G)**, Foveal VD in SCP of eyes with Macula-off RRD; **(H)**, Foveal VD in DCP of eyes with Macula-off RRD; **(I)**, Parafoveal VD in SCP of eyes with Macula-on RRD; **(J)**, Parafoveal VD in DCP of eyes with Macula-on RRD; **(K)**, Parafoveal VD in SCP of eyes with Macula-off RRD; **(L)**, Parafoveal VD in DCP of eyes with Macula-off RRD. FAZ, foveal avascular zone; SCP, superficial capillary plexus; DCP, deep capillary plexus, RRD, rhegmatogenous retinal detachment; VD, vascular density.

References

Adhi, M., Filho, M. A. B., Louzada, R. N., Kuehlewein, L., Carlo, T. E. D., Baumal, C. R., et al. (2016). Retinal capillary network and foveal avascular zone in eyes with vein occlusion and fellow eyes analyzed with optical coherence tomography angiography. *Invest. Ophthalmol. Vis. Sci.* 57, OCT486–94. doi:10.1167/iovs.15-18907

Agarwal, A., Aggarwal, K., Akella, M., Agrawal, R., Khandelwal, N., Bansal, R., et al. (2019). Fractal dimension and optical coherence tomography angiography features of the central macula after repair of rhegmatogenous retinal detachments. *Retina* 39 (11), 2167–2177. doi:10.1097/IAE.0000000000002276

Agnieszka, K-T., Joanna, K., and Bozena, R-D. (2011). Macular microcirculation blood flow after pars plana vitrectomy with silicone oil tamponade. *Klin. Ocz.* 113, 146–148.

Anegondi, N., Kshirsagar, A., Mochi, T. B., and Roy, A. S. (2018). Quantitative comparison of retinal vascular features in optical coherence tomography angiography images from three different devices. *Ophthalmic Surg. Lasers Imaging Retina* 49 (7), 488–496. doi:10.3928/23258160-20180628-04

Arfeen, S. A., Bahgat, N., Adel, N., Eissa, M., and Khafagy, M. M. (2020). Assessment of superficial and deep retinal vessel density in systemic lupus erythematosus patients using optical coherence tomography angiography. *Graefes Arch. Clin. Exp. Ophthalmol.* 258, 1261–1268. doi:10.1007/s00417-020-04626-7

Barca, F., Bacherini, D., Dragotto, F., Tartaro, R., Lenzetti, C., Finocchio, L., et al. (2020). OCT angiography findings in macula-on and macula-off rhegmatogenous retinal detachment: A prospective study. *J. Clin. Med.* 9 (12), 3982. doi:10.3390/jcm9123982

Birol, G., Wang, S., Budzynski, E., Wangsa-Wirawan, N. D., and Linsenmeier, R. A. (2007). Oxygen distribution and consumption in the macaque retina. *Am. J. Physiol. Heart Circ. Physiol.* 293, H1696–H1704. doi:10.1152/ajpheart.00221.2007

Bonfiglio, V., Ortisi, E., Scollo, D., Reibaldi, M., Russo, A., Pizzo, A., et al. (2020). Vascular changes after vitrectomy for rhegmatogenous retinal detachment: Optical coherence tomography angiography study. *Acta Ophthalmol.* 98 (5), E563–E9. doi:10.1111/aos.14315

Bonnin, S., Mané, V., Couturier, A., Julien, M., Paques, M., Tadayoni, R., et al. (2015). New insight into the macular deep vascular plexus imaged by optical coherence tomography angiography. *Retina* 35, 2347–2352. doi:10.1097/IAE.0000000000000839

Chatziralli, I., Theodossiadis, G., Chatzirallis, A., Dimitriou, E., Parikakis, E., and Theodossiadis, P. (2022). Evolution of macular microvasculature and retinal layers alterations in patients with macula off retinal detachment after vitrectomy. *Eur. J. Ophthalmol.* 32 (1), 520–526. doi:10.1177/1120672121992984

Christou, E. E., Kalogeropoulos, C., Georgalas, I., Stavrakas, P., Christodoulou, E., Batsos, G., et al. (2021). Assessment of anatomical and functional macular changes with optical coherence tomography angiography after macula-off rhegmatogenous retinal detachment repair. *Semin. Ophthalmol.* 36 (3), 119–127. doi:10.1080/08820538.2021.1889618

Chua, J., Chin, C. W. L., Hong, J., Chee, M. L., Le, T-T., Ting, D. S. W., et al. (2019). Impact of hypertension on retinal capillary microvasculature using optical coherence tomographic angiography. *J. Hypertens.* 37, 572–580. doi:10.1097/HJH.0000000000001916

D'Aloisio, R., Gironi, M., Verdina, T., Vivarelli, C., Leonelli, R., Mariotti, C., et al. (2022). Early structural and vascular changes after within-24 hours vitrectomy for recent onset rhegmatogenous retinal detachment treatment: A pilot study comparing bisected macula and not bisected macula. *J. Clin. Med.* 11 (12), 3498. doi:10.3390/jcm11123498

Dupas, B., Minvielle, W., Bonnin, S., Couturier, A., Erginay, A., Massin, P., et al. (2018). Association between vessel density and visual acuity in patients with diabetic retinopathy and poorly controlled type 1 diabetes. *JAMA Ophthalmol.* 136, 721–728. doi:10.1001/jamaophthalmol.2018.1319

Greig, E. C., Brigell, M., Cao, F., Levine, E. S., Peters, K., Moult, E. M., et al. (2020). Macular and peripapillary optical coherence tomography angiography metrics predict progression in diabetic retinopathy: A sub-analysis of TIME-2B study data. *Am. J. Ophthalmol.* 219, 66–76. doi:10.1016/j.ajo.2020.06.009

Hong, E. H., Cho, H., Kim, D. R., Kang, M. H., Shin, Y. U., and Seong, M. (2020). Changes in retinal vessel and retinal layer thickness after vitrectomy in retinal detachment via swept-source OCT angiography. *Invest. Ophthalmol. Vis. Sci.* 61 (2), 35. doi:10.1167/iovs.61.2.35

Kaderli, S. T., Karalezli, A., and Sul, S. (2021). Microvascular retinal alterations in rhegmatogenous retinal detachment after pneumatic retinopexy. *Acta Ophthalmol.* 99 (4), 383–389. doi:10.1111/aos.14624

Kuehlewein, L., Bansal, M., Lenis, T. L., Iafe, N. A., Sadda, S. R., Filho, M. A. B., et al. (2015). Optical coherence tomography angiography of type 1 neovascularization in age-related macular degeneration. *Am. J. Ophthalmol.* 160, 739–748. doi:10.1016/j.ajo.2015.06.030

Lavia, C., Bonnin, S., Maule, M., Erginay, A., Tadayoni, R., and Gaudric, A. (2019). Vessel density of superficial, intermediate, and deep capillary plexuses using optical coherence tomography angiography. *Retina* 39, 247–258. doi:10.1097/IAE.0000000000002413

Lee, J., Moon, B. G., Cho, A. R., and Yoon, Y. H. (2016). Optical coherence tomography angiography of DME and its association with anti-VEGF treatment response. *Ophthalmology* 123, 2368–2375. doi:10.1016/j.ophtha.2016.07.010

Lee, J. H., and Park, Y. G. (2021). Microvascular changes on optical coherence tomography angiography after rhegmatogenous retinal detachment vitrectomy with silicone tamponade. *PLoS One* 16 (3), e0248433. doi:10.1371/journal.pone.0248433

Liu, Y., Lei, B., Jiang, R., Huang, X., Zhou, M., and Xu, G. (2021). Changes of macular vessel density and thickness in gas and silicone oil tamponades after vitrectomy for macula-on rhegmatogenous retinal detachment. *BMC Ophthalmol.* 21 (1), 392. doi:10.1186/s12886-021-02160-6

Lu, Y., Wang, J. C., Cui, Y., Zhu, Y., Zeng, R., Lu, E. S., et al. (2021). A quantitative comparison of four optical coherence tomography angiography devices in healthy eyes. *Graefes Arch. Clin. Exp. Ophthalmol.* 259 (6), 1493–1501. doi:10.1007/s00417-020-04945-9

Ma, Y., Zhu, X. Q., and Peng, X. Y. (2020). Macular perfusion changes and ganglion cell complex loss in patients with silicone oil-related visual loss. *Biomed. Environ. Sci.* 33 (3), 151–157. doi:10.3967/bes2020.021

Masland, R. H. (2012). The neuronal organization of the retina. *Neuron* 76, 266–280. doi:10.1016/j.neuron.2012.10.002

McKay, K. M., Vingopoulos, F., Wang, J. C., Papakostas, T. D., Silverman, R. F., Marmalidou, A., et al. (2020). Retinal microvasculature changes after repair of macula-off retinal detachment assessed with optical coherence tomography angiography. *Clin. Ophthalmol.* 14, 1759–1767. doi:10.2147/OPTH.S214623

Nakazawa, T., Kayama, M., Ryu, M., Kunikata, H., Watanabe, R., Yasuda, M., et al. (2011). Tumor necrosis factor-alpha mediates photoreceptor death in a rodent model of retinal detachment. *Invest. Ophthalmol. Vis. Sci.* 52, 1384–1391. doi:10.1167/iovs.10-6509

Nakazawa, T., Matsubara, A., Noda, K., Hisatomi, T., She, H., Skondra, D., et al. (2006). Characterization of cytokine responses to retinal detachment in rats. *Mol. Vis.* 12, 867–878.

Ng, H., La Heij, E. C., Andrinopoulou, E. R., van Meurs, J. C., and Vermeer, K. A. (2020). Smaller foveal avascular zone in deep capillary plexus is associated with better visual acuity in patients after macula-off retinal detachment surgery. *Transl. Vis. Sci. Technol.* 9 (10), 25–12. doi:10.1167/tvst.9.10.25

Park, D. H., Choi, K. S., Sun, H. J., and Lee, S. J. (2018). Factors associated with visual outcome after macula-off rhegmatogenous retinal detachment surgery. *Retina* 38, 137–147. doi:10.1097/IAE.0000000000001512

Provis, J. M. (2001). Development of the primate retinal vasculature. *Prog. Retin. Eye Res.* 20, 799–821. doi:10.1016/s1350-9462(01)00012-x

Roohipoor, R., Tayebi, F., Riazi-Esfahani, H., Khodabandeh, A., Karkhaneh, R., Davoudi, S., et al. (2020). Optical coherence tomography angiography changes in macula-off rhegmatogenous retinal detachments repaired with silicone oil. *Int. Ophthalmol.* 40, 3295–3302. doi:10.1007/s10792-020-01516-z

Sato, E. A., Shinoda, K., Kimura, I., Ohtake, Y., and Inoue, M. (2007). Microcirculation in eyes after rhegmatogenous retinal detachment surgery. *Curr. Eye Res.* 32, 773–779. doi:10.1080/02713680701531108

Scarinci, F., Nesper, P. L., and Fawzi, A. A. (2016). Deep retinal capillary nonperfusion is associated with photoreceptor disruption in diabetic macular ischemia. *Am. J. Ophthalmol.* 168, 129–138. doi:10.1016/j.ajo.2016.05.002

Schocket, L. S., Witkin, A. J., Fujimoto, J. G., Ko, T. H., Schuman, J. S., Rogers, A. H., et al. (2006). Ultrahigh-resolution optical coherence tomography in patients with decreased visual acuity after retinal detachment repair. *Ophthalmology* 113, 666–672. doi:10.1016/j.ophtha.2006.01.003

Shimoda, Y., Sano, M., Hashimoto, H., Yokota, Y., and Kishi, S. (2010). Restoration of photoreceptor outer segment after vitrectomy for retinal detachment. *Am. J. Ophthalmol.* 149, 284–290. doi:10.1016/j.ajo.2009.08.025

Shlomit, S., Mark, P. S., Charles, C. B., and Henry, J. K. (2011). Primary retinal detachment repair: Comparison of 1-year outcomes of four surgical techniques. *Retina* 31, 1500–1504. doi:10.1097/IAE.0b013e31820d3f55

Stang, A. (2010). Critical evaluation of the Newcastle-Ottawa scale for the assessment of the quality of nonrandomized studies in meta-analyses. *Eur. J. Epidemiol.* 25 (9), 603–605. doi:10.1007/s10654-010-9491-z

Stroup, D. F., Berlin, J. A., Morton, S. C., Olkin, I., Williamson, G. D., Rennie, D., et al. (2000). Meta-analysis of observational studies in epidemiology: A proposal for reporting. Meta-Analysis of observational studies in epidemiology (MOOSE) group. *JAMA* 283 (25), 2008–2012. doi:10.1001/jama.283.15.2008

Sun, Z., Tang, F., Wong, R., Lok, J., Szeto, S. K. H., Chan, J. C. K., et al. (2019). OCT angiography metrics predict progression of diabetic retinopathy and development of diabetic macular edema: A prospective study. *Ophthalmology* 126, 1675–1684. doi:10.1016/j.ophtha.2019.06.016

Tasman, W., and Jaeger, J. (1991). *Duane's foudations of clinical ophthalmology*. New York: Lippincott Williams & Wilkins.

Tsen, C-L., Sheu, S-J., Chen, S-C., and Wu, T-T. (2019). Imaging analysis with optical coherence tomography angiography after primary repair of macula-off rhegmatogenous retinal detachment. *Graefes Archive Clin. Exp. Ophthalmol.* 257 (9), 1847–1855. doi:10.1007/s00417-019-04381-4

Usui, Y., Westenskow, P. D., Kurihara, T., Aguilar, E., Sakimoto, S., Paris, L. P., et al. (2015). Neurovascular crosstalk between interneurons and capillaries is required for vision. *J. Clin. Invest.* 125, 2335–2346. doi:10.1172/JCI80297

Wang, H., Xu, X., Sun, X., Ma, Y., and Sun, T. (2019). Macular perfusion changes assessed with optical coherence tomography angiography after vitrectomy for rhegmatogenous retinal detachment. *Graefes Archive Clin. Exp. Ophthalmol.* 257 (4), 733–740. doi:10.1007/s00417-019-04273-7

Woo, J. M., Yoon, Y. S., Woo, J. E., and Min, J. K. (2018). Foveal avascular zone area changes analyzed using OCT angiography after successful rhegmatogenous retinal detachment repair. *Curr. Eye Res.* 43 (5), 674–678. doi:10.1080/02713683.2018.1437922

Yarmohammadi, A., Zangwill, L. M., Diniz-Filho, A., Suh, M. H., Manalastas, P. I., Fatehee, N., et al. (2016). Optical coherence tomography angiography vessel density in healthy, glaucoma suspect, and glaucoma eyes. *Invest. Ophthalmol. Vis. Sci.* 57, OCT451–9. doi:10.1167/iovs.15-18944

Zhang, B., Chou, Y., Zhao, X., Yang, J., and Chen, Y. (2020). Early detection of microvascular impairments with optical coherence tomography angiography in diabetic patients without clinical retinopathy: A meta-analysis. *Am. J. Ophthalmol.* 222, 226–237. doi:10.1016/j.ajo.2020.09.032

frontiers | Frontiers in Medicine

TYPE Original Research
PUBLISHED 06 January 2023
DOI 10.3389/fmed.2022.1083601

OPEN ACCESS

EDITED BY
Doina Gherghel,
Aston University, United Kingdom

REVIEWED BY
Jacqueline Chua,
Singapore Eye Research Institute (SERI), Singapore
Maurizio Mete,
Sacro Cuore Don Calabria Hospital (IRCCS), Italy

*CORRESPONDENCE
Xuemin Li
✉ lxmlxm66@sina.com
Changguan Wang
✉ docwcg@126.com

†These authors have contributed equally to this work and share first authorship

SPECIALTY SECTION
This article was submitted to Ophthalmology, a section of the journal Frontiers in Medicine

RECEIVED 29 October 2022
ACCEPTED 16 December 2022
PUBLISHED 06 January 2023

CITATION
Wang X, Yang J, Wang C and Li X (2023) Choroidal morphologic and vascular features in patients with unilateral idiopathic epiretinal membranes: An optical coherence tomography analysis integrated with assessment of retinal layers. *Front. Med.* 9:1083601. doi: 10.3389/fmed.2022.1083601

Choroidal morphologic and vascular features in patients with unilateral idiopathic epiretinal membranes: An optical coherence tomography analysis integrated with assessment of retinal layers

Xinglin Wang[1,2†], Jiarui Yang[1,2†], Changguan Wang[1,2*] and Xuemin Li[1,2*]

[1]Department of Ophthalmology, Peking University Third Hospital, Beijing, China, [2]Beijing Key Laboratory of Restoration of Damaged Ocular Nerve, Beijing, China

Introduction: Integrated analysis of retinal and choroidal morphologic and vascular features is urgently needed to examine whether and how these two elements interact with each other, thus contributing to visual impairment in patients with idiopathic epiretinal membranes (iERMs).

Methods: An observational retrospective study consisting of 181 patients diagnosed with unilateral iERM between August 2019 and July 2022 was carried out at Peking University Third Hospital. All patients underwent a standardized set of ophthalmologic examinations, including EDI-OCT and OCTA scanning, and were subsequently categorized into four stages according to current classification schemes based on their OCT findings. Altogether, 15 qualitative and quantitative parameters of both the retina (full-layer, inner and outer layers) and choroid were identified.

Results: The results revealed variations in the choroidal vascularity index (CVI) among different stages of iERMs ($p < 0.001$) for the first time. Distributions of retinal parameters across four stages of iERMs were validated. Correlation analysis between choroidal and retinal parameters showed that the CVI was associated with both inner and outer retinal morphologic biomarkers. Functional damage to retinal integrity was determined to be a strong contributor to visual acuity reduction in iERMs.

Discussion: This study complemented our present understanding of posterior segment structural and vascular alterations in iERMs.

KEYWORDS

idiopathic epiretinal membrane, enhanced depth imaging optical coherence tomography (EDI-OCT), choroidal vascularity index, choroidal capillary perfusion, choroidal vasculature

Introduction

Idiopathic epiretinal membrane (iERM) is a common macular abnormality in elderly people characterized by aggregation of extracellular matrix and pre-retinal proliferation of myofibroblastic cells. Patients are often asymptomatic at first, but iERMs eventually induce progressive worsening of visual functions, including blurred vision and metamorphopsia (1, 2).

The introduction of current imaging modalities, such as spectral-domain optical coherence tomography (SD-OCT), enhanced depth imaging OCT (EDI-OCT), and optical coherence tomography angiography (OCTA) has enabled us to quantify the microstructure in the retina and choroid in patients with iERMs (3, 4). Previous studies have elucidated the morphologic alterations of different layers in the inner retina, including the ganglion cell layer (GCL) (5–10), inner plexiform layer (IPL) (5–10), inner nuclear layer (INL) (5–11), and ectopic inner foveal layer (EIFL) (12–17), which is defined as a unique inner retinal layer when distortion of the retina is present. The identification of EIFL also facilitated a four-stage iERM classification system which has been widely used and validated recently (13). The microstructure of the outer retina, including ellipsoid zone (EZ) and central bouquet (CB) abnormalities in iERMs was also investigated (14, 18–24). However, the tractional and tangential forces induced by iERM may transmit downward thus impacting the underlying choroid (14). In this regard, observations of retinal architecture alone are insufficient to understand the pathophysiology of iERMs. Besides, the incorporation of both retinal and choroidal parameters is urgently needed to examine whether and how these two elements interact with each other and with patient visual outcomes.

In this study, we aimed to determine the variations in retinal (both inner and outer layers) and choroidal parameters in different stages of iERMs and identify the factors related to best corrected visual acuity (BCVA). The association between retinal and choroidal parameters was also evaluated.

Materials and methods

Study design and participants

An observational, retrospective, institutional case series was carried out at Peking University Third Hospital in adherence to the tenets of the Declaration of Helsinki and was approved by the Institutional Review Board of Peking University Third Hospital.

Electronic records of patients diagnosed with unilateral iERM between August 1st 2019 and July 31st 2022 according to existing standards (1) were examined. The exclusion criteria were as follows: (1) secondary ERM (2) history of previous intraocular surgery with the exclusion of uncomplicated phacoemulsification at least 6 months ago; (3) presence of other ocular abnormalities that could have interfered with functional and morphologic results, as summarized in **Supplementary Table 1**; (4) contralateral eye suffering from any form of retinochoroidal diseases. Details of patient enrollment are illustrated in **Figure 1**.

Ocular examination

All patients underwent a standardized set of ophthalmologic examinations, including slit-lamp biomicroscopy, dilated fundus examination, EDI-OCT and OCTA scanning, as previously described (25, 26). Best-corrected visual acuity (BCVA) was obtained after autorefraction screening (Canon Autorefractor RK-F1; Canon Inc., Ltd., Tochigiken, Japan) and manifest refraction in the Snellen fraction and was converted into the logarithm of the minimum angle of resolution (logMAR) for statistical analysis. Intraocular pressure (Auto Non-contact Tonometer, NT-3000; Nidek, Gamagori, Japan) and biometric measurements (Non-contact Zeiss IOLMaster-700, Carl Zeiss Meditec AG, Jena, Germany) were also assessed. Both eyes of the included subjects were selected for examination and subsequent analysis.

Acquisition of retinal and choroidal parameters and grading of iERMs

All retinal and choroidal structural parameters were obtained using Heidelberg Spectralis SD-OCT (Heidelberg Engineering, Heidelberg, Germany) in EDI-OCT mode (cross-line scan spanning 30°) and OCTA (Optovue Inc., Freemont, California, USA). All OCT measurements were taken in a 2 mm-wide area centered at the fovea to match the 1 mm-radius circular calculation area in OCTA, which is elucidated below. Choroidal vascularity index (CVI) was defined as the ratio of choroidal luminal area (LA) and total choroidal area (TCA) based on post-binarization OCT images. Subfoveal choroidal thickness (SFCT), TCA, LA, choroidal stromal area (SA), and CVI were all measured and calculated automatically by a software which we developed as previously described (25). Images with poor identification of the choroidal-scleral interface or scanning quality below 6/10 after two rescan attempts were excluded. To avoid inaccurate segmentation of the retinal layers in advanced iERMs where disorganization of the retina is commonly present, two masked ophthalmologists were assigned to manually evaluate central retinal thickness (CRT) and the thickness of retinal GCL, IPL, INL, EIFL, and photoreceptor outer segment (PROS), with intraclass correlation coefficients (ICC) of 0.961 (CRT), 0.954 (GCL + IPL), 0.966 (INL), 0.928 (EIFL), and 0.957 (PROS), and the mean value of their measurements were selected for subsequent analysis.

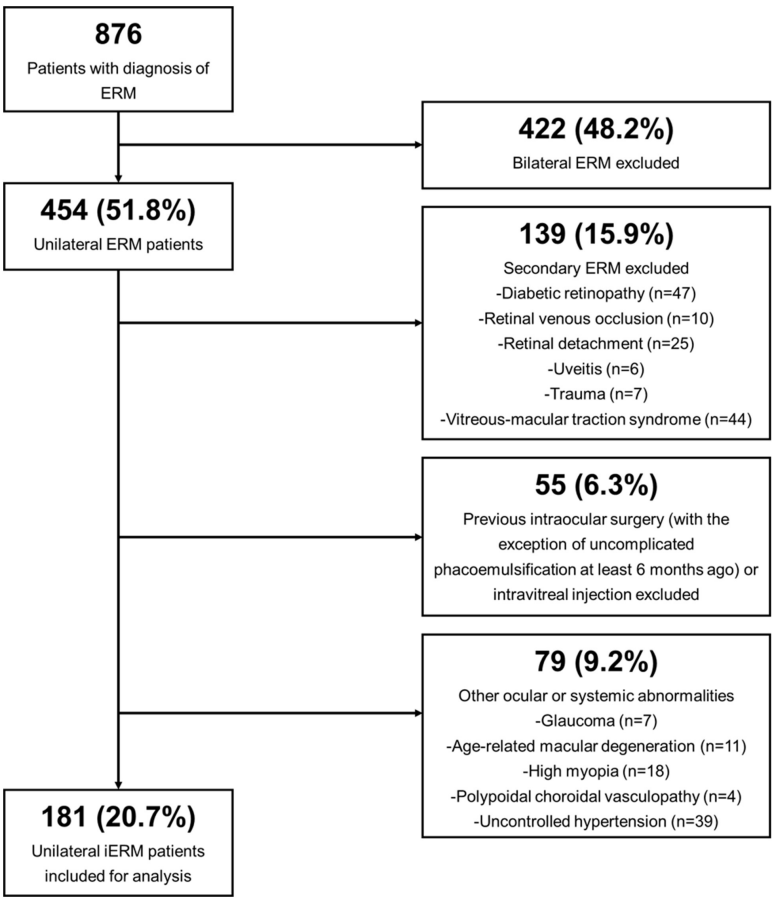

FIGURE 1
Flow diagram demonstrating the selection process of enrolled unilateral idiopathic epiretinal membrane (iERM) subjects.

Boundaries of each retinal layer evaluated are embedded in **Supplementary Table 2**, and an example of measurements of retinal thickness is illustrated in **Supplementary Figure 1**. EZ disruption and CB abnormalities were assessed according to a previous classification scheme (14). Choroidal capillary perfusion (CCP), as a reference for choroidal capillary blood flow, was quantitatively evaluated on OCTA in angio-retina scanning mode (840 nm, 70,000 A-scans/s, 3 mm × 3 mm) (27, 28).

Furthermore, iERMs were classified into four stages by the SD-OCT classification system proposed by Govetto et al. (13) depending on the preservation (Stage 1) or absence (Stage 2) of a foveal pit, presence of ectopic inner foveal layers (Stage 3) and disorganization of the retinal layers (Stage 4).

Statistical analysis

Statistical analysis was performed using SPSS version 20.0 (SPSS, Inc., Chicago, IL), and all values are represented as mean ± standard deviation unless indicated otherwise. The normality of the distributions of all variables was assessed using analytical methods (Shapiro-Wilk or Kolmogorov-Smirov tests). Independent *t*-tests or Mann-Whitney *U*-tests were used to compare continuous variables between two groups of iERMs. One-way ANOVA, Kruskal-Wallis or Welch tests were selected to compare continuous variables among three or more groups. Pearson Chi-Square test or Fisher's exact test was used to compare proportions among the study population. The correlations between retinal and choroidal parameters and between all parameters and BCVA were calculated by Spearman rank correlation or Kendall's tau-b correlation analysis. Multiple regression analysis was performed to determine the independent predictors of BCVA after a collinearity check. A two-sided *p*-value less than 0.05 was considered to be statistically significant.

Results

A total of 181 patients suffering from unilateral iERM were included in the study, consisting of 94 men and 87 women

from 53 to 81 years old (mean age: 66.73 ± 6.44 years). The average logMAR BCVA was 0.36 ± 0.28 (20/39) in affected eyes and 0.10 ± 0.08 (20/25) in contralateral eyes. Based on OCT imaging findings, the iERM status of all patients was classified into stage 1 (54 eyes, 29.8%), stage 2 (51 eyes, 28.2%), stage 3 (45 eyes, 24.9%), and stage 4 (31 eyes, 17.1%). No significant difference in age, gender distribution, axial length or refractive error was identified among all groups (Table 1).

Variations in retinal and choroidal parameters in different stages of iERMs

The anatomical and functional parameters in different stages of iERMs and fellow eyes are shown in Table 1. The overall retina and inner retinal layers, including the GCL, IPL, and INL, thickened in higher stages of iERMs ($p < 0.001$, Supplementary Figure 1), with a higher occurrence of complicated CME ($p < 0.001$). Structural disturbance in the outer retina varied significantly among the four groups ($p < 0.001$ for EZ

TABLE 1 Demographics and ocular characteristics in different stages of idiopathic epiretinal membrane and fellow eyes.

	Stage 1 (n = 54)	Stage 2 (n = 51)	Stage 3 (n = 45)	Stage 4 (n = 31)	P-value	Fellow eyes (n = 181)
Age (years)	65.94 ± 4.24	66.98 ± 6.99	66.24 ± 7.47	68.42 ± 7.01	0.331 [a]	/
Gender (Male/Female)	32/22	27/24	19/26	16/15	0.410 [b]	/
Presence of diabetes	6/54	8/51	7/45	3/31	0.813 [e]	/
Axial length (mm)	24.25 ± 1.21	24.52 ± 1.09	24.61 ± 1.33	24.58 ± 1.46	0.772 [a]	24.39 ± 1.78
Refractive error (D)	−0.49 ± 2.56	−0.26 ± 2.94	−0.17 ± 2.74	−0.44 ± 3.14	0.549 [a]	−0.24 ± 3.22
Retinal parameters						
CRT (μm)	292.87 ± 30.24	415.90 ± 34.68	518.00 ± 31.21	636.77 ± 49.01	<0.001[a]	253.12 ± 20.84***
GCL + IPL (μm)	102.25 ± 18.03	153.80 ± 23.94	173.86 ± 16.37	/	<0.001[c]	97.43 ± 10.26***
INL (μm)	46.82 ± 10.94	53.39 ± 10.81	56.80 ± 10.10	/	<0.001[d]	44.55 ± 5.19***
GCL + IPL + INL (μm)	149.08 ± 27.35	207.19 ± 31.94	230.66 ± 24.95	/	<0.001[d]	138.96 ± 10.85***
EIFL (μm)	/	/	186.07 ± 51.94	/		/
PROS length (μm)	61.78 ± 3.27	67.60 ± 11.23	69.47 ± 14.07	63.06 ± 6.13	0.097 [a]	63.80 ± 5.50*
EZ disruption	2/54 (3.7%)	9/51 (17.6%)	12/45 (26.7%)	14/31 (45.2%)	<0.001[b]	/
Central bouquet abnormalities	3/54 (5.6%)	13/51 (25.5%)	10/45 (22.2%)	3/31 (9.7%)	0.011[e]	
Cotton ball sign	3/54	7/51	2/45	0/31		/
Foveolar detachment	0/54	4/51	5/45	3/31		/
Vitelliform lesion	0/54	2/51	3/45	0/31		/
Presence of CME	0/54 (0%)	7/51 (13.7%)	9/45 (20.0%)	11/31 (35.5%)	<0.001[b]	/
Choroidal parameters						
SFCT (μm)	232.30 ± 25.29	226.88 ± 38.95	233.50 ± 43.75	238.62 ± 60.04	0.471[a]	233.16 ± 43.40
TCA (mm^2)	0.4435 ± 0.0575	0.4481 ± 0.0651	0.4621 ± 0.0535	0.4710 ± 0.0656	0.423 [a]	0.4614 ± 0.0822
LA (mm^2)	0.2822 ± 0.0370	0.2893 ± 0.0423	0.3015 ± 0.0351	0.3086 ± 0.0429	0.045 [a]	0.2922 ± 0.0521
SA (mm^2)	0.1613 ± 0.0205	0.1588 ± 0.0230	0.1606 ± 0.0188	0.1624 ± 0.0230	0.917 [a]	0.1693 ± 0.0302***
CVI	0.6362 ± 0.0035	0.6455 ± 0.0058	0.6524 ± 0.0060	0.6553 ± 0.0062	<0.001[a]	0.6332 ± 0.0038***
CCP (%)	57.37 ± 3.41	56.99 ± 5.41	55.58 ± 5.26	56.78 ± 5.81	0.406 [a]	63.45 ± 4.35***
BCVA (logMAR)	0.10 ± 0.07	0.29 ± 0.12	0.46 ± 0.18	0.79 ± 0.25	<0.001[a]	0.10 ± 0.08***

CRT, central retinal thickness; CME, cystoid macular edema; GCL + IPL, ganglion cell layer + inner plexiform layer; INL, inner nuclear layer; EIFL, ectopic inner foveal layer; EZ, ellipsoid zone; PROS, photoreceptor outer segment; SFCT, subfoveal choroidal thickness; TCA, total choroidal area; LA, luminal area; SA, stromal area; CVI, choroidal vascularity index; CCP, choroidal capillary perfusion; BCVA, best corrected visual acuity. Asterisks represent the significance comparing values in iERMs and their contralateral eyes. *$p < 0.05$; ***$p < 0.001$.
[a]Kruskal-Wallis test.
[b]Pearson Chi-Square test.
[c]Welch test.
[d]One-way ANOVA test.
[e]Fisher's exact test.

disruption, $p = 0.011$ for CB abnormalities). The subtype of CB abnormalities was also significantly associated with iERM stages ($p = 0.030$), where stage 2 iERMs had the most cotton ball signs (13.7%) and stage 3 iERMs had the most foveolar detachments (11.1%). The PROS length in iERMs was higher than that in the control group (65.55 ± 10.16 vs. 63.80 ± 5.50, $p = 0.047$), but was comparable among the four stages of iERMs ($p = 0.097$). CVI, the only choroidal parameter which was significantly different among the four groups, exhibited an increasing pattern as iERM advanced into higher stages ($p < 0.001$).

Associations of retinal and choroidal parameters in iERMs

The correlation analysis between retinal and choroidal parameters in eyes with iERMs revealed that a higher CVI correlated with a thicker CRT, GCL + IPL, INL, GCL + IPL + INL, and PROS (Table 2). As shown in Figure 2, eyes accompanied with CME had a higher CVI ($p < 0.001$) and statistically equivalent CCP ($p = 0.362$) and SFCT ($p = 0.768$) than uncomplicated iERM eyes. All choroidal parameters including CVI ($p < 0.001$), CCP ($p = 0.001$), and SFCT ($p = 0.005$) varied between eyes with and without EZ disruption. Additionally, only the CVI out of all choroidal parameters was affected in terms of CB status ($p < 0.001$, $p = 0.097$, $p = 0.141$ for CVI, CCP, and SFCT, respectively; detailed data are embedded in Table 3).

Predictive variables affecting BCVA in iERMs

Figure 3 demonstrates the correlation of BCVA and various OCT morphologic biomarkers in iERMs. Among all retinal and choroidal parameters, CRT, CVI, and GCL + IPL thickness had the strongest correlation with BCVA ($r = 0.896$, 0.817, 0.771, respectively. All $p < 0.001$), followed by GCL + IPL + INL thickness ($r = 0.743$, $p < 0.001$), EZ disruption ($r = 0.439$, $p < 0.001$), INL thickness ($r = 0.383$, $p < 0.001$), CB abnormalities ($r = 0.252$, $p < 0.001$), PROS length ($r = 0.197$, $p = 0.008$), and CCP ($r = -0.165$, $p = 0.026$). SFCT was found to be statistically irrelevant to BCVA ($r = -0.006$, $p = 0.937$). Subsequently, parameters with statistically solid and integral values across four stages of iERMs were included in multiple regression analysis, which ruled out GCL and IPL for the disrupted retinal structure in higher stages of iERMs. SFCT and choroidal area parameters were also excluded for

TABLE 2 The association between retinal and choroidal parameters in eyes with epiretinal membranes ($N = 181$).

	CRT, μm	GCL + IPL, μm[a]	INL, μm[a]	GCL + IPL + INL, μm[a]	EIFL, μm[b]	PROS, μm
CVI	$r = 0.792$* $p < 0.001$	$r = 0.690$* $p < 0.001$	$r = 0.272$* $p = 0.001$	$r = 0.655$* $p < 0.001$	$r = 0.197$ $p = 0.195$	$r = 0.343$* $p < 0.001$
CCP,%	$r = -0.089$ $p = 0.235$	$r = -0.119$ $p = 0.146$	$r = -0.113$ $p = 0.169$	$r = -0.124$ $p = 0.130$	$r = 0.012$ $p = 0.938$	$r = -0.113$ $p = 0.181$
SFCT, μ m	$r = -0.072$ $p = 0.335$	$r = -0.133$ $p = 0.104$	$r = -0.031$ $p = 0.702$	$r = -0.120$ $p = 0.145$	$r = -0.086$ $p = 0.573$	$r = -0.067$ $p = 0.369$

CRT, central retinal thickness; GCL + IPL, ganglion cell layer + inner plexiform layer; INL, inner nuclear layer; EIFL, ectopic inner foveal layer; PROS, photoreceptor outer segment; BCVA, best corrected visual acuity; CVI, choroidal vascularity index; CCP, choroidal capillary perfusion; SFCT, subfoveal choroidal thickness.
*Values with statistical significance were highlighted with asterisks.
[a]$N = 150$ (stage 1–3 epiretinal membranes with identifiable retinal layers).
[b]$N = 45$ (stage 3 epiretinal membranes).

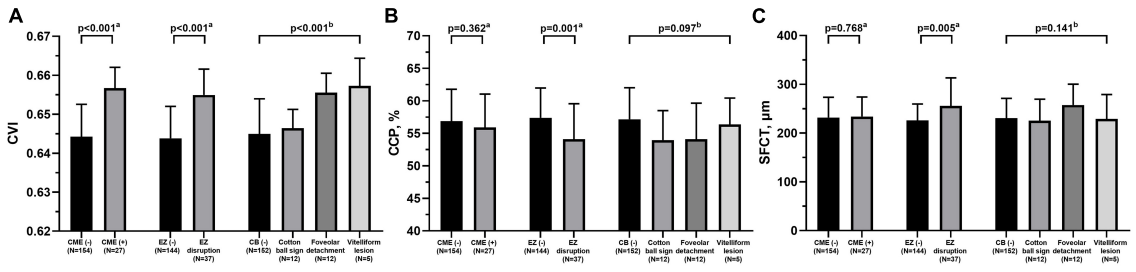

FIGURE 2
Comparisons of choroidal parameters including CVI **(A)**, CCP **(B)**, and SFCT **(C)** between eyes with different retinal features under idiopathic epiretinal membrane conditions. CVI, choroidal vascularity index; CCP, choroidal capillary perfusion; SFCT, subfoveal choroidal thickness; CME, cystoid macular edema; EZ, ellipsoid zone; CB, central bouquet abnormality. [a]Mann-Whitney test. [b]Kruskal-Wallis test.

TABLE 3 Distributions of choroidal parameters including CVI, CCP, and SFCT in iERMs eyes in terms of different structural retinal status.

	CVI	CCP	SFCT
CME (−) (N = 154)	0.6443 ± 0.0083	56.86 ± 4.91	231.87 ± 41.47
CME (+) (N = 27)	0.6567 ± 0.0053	55.90 ± 5.14	233.78 ± 40.05
P-value[a]	<0.001	0.362	0.768
EZ (−) (N = 144)	0.6438 ± 0.0082	57.40 ± 4.58	226.09 ± 33.42
EZ disruption (N = 37)	0.6550 ± 0.0066	54.08 ± 5.48	255.74 ± 57.57
P-value[a]	< 0.001	0.001	0.005
CB (−) (N = 152)	0.6450 ± 0.0090	57.15 ± 4.86	230.77 ± 40.28
CB (+) (N = 29)	0.6521 ± 0.0070	54.44 ± 4.81	239.41 ± 45.54
P-value[a]	<0.001	0.015	0.410
Cotton ball sign (N = 12)	0.6465 ± 0.0048	53.96 ± 4.53	225.39 ± 44.17
Foveolar detachment (N = 12)	0.6556 ± 0.0050	54.12 ± 5.52	257.69 ± 42.40
Vitelliform lesion (N = 5)	0.6573 ± 0.0071	56.37 ± 4.04	229.21 ± 49.88
P-value[b]	<0.001	0.097	0.141

CVI, choroidal vascularity index; CCP, choroidal capillary perfusion; SFCT, subfoveal choroidal thickness; CME, cystoid macular edema; EZ, ellipsoid zone; CB, central bouquet abnormality.
[a]Mann-Whitney test.
[b]Kruskal-Wallis test among three CB (+) groups and CB (−) group.

their comparable values among the four groups and lack of correlation with BCVA. The regression model (R^2 = 0.843, adjusted R^2 = 0.837) showed that the predictive variables for BCVA were CRT (standardized partial regression coefficient β = 0.772, $p < 0.001$), presence of CME (β = 0.102, $p = 0.004$), EZ disruption (β = 0.190, $p < 0.001$), and CB abnormalities (β = 0.112, $p = 0.002$). None of the choroidal parameters exhibited predictive value in terms of BCVA.

Discussion

Much evidence regarding the posterior segment microstructure using non-invasive OCT and OCTA has emerged in recent years, with attempts to identify predictive and prognostic factors of visual functioning in iERMs (6, 8, 9, 13–15, 17–22, 29). However, these investigations mostly focused on retinal features, and even with a handful of studies revealing the potential role of the choroid in iERMs (28, 30–33), all-around incorporation of OCT and OCTA biomarkers was still insufficient to achieve. Furthermore, fewer studies have been updated according to the ERM classification and staging scheme (1, 13). To the best of our knowledge, this is the first study to comprehensively quantify the variations in retinal morphology at the full-layer, inner retina and outer retina levels, together with choroidal morphological and vascular parameters in all four stages of iERMs.

Here, our study confirmed that CRT and the presence of CME were elevated in higher stages of iERMs, which has been widely described before (12–14, 16, 34, 35). The microstructure of the inner retina has also been quantitatively evaluated by previous investigators, but the conclusions were somewhat conflicting regarding some specific inner retinal parameters, including the thickness of the GCL + IPL and INL. In some cases, GCL + IPL was thinner in eyes with iERM than in healthy controls (6, 7), while others discovered the opposite results (5, 8–10). This is reasonable considering that the auto segmentation and assessment of the inner retina through the built-in ganglion cell analysis (GCA) algorithm on OCT usually fails when severe retinal layer distortion is present in cases of iERMs, which makes the identification of the GCL, IPL, and INL mostly dependent on manual measurements. Besides, the fact that patients in these studies were not classified or graded according to a unanimous staging scheme may also contribute to these contrary results. In the present study, we found that the thickness of both the GCL + IPL and INL varied among different stages of iERMs, with stage 3 iERMs being the thickest followed by stage 2 and stage 1 iERMs (stage 4 iERMs were excluded for their inner retinal distortion), and all iERMs had thicker GCL + IPL and INL than the control group, which was in accordance with most previous studies (5, 8–10). Although still relying on manual measurements, our study provides the first evidence to distinguish variations in inner retinal morphology in different stages of iERMs.

The tangential reaction caused by ERM, which induced lateral displacement of the inner retina and thickened the GCL, IPL, and INL within (8, 14, 36), also affected the outer retina in our subjects. The results here demonstrated that EZ disruptions were presented more frequently in higher stages of iERMs, and subtypes of CB abnormalities were also significantly associated with iERM stages, which is in line with a previous study by Govetto et al. (14). PROS length was longitudinally analyzed before and was found to be higher preoperatively and decreased after membrane peeling in iERMs (21, 37), but comparisons among different stages of iERMs and with healthy control eyes are still lacking. Our results here showed that iERMs had a higher PROS length than controls and that PROS length was not associated with iERM stages.

A few studies dug into choroidal morphologic and vascular features using SFCT, CVI, or CCP separately for observations of iERM patients (32, 38–41), but their investigation was neither integrated in terms of choroidal parameters nor did they distinguish the different stages of iERMs. Our systematic analysis of the choroid showed that SFCT was unaffected by the presence or severity of iERM. This was also validated by the comparable values of TCA, LA, and SA in all groups, suggesting that no expansion or shrinking of the choroid total volume was observed in iERMs. However, the choroid appeared more vascularized in higher stages of iERMs on the full-layer level ($P < 0.001$ for CVI among all groups),

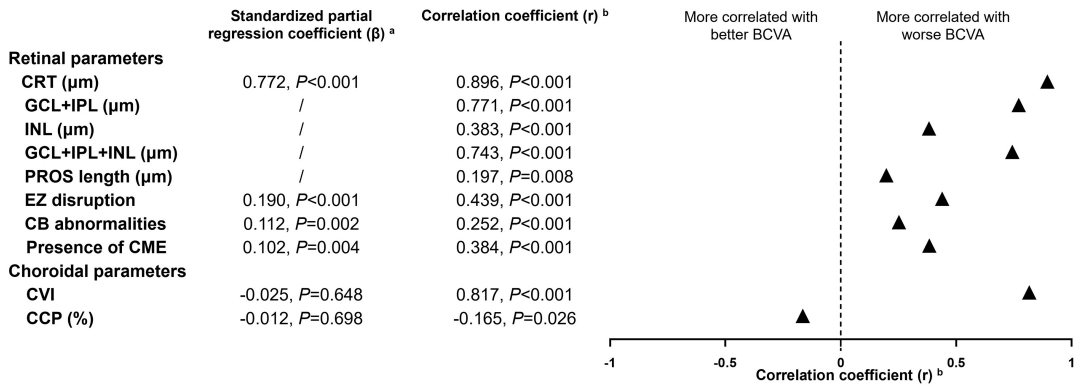

FIGURE 3
Multiple regression and correlation analysis to determine the OCT morphologic factors related to best-corrected visual acuity in idiopathic epiretinal membranes. CRT, central retinal thickness; CME, cystoid macular edema; GCL + IPL, ganglion cell layer + inner plexiform layer; INL, inner nuclear layer; EZ, ellipsoid zone; CB, central bouquet; PROS, photoreceptor outer segment; CVI, choroidal vascularity index; CCP, choroidal capillary perfusion; BCVA, best corrected visual acuity. [a]OCT parameters with statistically solid and integral values across four stages of idiopathic epiretinal membranes were included in multiple regression analysis, which ruled out thickness of specific retinal layer for the disrupted retinal structure in higher stages of iERMs. Subfoveal choroidal thickness and choroidal area parameters were also excluded for their comparable value among four groups and lack of correlation to BCVA. [b]Spearman correlation analysis was used for continuous variables and Kendall's tau-b correlation analysis was used for categorical variables.

which complemented the preliminary findings of a previous study where iERMs had a higher CVI than healthy eyes (39). In accordance with a recent study in which eyes with iERM had lower CCP than contralateral eyes (31), similar results were identified here [affected eyes vs. healthy eyes (%), 56.72 ± 4.94 vs. 63.45 ± 4.35, $P < 0.001$], but subsequent subgroup analysis revealed that CCP was independent of iERM stages.

All main choroidal parameters including SFCT, CVI, and CCP showed variations in terms of the presence of EZ disruption. Without longitudinal follow-up on iERM development, we cannot say for certain whether the altered choroidal morphology and vascularity affected EZ continuity or vice versa. Based on the fact that the densely vascularized choroid, especially its Haller's layer, provides nutrient and oxygen exchange with the outer retina (4, 42), we speculate that the tangential traction caused by iERMs not only mechanically stretches the EZ band (or all outer retina), but also disturbs choroidal function, which results in EZ injury. CVI was found to be correlated with all retinal parameters except the thickness of EIFL, indicating that the previously neglected choroid may actually play a crucial role in the development of retinal distortion under iERM status.

However, it is noteworthy that even with significant correlations to BCVA, choroidal parameters exhibited no predictive impact for BCVA in multiple regression analysis. Indeed, visual outcome has been proven to be determined by retinal morphology and functioning more directly (2, 43), but accompanying changes in the choroid may drive or facilitate the process of retinal deterioration in iERMs (28, 31). Future prospective observations and additional clinicopathologic studies are needed to examine the microanatomy of the outer retina and choroid, thus fully understanding the sequence of events in the development of retinal and choroidal alterations in iERMs.

There were several limitations in our study. First, the total number of enrolled subjects was relatively small considering that there were four subgroups altogether, and the variance in sample size among the four groups, although inevitable, may induce statistical unreliability regarding the study conclusion. Second, the observational nature of this study narrowed the generalization of our conclusions, and was also insufficient to explicate the precedence of retinal and choroidal changes during the progression of iERMs. Last, although many parameters were obtained using unbiased automated software, a few retinal biomarkers, including the thickness of inner retinal layer and outer retinal distortion were still manually assessed. Future robust tools are urgently needed to automatically segment and identify retinal and choroidal abnormalities.

In conclusion, this study complemented our present understanding of the posterior segment structural and vascular alterations in iERMs. CVI varied, while SFCT and CCP were comparable, among different stages of iERMs. Functional damage to retinal integrity was determined to be a strong contributor to visual acuity reduction in iERMs. Besides, the correlation of CVI to both inner and outer retinal morphologic biomarkers indicated that future studies with larger sample sizes and longitudinal observations are needed to fully examine the possible mechanisms of retinal and choroidal alterations in the development of iERMs.

Data availability statement

The raw data supporting the conclusions of this article will be made available by the authors, without undue reservation.

Ethics statement

The studies involving human participants were reviewed and approved by the Institutional Review Board of Peking University Third Hospital. Written informed consent for participation was not required for this study in accordance with the national legislation and the institutional requirements.

Author contributions

CW and XL: conceptualization. XL: data curation and funding acquisition. XW: formal analysis, investigation, and writing—original draft. XW and JY: methodology. CW: supervision. JY: writing—review and editing. All authors have read and agreed to the published version of the manuscript.

Conflict of interest

The authors declare that the research was conducted in the absence of any commercial or financial relationships that could be construed as a potential conflict of interest.

Publisher's note

All claims expressed in this article are solely those of the authors and do not necessarily represent those of their affiliated organizations, or those of the publisher, the editors and the reviewers. Any product that may be evaluated in this article, or claim that may be made by its manufacturer, is not guaranteed or endorsed by the publisher.

Supplementary material

The Supplementary Material for this article can be found online at: https://www.frontiersin.org/articles/10.3389/fmed.2022.1083601/full#supplementary-material

References

1. Folk J, Adelman R, Flaxel C, Hyman L, Pulido J, Olsen T. Idiopathic epiretinal membrane and vitreomacular traction preferred practice pattern(®) guidelines. *Ophthalmology.* (2016) 123:152–81. doi: 10.1016/j.ophtha.2015.10.048

2. Fung A, Galvin J, Tran T. Epiretinal membrane: a review. *Clin Exp Ophthalmol.* (2021) 49:289–308. doi: 10.1111/ceo.13914

3. Iovino C, Pellegrini M, Bernabei F, Borrelli E, Sacconi R, Govetto A, et al. Choroidal vascularity index: an in-depth analysis of this novel optical coherence tomography parameter. *J Clin Med.* (2020) 9:595. doi: 10.3390/jcm9020595

4. Borrelli E, Sarraf D, Freund K, Sadda SR. OCT angiography and evaluation of the choroid and choroidal vascular disorders. *Prog Retin Eye Res.* (2018) 67:30–55. doi: 10.1016/j.preteyeres.2018.07.002

5. Kim J, Kang S, Kong M, Ha H. Assessment of retinal layers and visual rehabilitation after epiretinal membrane removal. *Graefes Arch Clin Exp Ophthalmol.* (2013) 251:1055–64. doi: 10.1007/s00417-012-2120-7

6. Lee E, Yu H. Ganglion cell-inner plexiform layer thickness after epiretinal membrane surgery: a spectral-domain optical coherence tomography study. *Ophthalmology.* (2014) 121:1579–87. doi: 10.1016/j.ophtha.2014.02.010

7. Lee H, Kim M, Jo Y, Kim J. Thickness of the macula, retinal nerve fiber layer, and ganglion cell layer in the epiretinal membrane: the repeatability study of optical coherence tomography. *Invest Ophthalmol Vis Sci.* (2015) 56:4554–9. doi: 10.1167/iovs.15-16949

8. Park S, Byon I, Kim H, Lee J, Oum B. Analysis of the ganglion cell layer and photoreceptor layer using optical coherence tomography after idiopathic epiretinal membrane surgery. *Graefes Arch Clin Exp Ophthalmol.* (2015) 253:207–14. doi: 10.1007/s00417-014-2684-5

9. Pierro L, Iuliano L, Gagliardi M, Codenotti M, Ambrosi A, Bandello F. Role of ganglion cell complex in visual recovery following surgical internal limiting membrane peeling. *Graefes Arch Clin Exp Ophthalmol.* (2015) 253:37–45. doi: 10.1007/s00417-014-2665-8

10. Moon B, Yang Y, Chung H, Sohn J. Correlation between macular microstructures and aniseikonia after idiopathic epiretinal membrane removal. *Retina.* (2020) 40:1160–8. doi: 10.1097/IAE.0000000000002530

11. Takabatake M, Higashide T, Udagawa S, Sugiyama K. Postoperative changes and prognostic factors of visual acuity, metamorphopsia, and aniseikonia after vitrectomy for epiretinal membrane. *Retina.* (2018) 38:2118–27.

12. Govetto A, Virgili G, Rodriguez F, Figueroa M, Sarraf D, Hubschman J. Functional and anatomical significance of the ectopic inner foveal layers in eyes with idiopathic epiretinal membranes: surgical results at 12 Months. *Retina.* (2019) 39:347–57.

13. Govetto A, Lalane R, Sarraf D, Figueroa M, Hubschman J. Insights into epiretinal membranes: presence of ectopic inner foveal layers and a new optical coherence tomography staging scheme. *Am J Ophthalmol.* (2017) 175:99–113.

14. Govetto A, Bhavsar K, Virgili G, Gerber M, Freund K, Curcio C, et al. Tractional abnormalities of the central foveal bouquet in epiretinal membranes: clinical spectrum and pathophysiological perspectives. *Am J Ophthalmol.* (2017) 184:167–80. doi: 10.1016/j.ajo.2017.10.011

15. Doguizi S, Sekeroglu M, Ozkoyuncu D, Omay A, Yilmazbas P. Clinical significance of ectopic inner foveal layers in patients with idiopathic epiretinal membranes. *Eye.* (2018) 32:1652–60. doi: 10.1038/s41433-018-0153-9

16. Mavi Yildiz A, Avci R, Yilmaz S. The predictive value of ectopic inner retinal layer staging scheme for idiopathic epiretinal membrane: surgical results at 12 months. *Eye.* (2021) 35:2164–72. doi: 10.1038/s41433-021-01429-w

17. González-Saldivar G, Berger A, Wong D, Juncal V, Chow D. Ectopic inner foveal layer classification scheme predicts visual outcomes after epiretinal membrane surgery. *Retina.* (2020) 40:710–7. doi: 10.1097/IAE.0000000000002486

18. Kinoshita T, Imaizumi H, Miyamoto H, Katome T, Semba K, Mitamura Y. Two-year results of metamorphopsia, visual acuity, and optical coherence tomographic parameters after epiretinal membrane surgery. *Graefes Arch Clin Exp Ophthalmol.* (2016) 254:1041–9. doi: 10.1007/s00417-015-3147-3

19. Fang I, Hsu C, Chen L. Correlation between visual acuity changes and optical coherence tomography morphological findings in idiopathic epiretinal membranes. *Graefes Arch Clin Exp Ophthalmol.* (2016) 254:437–44.

20. Watanabe K, Tsunoda K, Mizuno Y, Akiyama K, Noda T. Outer retinal morphology and visual function in patients with idiopathic epiretinal membrane. *JAMA Ophthalmol.* (2013) 131:172–7.

21. Shiono A, Kogo J, Klose G, Takeda H, Ueno H, Tokuda N, et al. Photoreceptor outer segment length: a prognostic factor for idiopathic epiretinal membrane surgery. *Ophthalmology.* (2013) 120:788–94.

22. Ortoli M, Blanco-Garavito R, Blautain B, Mastorakos N, Souied E, Glacet-Bernard A. Prognostic factors of idiopathic epiretinal membrane surgery and evolution of alterations of the central cone bouquet. *Graefes Arch Clin Exp Ophthalmol.* (2021) 259:2139–47. doi: 10.1007/s00417-021-05110-6

23. Shimozono M, Oishi A, Hata M, Matsuki T, Ito S, Ishida K, et al. The significance of cone outer segment tips as a prognostic factor in epiretinal membrane surgery. *Am J Ophthalmol.* (2012) 153:698–704.

24. Itoh Y, Inoue M, Rii T, Hirota K, Hirakata A. Correlation between foveal cone outer segment tips line and visual recovery after epiretinal membrane surgery. *Invest Ophthalmol Vis Sci.* (2013) 54:7302–8. doi: 10.1167/iovs.13-12702

25. Yang J, Wang X, Wang Y, Li Z, Xia H, Hou Q, et al. CVIS: Automated OCT-scan-based software application for the measurements of choroidal vascularity index and choroidal thickness. *Acta Ophthalmol.* (2022) 100:e1553–60. doi: 10.1111/aos.15152

26. Wang X, Yang J, Liu Y, Yang L, Xia H, Ren X, et al. Choroidal morphologic and vascular features in patients with myopic choroidal neovascularization and different levels of myopia based on image binarization of optical coherence tomography. *Front Med.* (2021) 8:791012. doi: 10.3389/fmed.2021.791012

27. Jia Y, Bailey S, Wilson D, Tan O, Klein M, Flaxel C, et al. Quantitative optical coherence tomography angiography of choroidal neovascularization in age-related macular degeneration. *Ophthalmology.* (2014) 121:1435–44.

28. Li Z, Zhang J, Lin T, Peng W, Lu L, Hu J. Macular vascular circulation and retinal oxygen saturation changes for idiopathic macular epiretinal membrane after vitrectomy. *Acta Ophthalmol.* (2019) 97:296–302. doi: 10.1111/aos.14066

29. Cho K, Park S, Cho J, Woo S, Park K. Inner-Retinal irregularity index predicts postoperative visual prognosis in idiopathic epiretinal membrane. *Am J Ophthalmol.* (2016) 168:139–49.

30. Gediz B, Doguizi S, Ozen O, Sekeroglu M. Is choroidal vascularity index a useful marker in different stages of idiopathic epiretinal membranes? *Photodiagnosis Photodyn Ther.* (2021) 33:102110. doi: 10.1016/j.pdpdt.2020.102110

31. Chen H, Chi W, Cai X, Deng Y, Jiang X, Wei Y, et al. Macular microvasculature features before and after vitrectomy in idiopathic macular epiretinal membrane: an OCT angiography analysis. *Eye.* (2019) 33:619–28. doi: 10.1038/s41433-018-0272-3

32. Rommel F, Brinkmann M, Sochurek J, Prasuhn M, Grisanti S, Ranjbar M. Ocular blood flow changes impact visual acuity gain after surgical treatment for idiopathic epiretinal membrane. *J Clin Med.* (2020) 9:1768. doi: 10.3390/jcm9061768

33. D'Aloisio R, Carpineto P, Aharrh-Gnama A, Iafigliola C, Cerino L, Di Nicola M, et al. Early vascular and functional changes after vitreoretinal surgery: a comparison between the macular hole and epiretinal membrane. *Diagnostics.* (2021) 11:1031. doi: 10.3390/diagnostics11061031

34. Tung H, Chen Y, Tung H, Tung H, Chen S. Foveal displacement in eyes with epiretinal membrane after vitrectomy and membrane peeling. *Retina.* (2021) 41:2246–52.

35. Zobor G, Sacu S, Hollaus M, Aliyeva L, Schmalek A, Schmidt-Erfurth U, et al. The postoperative course of choroidal and central retinal thickness in epiretinal membranes with respect to membrane severity. *Ophthalmic Res.* (2021) 64:1020–8. doi: 10.1159/000519272

36. Yang H, Kim S, Jung Y, Kim K, Kim J, Yu H. Improvement of horizontal macular contraction after surgical removal of epiretinal membranes. *Eye.* (2011) 25:754–61.

37. Yüksel K, Karaküçük Y, Özkaya A, Pekel G, Baz Ö, Alagöz C, et al. Comparison of photoreceptor outer segment length in diabetic and idiopathic epiretinal membranes. *Eye.* (2015) 29:1446–52. doi: 10.1038/eye.2015.133

38. Kang E, Lee K, Koh H. Changes in choroidal thickness after vitrectomy for epiretinal membrane combined with vitreomacular traction. *Acta Ophthalmol.* (2017) 95:e393–8.

39. Rizzo S, Savastano A, Finocchio L, Savastano M, Khandelwal N, Agrawal R. Choroidal vascularity index changes after vitreomacular surgery. *Acta Ophthalmol.* (2018) 96:e950–5. doi: 10.1111/aos.13776

40. Yu Y, Teng Y, Gao M, Liu X, Chen J, Liu W. Quantitative choriocapillaris perfusion before and after vitrectomy in idiopathic epiretinal membrane by optical coherence tomography angiography. *Ophthalmic Surg Lasers Imaging Retina.* (2017) 48:906–15.

41. Casini G, Loiudice P, Lazzeri S, Pellegrini M, Ripandelli G, Figus M, et al. Analysis of choroidal thickness change after 25-gauge vitrectomy for idiopathic epiretinal membrane with or without phacoemulsification and intraocular lens implantation. *Ophthalmologica.* (2017) 237:78–84. doi: 10.1159/000452769

42. Lutty G, McLeod D. Development of the hyaloid, choroidal and retinal vasculatures in the fetal human eye. *Prog Retin Eye Res.* (2018) 62:58–76. doi: 10.1016/j.preteyeres.2017.10.001

43. Iuliano L, Fogliato G, Gorgoni F, Corbelli E, Bandello F, Codenotti M. Idiopathic epiretinal membrane surgery: safety, efficacy and patient related outcomes. *Clin Ophthalmol.* (2019) 13:1253–65. doi: 10.2147/OPTH.S176120

frontiers | Frontiers in Medicine

TYPE Original Research
PUBLISHED 06 January 2023
DOI 10.3389/fmed.2022.1037471

OPEN ACCESS

EDITED BY
Doina Gherghel,
Aston University, United Kingdom

REVIEWED BY
Doreen Schmidl,
Medical University of Vienna, Austria
Jacqueline Chua,
Singapore Eye Research Institute, Singapore

*CORRESPONDENCE
Ingeborg Stalmans
✉ ingeborg.stalmans@mac.com

SPECIALTY SECTION
This article was submitted to Ophthalmology, a section of the journal Frontiers in Medicine

RECEIVED 05 September 2022
ACCEPTED 16 December 2022
PUBLISHED 06 January 2023

CITATION
Van Eijgen J, Heintz A, van der Pluijm C, Delporte M, De Witte D, Molenberghs G, Barbosa-Breda J and Stalmans I (2023) Normal tension glaucoma: A dynamic optical coherence tomography angiography study. *Front. Med.* 9:1037471. doi: 10.3389/fmed.2022.1037471

Normal tension glaucoma: A dynamic optical coherence tomography angiography study

Jan Van Eijgen[1,2], Alexander Heintz[1], Claire van der Pluijm[1], Margaux Delporte[3], Dries De Witte[3], Geert Molenberghs[3], João Barbosa-Breda[1,4,5] and Ingeborg Stalmans[1,2]*

[1]Department of Neurosciences, Research Group of Ophthalmology, KU Leuven, Leuven, Belgium, [2]Department of Ophthalmology, University Hospitals UZ Leuven, Leuven, Belgium, [3]Leuven Biostatistics and Statistical Bioinformatics Centre (L-BioStat), KU Leuven, Leuven, Belgium, [4]Department of Surgery and Physiology, Cardiovascular R&D Centre - UnIC@RISE, University of Porto, Porto, Portugal, [5]Department of Ophthalmology, Centro Hospitalar Universitário de São João, Porto, Portugal

Purpose: Vascular dysregulation seems to play a role in the pathogenesis of glaucoma, in particular normal tension glaucoma (NTG). The development of optical coherence tomography angiography (OCTA) enabled the measurement of the retinal microvasculature non-invasively and with high repeatability. Nonetheless, only a few studies transformed OCTA into a dynamic examination employing a sympathomimetic stimulus. The goal of this study was to use this dynamic OCTA exam (1) to differentiate healthy individuals from glaucoma patients and (2) to distinguish glaucoma subcategories, NTG and high-tension primary open angle glaucoma (POAG).

Methods: Retinal vessel density (VD) in NTG patients (n = 16), POAG patients (n = 12), and healthy controls (n = 14) was compared before and during a hand grip test with a hydraulic dynamometer.

Results: At baseline, mean peripapillary VD was lower in POAG and NTG (42.6 and 48.5%) compared to healthy controls (58.1%; $p < 0.001$) and higher in NTG compared to POAG (p = 0.024) when corrected for mean arterial pressure (MAP). Peripapillary and macular (superficial and deep) VD differences were found for gender, age, and baseline MAP. No change in VD occurred (pre-/post-stimulus) in any of the groups.

Conclusion: Retinal VD loss in glaucoma patients was confirmed and the necessity to correct for gender, age and especially MAP was established. Although replication in a larger population is necessary, OCTA might not be the most suitable method to dynamically evaluate the retinal microvasculature.

KEYWORDS

glaucoma, retina, microvasculature, optical coherence tomography angiography, sympathomimetic stimulus, hand grip test

1. Introduction

Glaucoma is the leading cause of irreversible blindness globally and is estimated to affect more than 120 million people by 2040. It leads to a decline of the patient's visual field is caused by the chronic and progressive loss of the macular ganglion cell layer. Primary open angle glaucoma (POAG) represents 74% of cases and is characterized by high intraocular pressures (IOP; > 21 mmHg) without iridocorneal angle closure or other evident causes of IOP increase (1). Normal tension glaucoma (NTG; IOP ≤ 21 mmHg) is considered a subgroup of POAG and is treated similarly by lowering the IOP, even in the presence of normal IOP. This initially challenged the unquestioned association of glaucoma and elevated IOP (2). According to ethnic background the proportion of NTG can greatly differ, constituting up to 52–92% of POAG patients in Asia and 30–39% of POAG patients with European ancestry (1, 2).

The mechanical theory, for many years considered as mainstay etiology, states that the optic nerve head is mechanically damaged by elevated IOP (3, 4). The mechanical deformation of the lamina cribrosa generates axonal damage along the optic nerve (2). A thinner cornea, higher corneal hysteresis, and a higher translaminar pressure gradient over the lamina cribrosa have been reported to increase the sensitivity of the optic nerve to IOP changes (5, 6).

The vascular theorem claims that the optic neuropathy is elicited by repetitive ischaemia and reperfusion (7–9). Cardiovascular comorbidities such as ischemic heart disease, stroke, hypertension, hyperlipidemia, and metabolic syndrome are more prevalent in POAG, predominantly in NTG (7, 10, 11). Furthermore, increased vasoconstriction and decreased retinal blood flow (RBF) in response to sympathomimetic stimuli [e.g., cold pressor test (CPT) and handgrip test] in NTG and the higher prevalence of NTG in patients with migraine, Raynaud's disease, and Flammer syndrome are aligned with this theory (12–14). The development of optical coherence tomography angiography (OCTA) emphasized the focus on the vascular theory even further (15). Using OCTA, a significant constriction of the retinal vessels has been measured following a handgrip test in healthy individuals (16).

Autoregulation of the RBF, enabling continuous and stable oxygenation, is mostly dependent on the release of vasoactive metabolites, most importantly no (12, 14), and oxidative stress mediators (17, 18). Fluctuation of RBF, low systemic blood pressure (BP) with nocturnal dips and reduced nocturnal RBF have been reported in NTG (8, 19, 20). Low diastolic BP and reduced RBF in response to a handgrip test have been associated with progressive visual field (VF) defects (13, 21, 22). It is hypothesized that repetitive dipping of the BP in absence of effective autoregulation causes recurrent ischaemic damage, which is subsequently responsible for VF damage (8, 14, 23).

In recent years OCTA has been involved in dynamic measurements in combination with physiological stimuli as hypoxia, flicker light and isometric exercise (13, 24–27). Plexus-specific dilatator responses were seen after flicker stimulation, as well as dilation of the superficial capillary plexus after hypoxia, constriction of the deep capillary plexus after hyperoxia and a blunted response after hypoxia or isometric exercise in diabetes type 1 patients (24–27).

To date, only a few studies have studied the vascular reactivity in POAG and NTG separately (28). In another study comparing healthy eyes with POAG and NTG, baseline vessel density (VD) differed between healthy and glaucoma groups; but not between POAG and NTG (29).

This study aims to confirm the ability to distinguish both glaucoma groups from healthy individuals using OCTA and to, more importantly, distinguish NTG from POAG using OCTA and a sympathomimetic stimulus (handgrip test).

2. Materials and methods

2.1. Study

2.1.1. Participants

Ethical approval was obtained from the UZ/KU Leuven Ethical Research Commission (ethical approval number S62253). Patients with NTG (maximum untreated IOP ≤ 21 mmHg), high pressure POAG (maximum untreated IOP > 21 mmHg) and healthy controls were recruited from the existing cohort of the Leuven eye study (7). The most severely affected eye was selected in glaucoma patients. Exclusion criteria were: (i) diabetes mellitus, (ii) previous ocular trauma, (iii) myopia > −6D, (iv) hyperopia > 4D, or (v) aberrant BP response [drop of the mean arterial pressure (MAP) > 20 mmHg after hand grip test].

2.1.2. Protocol

Patients were instructed to avoid caffeinated drinks on the day of the examination. Baseline BP, routine ophthalmological examination, and baseline OCTA were obtained. Subsequently, maximal grip force was measured in the dominant arm using the Jamar® hydraulic dynamometer. After a 15-min break, OCTA was repeated 3 min into a handgrip test, in which the patient was instructed to hold at least one-third grip strength for 3–5 min. BP was measured every minute on the contralateral arm and the procedure was interrupted when the diastolic BP exceeded 120 mmHg or in the presence of any other adverse event.

The OCTA scan was made using the Angiovue® software (Optovue®, Fremont, CA, USA) providing an automatic quantitative measurement of VD in the fovea, perifovea and parafovea using the macular (6 mm × 6 mm) scan divided into a superficial [inner limiting membrane (ILM) to inner plexiform layer (IPL)] and deep layer [IPL to outer plexiform layer (OPL)]. Following the ETDRS grid, the peri- and parafoveal data were further divided into four quadrants: nasal, superior, temporal,

and inferior quadrant. The peripapillary vessel density was measured at the (superficial) "radial peripapillary capillary" level of the optic disc following the Garway-Heath map [six regions: temporal 90°, superotemporal (ST) 40°, inferotemporal (IT) 40°, nasal 110°, superonasal (SN) 40°, and inferonasal (IN) 40° regions] where the temporal and nasal part were divided in half [resulting in eight regions, including the new temporal-superior 45° (TS), temporal-inferior 45° (TI), nasal-superior (NS) 55°, and nasal-inferior (NI) regions 55°]. No IOP-lowering medication was discontinued for this study.

2.2. Statistical analysis

Statistical analysis was conducted in SAS9.4. The responses were not normally distributed (Shapiro–Wilk test not shown). The Kruskal–Wallis test was applied to compare unpaired continuous responses between groups. The Chi-squared test was performed in order to examine the presence of an association between categorical variables and group membership. Given the central limit theorem, linear mixed models (LMM) with random intercept (allowing subject-specific values at baseline) were considered to evaluate the effect of the hand grip test on retinal parameters while accounting for age, diagnosis, gender, baseline MAP, as well as their time dependent effect as the extent of BP change during the test. Significance was defined as $p < 0.05$.

3. Results

Fifty-one eyes of 51 patients were examined. Four participants were forced to stop within 90 s because of a diastolic BP exceeding 120 mmHg, three experienced adverse effects and two exhibited a paradoxal decrease of their MAP after the hand grip test (−30 and −35 mmHg). These data were excluded ($n = 9$).

An overview of cohort characteristics in terms of disease severity, age and gender can be found in **Table 1** (no significant differences between groups). Eventually 16 patients with NTG, 12 with POAG and 14 healthy controls participated. Ages ranged from 47 to 75 years. Few participants used antihypertensive medication: only one healthy participant used a beta blocker together with four NTG patients (one ACE inhibitor, one angiotensin II receptor blocker, one calcium channel blocker and one angiotensin II receptor blocker combined with a beta blocker). No antihypertensive medication featured in the POAG subgroup. **Supplementary Table 1** summarizes the IOP-lowering medication and surgical antecedents of the glaucoma subgroups. All glaucoma patients but one NTG patient reported chronic use of topical IOP-lowering medication. Eight NTG patients and seven POAG patients had previous IOP-lowering surgery (phaco-emulsification not included). Healthy participants were free of surgical precedents and topical medication.

3.1. Effect of the handgrip test on arterial blood pressure

At baseline, there was no significant difference in systolic, diastolic, or mean arterial BP between the three populations (**Table 2**; $p > 0.2$). In all three groups, a significant elevation of both systolic as diastolic BP (**Table 2**) during the handgrip test was noted (median 32 and 25 mmHg; $p < 0.001$).

3.2. Effect of the handgrip test on vessel density

Tables 3–5 summarize the inferred estimates of peripapillary (**Table 3**), macular superficial (**Table 4**; ILM to IPL) and macular deep (**Table 5**, IPL to OPL) VD parameters during the test. Only cells with significant estimates are shown ($p < 0.05$), others were left blank. The mean VD values and standard deviation of all regions can be found in **Supplementary Tables 2, 3**. The p-values of the LMM models can be found in the **Supplementary Tables 4–6**. The handgrip effect and matching p-values were also described for total retinal thickness parameters in the **Supplementary Tables 7–10**. The intercepts in **Tables 3–5** represent the inferred VD for male healthy participants. If significant, the other variables show an additional effect on the intercept VD. By example, adding the value for gender results in the inferred VD for female healthy participants. The variable time represents the overall effect of the handgrip test. The group (diagnosis) effect can be read from the comparative lines indicated in gray in the tables. The combination variables refer to how a certain variable influenced the VD change during the handgrip test. LMM variable changes can only be separately considered bearing in mind that the other variables -theoretically- need to remain constant.

In all peripapillary (inferred average difference for POAG of −12.9%, $p < 0.001$ and for NTG of −8.7%, $p < 0.001$) and superficial macular areas (but the fovea) (POAG and NTG −10.1%, $p < 0.001$), the baseline vessel densities in the NTG and POAG groups were significantly lower than in the control group. No significant difference was found in the VD of the fovea ($p = 0.406$), possibly due to its mainly avascular nature. The stimulus itself did, however, result in a strong decrease in the deep foveal VD (−20%, $p = 0.025$) over all groups, with even more decrease in the NTG group (−4.0 and −4.5%, $p = 0.012$ and $p = 0.008$). NTG patients systemically exhibit a significant higher baseline peripapillary VD compared to their POAG counterparts, especially in the superonasal region (+9.4%, $p = 0.006$), without significant mean deviation (MD) differences. All these baseline differences lose significance when not corrected for the baseline MAP ($p > 0.05$, data not shown). In the deep macular plexus baseline differences were only found in the NTG group compared to healthy controls on average (−5.2%, $p = 0.023$), in the superior paramacular (−5%,

TABLE 1 Descriptive statistics of the analyzed study cohort.

Group	POAG	NTG	Controls	P1	P2	P3
Number of participants	12	16	14			
Median age in years (interval)	60 (47–75)	67 (52–74)	58 (48–73)	0.424	0.045	0.025
Gender female:male	7:5	8:8	9:5	0.786	0.557	0.278
Median MD in decibels (interval)	−2.35 (−20.1–1.9)	−5.6 (−10–2.9)	NA	0.587	NA	NA

P1: Comparison of POAG patients vs. NTG patients (Kruskal–Wallis test for continuous variables. Chi-square test for categorical variables). P2: Comparison of POAG patients vs. controls (Kruskal–Wallis test for continuous variables. Chi-square test for categorical variables). P3: Comparison of NTG patients vs. controls (Kruskal–Wallis test for continuous variables. Chi-square test for categorical variables). POAG, primary open angle glaucoma; NTG, normal tension glaucoma; MD, mean deviation.

TABLE 2 Baseline and during handgrip median arterial blood pressures (mmHg).

Group	All groups	NTG	POAG	Controls	P1	P2	P3
MAP baseline (interval)	100 (73–129)	99 (73–121)	105 (89–126)	100 (83–129)	0.236	0.624	0.630
MAP handgrip (interval)	130 (97–168)	128 (97–166)	130 (98–151)	130 (107–168)	0.763	0.870	0.983
MAP difference (interval)	29 (2–80)	30 (2–54)	26 (9–38)	26 (9–80)	0.134	0.724	0.381
SYS BP baseline (interval)	141 (109–183)	139 (109–174)	140 (127–183)	139 (120–183)	0.515	0.913	0.553
SYS BP handgrip (interval)	179 (122–232)	176 (122–210)	178 (130–208)	181 (146–216)	1.000	0.496	0.456
SYS BP difference (interval)	32 (−1–96)	32 (4–63)	32 (−1–50)	32 (11–74)	0.457	0.301	0.809
DIA BP baseline (interval)	82 (55–105)	80 (55–98)	86 (68–98)	84 (56–105)	0.236	0.644	0.417
DIA BP handgrip (interval)	108 (65–145)	110 (82–144)	107 (82–127)	100 (65–145)	0.871	0.683	0.843
DIA BP difference (interval)	25 (−9–72)	28 (−9–54)	23 (8–34)	21 (−5–47)	0.109	0.957	0.392

P1: Comparison of POAG patients vs. NTG patients (Kruskal–Wallis test). P2: Comparison of POAG patients vs. controls (Kruskal–Wallis test). P3: Comparison of NTG patients vs. controls (Kruskal–Wallis test). MAP, mean arterial pressure; SYS BP, systolic blood pressure; DIA BP, diastolic blood pressure; POAG, primary open angle glaucoma; NTG, normal tension glaucoma.

$p = 0.036$) and in the perifoveal regions (inferred average −5.9%, $p = 0.021$).

Women showed a slightly higher peripapillary VD (+4.6%, $p = 0.02$) and had a more pronounced decrease of VD during handgrip test in the superficial paramacular plexus (ranging from −2.9 to −3.6%, $p < 0.048$), keeping the other covariates fixed.

Controlling for the other variables, the higher the baseline MAP, the more the superficial paramacular plexus and all regions of the deep perifoveal plexus decreased in VD during the handgrip test (ca. −0.2%/mmHg, highest $p = 0.022$).

Lastly the VD of all deep macular regions increased more (ca. +0.5%/year, highest $p = 0.003$) during the handgrip test the older the participants were, if, again, the other variables are kept constant.

4. Discussion

Known for its repeatability and discriminative power, OCTA is finding its way into glaucoma clinical care (30). So far, most OCTA research in glaucoma focussed on non-dynamic VD comparison and most time without access to normative datasets. Overall these studies show a lower circumpapillary VD, reduced prelaminar optic disc perfusion, and lower systolic acceleration of the central retinal artery in patients with glaucoma when compared to healthy controls (7, 31–33). Lower blood flow and VD at the optic disc correlates with glaucoma severity in terms of visual field mean deviation, ganglion cell complex thickness and retinal nerve fiber layer (RNFL) thickness (34). VD is also shown to decrease faster in glaucomatous eyes than in their normal counterparts (35). Even within glaucoma subclasses, the reduction in peripapillary VD is apparent in both NTG and POAG separately (36, 37). In this study, we were able to replicate this baseline, non-dynamic VD differences between glaucoma patients (NTG and POAG) and healthy controls. The key findings are summarized in the synopsis text **Box 1**.

In accordance to Lommatzsch et al. (nasal peripapillary region) (28) and Scripsema et al. (average perfused capillary density) (29) we also report on slightly higher superficial peripapillary VD in patients with NTG patients compared to POAG ones. Lommatzsch et al. only reached significance nasally, but the trend is visible in all regions (28). The race (Caucasian) and severity of the studied glaucoma groups are more or less similar in these study cohorts and the same device was used (Optovue). Secondly, Bojikian et al. reported on a lower optic disc perfusion of the prelaminar tissue in glaucoma compared to healthy controls, but without differences between NTG and POAG specifically, the latter partly in accordance to our lack of differences of within-disc VD between all groups (31). One might argue that the proclivity NTG discs have for focal defects/notching can explain why

TABLE 3 Optic nerve head vessel density optical coherence tomography angiography (OCTA) adjusted linear mixed model estimates (%).

VD region	All	Disc	Peripapil	SUP Hemi	INF Hemi	NS	NI	IN	IT	TI	TS	ST	SN
Intercept	62.4	67.0	64.3	65.9	62.8	47.2	51.4	61.3	64.8	49.5	70.1	60.0	59.0
Gender			4.6	4.4	4.6	5.7							
MAP_0													
Age													
Diagnosis													
POAG (vs. normal)	−12.9		−15.0	−13.6	−15.9	−13.6	−13.1	−17.1	−26.0	−7.8	−9.3	−19.9	−15.7
NTG (vs. normal)	−8.7		−10.0	−8.5	−12.0	−7.7	−7.9	−14.4	−20.7			−14.2	−6.3
NTG (vs. POAG)	4.3		5.0	5.2		5.9	5.1			4.5	6.2		9.4
Time													
Gender*time											−3.1		
MAP_0*time													
MAPdiff*time													
Age*time													
Diagnosis*time													
POAG (vs. normal)													
NTG (vs. normal)													
NTG (vs. POAG)													

Only significant responses ($p < 0.05$) are reported. Blank cells indicate a non-significant result. The intercept represents the inferred VD for male healthy participants. If significant, the other variables show an additional effect on the intercept VD. E.g., adding the value for gender results in the inferred VD for female healthy participants. The variable time represents the overall effect of the handgrip test. The combination variables refer to how a certain variable influenced the VD change during the handgrip test. LMM variable changes can only be separately considered bearing in mind that the other variables -theoretically- need to remain constant. VD, vessel density; MAP_0, mean arterial pressure at baseline; POAG, primary open angle glaucoma; NTG, normal tension glaucoma; MAPdiff, difference of mean arterial pressure during examination; Peripapil, peripapillary mean; SUP, superior; Hemi, hemisphere. INF, inferior; NS, NI, IN, IT, TI, TS, ST, and SN as explained in the section "2 Materials and methods".

VD might be slightly higher in all regions when comparing patients with similar visual field severity. Inferotemporally and superotemporally no differences were detected between NTG and high-tension POAG, which supports this claim since rim loss preferentially occurs in these regions for NTG. It has to be noted that the reverse was found at the Fudan University in Shanghai: lower peripapillary VD in NTG than POAG. Racial differences, higher severity levels of glaucoma (−9.11 and −9.76 dB MD for POAG and NTG, respectively where the focal differences between both groups may diminish) and the lack of BP correction might possibly explain these differences (37).

To our knowledge, we are the first to report on gender differences in VD, namely, higher peripapillary VD in women and lower VD after BP rise in the superficial parafoveal plexus.

In addition, we are the first to report on the importance of MAP measurement and correction thereof in the analysis of OCTA. Baseline VD differences between POAG and NTG only become apparent when corrected for baseline MAP. Baseline MAP was also significantly associated with macular VD changes after BP rise, possibly pointing toward an impaired dilator capacity due to endothelial damage. This strongly advocates to analyze and correct for BP levels in future OCTA research. Simultaneous correction for BP and mean ocular perfusion pressure results in collinearity and should be avoided.

In this paper, age is shown to modulate the effect of the BP rise on the VD of the deep plexus. Higher age gives rise to relatively higher post-stimulus VD. Lin et al. showed a decrease in the retinal VD of the deep vascular plexus in an aging population, corrected for confounders such as sex and controlled hypertension (38). A lower starting point (although not significant in this study) might explain why the VD change is less pronounced in the elderly compared to the young. Further research is needed regarding this point.

Interestingly, we noted a strong decrease of deep foveal VD during handgrip in all groups, even more pronounced in NTG. Further research is needed to clarify the discriminative power of the deep foveal vasculature.

In contrast to the static evaluation of VD described above, we propose a dynamic alternative to assess vascular reactivity following a sympathomimetic stimulus. Isometric exercise, as is the hand grip test, results in BP rise and retinal vasoconstriction in the healthy retina according to the protocol of Sousa et al. (16). This vasoconstrictive response was first reported in healthy individuals by Blum et al. using a retinal vessel analyser (39), later corroborated using a compacted laser

TABLE 4 Macular superficial [inner limiting membrane (ILM)-IPL] vascular plexus vessel density (OCTA) adjusted linear mixed model estimates (%).

Vessel density region (ETDRS)	All	All SUP Hemi	All INF Hemi	FAZ area	Fovea	Para fovea	Para SUP Hemi	Para INF Hemi	Para SUP	Para INF	Para NAS	Para TEM	Peri fovea	Peri SUP Hemi	Peri INF Hemi	Peri SUP	Peri INF	Peri NAS	Peri TEM
Intercept	61.4	62.2	60.5	0.4	21.2	56.6	56.8	56.3	54.9	60.0	51.4	59.9	65.5	67.6	63.3	72.7	64.1	66.9	57.8
Gender																			
MAP_0																			
Age		−0.2							−0.3					−0.3		−0.3		−0.3	
Diagnosis																			
POAG (vs. normal)	−10.1	−9.4	−10.9			−7.8	−7.5	−8.1	−7.8	−7.9	−6.3	−9.0	−10.6	−9.8	−11.4	−12.0	−12.0	−8.5	−10.0
NTG (vs. normal)	−10.1	−9.0	−11.4			−8.7	−7.6	−9.8	−8.4	−10.8	−5.8	−9.9	−10.6	−9.1	−12.1	−10.3	−13.0	−8.6	−10.5
NTG (vs. POAG)																			
Time																			
Gender*time						−3.1	−3.2	−3.0		−2.9	−3.6								
MAP_0*time						−0.1	−0.1	−0.2	−0.2	−0.2	−0.1								
MAPdiff*time				−0.001															
Age*time					0.2														
Diagnosis*time																			
POAG (vs. normal)																			
NTG (vs. normal)																			
NTG (vs. POAG)																			

Only significant responses ($p < 0.05$) are reported. Blank cells indicate a non-significant result. The intercept represents the inferred VD for male healthy participants. If significant, the other variables show an additional effect on the intercept VD. E.g., adding the value for gender results in the inferred VD for female healthy participants. The variable time represents the overall effect of the handgrip test. The combination variables refer to how a certain variable influenced the VD change during the handgrip test. LMM variable changes can only be separately considered bearing in mind that the other variables -theoretically- need to remain constant. MAP_0, mean arterial pressure at baseline; POAG, primary open angle glaucoma; NTG, normal tension glaucoma; MAPdiff, difference of mean arterial pressure during examination; SUP, superior; Hemi, hemisphere; INF, inferior; FAZ, foveal avascular zone; Para, parafovea; NAS, nasal; TEM, temporal.

10.3389/fmed.2022.1037471

TABLE 5 Macular deep [inner plexiform layer (IPL)-outer plexiform layer (OPL)] vascular plexus vessel density (OCTA) adjusted linear mixed model estimates (%).

Vessel density region (ETDRS)	All	All SUP Hemi	All INF Hemi	Fovea	Para fovea	Para SUP Hemi	Para INF Hemi	Para SUP	Para INF	Para NAS	Para TEM	Peri fovea	Peri SUP Hemi	Peri INF Hemi	Peri SUP	Peri INF	Peri NAS	Peri TEM
Intercept	52.5	49.3	55.8	39.8	54.8	54.8	54.9	52.7	59.7	50.2	56.8	55.1	51.8	58.4	51.7	55.9	49.3	63.1
Gender																		
MAP_0										0.2								
Age										−0.2								
Diagnosis																		
POAG (vs. normal)															−5.8			−5.7
NTG (vs. normal)	−5.2	−4.8	−5.5		−3.7	−4.0		−5.0				−5.9	−5.2	−6.6	−5.7	−6.7		−6.3
NTG (vs. POAG)																		
Time				−20.0														
Gender*time																		
MAP_0*time	−0.2	−0.2	−0.2		−0.2	−0.2	−0.2	−0.3	−0.2	−0.2	−0.2	−0.2	−0.2	−0.2	−0.2	−0.2	−0.3	−0.2
MAPdiff*time																		
Age*time	0.5	0.5	0.5	0.4	0.4	0.4	0.5	0.5	0.5		0.4	0.5	0.5	0.5	0.5	0.5	0.6	0.4
Diagnosis*time																		
POAG (vs. normal)																		
NTG (vs. normal)				−4.0					−4.6	−4.3								
NTG (vs. POAG)				−4.5														

Only significant responses ($p < 0.05$) are reported, blank cells indicate a non-significant result. The intercept represents the inferred VD for male healthy participants. If significant, the other variables show an additional effect on the intercept VD. E.g., adding the value for gender results in the inferred VD for female healthy participants. The variable time represents the overall effect of the handgrip test. The combination variables refer to how a certain variable influenced the VD change during the handgrip test. LMM variable changes can only be separately considered bearing in mind that the other variables -theoretically- need to remain constant. MAP_0, mean arterial pressure at baseline; POAG, primary open angle glaucoma; NTG, normal tension glaucoma; MAPdiff, difference of mean arterial pressure during examination; SUP, superior; Hemi, hemisphere; INF, inferior; Para, parafovea; NAS, nasal; TEM, temporal.

10.3389/fmed.2022.1037471

BOX 1 Synopsis.

Previously known
- Baseline peripapillary vessel density in healthy individuals is higher compared to glaucoma patients.
- Baseline peripapillary vessel density is higher in NTG than POAG for a similar level of VF damage.
- The handgrip test induces a vasoconstriction response in the retinal vessels.
- Vascular dysregulation measured following sympathomimetic test is more common found in patients with history of cold hands.

This study
- Is the first study comparing OCTA responses between POAG, NTG and healthy eyes after induced BP rise.
- Confirms higher baseline peripapillary vessel density measures in healthy individuals compared to glaucoma patients, and in NTG compared to POAG separately.
- Could not find VD changes with OCTA after BP rise in either of the studied groups.
- Proves the importance of statistical correction of OCTA measures for age, gender and especially MAP.

Doppler flowmeter (13), and lastly confirmed by Sousa et al. using OCTA (16). We, however, were unable to replicate this vasoconstriction in healthy controls except for the deep foveal vessels (all groups).

Possible explanations for this non-significant finding are multiple: (1) We used a linear mixed model to correct for participant characteristics and absolute BP values, thereby properly taking into account between- and within-patient variability, whereas Sousa et al. did not; (2) Lack of power as denoted in the post how power analysis (14 healthy participants instead of 24 in Sousa's test), but both the expected decrease of retinal thickness and VD in the glaucomatous groups favor external validity of the test; (3) Patients in our study might not always have maintained one third of their maximal measured force, however, the amplitude of our mean MAP increase (30 mmHg) matches that from Sousa et al. (28 mmHg) (16); (4) Our participants were recruited from the Leuven eye study cohort (10). Therefore, only subjects with diabetes mellitus, ocular trauma and high ametropia were excluded, whereas Sousa et al. excluded hypertensive patients, smokers, and patients using vasoactive drugs. The mean MAP values of the study of Sousa et al. going from a 91 to 118 mmHg, are ca 10 mmHg lower than ours. The Bayliss effect is the immediate constrictive, physiological reaction suggested to be the mechanism for retinal vascular constriction following sympathomimetic stimulation using the handgrip test (16, 39). While we correct for the absolute BP values in our model, chronic arterial hypertension might be responsible for this difference since it results in systemic endothelial dysfunction, thus permanently impaired vasodilation, and therefore (retinal) arteriolar narrowing (40, 41). However, exact data regarding the influence of vasoactive (systemic and topical) drugs and long lasting hypertension on retinal vascular reactivity are lacking (32).

Similar to the hand-grip test, the CPT is another sympathomimetic test used to compare autonomic dysregulation in healthy individuals and glaucoma (42, 43). Next to the Bayliss effect in isometric exercise, an additional underlying mechanism for both tests is thought to rely on an elevation in ET-1 (42). Gherghel et al. reported a significant decrease in flow velocity (retinal flowmeter) in POAG patients, without concomitant BP increase. The absent or blunted BP response following CPT might be the result of autonomic vascular dysregulation (43).

Chou et al. on the other hand showed no significant VD change after CPT (OCTA), neither when categorization was based on a history of cold hands. However, the 5-min waiting period between the end of CPT and the beginning of OCTA measurement could explain the absence of significant VD change. In fact, peripheral vascular change following a sympathetic stimulus has been reported to decline after 1 min. For this reason, we chose not to delay the OCTA exam in our current study. Additionally, it has to be noted that Chou et al. did not differentiate between glaucoma subcategories (POAG/NTG). (42) Contrary to the retinal flowmeter, OCTA cannot directly measure flow velocity (44). As flow velocity might represent haemodynamic changes more directly, this could also explain the absence of a significant haemodynamic response in our study and the study of Chou et al.

First the idea OCTA might not be suited for dynamic evaluation after isometric exercise is contradicted by other studies with significant findings (27). Second it can be argued that autoregulatory capacity could theoretically be better evaluated on larger effector vessels. More recently, Streese et al. published standard operating procedures for dynamic vessel analysis with flicker light stimulation using the dynamic vessel analyzer (DVA) (45). The vascular response measured with DVA is diminished in POAG and is proven to improve after surgical glaucoma treatment such as trabeculectomy or transscleral photocyclocoagulation (46, 47). DVA constitutes therefore a promising candidate for future dynamic studies in glaucoma given the multitude of dynamic parameters that can be extracted from its continuous measurement during flicker light stimulation.

4.1. Limitations

Due to the relatively small sample size, our study might not have had the power to pick up all VD changes, specifically for the healthy controls. Secondly, IOP was not measured during the handgrip test which disabled analysis or adjustment

for perfusion pressures. Future studies should include the simultaneous recording of IOP. Thirdly, the biasing effect of concomitant antihypertensive or topical medication use and the presence of arterial hypertension were not assessed.

5. Conclusion

We were able to validate baseline VD differences between glaucoma patients (NTG and POAG) and healthy controls. Additionally, NTG exhibited higher baseline peripapillary VDs than POAG [except for the inferotemporal and superotemporal regions, where focal rim thinning (notching) typically occurs]. Further, the importance of statistical correction for BP (MAP), gender and age in OCTA studies was proven. Future studies on OCTA should therefore correct for confounders as BP, gender and age (e.g., *via* adjusted linear mixed models). Finally, there was no significant VD change after isometric exercise in any of the groups. Further investigation with larger populations or other dynamic examination methods are recommended.

Data availability statement

The raw data supporting the conclusions of this article will be made available by the authors, without undue reservation.

Ethics statement

The studies involving human participants were reviewed and approved by the De Ethische Commissie Onderzoek UZ/KU Leuven (EC Onderzoek). The patients/participants provided their written informed consent to participate in this study.

Author contributions

JVE, JBB, and IS analyzed and interpreted the data and wrote the manuscript. DDW, MD, and GM contributed to statistical guidance, and reviewed and approved the manuscript. CP and AH reviewed and approved the manuscript. JVE, JBB, IS, and AH designed the study. IS was the guarantor of the work and had full access to all the data in the study, takes responsibility for the integrity of the data, and the accuracy of the data analysis. All authors contributed to the article and approved the submitted version.

Funding

JVE was granted a Ph.D. fellowship fundamental research from the FWO (Research Foundation Flanders).

Conflict of interest

The authors declare that the research was conducted in the absence of any commercial or financial relationships that could be construed as a potential conflict of interest.

Publisher's note

All claims expressed in this article are solely those of the authors and do not necessarily represent those of their affiliated organizations, or those of the publisher, the editors and the reviewers. Any product that may be evaluated in this article, or claim that may be made by its manufacturer, is not guaranteed or endorsed by the publisher.

Supplementary material

The Supplementary Material for this article can be found online at: https://www.frontiersin.org/articles/10.3389/fmed.2022.1037471/full#supplementary-material

References

1. Tham YC, Li X, Wong TY, Quigley HA, Aung T, Cheng CY. Global prevalence of glaucoma and projections of glaucoma burden through 2040: a systematic review and meta-analysis. *Ophthalmology.* (2014) 121:2081–90. doi: 10.1016/j.ophtha.2014.05.013

2. Esporcatte BL, Tavares IM. Normal-tension glaucoma: an update. *Arq Bras Oftalmol.* (2016) 79:270–6. doi: 10.5935/0004-2749.20160077

3. Agnifili L, Mastropasqua R, Frezzotti P, Fasanella V, Motolese I, Pedrotti E, et al. Circadian intraocular pressure patterns in healthy subjects, primary open angle and normal tension glaucoma patients with a contact lens sensor. *Acta Ophthalmol.* (2015) 93:e14–21. doi: 10.1111/aos.12408

4. Costagliola C, Agnifili L, Mastropasqua L, di Costanzo A. Low-tension glaucoma: an oxymoron in ophthalmology. *Prevent Chronic Dis.* (2019) 16:E10. doi: 10.5888/pcd16.180534

5. Vu DM, Silva FQ, Haseltine SJ, Ehrlich JR, Radcliffe NM. Relationship between corneal hysteresis and optic nerve parameters measured with spectral domain optical coherence tomography. *Graefes Arch Clin Exp Ophthalmol.* (2013) 251:1777–83. doi: 10.1007/s00417-013-2311-x

6. Hussnain SA, Alsberge JB, Ehrlich JR, Shimmyo M, Radcliffe NM. Change in corneal hysteresis over time in normal, glaucomatous and diabetic eyes. *Acta Ophthalmol.* (2015) 93:e627–30. doi: 10.1111/aos.12726

7. Barbosa-Breda J, Van Keer K, Abegão-Pinto L, Nassiri V, Molenberghs G, Willekens K, et al. Improved discrimination between normal-tension and primary open-angle glaucoma with advanced vascular examinations - the Leuven Eye Study. *Acta Ophthalmol.* (2019) 97:e50–6. doi: 10.1111/aos.13809

8. Choi J, Kook MS. Systemic and ocular hemodynamic risk factors in glaucoma. *Biomed Res Int.* (2015) 2015:141905.

9. Lestak J, Pitrova S, Nutterova E, Bartosova L. Normal tension vs high tension glaucoma: an - overview. *Cesk Slov Oftalmol Casopis Cesk Oftalmologicke Spolecnosti Slovenske Oftalmologicke Spolecnosti.* (2019) 75:55–60. doi: 10.31348/2019/2/1

10. Abegao Pinto L, Willekens K, Van Keer K, Shibesh A, Molenberghs G, Vandewalle E, et al. Ocular blood flow in glaucoma - the Leuven Eye Study. *Acta Ophthalmol.* (2016) 94:592–8.

11. Lee SH, Kim GA, Lee W, Bae HW, Seong GJ, Kim CY. Vascular and metabolic comorbidities in open-angle glaucoma with low- and high-teen intraocular pressure: a cross-sectional study from South Korea. *Acta Ophthalmol.* (2017) 95:e564–74. doi: 10.1111/aos.13487

12. Trivli A, Koliarakis I, Terzidou C, Goulielmos GN, Siganos CS, Spandidos DA, et al. Normal-tension glaucoma: pathogenesis and genetics (Review). *Exp Ther Med.* (2019) 17:563–74.

13. Gugleta K, Orgül S, Hasler PW, Picornell T, Gherghel D, Flammer J. Choroidal vascular reaction to hand-grip stress in subjects with vasospasm and its relevance in glaucoma. *Invest Ophthalmol Vis Sci.* (2003) 44:1573–80. doi: 10.1167/iovs.02-0521

14. Flammer J, Orgül S, Costa VP, Orzalesi N, Krieglstein GK, Serra LM, et al. The impact of ocular blood flow in glaucoma. *Prog Retin Eye Res.* (2002) 21:359–93. doi: 10.1016/S1350-9462(02)00008-3

15. Van Melkebeke L, Barbosa-Breda J, Huygens M, Stalmans I. Optical coherence tomography angiography in glaucoma: a review. *Ophthalmic Res.* (2018) 60:139–51. doi: 10.1159/000488495

16. Sousa DC, Leal I, Moreira S, do Vale S, Silva-Herdade AS, Aguiar P, et al. A protocol to evaluate retinal vascular response using optical coherence tomography angiography. *Front Neurosci.* (2019) 13:566. doi: 10.3389/fnins.2019.00566

17. Himori N, Kunikata H, Shiga Y, Omodaka K, Maruyama K, Takahashi H, et al. The association between systemic oxidative stress and ocular blood flow in patients with normal-tension glaucoma. *Graefes Arch Clin Exp Ophthalmol.* (2016) 254:333–41.

18. Yilmaz N, Coban DT, Bayindir A, Erol MK, Ellidag HY, Giray O, et al. Higher serum lipids and oxidative stress in patients with normal tension glaucoma, but not pseudoexfoliative glaucoma. *Bosn J Basic Med Sci.* (2016) 16:21–7. doi: 10.17305/bjbms.2016.830

19. Mroczkowska S, Ekart A, Sung V, Negi A, Qin L, Patel SR, et al. Coexistence of macro- and micro-vascular abnormalities in newly diagnosed normal tension glaucoma patients. *Acta Ophthalmol.* (2012) 90:e553–9. doi: 10.1111/j.1755-3768.2012.02494.x

20. Melgarejo JD, Eijgen JV, Maestre GE, Al-Aswad LA, Thijs L, Mena LJ, et al. Open-angle glaucomatous optic neuropathy is related to dips rather than increases in the mean arterial pressure over 24-H. *Am J Hypertens.* (2022) 35:703–14. doi: 10.1093/ajh/hpac028

21. Mallick J, Devi L, Malik PK, Mallick J. Update on normal tension glaucoma. *J Ophthalmic Vis Res.* (2016) 11:204–8. doi: 10.4103/2008-322X.183914

22. Killer HE, Pircher A. Normal tension glaucoma: review of current understanding and mechanisms of the pathogenesis. *Eye (Lond).* (2018) 32:924–30. doi: 10.1038/s41433-018-0042-2

23. Fan N, Wang P, Tang L, Liu X. Ocular blood flow and normal tension glaucoma. *Biomed Res Int.* (2015) 2015:308505. doi: 10.1155/2015/308505

24. Hommer N, Kallab M, Sim YC, Lee AX, Chua J, Tan B, et al. Effect of hyperoxia and hypoxia on retinal vascular parameters assessed with optical coherence tomography angiography. *Acta Ophthalmol.* (2022) 100:e1272–9. doi: 10.1111/aos.15077

25. Kallab M, Hommer N, Tan B, Pfister M, Schlatter A, Werkmeister RM, et al. Plexus-specific effect of flicker-light stimulation on the retinal microvasculature assessed with optical coherence tomography angiography. *Am J Physiol Heart Circ Physiol.* (2021) 320:H23–8. doi: 10.1152/ajpheart.00495.2020

26. Nesper PL, Lee HE, Fayed AE, Schwartz GW, Yu F, Fawzi AA. Hemodynamic response of the three macular capillary plexuses in dark adaptation and flicker stimulation using optical coherence tomography angiography. *Invest Ophthalmol Vis Sci.* (2019) 60:694–703. doi: 10.1167/iovs.18-25478

27. Sousa DC, Leal I, Moreira S, do Vale S, Silva-Herdade AS, Aguiar P, et al. Retinal vascular reactivity in Type 1 diabetes patients without retinopathy using optical coherence tomography angiography. *Invest Ophthalmol Vis Sci.* (2020) 61:49. doi: 10.1167/iovs.61.6.49

28. Lommatzsch C, Rothaus K, Koch JM, Heinz C, Grisanti S. Vessel density in glaucoma of different entities as measured with optical coherence tomography angiography. *Clin Ophthalmol.* (2019) 13:2527–34.

29. Scripsema NK, Garcia PM, Bavier RD, Chui TY, Krawitz BD, Mo S, et al. Optical coherence tomography angiography analysis of perfused peripapillary capillaries in primary open-angle glaucoma and normal-tension glaucoma. *Invest Ophthalmol Vis Sci.* (2016) 57:OCT611–20. doi: 10.1167/iovs.15-18945

30. Hosari S, Hohberger B, Theelke L, Sari H, Lucio M, Mardin CYOCT. Angiography: measurement of retinal macular microvasculature with spectralis II OCT angiography - reliability and reproducibility. *Ophthalmologica.* (2020) 243:75–84. doi: 10.1159/000502458

31. Bojikian KD, Chen CL, Wen JC, Zhang Q, Xin C, Gupta D, et al. Optic disc perfusion in primary open angle and normal tension glaucoma eyes using optical coherence tomography-based microangiography. *PLoS One.* (2016) 11:e0154691. doi: 10.1371/journal.pone.0154691

32. Wang YM, Shen R, Lin TPH, Chan PP, Wong MOM, Chan NCY, et al. Optical coherence tomography angiography metrics predict normal tension glaucoma progression. *Acta Ophthalmol.* (2022) 100:e1455–62. doi: 10.1111/aos.15117

33. Ko CK, Huang KI, Su FY, Ko ML. Vessel density in the macular and peripapillary areas in preperimetric glaucoma to various stages of primary open-angle glaucoma in Taiwan. *J Clin Med.* (2021) 10:5490. doi: 10.3390/jcm10235490

34. Wang X, Jiang C, Ko T, Kong X, Yu X, Min W, et al. Correlation between optic disc perfusion and glaucomatous severity in patients with open-angle glaucoma: an optical coherence tomography angiography study. *Graefes Arch Clin Exp Ophthalmol.* (2015) 253:1557–64.

35. Miguel A, Silva A, Barbosa-Breda J, Azevedo L, Abdulrahman A, Hereth E, et al. OCT-angiography detects longitudinal microvascular changes in glaucoma: a systematic review. *Br J Ophthalmol.* (2021) 106:667–75. doi: 10.1136/bjophthalmol-2020-318166

36. Shin JW, Sung KR, Lee JY, Kwon J, Seong M. Optical coherence tomography angiography vessel density mapping at various retinal layers in healthy and normal tension glaucoma eyes. *Graefes Arch Clin Exp Ophthalmol.* (2017) 255:1193–202. doi: 10.1007/s00417-017-3671-4

37. Xu H, Zhai R, Zong Y, Kong X, Jiang C, Sun X, et al. Comparison of retinal microvascular changes in eyes with high-tension glaucoma or normal-tension glaucoma: a quantitative optic coherence tomography angiographic study. *Graefes Arch Clin Exp Ophthalmol.* (2018) 256:1179–86. doi: 10.1007/s00417-018-3930-z

38. Lin Y, Jiang H, Liu Y, Rosa Gameiro G, Gregori G, Dong C, et al. Age-related alterations in retinal tissue perfusion and volumetric vessel density. *Invest Ophthalmol Vis Sci.* (2019) 60:685–93. doi: 10.1167/iovs.18-25864

39. Blum M, Bachmann K, Wintzer D, Riemer T, Vilser W, Strobel J. Noninvasive measurement of the Bayliss effect in retinal autoregulation. *Graefes Arch Clin Exp Ophthalmol.* (1999) 237:296–300.

40. Köchli S, Endes K, Infanger D, Zahner L, Hanssen H. Obesity, blood pressure, and retinal vessels: a meta-analysis. *Pediatrics.* (2018) 141:e20174090. doi: 10.1542/peds.2017-4090

41. Konukoglu D, Uzun H. Endothelial dysfunction and hypertension. *Adv Exp Med Biol.* (2017) 956:511–40.

42. Chou WY, Liu CJ, Chen MJ, Chiou SH, Chen WT, Ko YC. Effect of cold provocation on vessel density in eyes with primary open angle glaucoma: an optical coherence tomography angiography study. *Sci Rep.* (2019) 9:9384. doi: 10.1038/s41598-019-45386-7

43. Gherghel D, Hosking SL, Cunliffe IA. Abnormal systemic and ocular vascular response to temperature provocation in primary open-angle glaucoma patients: a case for autonomic failure? *Invest Ophthalmol Vis Sci.* (2004) 45:3546–54. doi: 10.1167/iovs.04-0290

44. Zhu J, Merkle CW, Bernucci MT, Chong SP, Srinivasan VJ. Can OCT angiography be made a quantitative blood measurement tool? *Appl Sci (Basel).* (2017) 7:687. doi: 10.3390/app7070687

45. Streese L, Lona G, Wagner J, Knaier R, Burri A, Nève G, et al. Normative data and standard operating procedures for static and dynamic retinal vessel analysis as biomarker for cardiovascular risk. *Sci Rep.* (2021) 11:14136. doi: 10.1038/s41598-021-93617-7

46. Gugleta K, Kochkorov A, Waldmann N, Polunina A, Katamay R, Flammer J, et al. Dynamics of retinal vessel response to flicker light in glaucoma patients and ocular hypertensives. *Graefes Arch Clin Exp Ophthalmol.* (2012) 250:589–94. doi: 10.1007/s00417-011-1842-2

47. Selbach JM, Schallenberg M, Kramer S, Anastassiou G, Steuhl KP, Vilser W, et al. Trabeculectomy improves vessel response measured by dynamic vessel analysis (DVA) in glaucoma patients. *Open Ophthalmol J.* (2014) 8:75–81. doi: 10.2174/1874364101408010075

frontiers | Frontiers in Medicine

TYPE Original Research
PUBLISHED 09 January 2023
DOI 10.3389/fmed.2022.1080052

OPEN ACCESS

EDITED BY
Doina Gherghel,
Aston University, United Kingdom

REVIEWED BY
Hui Xiao,
Sun Yat-sen University, China
André Ferreira,
Centro Hospitalar Universitário do Porto, Portugal

*CORRESPONDENCE
Katja Hatz
✉ katja.hatz@vista.ch

†These authors have contributed equally to this work

SPECIALTY SECTION
This article was submitted to Ophthalmology, a section of the journal Frontiers in Medicine

RECEIVED 25 October 2022
ACCEPTED 16 December 2022
PUBLISHED 09 January 2023

CITATION
Türksever C, Hoffmann L and Hatz K (2023) Peripapillary and macular microvasculature in neovascular age-related macular degeneration in long-term and recently started anti-VEGF therapy versus healthy controls.
Front. Med. 9:1080052.
doi: 10.3389/fmed.2022.1080052

Peripapillary and macular microvasculature in neovascular age-related macular degeneration in long-term and recently started anti-VEGF therapy versus healthy controls

Cengiz Türksever[1,2†], Laura Hoffmann[1,3†] and Katja Hatz[1,2*]

[1]Medical Retina Department, Vista Augenklinik Binningen, Binningen, Switzerland, [2]Faculty of Medicine, University of Basel, Basel, Switzerland, [3]Augenklinik, Charité – Universitätsmedizin Berlin, Berlin, Germany

Aim: To investigate the peripapillary and macular microvasculature in neovascular age-related macular degeneration (nAMD) in recently started versus long-term anti-vascular endothelial growth factor (VEGF) therapy and healthy controls.

Methods: Eyes with nAMD treated in a treat-and-extend regimen were assigned to group 1 (<5 injections) or 2 (≥20 injections) whereas group 3 constituted the healthy age-matched controls. Blood flow signals were acquired using PLEX® Elite 9000 swept-source optical coherence tomography angiography (OCTA) of the macular and peripapillary regions. Mean ganglion cell complex (GCC) thickness values were quantified using spectral-domain optical coherence tomography (SD-OCT).

Results: Including 80 eyes whereof 40 controls, macular superficial perfusion density was significantly reduced in group 1 and 2 compared to controls ($p < 0.001$; $p = 0.010$) without a difference between groups 1 and 2. Peripapillary perfusion parameters did not correlate with post-operative intraocular pressure (IOP) or number of anti-VEGF injections. Mean peripapillary flux index was significantly lower in group 2 than in controls ($p = 0.023$) and significantly decreased in the nasal quadrants for both AMD groups compared to group 3 ($p = 0.013$; $p < 0.001$). Mean peripapillary perfusion density was significantly reduced in both AMD groups compared to controls (0.515 ± 0.02 versus 0.556 ± 0.03, $p < 0.0001$).

Conclusion: Frequency of anti-VEGF treatment in nAMD and post-operative IOP showed no correlation with peripapillary perfusion parameters, but anti-VEGF treated nAMD patients exhibited partly altered peripapillary perfusion

compared to healthy controls. Reduced macular perfusion density of the inner retina in anti-VEGF treated nAMD compared to healthy controls might be discussed as an anti-VEGF treatment effect or a characteristic of nAMD.

KEYWORDS

optical coherence tomography angiography, age-related macular degeneration, microvasculature, intraocular pressure, perfusion density, flux index

Introduction

Neovascular age-related macular degeneration (nAMD) is the leading cause of blindness in elderly patients in industrialized countries (1). Currently, standard treatment of nAMD follows vascular endothelial growth factor (VEGF) inhibition using approved drugs such as ranibizumab, aflibercept, and brolucizumab in different treatment regimens. Efficacy and safety of the molecules were proved by large scale studies (2–5).

Short-term rise of intraocular pressure (IOP) is a well-recognized and very common complication of intravitreal anti-VEGF injection. A recent meta-analysis reported a significantly increased IOP on the day of injection with a normalization of IOP after 1 week (6). Some studies also suggest a sustained rise in IOP after 2 years of treatment in repeatedly injected eyes (7, 8). Recurrent anti-VEGF injections have been associated with a significant reduction in retinal nerve fiber layer (RNFL) thickness after 12 months, yet its clinical relevance remains uncertain (6).

With increased IOP after intravitreal anti-VEGF injection possible consequences on retinal perfusion have been assessed by retinal oximetry. An altered retinal oxygen metabolism has been discovered in different retinal diseases (9). A reduced oxygen extraction, which corresponds to the arteriovenous difference (AVD) in oxygen saturation, compared to healthy controls has been shown in nAMD whereas the vessel diameters were similar (10). While the impact of the choroidal vasculature in nAMD has been well-established, a decrease in blood flow velocity in retinal arteries as measured by the retinal function imager has been reported in patients with nAMD as well (11).

The development of optical coherence tomography angiography (OCTA) enables a non-invasive analysis of the vessel density in the different layers of the retina and the choriocapillaris (CC). A parapapillary microvascular dropout correlating with the reduced RNFL thickness has been described in glaucomatous eyes (12). A retrospective analysis comparing eyes with exudative AMD and non-exudative AMD revealed a significantly decreased retinal vessel density in the superficial capillary plexus in the group with exudative AMD, especially in the parafoveal region (13). However, in nAMD after a loading phase of anti-VEGF injections the macular vessel density of the retina and the CC remained unchanged compared to baseline (14).

Currently, there is still limited data on the effects of repeated intravitreal injections on peripapillary and macular retinal vessel density. Therefore, the aim of this study was to examine and compare OCTA blood flow indices of the macular and optic nerve head (ONH) regions in patients with nAMD with recently started and long-term anti-VEGF treatment, respectively, and healthy controls.

Materials and methods

This cross-sectional, single-visit study was conducted at Vista Augenklinik Binningen, Switzerland. The study was approved by the local ethics committee (Ethikkommission Nordwestschweiz–EKNZ, EKNZ-No 2018-02043) and registered at clinicaltrials.gov (NCT 03833830). The research was conducted in accordance with the tenets of the Declaration of Helsinki and Good Clinical Practice (ICH-GCP).

All subjects gave written informed consent after information about the study. Patients with a clinical diagnosis of nAMD confirmed by a retina specialist and fulfilling the inclusion criteria were recruited consecutively at the Medical Retina department. Eligible patients were required to have been treated for sub- or juxtafoveal MNV due to nAMD with anti-VEGF intravitreal injections either for <5 times (group 1; short-term treatment eyes) or at least 20 times (group 2; long-term treatment eyes). Exclusion criteria were a diagnosis of glaucoma/ocular hypertension at baseline of anti-VEGF treatment, history of retinal vascular disorders like diabetic retinopathy, retinal vein/arterial occlusive disease, or uveitis, history of papillary disease which might interfere with interpretation of peripapillary imaging evaluation such as severe tilted disc, parapapillary MNV, papillary drusen, optic nerve neuritis, or papillary edema and inability to perform study imaging of sufficient quality. For each patient, only one eye was selected and included in the study. Age- and sex-matched healthy volunteers were recruited at the General Ophthalmology department. Study examinations took place between December 2018 and

January 2021. Intravitreal injections (0.5 mg ranibizumab–Lucentis®, Novartis, Basel, Switzerland; 2 mg aflibercept – Eylea®, Bayer, Basel, Switzerland) were performed following a standardized procedure (15) in an operating room setting.

For each patient and healthy subject one study visit was performed including best-corrected visual acuity measurement (BCVA), dilated biomicroscopic fundus examination, IOP measurement prior and 10 min after the intravitreal injection, spectral-domain optical coherence tomography (SD-OCT) (Spectralis, Heidelberg Engineering, Inc., Heidelberg, Germany) and swept source OCTA (SS-OCTA) (PLEX Elite 9000, Carl Zeiss Meditec, Dublin, USA) (**Figure 1**). Apart from BCVA measurement all examinations were performed in mydriatic pupil state. SD-OCT scans were acquired using an established protocol comprising 19 horizontal scans of 6 mm length (volume scan) in follow-up modus and a 6 mm star scan centered on the fovea. After manual correction of segmentation errors, macular SD-OCT scans were analyzed for central retinal thickness (CRT), characteristics of sub- and intraretinal fluid and vitreomacular interface. Circumpapillary RNFL thickness and macular ganglion cell complex (GCC) thickness (RNFL + ganglion cell layer + inner plexiform layer) were measured within the central 3 mm using an ETDRS grid overlay (**Figure 1E**). All SD-OCT images were reviewed and assessed by the same observer (CT) following standard evaluation protocols. IOP elevation following the intravitreal injection was calculated as the difference in IOP value prior and 10 min after the injection.

The OCTA scan protocols for imaging vessel density and peripapillary flux index included a 6 × 6 mm scan centered on the fovea and a 6 × 6 mm scan centered on the ONH (**Figure 2**). Each 6 × 6 mm section consisted of 500 A-scans per B-scan. Vessel density measurement for superficial and deep retinal layer were performed separately in the macular region. Vessel density and flux index measurements within the 2 mm annulus of the 6 × 6 mm ONH-centered scan were evaluated.

Quality assessment of each SS-OCTA measurement was performed by an OCTA-experienced ophthalmologist (CT) and similarly graded as previously described by Ali et al. (16):

- Grade 0 (degraded image quality): vascular structures are hardly visible, loss of signal, band of motion artefacts (excluded from study).
- Grade I (good image quality): visible vascular structures, no or very decent motion artefacts, visible vascular margins at the 6 mm central part of the OCTA image.
- Grade II (very good image quality): continuous vascular structures, very subtle lines of motion artefact, vessels are clearly visible.
- Grade III (excellent image quality): continuous vascular structures, no lines of motion artefact, vessels are perfectly visible.

In addition, blood pressure, body mass-index (BMI), and pulse pressure were measured and calculated for each subject.

Statistical analysis

Statistical analyses were carried out with SPSS version 24.0 for Windows (SPSS, Chicago, IL, USA). Continuous variables were described as mean ± standard deviation (SD) or percentages. For comparison of means between different subgroups an ANOVA analysis applying a Bonferroni adjustment were performed. Correlation analyses (univariate) followed Pearson's test. A p-value < 0.05 was considered statistically significant.

Results

While a total of 94 eyes of 94 subjects were recruited in this study, 14 eyes were excluded due to insufficient (grade 0) image quality. In total, 80 eyes of 80 subjects with good, very good or excellent OCTA image quality (grade 1, 2, or 3) were included for further analysis. Forty eyes were included in the nAMD groups whereof 19 eyes in group 1 (<5 injections) and 21 eyes in group 2 (>20 anti-VEGF injections) at the time of the study visit as well as 40 eyes in the control group. Twenty-two eyes (55%) received ranibizumab, 6 (15%) aflibercept, and 12 (30%) mixed agents. Treatment distribution in group 1 was 94.7% (n = 18) ranibizumab and 5.3% (n = 1) aflibercept and in group 2 19% (n = 4) ranibizumab, 23.8% (n = 5) aflibercept, and 57.1% (n = 12) mixed agents. Demographic and functional characteristics are summarized in **Table 1**.

The mean number of prior intravitreal injections in eyes with nAMD was 19.97 ± 20.56 (range 1– 85) with on average 2.79 ± 1.03 in group 1 and 35.52 ± 17.00 in group 2. The OCTA examination in groups 1 and 2 took place after on average 41.45 ± 16.5 days following the last intravitreal injection. A total of 13 (32.5%) out of 40 eyes showed an elevation of IOP > 25 mmHg 10 min after the intravitreal injection with a maximal increase of 25 mmHg following the injection. Interestingly, in one eye IOP was significantly reduced from 18 to 6 mmHg after the injection, probably due to a subtle leakage in a very thin sclera after 31 intravitreal injections.

Hemodynamics in patients with nAMD

Hemodynamic parameters are shown in **Table 1**. While there was no significant difference between the subgroups in

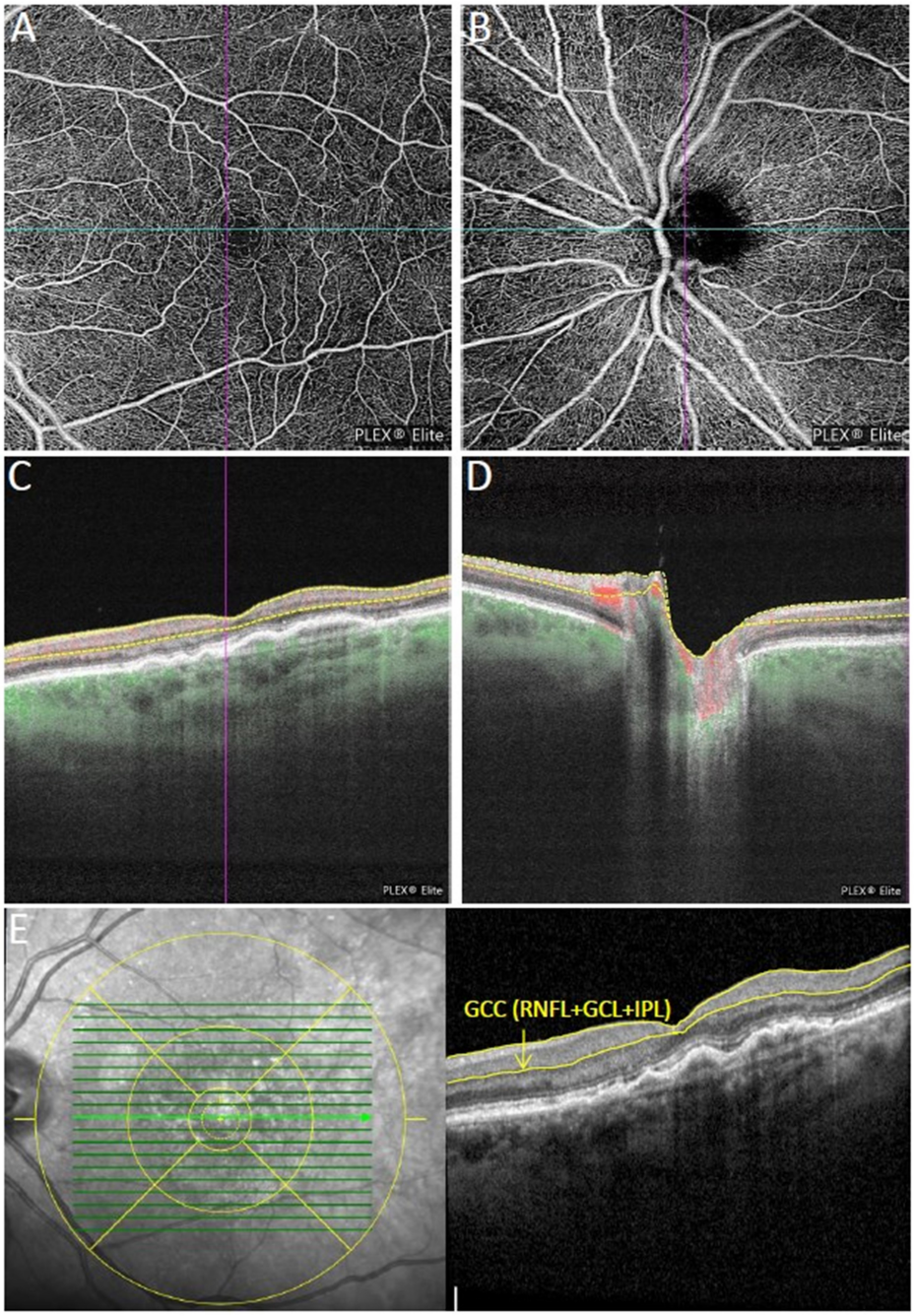

FIGURE 1
Multimodal imaging of an eye with neovascular age-related macular degeneration (nAMD) previously treated with four intravitreal injections of aflibercept. **(A,B)** Show the macular and peripapillary optical coherence tomography angiography (OCTA) 6 × 6 mm en-face scans graded as qualitatively very good. Vessel density measurement for superficial **(C)**, and deep retinal layer were performed separately in the macular region, while vessel density and flux index measurements of the optic nerve head (ONH) were evaluated within the 2 mm annulus of the 6 × 6 mm ONH-centered scan **(D)**. **(E)** Macular ganglion cell complex (GCC) thickness in the central 3 mm (retinal nerve fiber layer (RNFL) + ganglion cell layer + inner plexiform layer) were measured using the segmentation tool with an ETDRS grid overlay centered on the fovea.

mean BMI, heart rate per minute, and diastolic blood pressure, mean systolic blood pressure was significantly higher in group 2 compared to group 1 and the controls (p = 0.048; p = 0.003, respectively). Likewise, pulse pressure was significantly higher in group 2 than in group 1 (p = 0.003) and controls (p = 0.012). The BMI of the subjects was equally distributed with 11 and 14 cases of overweight as well as 5 and 4 cases of obesity in the control group and the nAMD subgroups, respectively.

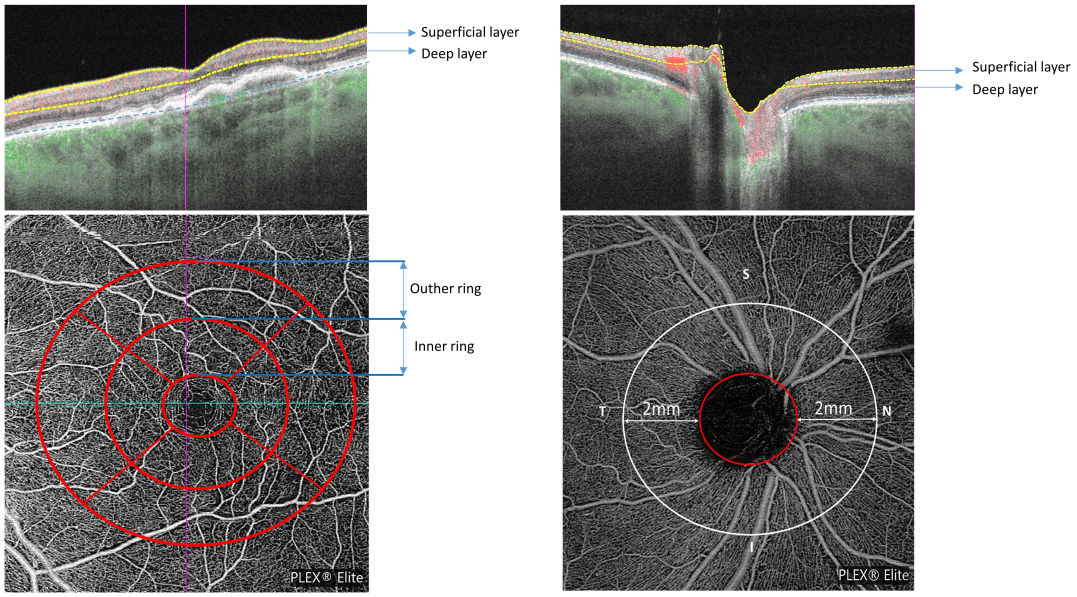

FIGURE 2
Macular and peripapillary optical coherence tomography angiography (OCTA) 6 × 6 mm scans with B-scans **(top row)** showing the location of superficial and deep layers and en-face scans **(bottom row)** with macular ETDRS grid **(left)** and the 2 mm annulus of the 6 × 6 mm optic nerve head (ONH)-centered scan **(right)**.

Spectral domain optical coherence tomography of the optic disc and macula

Main OCT parameters are summarized in Table 2.

In the nAMD groups, 20 eyes (50%) exhibited macular subretinal and 5 (12.5%) intraretinal fluid. The mean peripapillary RNFL was not significantly different between the subgroups (Table 2). There was no correlation between RNFL thickness and number of anti-VEGF injections in the subgroups ($r = 0.215$; $p = 0.183$). The mean GGC in the central 3 mm was thicker in group 2 compared to group 1 (103.8 μm ± 9.49 versus 97.68 μm ± 9.95; $p = 0.093$), particularly in the inferior part of the macula (120.95 μm ± 12.93 versus 110.42 μm ± 14.93, $p = 0.018$).

OCTA image quality

All images of the 80 included patients fulfilled the eligibility criteria for inclusion to study. However, due to fixation difficulties the image quality was better in controls than in eyes with nAMD. In the latter macular OCTA image quality was graded as excellent in 13 eyes (32.5%), as very good in 18 eyes (45%), and as good in 9 eyes (22.5%). Regarding the peripapillary area OCTA image quality was excellent in 12 eyes (30%), very good in 16 eyes (40%), and good in 12 eyes (30%). In the control group 26 eyes (65%) had excellent macular OCTA image quality, 10 eyes had very good (25%), and only 4 eyes (10%) showed good image quality. In the peripapillary region, the distribution of excellent, very good, and good image quality was 60, 30, and 10%, respectively. While the proportion of pseudophakic eyes was comparable between the nAMD groups and the control group (55 versus 60%), no subject presented with significant cataract formation.

Macular perfusion characteristics

Perfusion characteristics of the macula are shown in Table 3.

The deep perfusion density in both the central 3 and 6 mm were not significantly different between the three subgroups. However, the superficial perfusion density in the central 3 and 6 mm were found to be higher in controls than in group 1 ($p < 0.0001$; $p = 0.001$, respectively) and group 2 ($p = 0.01$; $p = 0.001$, respectively) (Table 3). Furthermore, in eyes with nAMD the presence of subretinal fluid within the 6 mm ETDRS grid ($N = 20$) was associated with a better superficial macular perfusion density in the central 6 mm ($p = 0.036$) compared to eyes without subretinal fluid ($n = 20$).

Peripapillary perfusion characteristics

The mean average peripapillary flux index was significantly reduced in group 2 compared to the control group (0.377 ± 0.04 versus 0.415 ± 0.06; $p = 0.023$) (see Table 4).

TABLE 1 Demographic and hemodynamic characteristics of subjects.

Groups	Number of subjects	Mean age, years (±SD)	Female sex (*n*, %)	Mean BCVA (±SD), (ETDRS letters)	Mean IOP change after injection; mmHg
Demographic characteristics					
Controls	40	78.4 ± 5.1	21 (52.5)	81.4 ± 5.4	
Group 1	19	79.0 ± 6.6	12 (63.1)	74.7 ± 13.6	7.57 ± 6.9
Group 2	21	77.9 ± 7.2	9 (42.9)	70.0 ± 20.6	10.0 ± 8.1
	Mean ± SD		Comparison between groups		*p*-values between groups *post-hoc* test with ANOVA
Hemodynamic characteristics					
BMI (kg/mm^2)	Controls	24.6 ± 3.35	Controls	Group 1	1.000
	Group 1	24.4 ± 4.06	Controls	Group 2	1.000
	Group 2	25.2 ± 3.26	Group 1	Group 2	1.000
Pulse pressure (mmHg)	Controls	61 ± 15.68	Controls	Group 1	0.863
	Group 1	55.9 ± 21.35	Controls	Group 2	**0.012**
	Group 2	74.6 ± 15.03	Group 1	Group 2	**0.003**
Systolic blood pressure (mmHg)	Controls	143 ± 16.66	Controls	Group 1	0.365
	Group 1	134.5 ± 26.58	Controls	Group 2	**0.048**
	Group 2	155.9 ± 16.89	Group 1	Group 2	0.003
Diastolic blood pressure (mmHg)	Controls	81.9 ± 8.36	Controls	Group 1	0.793
	Group 1	78.6 ± 11.23	Controls	Group 2	1.000
	Group 2	81.4 ± 13	Group 1	Group 2	1.000
Heart rate per minute	Controls	69.7 ± 7.96	Controls	Group 1	*0.092*
	Group 1	76 ± 12.41	Controls	Group 2	1.000
	Group 2	70.7 ± 12.15	Group 1	Group 2	0.329

Bold values represented the significant *p*-values.

The biggest differences when comparing group 2 and the controls were observed for the nasal peripapillary flux index (0.354 ± 0.03 versus 0.407 ± 0.05; $p < 0.0001$) and the temporal flux index of the ONH ($p = 0.012$). While in group 1 mean average peripapillary flux index was not significantly lower compared to the controls (0.392 ± 0.05 versus 0.415 ± 0.06, $p = 0.383$), the nasal peripapillary flux index was also significantly decreased compared to controls ($p = 0.013$). Interestingly, there was no significant difference in the flux indices between the two nAMD subgroups (0.371 ± 0.05 versus 0.407 ± 0.05, $p = 0.995$). Furthermore, there was no correlation between the peripapillary flux index in eyes with nAMD and neither IOP elevation after the injection nor the number of anti-VEGF injections received ($r = 0.130$, $p = 0.425$; $r = -0.135$, $p = 0.405$). The time period after the last injection was not significantly associated with neither peripapillary nor macular microvascular parameters.

The mean average peripapillary perfusion density was significantly reduced in the AMD groups compared to controls (0.515 ± 0.02 versus 0.556 ± 0.03, $p < 0.0001$) while there was no difference between group 1 and 2 ($p = 0.779$). This difference in peripapillary perfusion density between AMD subjects and controls persisted in all four peripapillary subquadrants ($p < 0.01$).

Discussion

While several studies evaluated macular microvasculature in macular diseases treated with intravitreal anti-VEGF injections (13, 14) to the best of our knowledge, this study is the first to evaluate peripapillary microvasculature in eyes with long-term versus recently started anti-VEGF therapy for nAMD compared to healthy controls.

Previous OCTA studies described the impact of OCTA image quality on the measurement itself (17, 18). Therefore, in our study we only included eyes with good, very good or excellent OCTA images based on the quality assessment as described by Ali et al. (16). In our study, better macular and peripapillary image quality was found

TABLE 2 Main optical coherence tomography (OCT) parameters.

SD-OCT parameters	Mean ± SD		Comparison between groups		*p*-values between groups *post-hoc* test with ANOVA
Central retinal thickness (μm)	Controls	278.1 ± 23.9	Controls	Group 1	0.603
	Group 1	294.1 ± 74.1	Controls	Group 2	1.000
	Group 2	270.1 ± 40.4	Group 1	Group 2	0.279
Mean peripapillary RNFL thickness (μm)	Controls	83.3 ± 7.5	Controls	Group 1	0.776
	Group 1	80.7 ± 9.1	Controls	Group 2	0.683
	Group 2	86.0 ± 8.6	Group 1	Group 2	0.136
Mean macular GCC thickness in central 3 mm (μm)	Controls	99.3 ± 7.8	Controls	Group 1	1
	Group 1	97.7 ± 9.9	Controls	Group 2	0.190
	Group 2	103.8 ± 9.5	Group 1	Group 2	0.093

TABLE 3 Macular perfusion characteristics.

Macular perfusion density based on SS-OCTA	Mean ± SD		Comparison between groups		Mean difference	*p*-values between groups* *post-hoc* test with ANOVA
Superficial perfusion density of the macula						
Central 3 mm	Controls	0.409 ± 0.035	Controls	Group 1	0.052	**0.000**
	Group 1	0.357 ± 0.047	Controls	Group 2	0.032	**0.010**
	Group 2	0.376 ± 0.04	Group 1	Group 2	−0.02	0.374
Central 6 mm	Controls	0.421 ± 0.036	Controls	Group 1	0.043	**0.001**
	Group 1	0.378 ± 0.043	Controls	Group 2	0.039	**0.001**
	Group 2	0.382 ± 0.039	Group 1	Group 2	−0.003	1.000
Deep perfusion density of the macula						
Central 3 mm	Controls	0.234 ± 0.064	Controls	Group 1	0.019	1.000
	Group 1	0.215 ± 0.095	Controls	Group 2	0.009	1.000
	Group 2	0.225 ± 0.093	Group 1	Group 2	−0.01	1.000
Central 6 mm	Controls	0.196 ± 0.060	Controls	Group 1	−0.024	0.776
	Group 1	0.220 ± 0.095	Controls	Group 2	−0.01	1.000
	Group 2	0.210 ± 0.090	Group 1	Group 2	0.014	1.000

*p-values adjusted with the Bonferroni adjustment.
Bold values represented the significant p-values.

in healthy controls compared to eyes with nAMD. This difference probably resulted from the impaired fixation ability due to the reduced visual acuity and/or central scotomas in nAMD patients.

While the subgroups were well balanced in terms of age, sex and BMI, an increased systolic blood pressure, and pulse pressure in nAMD patients following long-term anti-VEGF therapy compared to controls and nAMD patients with recently started intravitreal anti-VEGF treatment was noted. Higher pulse pressure is defined as an increased arterial stiffness and is a well-known risk factor for several cardiovascular diseases. While higher pulse pressure has been associated with an increased risk for late nAMD, (19) it cannot be excluded to be a systemic side-effect of the long-term anti-VEGF therapy (20). Furthermore, the FEAR study described a transient increase in blood pressure associated with intravitreal injections attributed to an anxiety response which may constitute a cardiovascular risk factor in frequent injections (21).

Due to the acute IOP changes caused by intravitreal injections, an acute decrease in angiographic PD in the overall optic nerve head, especially temporally, has been shown (22). A recent meta-analysis reported on a reduction of peripapillary RNFL thickness after recurrent injection of anti-VEGF with questionable clinical relevance (6).

TABLE 4 Peripapillary perfusion characteristics.

Peripapillary flux index based on SS-OCTA	Mean ± SD		Comparison between groups		*p*-values between groups* *post-hoc* test with ANOVA
Average	Controls	0.415 ± 0.056	Controls	Group 1	0.383
	Group 1	0.392 ± 0.049	Controls	Group 2	**0.023**
	Group 2	0.377 ± 0.042	Group 1	Group 2	0.995
Temporal	Controls	0.402 ± 0.052	Controls	Group 1	*0.099*
	Group 1	0.375 ± 0.034	Controls	Group 2	**0.012**
	Group 2	0.367 ± 0.036	Group 1	Group 2	1.000
Superior	Controls	0.425 ± 0.070	Controls	Group 1	1.000
	Group 1	0.414 ± 0.067	Controls	Group 2	0.309
	Group 2	0.395 ± 0.061	Group 1	Group 2	1.000
Nasal	Controls	0.407 ± 0.048	Controls	Group 1	**0.013**
	Group 1	0.371 ± 0.045	Controls	Group 2	**0.000**
	Group 2	0.354 ± 0.033	Group 1	Group 2	0.668
Inferior	Controls	0.434 ± 0.070	Controls	Group 1	0.602
	Group 1	0.410 ± 0.062	Controls	Group 2	*0.065*
	Group 2	0.392 ± 0.059	Group 1	Group 2	1.000

*p-values adjusted with the Bonferroni adjustment.
Bold values represented the significant p-values.

However, studies assessing the impact of repeated IVIs on the peripapillary microvasculature are lacking so far. In our study mean peripapillary perfusion density in all subquadrants was significantly reduced in both AMD groups compared to controls without a difference between the AMD eyes. Further, the average peripapillary flux index in eyes with frequent injections was significantly reduced, preferentially in the temporal and nasal area, compared to the controls in the absence of a correlation with neither IOP elevation after the injection nor the number of anti-VEGF injections received. No differences in peripapillary RNFL thickness between the subgroups were found. While several risk factors for a sustained and delayed elevation of IOP in eyes undergoing anti-VEGF injections like the cumulative number of IVIs, intervals between injections and preexisting glaucoma have been described, (23) the etiology of the decrease in peripapillary flux index in frequently treated eyes likely seems multifactorial. Hence, altered peripapillary perfusion may as well represent a characteristic of AMD itself.

In our study, superficial but not deep macular perfusion density were reduced in both nAMD groups compared to controls supporting previously reported results showing decreased superficial macular vessel density in nAMD compared to healthy controls and non-exudative AMD (13). Lee at al. showed a decreased macular vessel density with age but failed to report a linear correlation with the number of previous intravitreal injections (13). Likewise in our study, no difference in perfusion density was observed between long-term and short-term treated nAMD groups. Given the cross-sectional character of our study the pathogenesis of the reduced superficial perfusion density remains unclear but a possible explanations might include a vasoconstrictor effect of anti-VEGF therapy with immediate effect upon the first injection as well as a characteristic of AMD itself. Rosen et al. described a decrease of the superficial parafoveal perfusion density immediately after intravitreal injection (22). Hikichi et al. reported a deterioration of the vessel density of the deep capillary plexus and the CC but not the superficial capillary plexus with long-term anti-VEGF therapy (24). However, given the different OCTA algorithms applying variable boundaries for layer segmentation, comparisons between studies must consider the differing measurement methodologies (25).

It has been suggested that in nAMD proportionally less oxygen is extracted by the retinal vessels as a consequence of decreased oxygen demand by the atrophic tissue. However, minutes after anti-VEGF injection, a significant increase in AVD has been observed in patients with nAMD while vessel diameter remained unchanged (26). This short-term elevation in oxygen consumption is attributed either to an increased metabolism or a reduced blood flow due to a transient peak in IOP. However, in healthy controls a similar rise in AVD after an induced increase in IOP has been observed while retinal blood flow remained stable (27). Mendrinos et al. reported on a long-term a reduction in retinal artery diameter after single or repeated intravitreal anti-VEGF injections in nAMD (28). These findings could suggest a pharmacological vasoconstrictor effect of anti-VEGF treatment.

Another novel finding of our study consists in the better macular perfusion density in eyes with central subretinal fluid. Possibly, these eyes exhibit greater nAMD activity resulting in an increased oxygen demand. Beforehand, subretinal fluid has been discussed to be associated with an improved long-term BCVA outcome (29). Likewise, the FLUID study suggested to tolerate SRF while shifting toward an intraretinal fluid focused disease management (30).

Limitations of this study are its cross-sectional character rather than a long-term follow-up study and the limited number of patients. On the other hand, strengths of our study consisted in the recruiting of a sex- and age-matched healthy control group and the exclusion of images with poor image quality.

To conclude, we report an increased pulse pressure in long-term anti-VEGF treated subjects and decreased macular superficial perfusion density in nAMD eyes which might be linked to systemic and local side-effects of the treatment or reflect characteristics of nAMD. While alterations in the peripapillary microvasculature were observed partly in all nAMD, but especially in frequently treated eyes, neither a correlation to post-operative IOP elevation nor number of previous injections could be established. Due to the cross-sectional character of the study definite conclusion concerning the pathogenesis of the observed alterations cannot be deduced. However, closer clinical evaluation of patients in need of frequent intravitreal injections over the long-term is advisable. Therefore, larger prospective studies including possible confounders are warranted to assess the impact of repeated intravitreal injections on the retinal microvasculature and possible cardiovascular side-effects.

Data availability statement

On-request anonymized data can be shared if local ethics committee agrees. Requests to access the datasets should be directed to KH, katja.hatz@vista.ch.

Ethics statement

The studies involving human participants were reviewed and approved by Ethikkommission Nordwestschweiz EKNZ. The patients/participants provided their written informed consent to participate in this study.

Author contributions

CT: study concept, acquisition and interpretation of data, statistics, and writing of manuscript. LH: acquisition and interpretation of data, statistics, and writing of the manuscript. KH: study concept, supervision, and revision of the manuscript. All authors critically reviewed the manuscript and approved the final version.

Funding

This study was supported in part by CENAUG Foundation Liechtenstein (grant to KH, Vista Augenklinik).

Acknowledgments

The authors thank Mrs. Christine Knodel and Mrs. Susanne Müller for their valuable support in data and image acquisition as well as manuscript preparation.

Conflict of interest

The authors declare that the research was conducted in the absence of any commercial or financial relationships that could be construed as a potential conflict of interest.

Publisher's note

References

1. Wong WL, Su X, Li X, Cheung CM, Klein R, Cheng CY, et al. Global prevalence of age-related macular degeneration and disease burden projection for 2020 and 2040: a systematic review and meta-analysis. *Lancet Glob Health.* (2014) 2:e106–16. doi: 10.1016/S2214-109X(13)70145-1

2. Rosenfeld PJ, Brown DM, Heier JS, Boyer DS, Kaiser PK, Chung CY, et al. Ranibizumab for neovascular age-related macular degeneration. *N Engl J Med.* (2006) 355:1419–31. doi: 10.1056/NEJMoa054481

3. Brown DM, Kaiser PK, Michels M, Soubrane G, Heier JS, Kim RY, et al. Ranibizumab versus verteporfin for neovascular age-related macular degeneration. *N Engl J Med.* (2006) 355:1432–44. doi: 10.1056/NEJMoa062655

4. Heier JS, Brown DM, Chong V, Korobelnik JF, Kaiser PK, Nguyen QD, et al. Intravitreal aflibercept (VEGF trap-eye) in wet age-related macular degeneration. *Ophthalmology*. (2012) 119:2537–48. doi: 10.1016/j.ophtha.2012.09.006

5. Dugel PU, Koh A, Ogura Y, Jaffe GJ, Schmidt-Erfurth U, Brown DM, et al. HAWK and HARRIER: phase 3, multicenter, randomized, double-masked trials of brolucizumab for neovascular age-related macular degeneration. *Ophthalmology*. (2020) 127:72–84. doi: 10.1016/j.ophtha.2019.04.017

6. de Vries VA, Bassil FL, Ramdas WD. The effects of intravitreal injections on intraocular pressure and retinal nerve fiber layer: a systematic review and meta-analysis. *Sci Rep*. (2020) 10:13248. doi: 10.1038/s41598-020-70269-7

7. Hoguet A, Chen PP, Junk AK, Mruthyunjaya P, Nouri-Mahdavi K, Radhakrishnan S, et al. The effect of anti-vascular endothelial growth factor agents on intraocular pressure and glaucoma: a report by the american academy of ophthalmology. *Ophthalmology*. (2019) 126:611–22. doi: 10.1016/j.ophtha.2018.11.019

8. Baek SU, Park IW, Suh W. Long-term intraocular pressure changes after intravitreal injection of bevacizumab. *Cutan Ocul Toxicol*. (2016) 35:310–4. doi: 10.3109/15569527.2015.1124886

9. Stefánsson E, Olafsdottir OB, Eliasdottir TS, Vehmeijer W, Einarsdottir AB, Bek T, et al. Retinal oximetry: metabolic imaging for diseases of the retina and brain. *Prog Retin Eye Res*. (2019) 70:1–22. doi: 10.1016/j.preteyeres.2019.04.001

10. Geirsdottir A, Hardarson SH, Olafsdottir OB, Stefánsson E. Retinal oxygen metabolism in exudative age-related macular degeneration. *Acta Ophthalmol*. (2014) 92:27–33. doi: 10.1111/aos.12294

11. Burgansky-Eliash Z, Barash H, Nelson D, Grinvald A, Sorkin A, Loewenstein A, et al. Retinal blood flow velocity in patients with age-related macular degeneration. *Curr Eye Res*. (2014) 39:304–11. doi: 10.3109/02713683.2013.840384

12. Yarmohammadi A, Zangwill LM, Diniz-Filho A, Suh MH, Manalastas PI, Fatehee N, et al. Optical coherence tomography angiography vessel density in healthy, glaucoma suspect, and glaucoma eyes. *Invest Ophthalmol Vis Sci*. (2016) 57:OCT451–9. doi: 10.1167/iovs.15-18944

13. Lee SC, Tran S, Amin A, Morse LS, Moshiri A, Park SS, et al. Retinal vessel density in exudative and nonexudative age-related macular degeneration on optical coherence tomography angiography. *Am J Ophthalmol*. (2020) 212:7–16. doi: 10.1016/j.ajo.2019.11.031

14. Cennamo G, Montorio D, D'Alessandro A, Napolitano P, D'Andrea L, Tranfa F. Prospective study of vessel density by optical coherence tomography angiography after intravitreal bevacizumab in exudative age-related macular degeneration. *Ophthalmol Ther*. (2020) 9:77–85. doi: 10.1007/s40123-019-00221-0

15. Grzybowski A, Told R, Sacu S, Bandello F, Moisseiev E, Loewenstein A, et al. Update on intravitreal injections: euretina expert consensus recommendations. *Ophthalmologica*. (2018) 239:181–93. doi: 10.1159/000486145

16. Ali N, Sampson DM, Au Yong A, Jeewa R, Rajgopal S, Dutt D, et al. Clinical validation of the RTVue optical coherence tomography angiography image quality indicators. *Clin Exp Ophthalmol*. (2020) 48:192–203. doi: 10.1111/ceo.13680

17. Spaide RF, Fujimoto JG, Waheed NK. Image artifacts in optical coherence tomography angiography. *Retina*. (2015) 35:2163–80. doi: 10.1097/IAE.0000000000000765

18. Fenner BJ, Tan G, Tan A, Yeo I, Wong TY, Cheung G. Identification of imaging features that determine quality and repeatability of retinal capillary plexus density measurements in OCT angiography. *Br J Ophthalmol*. (2018) 102:509–14. doi: 10.1136/bjophthalmol-2017-310700

19. Cougnard-Gregoire A, Delyfer MN, Korobelnik JF, Rougier MB, Malet F, Le Goff M, et al. Long-term blood pressure and age-related macular degeneration: the ALIENOR study. *Invest Ophthalmol Vis Sci*. (2013) 54:1905–12. doi: 10.1167/iovs.12-10192

20. Porta M, Striglia E. Intravitreal anti-VEGF agents and cardiovascular risk. *Intern Emerg Med*. (2020) 15:199–210. doi: 10.1007/s11739-019-02253-7

21. Berger V, Munk MR, Lersch F, Wolf S, Ebneter A, Zinkernagel MS. Association of intravitreal injections with blood pressure increase: the following excitement and anxiety response under intravitreal injection study. *JAMA Ophthalmol*. (2018) 137:87–90. doi: 10.1001/jamaophthalmol.2018.4892

22. Barash A, Chui T, Garcia P, Rosen RB. Acute macular and peripapillary angiographic changes with intravitreal injections. *Retina*. (2020) 40:648–56. doi: 10.1097/IAE.0000000000002433

23. Dedania VS, Bakri SJ. Sustained elevation of intraocular pressure after intravitreal anti-vegf agents: what is the evidence? *Retina*. (2015) 35:841–58. doi: 10.1097/IAE.0000000000000520

24. Hikichi T, Agarie M. Reduced vessel density of the choriocapillaris during anti-vascular endothelial growth factor therapy for neovascular age-related macular degeneration. *Invest Ophthalmol Vis Sci*. (2019) 60:1088–95. doi: 10.1167/iovs.18-24522

25. Spaide RF, Curcio CA. Evaluation of segmentation of the superficial and deep vascular layers of the retina by optical coherence tomography angiography instruments in normal eyes. *JAMA Ophthalmol*. (2016) 135:259–62. doi: 10.1001/jamaophthalmol.2016.5327

26. Mitsch C, Pemp B, Pollreisz A, Gleiss A, Karst S, Scholda C, et al. Short-time effect of intravitreal injections on retinal vascular oxygenation and vessel diameter in patients with diabetic macular oedema or neovascular age-related macular degeneration. *Acta Ophthalmol*. (2020) 98:e301–8. doi: 10.1111/aos.14276

27. O'Connell RA, Anderson AJ, Hosking SL, Bui BV. Provocative intraocular pressure challenge preferentially decreases venous oxygen saturation despite no reduction in blood flow. *Ophthalmic Physiol Opt*. (2015) 35:114–24. doi: 10.1111/opo.12170

28. Mendrinos E, Mangioris G, Papadopoulou DN, Donati G, Pournaras CJ. Long-term results of the effect of intravitreal ranibizumab on the retinal arteriolar diameter in patients with neovascular age-related macular degeneration. *Acta Ophthalmol*. (2013) 91:e184–90. doi: 10.1111/aos.12008

29. Sharma S, Toth CA, Daniel E, Grunwald JE, Maguire MG, Ying GS, et al. Macular morphology and visual acuity in the second year of the comparison of age-related macular degeneration treatments trials. *Ophthalmology*. (2016) 123:865–75. doi: 10.1016/j.ophtha.2015.12.002

30. Guymer RH, Markey CM, McAllister IL, Gillies MC, Hunyor AP, Arnold JJ, et al. Tolerating subretinal fluid in neovascular age-related macular degeneration treated with ranibizumab using a treat-and-extend regimen: FLUID study 24-month results. *Ophthalmology*. (2019) 126:723–34. doi: 10.1016/j.ophtha.2018.11.025

frontiers | Frontiers in Medicine

TYPE Case Report
PUBLISHED 18 January 2023
DOI 10.3389/fmed.2023.1051089

OPEN ACCESS

EDITED BY
Doina Gherghel,
Aston University, United Kingdom

REVIEWED BY
Cheng-Rong Yu,
National Eye Institute (NIH), United States
Peiquan Zhao,
Shanghai Jiao Tong University, China

*CORRESPONDENCE
Fang Lu
✉ lufang@wchscu.cn

SPECIALTY SECTION
This article was submitted to Ophthalmology, a section of the journal Frontiers in Medicine

RECEIVED 22 September 2022
ACCEPTED 03 January 2023
PUBLISHED 18 January 2023

CITATION
Jiang X, Shen M, Liang L, Rosenfeld PJ and Lu F (2023) Severe retinal hemorrhages at various levels with a serous retinal detachment in a pediatric patient with aplastic anemia–A case report.
Front. Med. 10:1051089.
doi: 10.3389/fmed.2023.1051089

Severe retinal hemorrhages at various levels with a serous retinal detachment in a pediatric patient with aplastic anemia–A case report

Xiaoshuang Jiang[1], Mengxi Shen[2], Licong Liang[1], Philip J. Rosenfeld[2] and Fang Lu[1]*

[1]Department of Ophthalmology, West China Hospital, Sichuan University, Chengdu, China, [2]Department of Ophthalmology, Bascom Palmer Eye Institute, University of Miami Miller School of Medicine, Miami, FL, United States

Background: Aplastic anemia can cause ophthalmic abnormalities in patients. Vision loss in a child with aplastic anemia due to massive retinal hemorrhages at various levels is rare.

Case presentation: A pediatric patient with aplastic anemia presented with retinal hemorrhages at multiple levels along with a serous retinal detachment in both eyes and subsequent retinal changes after pars plana vitrectomy.

Conclusion: Anemia and thrombocytopenia in aplastic anemia could cause severe retinal hemorrhages and result in retinal atrophy and retinal edema. Vitrectomy can be performed to remove vitreous hemorrhage, but risk factors for retinal atrophy and edema need further investigation.

KEYWORDS

aplastic anemia, retinal hemorrhage, serous retinal detachment, vitrectomy, retinal atrophy, retinal edema

Introduction

Aplastic anemia is a bone marrow failure syndrome with high mortality if untreated. Aplastic anemia commonly presents in patients between 15 and 25 years of age, with a second smaller peak after age 60. Patients with aplastic anemia may present with malaise and fatigue from severe anemia, hemorrhagic sequalae due to thrombocytopenia, and infection from neutropenia. Current treatment options for aplastic anemia include hematopoietic stem cell transplantation, immunosuppressive therapy, and supportive care (1).

Ophthalmic findings reported in aplastic anemia include conjunctival pallor, subconjunctival hemorrhage, orbital hematoma, hyphema, and retinal abnormalities. Specifically, cotton-wool spots, nerve fiber layer hemorrhages, central retinal vein occlusion, vitreous hemorrhage, retinal neovascularization, and serous retinal detachment have been described as abnormal retinal findings in aplastic anemia (2–9). Most of time, the retinal abnormalities need only observation without intervention. We are unaware of any reports about massive multi-level retinal hemorrhages with serous retinal detachment in pediatric aplastic anemia. We report here on the ophthalmic course of a pediatric patient with aplastic anemia who presented with severe retinal and vitreous hemorrhages with serous retinal detachment in both eyes and subsequent retinal changes after pars plana vitrectomy.

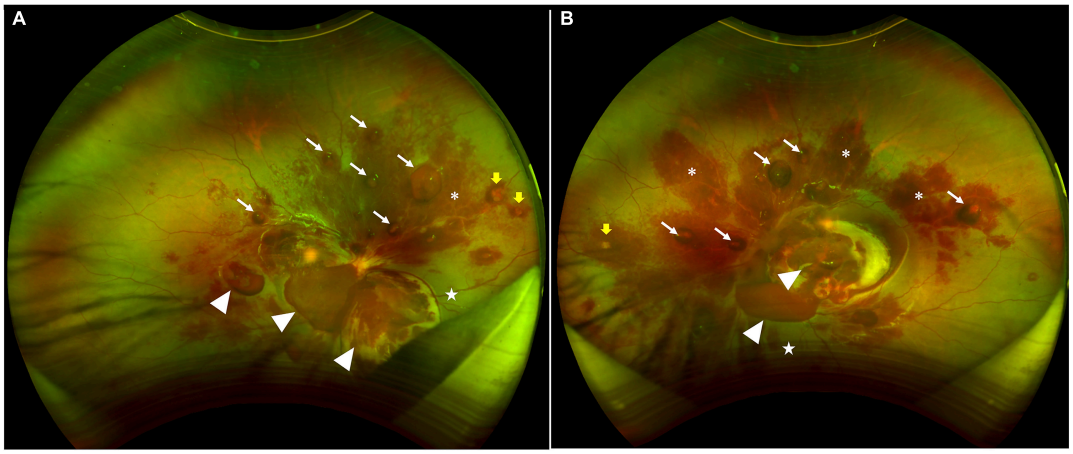

FIGURE 1
Scanning laser ophthalmoscopic images showing extensive dense preretinal, intraretinal, and subretinal hemorrhages in both retinas. **(A)** The right eye shows subhyloid hemorrhages (white arrows), hemorrhages between ILM and retina (white arrow heads), hemorrhages within the retina (asterisks), and sub-retinal hemorrhages (stars). Yellow arrows point at Roth spots. **(B)** The left eye shows subhyloid hemorrhages (white arrows), hemorrhages between ILM and retina (white arrow heads), hemorrhages within the retina (asterisks), at sub-retinal hemorrhages (stars). Yellow arrows point at Roth spots.

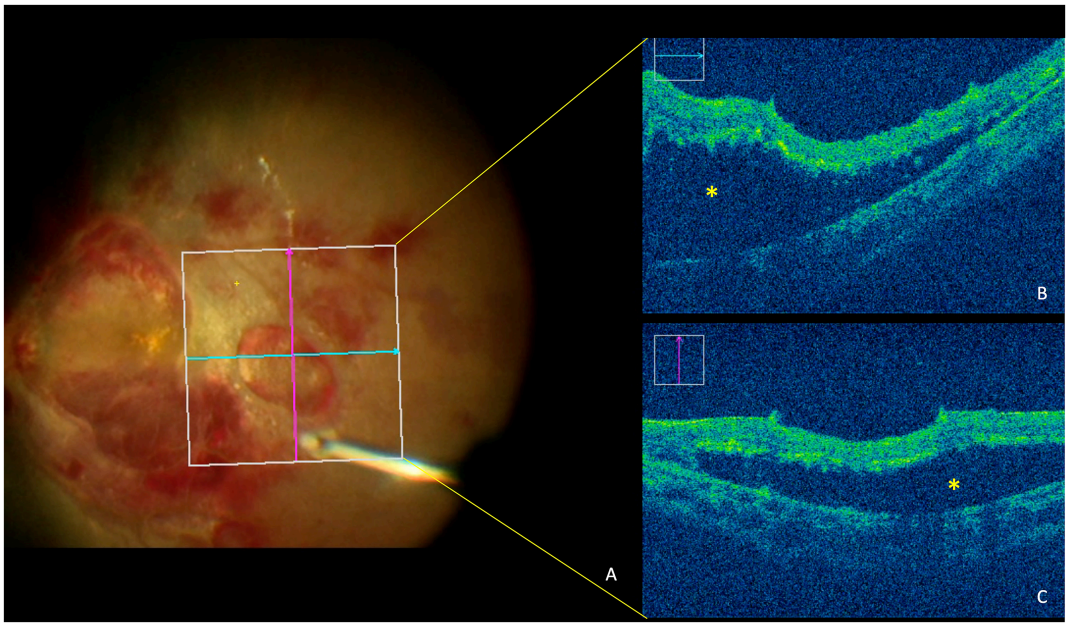

FIGURE 2
Optical coherence tomography (OCT) image during surgery shows serous retinal detachment in posterior fundus of the right eye. **(A)** Fundus imaging from the retina's view during surgery. **(B)** OCT imaging shows the horizontal B-scan of retina. **(C)** OCT imaging shows vertical B-scan of retina. Asterisks denote detachment of the neuroretina from the retinal pigment epithelium.

Case presentation

A 10-year-old boy with a history of aplastic anemia diagnosed in December 2019 presented to our clinic in December 2021 complaining of sudden vision loss in both eyes of 1 week duration without improvement. The patient denied any excessive physical exertion. Visual acuity was counting fingers at 20 cm in the right eye and hand movement in the left eye. Intraocular pressures were 10.2 mmHg in the right eye and 10.9 mmHg in the left eye using full auto tonometer (Canon, Japan, TX-20). The anterior segments of both eyes were quiet. Dilated funduscopic examination revealed extensive dense preretinal, intraretinal, and subretinal hemorrhages in both eyes (Figure 1). It was also noted that preretinal fibrosis was present along with hard exudates and Roth spots in retina.

Laboratory testing revealed hemoglobin of 81 g/L, leukocyte count of $1.79*10^9$/L, and platelets of $66*10^9$/L using the Coulter Prinicple (Systemx, Germany, XN-9000). Normal ranges are usually 115–150 g/L for hemoglobin, $3.5–9.5*10^9$/L for leukocyte count, $100–300*10^9$/L for platelets. Platelet counts varied between $72*10^9$/L and $81*10^9$/L before surgery after platelet transfusions.

Pars plana vitrectomy was performed to remove the vitreous haze and hemorrhage as well as the preretinal fibrosis 1 week after his presentation. Intraoperatively, several large and dense preretinal

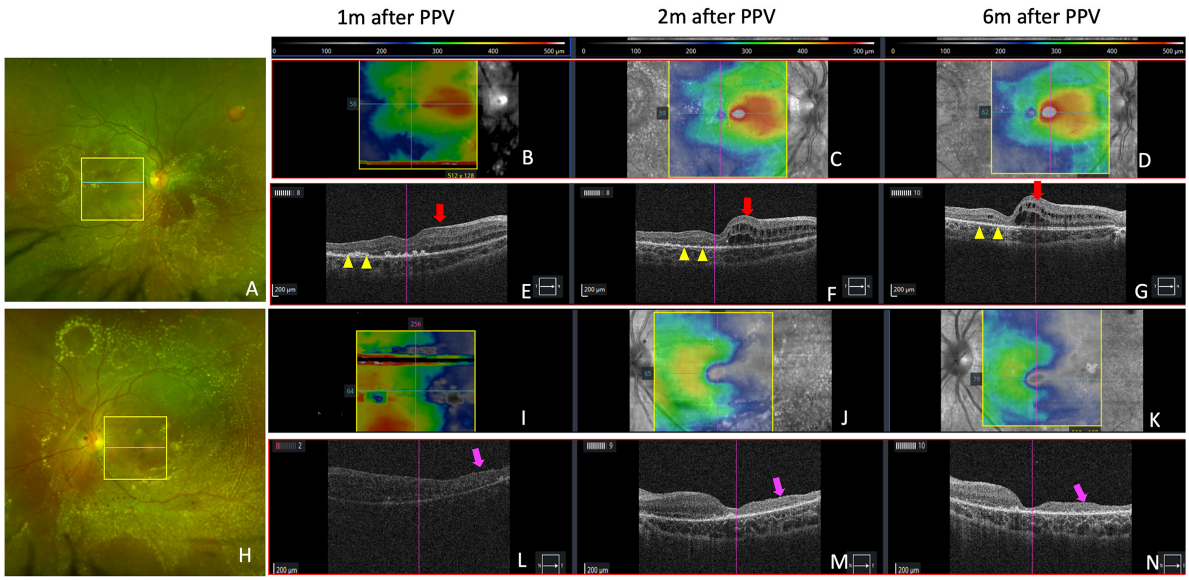

FIGURE 3
Retinal and optical coherence tomography (OCT) images showing retinal changes after vitrectomy. **(A,H)** Show retinal imaging by scanning laser ophthalmoscopy at 2 months. Yellow boxes in **(A,H)** show the area of OCT scanning in **(C,J)** with bule lines indicating the location of B-scans in **(F,M)**. **(B–D)** Show retinal thickness maps of right eye at 1 month, 2 months, and 6 months after vitrectomy. The color bars are shown above the panels. **(E–G)** Show horizontal OCT B-scans in the macular fovea of right eye. Yellow arrow heads show where hard exudates in the macular gradually absorbed without damage to outer retina. **(I–K)** Show retinal thickness maps of left eye at 1 month, 2 months, and 6 months after vitrectomy. **(L–N)** Show horizontal OCT B-scans in macular fovea of left eye. Red arrows show nasal macular edema after vitrectomy. Purple arrows show temporal macular atrophy.

hemorrhages were removed. During the surgery, both intraretinal and subretinal exudation was observed along with a temporal neuroretinal detachment in the right eye as appreciated in the surgical optical coherence tomography (OCT) images (Rescan 700, Carl Zeiss Meditec, Dublin, CA, USA) (Figure 2). During surgery, the dense vitreous haze contained hemosiderin with blood clots adherent to the retina. This material was evacuated using the vitrectomy instrument. After the preretinal hemorrhages were removed, the temporal serous retinal detachment was observed in both eyes less than 1 month, and the laboratory testing revealed hemoglobin of 79 g/L, leukocyte count of $2.37*10^9$/L, and platelets of $72*10^9$/L.

At 6 months of follow-up, visual acuity was 10/20 in right eye and 20/200 in left eye. OCT imaging (Cirrus HD-OCT, Carl Zeiss Meditec, Dublin, CA, USA) was performed on both eyes at 1 month, 2 months, and 6 months after surgery. In right eye, hard exudates gradually absorbed in the macula without damage to the outer retina as seen on OCT imaging; however, macular edema appeared nasally 2 months after pars plana vitrectomy. In left eye, temporal macular atrophy was observed after reattachment of the retina (Figure 3).

Discussion and conclusion

Anemia and thrombocytopenia were found to be important risk factors for developing hemorrhagic retinopathies. When anemia and thrombocytopenia were present at the same time, the frequency of retinopathy was 42% (10). In aplastic anemia, retinopathy was more frequently due to anemia and thrombocytopenia. This retinopathy was found in 69% of aplastic anemia patients who had Hb < 80 g/L and platelet counts of $<50 \times 10^9$/L. In a literature review of retinal findings in 200 patients with idiopathic aplastic anemia without any surgical treatment (bone marrow transplant), retinal hemorrhages were the most common reported manifestation which accounted for 56% of retinal abnormalities with subhyaloid/vitreous hemorrhages in 9%, peripheral retinal vasculopathy in 5.5%, and cotton-wool spots and optic disc edema in 4% each (9). Decreased visual acuity was usually due to preretinal and vitreous hemorrhages. In our case, vision impairment in both eyes was secondary to a large preretinal hemorrhage overlying the macular fovea.

The mechanism of retinal hemorrhages is likely to be multifactorial. Due to the presence of anemia in this disease, there is a compensatory increase in the cardiac output with increased turbulent flow that can lead to vascular endothelial damage and impairment of endothelial cell tight junctions, which may be responsible for the observed exudation and hemorrhage. Meanwhile, the impaired coagulation status in aplastic anemia due to a deficiency of platelets exacerbate the risk of hemorrhage. Observation without vitrectomy has been recommended for small vitreous and preretinal hemorrhages since most improve spontaneously, while vitrectomy should be performed to remove massive subhyloid and preretinal hemorrhages that impact vision since blood may cause permanent macular damage before it resolves.

Serous retinal detachment could also occur in pathological conditions that disrupt the integrity of blood-retinal barrier, which may be associated with inflammatory, infectious, infiltrative, neoplastic, vascular, and degenerative conditions (11). During the pars plana vitrectomy in our case, a serous retinal detachment was observed after the hemorrhage was removed. We speculated that ischemia in the retina and choroid impaired the blood-retinal barrier in our aplastic anemia patient, resulting in exudation from the

retinal vasculature and the choroid. At the 6 month follow up visit, outer retinal atrophy and retinal edema were observed in the area of the exudative retinal detachment. We propose that the cystic macular edema results from the ischemia and hypoxia that still exists in the retina of this child patient.

In conclusion, this report illustrated a pediatric case of aplastic anemia presenting with sudden vision loss, significant retinal hemorrhages at various levels and a serous retinal detachment, which were successfully managed with vitrectomy. The identification of risk factors and the long-term prevention of retinal atrophy and edema require further investigation.

Data availability statement

The raw data supporting the conclusions of this article will be made available by the authors, without undue reservation.

Author contributions

XJ performed the literature search, collection, and drafted the manuscript. MS contributed to image and photo illustration. LL contributed to the data collection. PR edited the manuscript and gave consultation. FL completed the all examination, confirmed the diagnosis, and performed the vitrectomy. All authors read, edited, and approved the final version of the manuscript.

Funding

This work was supported by National Natural Science Foundation of China (NSFC, Grant No. 281500728).

Acknowledgments

We would like to extend thanks to the patient and his father for their cooperation in this study.

Conflict of interest

The authors declare that the research was conducted in the absence of any commercial or financial relationships that could be construed as a potential conflict of interest.

Publisher's note

All claims expressed in this article are solely those of the authors and do not necessarily represent those of their affiliated organizations, or those of the publisher, the editors and the reviewers. Any product that may be evaluated in this article, or claim that may be made by its manufacturer, is not guaranteed or endorsed by the publisher.

References

1. Furlong E, Carter T. Aplastic anaemia: current concepts in diagnosis and management. *J Paediatr Child Health.* (2020) 56:1023–8.

2. Mansour A. Aplastic anemia simulating central retinal vein occlusion. *Am J Ophthalmol.* (1985) 100:478–9. doi: 10.1016/0002-9394(85)90519-7

3. Lilley E, Bruggers C, Pollock S. Papilledema in a patient with aplastic anemia. *Arch Ophthalmol.* (1990) 108:1674–5. doi: 10.1001/archopht.1990.01070140028014

4. Mansour A, Salti H, Han D, Khoury A, Friedman S, Salem Z, et al. Ocular findings in aplastic anemia. *Ophthalmologica.* (2000) 214:399–402.

5. Chan W, Liu D, Tham C, Wu R, Lam D. Bilateral subhyaloid haemorrhage in aplastic anaemia. *Br J Haematol.* (2003) 123:757.

6. Bahar I, Weinberger D, Kramer M, Axer-Siegel R. Retinal vasculopathy in fanconi anemia: a case report. *Retina.* (2005) 25:799–800.

7. Yahia S, Touffahi S, Zeghidi H, Zaouali S, Khairallah M. Ocular neovascularization in a patient with Fanconi anemia. *Can J Ophthalmol.* (2006) 41:778–9. doi: 10.3129/i06-078

8. Suzuki J, Goto H, Usui M, Sakai J. Serous retinal detachment in a patient with aplastic anemia associated with parvovirus B19 infection. *Graefes Arch Clin Exp Ophthalmol.* (2007) 245:324–6. doi: 10.1007/s00417-006-0315-5

9. Mansour A, Lee J, Yahng S, Kim K, Shahin M, Hamerschlak N, et al. Ocular manifestations of idiopathic aplastic anemia: retrospective study and literature review. *Clin Ophthalmol.* (2014) 8:777–87. doi: 10.2147/OPTH.S62163

10. Carraro M, Rossetti L, Gerli G. Prevalence of retinopathy in patients with anemia or thrombocytopenia. *Eur J Haematol.* (2001) 67:238–44.

11. Amer R, Nalcı H, Yalçındağ N. Exudative retinal detachment. *Surv Ophthalmol.* (2017) 62:723–69.

frontiers | Frontiers in Medicine

TYPE Mini Review
PUBLISHED 24 January 2023
DOI 10.3389/fmed.2023.1087123

OPEN ACCESS

EDITED BY
Yukihiro Shiga,
University of Montreal Hospital Research Centre (CRCHUM), Canada

REVIEWED BY
Zhengbo Shao,
The Second Affiliated Hospital of Harbin Medical University, China

*CORRESPONDENCE
Rachel S. Chong
✉ Rachel.chong.s.j@snec.com.sg

SPECIALTY SECTION
This article was submitted to Ophthalmology, a section of the journal Frontiers in Medicine

RECEIVED 02 November 2022
ACCEPTED 04 January 2023
PUBLISHED 24 January 2023

CITATION
Loo JH, Wang Z and Chong RS (2023) Caveolin-1 in vascular health and glaucoma: A critical vascular regulator and potential therapeutic target. *Front. Med.* 10:1087123. doi: 10.3389/fmed.2023.1087123

Caveolin-1 in vascular health and glaucoma: A critical vascular regulator and potential therapeutic target

Jing Hong Loo[1], Zhaoran Wang[2] and Rachel S. Chong[3,4]*

[1]Yong Loo Lin School of Medicine, National University of Singapore, Singapore, Singapore, [2]Duke-NUS Medical School, Singapore, Singapore, [3]Glaucoma Department, Singapore National Eye Center, Singapore, Singapore, [4]Ocular Imaging Department, Singapore Eye Research Institute, Singapore, Singapore

Caveolin-1 (Cav-1) is an integral scaffolding membrane protein found in most cell types. Cav-1 has been found to contribute significantly to ocular function, with mutations of Cav-1 being associated with a genetic risk of glaucoma development. Raised intraocular pressure (IOP) is a major modifiable risk factor for glaucoma. Cav-1 may be involved in both IOP-dependent and independent mechanisms involving vascular dysregulation. Systemic vascular diseases including hypertension, diabetes and hyperlipidaemia, have been shown to be associated with glaucoma development. Cav-1 is closely interlinked with endothelial nitric oxide synthase pathways that mediate vascular function and prevent cardiovascular diseases. Endothelial nitric oxide synthase and endothelin-1 are key vasoactive molecules expressed in retinal blood vessels that function to autoregulate ocular blood flow (OBF). Disruptions in the homeostasis of OBF have led to a growing concept of impaired neurovascular coupling in glaucoma. The imbalance between perfusion and neuronal stimulation arising from Cav-1 depletion may result in relative ischemia of the optic nerve head and glaucomatous injury. OBF is also governed by circadian variation in IOP and systemic blood pressure (BP). Cav-1 has been shown to influence central BP variability and other circadian rhythms such as the diurnal phagolysosomal digestion of photoreceptor fragments and toxic substrates to maintain ocular health. Overall, the vast implications of Cav-1 on various ocular mechanisms leading to glaucoma suggest a potential for new therapeutics to enhance Cav-1 expression, which has seen success in other neurodegenerative diseases.

KEYWORDS

glaucoma, Caveolin-1 (Cav-1), systemic vascular risk factors, ocular blood flow, neurovascular coupling (NVC), glaucoma therapy

Caveolin-1 in vascular health

Caveolin-1 (Cav-1) is a major coat protein of caveolae, which are flask-shaped invaginations of the plasma membrane ubiquitously found in various cell types, particularly adipocytes, endothelial cells, epithelial cells and fibroblasts. Caveolae have been discovered to play roles in lipid transportation (1), membrane traffic (2), and signal transduction (3). Although there are three caveolin genes identified in mammals, namely Cav-1, -2, and -3, Cav-1 is notably essential for caveolae formation and function (4, 5). Through a multitude of signaling cascades, Cav-1 has been implicated in cardiovascular disease, atherosclerosis, diabetes, cancer, and a variety of degenerative muscular dystrophies (6). In the cardiovascular system, Cav-1 particularly contributes to the functions of endothelial cells *via* interacting with endothelial nitric oxide synthase (eNOS) and regulating the release of nitric oxide (NO) (7).

Caveolin-1 involvement in glaucoma

While Cav-1 has been extensively studied in extra-ocular diseases, its role in ocular function and diseases has only recently received attention. Cav-1 is expressed abundantly in Muller glia, retinal and choroidal vasculature, and retinal pigment epithelium (RPE) (8). Mutations of Cav-1 gene are associated with an increased genetic risk of primary open-angle glaucoma development across various population cohorts (9–12).

Glaucoma is a neurodegenerative disease characterized by progressive loss of retinal ganglion cells (RGC) and optic nerve degeneration that results in irreversible visual field deficits. Raised intraocular pressure (IOP) is a major modifiable risk factor for glaucoma (13). The effect of Cav-1 deficiency on IOP homeostasis has been evaluated in various pre-clinical studies, with Cav-1 deficient mice displaying significantly higher IOP (14–16). A postulated mechanism underlying ocular hypertension in Cav-1 deficiency is the resultant overreactive eNOS signaling pathways. While NO is a potent vasodilator and has a crucial role in lowering IOP, chronic dysregulation of eNOS may lead to outflow tract dysfunction. Indeed, Cav-1 depletion has been independently associated with increased conventional outflow resistance leading to decreased drainage of aqueous humor from the anterior chamber (17). Additionally, new findings have shed light on Cav-1 potential role as mechanosensors in the Schlemm's canal and trabecular meshwork that protects against mechanical stress from IOP fluctuations (18). Cav-1 may contribute to increased IOP and increase the susceptibility of the optic nerve head (ONH) to cellular damage due to altered outflow tract mechanoprotection.

Cav-1 has also been implicated in altering vascular function, both systemically and within the eye. These alterations in vascular profile may contribute to greater glaucoma risk, as described in this mini-review.

The role of Cav-1 in mediating systemic vascular risk factors for glaucoma

Various systemic vascular risk factors including hypertension or hypotension, diabetes mellitus, hyperlipidaemia, atherosclerotic diseases and migraine have been associated with glaucoma development. Hypertension has a direct causative link to glaucoma risk by means of increased ciliary blood flow and aqueous humor production coupled with decrease outflow due to elevated episcleral venous pressure (19). Hypotension is particularly associated with normal-tension glaucoma since it lowers ocular perfusion pressure (OPP), resulting in optic nerve ischemia and glaucomatous degeneration (20). Circadian variation of blood pressure (BP) may have a role in glaucoma development too. A meta-analysis in 2015 pooled evidence from epidemiological studies and established nocturnal BP fall as a risk factor for progressive visual field losses in glaucoma (21). In presence of the other vascular risk factors, nocturnal dipping exacerbates poor optic nerve perfusion and glaucomatous optic neuropathy (22). The association between diabetes and glaucoma may be explained by a few key mechanisms. Hyperglycaemia and dysregulation in lipid metabolism results in oxidative stress, vascular dysregulation and eventual neuronal injury (23–25). Hyperglycaemia of the aqueous humor also leads to structural remodeling at the trabecular meshwork and impaired aqueous humor outflow (26). Atherosclerotic diseases include a spectrum of disease conditions from coronary artery disease to peripheral vascular disease and stroke. The association between atherosclerotic diseases and glaucoma has been extensively studied (27–30), however current evidence is insufficient to support a direct causal relationship between the two due to potential confounding factors from the underlying pathophysiological processes involved. Finally, migraine is associated with systemic vasospasm causing relative ischemia, thereby increasing the risk of glaucoma, particularly normal-tension glaucoma (31–33).

Many of the aforementioned systemic vascular risk factors have been linked to Cav-1. From diabetes to lipid disorders and pulmonary fibrosis, Cav-1 plays an integral role in maintaining vascular homeostasis and controlling atherosclerosis formation through lipoprotein trafficking across the vascular endothelium (34–36). Central to this physiology is the regulatory setup of Cav-1/eNOS. eNOS is constitutively expressed in vascular endothelium and produces the vasodilatory gas NO which maintains endothelial function and health (37). eNOS bounded to caveolae is rendered inactive by its direct association with caveolin scaffolding domain of Cav-1 (38). Cav-1 directly competes with calmodulin (an activator of eNOS) for binding to the active site of eNOS (39). Furthermore, Cav-1 also regulates eNOS expression levels by inhibiting serine/threonine amino acid kinase Akt phosphorylation of eNOS, thus governing the basal level of NO in endothelial cells (40). While Cav-1 depletion is characterized by chronic hyperactivation of eNOS, a decoupling of the de-inhibited eNOS may occur, thus resulting in a decreased bioavailability of NO (41). Reduced NO production is associated with vascular dysfunction and cardiovascular mortality (42).

Cav-1 mediated regulation of ocular blood flow *via* NO-dependent and independent pathways

Autoregulation of ocular blood flow (OBF) in the retinal vasculature enables a relatively stable supply of blood and metabolites despite fluctuation in OPP (43). OPP is calculated as derived from the subtraction of IOP from mean arterial pressure (44). Variations in mean arterial pressure and IOP results in corresponding variations in OPP. Within a range of OPP, OBF remains constant due to autoregulation of vascular tone in the retinal and ONH (45).

Two vasoactive factors, namely NO and ET-1, are crucial in the autoregulatory mechanism (46). NO is a potent vasodilator released by endothelial cells and acts on pericytes to cause vasodilation (47). ET-1 is a potent vasoconstrictor that exerts its effect *via* ETA, ETB1, and ETB2 receptors. ETA and ETB2 receptors are found on vascular smooth muscle cells and causes vasoconstriction while ETB1 is found on endothelial cells and cause vasodilation (48). The counterregulatory effects of NO and ET-1 maintains an appropriate vascular tone and constant blood flow to the ONH.

Impaired autoregulation is seen in glaucomatous optic neuropathy. This arises from cellular dysfunction leading to an imbalance of vasoactive factors and ischemia at the ONH (49, 50). Numerous studies have shown that elevated levels of ET-1 are associated with disease pathology (51–54). Blocking of ET-1 receptors in mice increased OBF and protects from glaucomatous

injury (55). Alterations in NO signaling pathways either through upregulation or downregulation are also implicated in glaucoma. High NO may increase ocular perfusion but cause oxidative stress and injury to neurons due to formation of reactive oxygen species (56). Decreased NO levels are found in the aqueous humor of glaucoma patients (57). Characteristic RGC loss and vascular dysfunction seen in glaucoma are more prominent with decreased NO production and impairment in its downstream NO-cGMP signaling pathways (58).

ET-1 and NO dysregulation is partly mediated by Cav-1. The effect of Cav-1 on NO homeostasis has been explained in the previous section. An intrinsic regulatory interaction also exists between Cav-1 and ET-1. Both the scaffolding domain and C-terminal domain of Cav-1 can bind to ET receptors and this localizes the complex to the caveolae membrane (59); it has been suggested that compartmentalization of ETB receptor/Cav-1 complexes within caveolae ensures signal transduction and prevents rapid endocytosis of the receptor (60). An early study demonstrated that disruption of caveolae structure significantly diminishes ET-1-induced phosphorylation of ERK 1/2 and subsequent signal propagation (60). This interplay between Cav-1 and mediators of vascular tone suggests the crucial role of Cav-1 in ocular vascular health. Cav-1 deficiency is associated with vascular dysregulation which may predispose to structural neuronal injury at the ONH in the presence of existing stressors like IOP, thus exacerbating disease progression (61).

Cav-1 depletion is also associated with disruptions in blood-retinal barrier integrity and venous morphology, that are independent of eNOS activity. Gu et al. have reported hyperpermeability of the large branch retinal veins of the superficial retina, and enlargement of retinal veins in Cav-1 knockout mice (62). These alterations were found to be independent of NOS-expression and activity. It is therefore possible that Cav-1 mediates vascular dysfunction in the eye through both NO-dependent and independent mechanisms, where the former regulates capillary dilation and the latter stabilizes vessel wall integrity in retinal veins.

Neurovascular coupling in glaucoma

Neuronal activity is tightly matched to OBF in the eye in what is termed as neurovascular coupling (NVC) (45). An increase in neuronal stimulation is associated with a corresponding increase in blood flow to meet the metabolic requirements of the retinal tissue. This NVC response is mediated by the neurovascular unit which comprises vascular cells, glial cells and neurons (63, 64). Defective NVC has been described in primary open-angle glaucoma (65, 66). In response to flicker-light stimulation, the increase in OBF in glaucoma patients was found to be significantly lower than that of healthy subjects (67). Various mechanisms may explain the defective NVC response in glaucoma. Firstly, glaucoma is characterized by RGC apoptosis due to various possible causes involving raised IOP, oxidative stress and mitochondrial dysfunction—decreased neuronal signaling from RGCs may drive reduced NVC (68–70). Secondly, decreased gap junction expression in the retinal and ONH also affects communication between cells of the neurovascular unit (71, 72). Lastly, the integrity of retinal barrier is compromised due to the loss of tight junctions (73), leading to both compromised blood supply and transendothelial migration of inflammatory cells causing further neuronal injury (74).

On the back of increasing evidence of Cav-1 involvement in glaucoma, our own study in Cav-1 knockout mice showed defective NVC at the ONH as assessed by laser speckle flowgraphy (16). This is associated with changes in vessel morphology as well as a decrease in electrophysiological function of RGCs (16). While the temporal association has yet to be clearly-established, it is possible that vascular dysfunction contributes to defective NVC which is associated with early functional RGC injury before structural losses are seen. Apart from its role in mediating vascular tone as described in the previous sections, Cav-1 may influence microvascular structural characteristics by downregulating vascular endothelial growth factor (75). Defective Cav-1 promotes angiogenesis, but the excessive vascular branching pattern may lead to poorer perfusion instead (76). These findings support the theory that defective Cav-1 is associated with vascular dysfunction and impaired NVC. However, the precise involvement of glial cells or retinal microvasculature in regulating the NVC process remains to be seen—particularly in the context of glaucoma.

Cav-1 and disruption of circadian rhythms

Numerous studies have shown that circadian variation in BP, IOP, and OPP are risk factors for the development of glaucoma. Progression of visual field loss in glaucoma patients has been associated with a larger range of diurnal IOP fluctuations and nocturnal pressure spikes (77–79). IOP tends to be higher at night due to decreased aqueous humor drainage *via* the trabecular meshwork and uveoscleral pathway (80). Similarly, diurnal variation in BP and nocturnal dipping may contribute to glaucoma pathogenesis as well (81, 82). Nocturnal BP reduction is attributed to a fall in sympathetic tone with reduced circulating levels of catecholamines (83). OPP is driven by a complex interplay between BP and IOP; fluctuations in either will translate to variations in OPP (84). Abrupt variations in OPP beyond the capacity of autoregulatory mechanisms may thus cause unstable OBF (85, 86), triggering a sequence of ischemic and reperfusion injury at the ONH.

Limited studies have described Cav-1 involvement in circadian rhythms disruptions causing glaucoma development. An experimental study by Desjardins et al. (87) showed that Cav-1 deficient mice exhibit decreased very low frequency BP variability. Administration of caveolin scaffolding domain reversed this drop in BP variability. The authors attributed this to the increased NO production *ex vivo* arising from reduced allosteric inhibition by Cav-1. While the bandwidth of spectral analysis cannot be directly applicable to human, the study does provide invaluable insights regarding the function of Cav-1 on NO production and control of central BP variability. Another circadian rhythm implicated in Cav-1 depletion is the diurnal pattern of renewal of photoreceptor outer segment (88). RPE supports photoreceptors neurons *via* the diurnal clearance of outer segment fragments (89). Cav-1 depletion impairs phagolysosome degradation by reversing the diurnal activity of enzymes in the RPE (88). Rod photoreceptor visual function is found be decreased with Cav-1 knockout (8).

While the present evidence for cav-1 involvement in circadian regulation remains scant, the unique role of Cav-1 in mediating ocular perfusion *via* multiple pathways warrants further studies into how circadian disruptions may influence Cav-1 function.

Potential therapeutic targets

Current treatment for glaucoma relies heavily on ocular hypotensive medications. Reduction in IOP has proven effective in preventing and slowing disease progression (85). In addition to its effectiveness, IOP-lowering medications exhibit minimal systemic adverse effects and high rates of patient tolerability (90). However, continued disease progression occurs in a small subset of patients despite adequate IOP lowering (91, 92). Furthermore, a modest proportion of patient experienced glaucomatous optic neuropathy despite having normal IOP, in what is termed as normal-tension glaucoma (93). This suggests that there are other IOP-independent mechanisms that may contribute to glaucoma development (94).

The multiple roles of Cav-1 in modulating ocular health and glaucoma risk suggest the potential for new therapeutic strategies that increase Cav-1 expression or augment its downstream signaling. While research on Cav-1 therapeutics remains in its infancy, success with Cav-1 gene therapy for chronic diseases have been described in few recent studies. Lin et al. demonstrated that electroporation-mediated transfer of the Cav-1 gene protects against bleomycin-induced pulmonary fibrosis in mouse lungs *via* downregulation of inflammasome activity and reduction in monocyte recruitment and circulating cytokines (95). The use of electroporation to deliver gene targets is currently being explored in clinical trials for cancer and vaccines (96). It thus remains to be seen if the promising outcomes of Cav-1 gene therapy for idiopathic pulmonary fibrosis can be replicated in humans as well. Cav-1 therapy has also been shown to preserve or delay neurodegeneration in a preclinical model of Alzheimer's disease. Wang et al. showed that synapsin-promoted Cav-1 gene therapy was able to maintain neuronal and synaptic morphology and preserve hippocampal function such as memory and learning in mice with Alzheimer's disease (97). Further translational or clinical research may focus on whether the therapeutic potential of Cav-1 can be exploited for neuroprotective effects in the human eye, possibly averting RGC loss and glaucoma development.

Conclusions

Raised IOP has long been regarded as the only modifiable risk factor for glaucoma. However, adequate IOP lowering with anti-glaucoma medications may not always deter glaucoma progression. Hence, other factors independent of IOP may be involved in the complex pathogenesis of glaucoma. The "vascular theory" affecting neuronal function has gained attention recently with new evidence showing vascular dysregulation may precede RGC loss (98). Patients with cardiovascular risk factors are at an increased risk of glaucoma. Dysregulation of OBF due to altered levels of vasoactive substances may lead to disruption in blood supply of the ONH. Impaired NVC can also cause a mismatch of neuronal stimulation and ocular perfusion. All these disturbances in vascular function may manifest as altered vessel morphology and vascular dropout seen in early glaucoma (99).

Cav-1 plays an important role in regulating various pathways involved in the "vascular theory" of glaucoma. There is consistent evidence describing the association between Cav-1 depletion and systemic cardiovascular disease, impaired autoregulation and defective NVC. While the underlying mechanism has not been fully elucidated, understanding this crucial association may pave the way for future therapeutics that focus on restoring vascular health to avert glaucomatous degeneration. Cav-1 therapeutics have shown promising outcomes for other disease, raising hopes that a similar approach can be applied to glaucoma prevention. Future research should focus on exploring the intricate interplay between Cav-1 and vascular dysregulation and exploiting the translative potential of Cav-1 therapy for alternative glaucoma treatment.

Author contributions

JHL wrote the first draft of the manuscript. ZW formatted and proofread the manuscript. RC provided overall leadership and wrote sections of the manuscript. All authors contributed to manuscript revision, read, and approved the submitted version.

Funding

Supported by NMRC Clinician-Scientist Individual Grant JRNMRR177301 to investigate the role of Caveolin-1 in Inner Retina Neurovascular Coupling in Experimental Glaucoma.

Conflict of interest

The authors declare that the research was conducted in the absence of any commercial or financial relationships that could be construed as a potential conflict of interest.

Publisher's note

References

1. Li WP, Liu P, Pilcher BK, Anderson R. Cell-specific targeting of caveolin-1 to caveolae, secretory vesicles, cytoplasm or mitochondria. *J Cell Sci.* (2001) 114:1397–408. doi: 10.1242/jcs.114.7.1397

2. Anderson RG. The caveolae membrane system. *Annu Rev Biochem.* (1998) 67:199–225.

3. Smart EJ, Graf GA, McNiven MA, Sessa WC, Engelman JA, Scherer PE, et al. Caveolins, liquid-ordered domains, and signal transduction. *Mol Cell Biol.* (1999) 19:7289–304.

4. Liu P, Rudick M, Anderson RG. Multiple functions of caveolin-1. *J Biol Chem.* (2002) 277:41295–8. doi: 10.1074/jbc.R200020200

5. Drab M, Verkade P, Elger M, Kasper M, Lohn M, Lauterbach B, et al. Loss of caveolae, vascular dysfunction, and pulmonary defects in caveolin-1 gene-disrupted mice. *Science.* (2001) 293:2449–52. doi: 10.1126/science.1062688

6. Cohen AW, Hnasko R, Schubert W, Lisanti MP. Role of caveolae and caveolins in health and disease. *Physiol Rev.* (2004) 84:1341–79. doi: 10.1152/physrev.00046.2003

7. Goligorsky MS, Li H, Brodsky S, Chen J. Relationships between caveolae and eNOS: everything in proximity and the proximity of everything. *Am J Physiol Renal Physiol.* (2002) 283:F1–10. doi: 10.1152/ajprenal.00377.2001

8. Li X, McClellan ME, Tanito M, Garteiser P, Towner R, Bissig D, et al. Loss of caveolin-1 impairs retinal function due to disturbance of subretinal microenvironment. *J Biol Chem.* (2012) 287:16424–34. doi: 10.1074/jbc.M112.353763

9. Loomis SJ, Kang JH, Weinreb RN, Yaspan BL, Cooke Bailey JN, Gaasterland D, et al. Association of CAV1/CAV2 genomic variants with primary open-angle glaucoma overall and by gender and pattern of visual field loss. *Ophthalmology.* (2014) 121:508–16. doi: 10.1016/j.ophtha.2013.09.012

10. Thorleifsson G, Walters GB, Hewitt AW, Masson G, Helgason A, DeWan A, et al. Common variants near CAV1 and CAV2 are associated with primary open-angle glaucoma. *Nat Genet.* (2010) 42:906–9. doi: 10.1038/ng.661

11. Rong SS, Chen LJ, Leung CK, Matsushita K, Jia L, Miki A, et al. Ethnic specific association of the CAV1/CAV2 locus with primary open-angle glaucoma. *Sci Rep.* (2016) 6:27837. doi: 10.1038/srep27837

12. Kim S, Kim K, Heo DW, Kim JS, Park CK, Kim CS, et al. Expression-associated polymorphisms of CAV1-CAV2 affect intraocular pressure and high-tension glaucoma risk. *Mol Vis.* (2015) 21:548–54.

13. Weinreb RN, Aung T, Medeiros FA. The pathophysiology and treatment of glaucoma: a review. *JAMA.* (2014) 311:1901–11. doi: 10.1001/jama.2014.3192

14. Lei Y, Song M, Wu J, Xing C, Sun X. eNOS activity in CAV1 knockout mouse eyes. *Invest Ophthalmol Vis Sci.* (2016) 57:2805–13. doi: 10.1167/iovs.15-18841

15. Song M, Wu J, Lei Y, Sun X. Genetic deletion of the NOS3 gene in CAV1-/- mice restores aqueous humor outflow function. *Invest Ophthalmol Vis Sci.* (2017) 58:4976–87. doi: 10.1167/iovs.16-21072

16. Loo JH, Lee YS, Woon CY, Yong VHK, Tan B, Schmetterer L, et al. Loss of caveolin-1 impairs light flicker-induced neurovascular coupling at the optic nerve head. *Front Neurosci.* (2021) 15:764898. doi: 10.3389/fnins.2021.764898

17. Kizhatil K, Chlebowski A, Tolman NG, Freeburg NF, Ryan MM, Shaw NN, et al. An *in vitro* perfusion system to enhance outflow studies in mouse eyes. *Invest Ophthalmol Vis Sci.* (2016) 57:5207–15. doi: 10.1167/iovs.16-19481

18. Elliott MH, Ashpole NE, Gu X, Herrnberger L, McClellan ME, Griffith GL, et al. Caveolin-1 modulates intraocular pressure: implications for caveolae mechanoprotection in glaucoma. *Sci Rep.* (2016) 6:37127. doi: 10.1038/srep37127

19. Zhao D, Cho J, Kim MH, Guallar E. The association of blood pressure and primary open-angle glaucoma: a meta-analysis. *Am J Ophthalmol.* (2014) 158:615–27.e9. doi: 10.1016/j.ajo.2014.05.029

20. Binggeli T, Schoetzau A, Konieczka K. In glaucoma patients, low blood pressure is accompanied by vascular dysregulation. *EPMA J.* (2018) 9:387–91. doi: 10.1007/s13167-018-0155-5

21. Bowe A, Grünig M, Schubert J, Demir M, Hoffmann V, Kütting F, et al. Circadian variation in arterial blood pressure and glaucomatous optic neuropathy: a systematic review and meta-analysis. *Am J Hypertens.* (2015) 28:1077–82. doi: 10.1093/ajh/hpv016

22. Grzybowski A, Och M, Kanclerz P, Leffler C, Moraes CG. Primary open angle glaucoma and vascular risk factors: a review of population based studies from 1990 to 2019. *J Clin Med.* (2020) 9:761. doi: 10.3390/jcm9030761

23. Chopra V, Varma R, Francis BA, Wu J, Torres M, Azen SP, et al. Type 2 diabetes mellitus and the risk of open-angle glaucoma the Los Angeles Latino Eye Study. *Ophthalmology.* (2008) 115:227–32.e1. doi: 10.1016/j.ophtha.2007.04.049

24. Su DH, Wong TY, Wong WL, Saw SM, Tan DT, Shen SY, et al. Diabetes, hyperglycemia, and central corneal thickness: the Singapore Malay Eye Study. *Ophthalmology.* (2008) 115:964–8.e1. doi: 10.1016/j.ophtha.2007.08.021

25. Nakamura M, Kanamori A, Negi A. Diabetes mellitus as a risk factor for glaucomatous optic neuropathy. *Ophthalmologica.* (2005) 219:1–10. doi: 10.1159/000081775

26. Sato T, Roy S. Effect of high glucose on fibronectin expression and cell proliferation in trabecular meshwork cells. *Invest Ophthalmol Vis Sci.* (2002) 43:170–5.

27. Jeganathan VS, Wong TY, Foster PJ, Crowston JG, Tay WT, Lim SC, et al. Peripheral artery disease and glaucoma: the singapore malay eye study. *Arch Ophthalmol.* (2009) 127:888–93. doi: 10.1001/archophthalmol.2009.136

28. Chen YY, Hu HY, Chu D, Chen HH, Chang CK, Chou P, et al. Patients with primary open-angle glaucoma may develop ischemic heart disease more often than those without glaucoma: an 11-year population-based cohort study. *PLoS ONE.* (2016) 11:e0163210. doi: 10.1371/journal.pone.0163210

29. Marshall H, Mullany S, Qassim A, Siggs O, Hassall M, Ridge B, et al. Cardiovascular disease predicts structural and functional progression in early glaucoma. *Ophthalmology.* (2021) 128:58–69. doi: 10.1016/j.ophtha.2020.06.067

30. Song X, Li P, Li Y, Yan X, Yuan L, Zhao C, et al. Strong association of glaucoma with atherosclerosis. *Sci Rep.* (2021) 11:8792. doi: 10.1038/s41598-021-88322-4

31. Wang JJ, Mitchell P, Smith W. Is there an association between migraine headache and open-angle glaucoma? Findings from the Blue Mountains Eye Study. *Ophthalmology.* (1997) 104:1714–9.

32. Cursiefen C, Wisse M, Cursiefen S, Jünemann A, Martus P, Korth M, et al. Migraine and tension headache in high-pressure and normal-pressure glaucoma. *Am J Ophthalmol.* (2000) 129:102–4. doi: 10.1016/S0002-9394(99)00289-5

33. McKendrick AM, Vingrys AJ, Badcock DR, Heywood JT. Visual field losses in subjects with migraine headaches. *Invest Ophthalmol Vis Sci.* (2000) 41:1239–47.

34. Frank PG, Pavlides S, Lisanti MP. Caveolae and transcytosis in endothelial cells: role in atherosclerosis. *Cell Tissue Res.* (2009) 335:41–7. doi: 10.1007/s00441-008-0659-8

35. Le Lay S, Blouin CM, Hajduch E, Dugail I. Filling up adipocytes with lipids. Lessons from caveolin-1 deficiency. *Biochim Biophys Acta.* (2009) 1791:514–8. doi: 10.1016/j.bbalip.2008.10.008

36. Bakhshi FR, Mao M, Shajahan AN, Piegeler T, Chen Z, Chernaya O, et al. Nitrosation-dependent caveolin 1 phosphorylation, ubiquitination, and degradation and its association with idiopathic pulmonary arterial hypertension. *Pulm Circ.* (2013) 3:816–30. doi: 10.1086/674753

37. Albrecht EW, Stegeman CA, Heeringa P, Henning RH, van Goor H. Protective role of endothelial nitric oxide synthase. *J Pathol.* (2003) 199:8–17. doi: 10.1002/path.1250

38. Bernatchez PN, Bauer PM, Yu J, Prendergast JS, He P, Sessa WC, et al. Dissecting the molecular control of endothelial NO synthase by caveolin-1 using cell-permeable peptides. *Proc Natl Acad Sci U S A.* (2005) 102:761–6. doi: 10.1073/pnas.0407224102

39. Michel JB, Feron O, Sacks D, Michel T. Reciprocal regulation of endothelial nitric-oxide synthase by Ca^{2+}-calmodulin and caveolin. *J Biol Chem.* (1997) 272:15583–6.

40. Chen Z, Oliveira S, Zimnicka AM, Jiang Y, Sharma T, Chen S, et al. Reciprocal regulation of eNOS and caveolin-1 functions in endothelial cells. *Mol Biol Cell.* (2018) 29:1190–202. doi: 10.1091/mbc.E17-01-0049

41. Bendall JK, Alp NJ, Warrick N, Cai S, Adlam D, Rockett K, et al. Stoichiometric relationships between endothelial tetrahydrobiopterin, endothelial NO synthase (eNOS) activity, and eNOS coupling *in vivo*: insights from transgenic mice with endothelial-targeted GTP cyclohydrolase 1 and eNOS overexpression. *Circ Res.* (2005) 97:864–71. doi: 10.1161/01.RES.0000187447.03525.72

42. Qian J, Fulton D. Post-translational regulation of endothelial nitric oxide synthase in vascular endothelium. *Front Physiol.* (2013) 4:347. doi: 10.3389/fphys.2013.00347

43. Luo X, Shen YM, Jiang MN, Lou XF, Shen Y. Ocular blood flow autoregulation mechanisms and methods. *J Ophthalmol.* (2015) 2015:864871. doi: 10.1155/2015/864871

44. Prada D, Harris A, Guidoboni G, Siesky B, Huang AM, Arciero J, et al. Autoregulation and neurovascular coupling in the optic nerve head. *Surv Ophthalmol.* (2016) 61:164–86. doi: 10.1016/j.survophthal.2015.10.004

45. Wareham LK, Calkins DJ. The Neurovascular Unit in Glaucomatous Neurodegeneration. *Front Cell Dev Biol.* (2020) 8:452. doi: 10.3389/fcell.2020.00452

46. Nyborg NC, Nielsen PJ. The level of spontaneous myogenic tone in isolated human posterior ciliary arteries decreases with age. *Exp Eye Res.* (1990) 51:711–5.

47. Polak K, Luksch A, Berisha F, Fuchsjaeger-Mayrl G, Dallinger S, Schmetterer L, et al. Altered nitric oxide system in patients with open-angle glaucoma. *Arch Ophthalmol.* (2007) 125:494–8. doi: 10.1001/archopht.125.4.494

48. Schmidl D, Garhofer G, Schmetterer L. The complex interaction between ocular perfusion pressure and ocular blood flow: relevance for glaucoma. *Exp Eye Res.* (2011) 93:141–55. doi: 10.1016/j.exer.2010.09.002

49. Moore D, Harris A, Wudunn D, Kheradiya N, Siesky B. Dysfunctional regulation of ocular blood flow: a risk factor for glaucoma? *Clin Ophthalmol.* (2008) 2:849–61. doi: 10.2147/OPTH.S2774

50. Feke GT, Pasquale LR. Retinal blood flow response to posture change in glaucoma patients compared with healthy subjects. *Ophthalmology.* (2008) 115:246–52. doi: 10.1016/j.ophtha.2007.04.055

51. Emre M, Orgül S, Haufschild T, Shaw SG, Flammer J. Increased plasma endothelin-1 levels in patients with progressive open angle glaucoma. *Br J Ophthalmol.* (2005) 89:60–3. doi: 10.1136/bjo.2004.046755

52. Kunimatsu S, Mayama C, Tomidokoro A, Araie M. Plasma endothelin-1 level in Japanese normal tension glaucoma patients. *Curr Eye Res.* (2006) 31:727–31. doi: 10.1080/02713680600837382

53. Cellini M, Strobbe E, Gizzi C, Balducci N, Toschi PG, Campos EC, et al. Endothelin-1 plasma levels and vascular endothelial dysfunction in primary open angle glaucoma. *Life Sci.* (2012) 91:699–702. doi: 10.1016/j.lfs.2012.02.013

54. Chen HY, Chang YC, Chen WC, Lane HY. Association between plasma endothelin-1 and severity of different types of glaucoma. *J Glaucoma.* (2013) 22:117–22. doi: 10.1097/IJG.0b013e31822e8c65

55. Howell GR, Macalinao DG, Sousa GL, Walden M, Soto I, Kneeland SC, et al. Molecular clustering identifies complement and endothelin induction as early events in a mouse model of glaucoma. *J Clin Invest.* (2011) 121:1429–44. doi: 10.1172/JCI44646

56. Tezel G. Oxidative stress in glaucomatous neurodegeneration: mechanisms and consequences. *Prog Retin Eye Res.* (2006) 25:490–513. doi: 10.1016/j.preteyeres.2006.07.003

57. Doganay S, Evereklioglu C, Turkoz Y, Er H. Decreased nitric oxide production in primary open-angle glaucoma. *Eur J Ophthalmol.* (2002) 12:44–8. doi: 10.1177/112067210201200109

58. Galassi F, Renieri G, Sodi A, Ucci F, Vannozzi L, Masini E, et al. Nitric oxide proxies and ocular perfusion pressure in primary open angle glaucoma. *Br J Ophthalmol.* (2004) 88:757–60. doi: 10.1136/bjo.2003.028357

59. Chun M, Liyanage UK, Lisanti MP, Lodish HF. Signal transduction of a G protein-coupled receptor in caveolae: colocalization of endothelin and its receptor with caveolin. *Proc Natl Acad Sci U S A.* (1994) 91:11728–32.

60. Yamaguchi T, Murata Y, Fujiyoshi Y, Doi T. Regulated interaction of endothelin B receptor with caveolin-1. *Eur J Biochem.* (2003) 270:1816–27. doi: 10.1046/j.1432-1033.2003.03544.x

61. Trible JR, Costa VP, Sergott RC, Spaeth GL, Smith M, Wilson RP, et al. The influence of primary open-angle glaucoma upon the retrobulbar circulation: baseline, postoperative and reproducibility analysis. *Trans Am Ophthalmol Soc.* (1993) 91:245–61; discussion 61–5.

62. Gu X, Fliesler SJ, Zhao YY, Stallcup WB, Cohen AW, Elliott MH, et al. Loss of caveolin-1 causes blood-retinal barrier breakdown, venous enlargement, and mural cell alteration. *Am J Pathol.* (2014) 184:541–55. doi: 10.1016/j.ajpath.2013.10.022

63. Hamilton NB, Attwell D, Hall CN. Pericyte-mediated regulation of capillary diameter: a component of neurovascular coupling in health and disease. *Front Neuroenerg.* (2010) 2:5. doi: 10.3389/fnene.2010.00005

64. Attwell D, Buchan AM, Charpak S, Lauritzen M, Macvicar BA, Newman EA, et al. Glial and neuronal control of brain blood flow. *Nature.* (2010) 468:232–43. doi: 10.1038/nature09613

65. Garhöfer G, Zawinka C, Huemer KH, Schmetterer L, Dorner GT. Flicker light-induced vasodilatation in the human retina: effect of lactate and changes in mean arterial pressure. *Invest Ophthalmol Vis Sci.* (2003) 44:5309–14. doi: 10.1167/iovs.03-0587

66. Gugleta K, Kochkorov A, Waldmann N, Polunina A, Katamay R, Flammer J, et al. Dynamics of retinal vessel response to flicker light in glaucoma patients and ocular hypertensives. *Graefes Arch Clin Exp Ophthalmol.* (2012) 250:589–94. doi: 10.1007/s00417-011-1842-2

67. Gugleta K, Fuchsjäger-Mayrl G, Orgül S. Is neurovascular coupling of relevance in glaucoma? *Surv Ophthalmol.* (2007) 52:S139–43. doi: 10.1016/j.survophthal.2007.08.009

68. Qu J, Wang D, Grosskreutz CL. Mechanisms of retinal ganglion cell injury and defense in glaucoma. *Exp Eye Res.* (2010) 91:48–53. doi: 10.1016/j.exer.2010.04.002

69. Liu B, Neufeld AH. Expression of nitric oxide synthase-2 (NOS-2) in reactive astrocytes of the human glaucomatous optic nerve head. *Glia.* (2000) 30:178–86. doi: 10.1002/(SICI)1098-1136(200004)30:2<178::AID-GLIA7>3.0.CO;2-C

70. Saccà SC, Izzotti A. Oxidative stress and glaucoma: injury in the anterior segment of the eye. *Prog Brain Res.* (2008) 173:385–407. doi: 10.1016/S0079-6123(08)01127-8

71. Shibata M, Oku H, Sugiyama T, Kobayashi T, Tsujimoto M, Okuno T, et al. Disruption of gap junctions may be involved in impairment of autoregulation in optic nerve head blood flow of diabetic rabbits. *Invest Ophthalmol Vis Sci.* (2011) 52:2153–9. doi: 10.1167/iovs.10-6605

72. Malone P, Miao H, Parker A, Juarez S, Hernandez MR. Pressure induces loss of gap junction communication and redistribution of connexin 43 in astrocytes. *Glia.* (2007) 55:1085–98. doi: 10.1002/glia.20527

73. Ivanova E, Kovacs-Oller T, Sagdullaev BT. Domain-specific distribution of gap junctions defines cellular coupling to establish a vascular relay in the retina. *J Comp Neurol.* (2019) 527:2675–93. doi: 10.1002/cne.24699

74. Soto I, Howell GR. The complex role of neuroinflammation in glaucoma. *Cold Spring Harb Perspect Med.* (2014) 4:8. doi: 10.1101/cshperspect.a017269

75. Liu J, Razani B, Tang S, Terman BI, Ware JA, Lisanti MP, et al. Angiogenesis activators and inhibitors differentially regulate caveolin-1 expression and caveolae formation in vascular endothelial cells. Angiogenesis inhibitors block vascular endothelial growth factor-induced down-regulation of caveolin-1. *J Biol Chem.* (1999) 274: 15781–5.

76. Mirzapour-Shafiyi F, Kametani Y, Hikita T, Hasegawa Y, Nakayama M. Numerical evaluation reveals the effect of branching morphology on vessel transport properties during angiogenesis. *PLoS Comput Biol.* (2021) 17:e1008398. doi: 10.1371/journal.pcbi.1008398

77. Asrani S, Zeimer R, Wilensky J, Gieser D, Vitale S, Lindenmuth K, et al. Large diurnal fluctuations in intraocular pressure are an independent risk factor in patients with glaucoma. *J Glaucoma.* (2000) 9:134–42. doi: 10.1097/00061198-200004000-00002

78. Liu JH, Zhang X, Kripke DF, Weinreb RN. Twenty-four-hour intraocular pressure pattern associated with early glaucomatous changes. *Invest Ophthalmol Vis Sci.* (2003) 44:1586–90. doi: 10.1167/iovs.02-0666

79. Wax MB, Camras CB, Fiscella RG, Girkin C, Singh K, Weinreb RN, et al. Emerging perspectives in glaucoma: optimizing 24-h control of intraocular pressure. *Am J Ophthalmol.* (2002) 133:S1–10. doi: 10.1016/S0002-9394(02)01459-9

80. Liu H, Fan S, Gulati V, Camras LJ, Zhan G, Ghate D, et al. Aqueous humor dynamics during the day and night in healthy mature volunteers. *Arch Ophthalmol.* (2011) 129:269–75. doi: 10.1001/archophthalmol.2011.4

81. Melgarejo JD, Maestre GE, Mena LJ, Lee JH, Petitto M, Chávez CA, et al. Normal-tension glaucomatous optic neuropathy is related to blood pressure variability in the Maracaibo Aging Study. *Hypertens Res.* (2021) 44:1105–12. doi: 10.1038/s41440-021-00687-1

82. Shin JW, Jo YH, Song MK, Won HJ, Kook MS. Nocturnal blood pressure dip and parapapillary choroidal microvasculature dropout in normal-tension glaucoma. *Sci Rep.* (2021) 11:206. doi: 10.1038/s41598-020-80705-3

83. Sherwood A, Steffen PR, Blumenthal JA, Kuhn C, Hinderliter AL. Nighttime blood pressure dipping: the role of the sympathetic nervous system. *Am J Hypertens.* (2002) 15:111–8. doi: 10.1016/S0895-7061(01)02251-8

84. Choi J, Jeong J, Cho HS, Kook MS. Effect of nocturnal blood pressure reduction on circadian fluctuation of mean ocular perfusion pressure: a risk factor for normal tension glaucoma. *Invest Ophthalmol Vis Sci.* (2006) 47:831–6. doi: 10.1167/iovs.05-1053

85. Heijl A, Leske MC, Bengtsson B, Hyman L, Bengtsson B, Hussein M, et al. Reduction of intraocular pressure and glaucoma progression: results from the Early Manifest Glaucoma Trial. *Arch Ophthalmol.* (2002) 120:1268–79. doi: 10.1001/archopht.120.10.1268

86. Delaney Y, Walshe TE, O'Brien C. Vasospasm in glaucoma: clinical and laboratory aspects. *Optom Vis Sci.* (2006) 83:406–14. doi: 10.1097/01.opx.0000225877.13217.01

87. Desjardins F, Lobysheva I, Pelat M, Gallez B, Feron O, Dessy C, et al. Control of blood pressure variability in caveolin-1-deficient mice: role of nitric oxide identified *in vivo* through spectral analysis. *Cardiovasc Res.* (2008) 79:527–36. doi: 10.1093/cvr/cvn080

88. Sethna S, Chamakkala T, Gu X, Thompson TC, Cao G, Elliott MH, et al. Regulation of phagolysosomal digestion by caveolin-1 of the retinal pigment epithelium is essential for vision. *J Biol Chem.* (2016) 291:6494–506. doi: 10.1074/jbc.M115.687004

89. Baba K, Goyal V, Tosini G. Circadian regulation of retinal pigment epithelium function. *Int J Mol Sci.* (2022) 23:5. doi: 10.3390/ijms23052699

90. Beckers HJ, Schouten JS, Webers CA, van der Valk R, Hendrikse FS. A effects of commonly used glaucoma medications: comparison of tolerability, chance of discontinuation, and patient satisfaction. *Graefes Arch Clin Exp Ophthalmol.* (2008) 246:1485–90. doi: 10.1007/s00417-008-0875-7

91. Anderson DR. Collaborative normal tension glaucoma study. *Curr Opin Ophthalmol.* (2003) 14:86–90. doi: 10.1097/00055735-200304000-00006

92. Cockburn DM. Does reduction of intraocular pressure (IOP) prevent visual field loss in glaucoma? *Am J Optom Physiol Opt.* (1983) 60:705–11.

93. Chen MJ. Normal tension glaucoma in Asia: epidemiology, pathogenesis, diagnosis, and management. *Taiwan J Ophthalmol.* (2020) 10:250–4. doi: 10.4103/tjo.tjo_30_20

94. Killer HE, Pircher A. Normal tension glaucoma: review of current understanding and mechanisms of the pathogenesis. *Eye.* (2018) 32:924–30. doi: 10.1038/s41433-018-0042-2

95. Lin X, Barravecchia M, Matthew Kottmann R, Sime P, Dean DA. Caveolin-1 gene therapy inhibits inflammasome activation to protect from bleomycin-induced pulmonary fibrosis. *Sci Rep.* (2019) 9:19643. doi: 10.1038/s41598-019-55819-y

96. Heller R, Heller LC. Gene electrotransfer clinical trials. *Adv Genet.* (2015) 89:235–62. doi: 10.1016/bs.adgen.2014.10.006

97. Wang S, Leem JS, Podvin S, Hook V, Kleschevnikov N, Savchenko P, et al. Synapsin-caveolin-1 gene therapy preserves neuronal and synaptic morphology and prevents neurodegeneration in a mouse model of AD. *Mol Ther Methods Clin Dev.* (2021) 21:434–50. doi: 10.1016/j.omtm.2021.03.021

98. Jia Y, Wei E, Wang X, Zhang X, Morrison JC, Parikh M, et al. Optical coherence tomography angiography of optic disc perfusion in glaucoma. *Ophthalmology.* (2014) 121:1322–32. doi: 10.1016/j.ophtha.2014.01.021

99. Liu L, Jia Y, Takusagawa HL, Pechauer AD, Edmunds B, Lombardi L, et al. Optical coherence tomography angiography of the peripapillary retina in glaucoma. *JAMA Ophthalmol.* (2015) 133:1045–52. doi: 10.1001/jamaophthalmol.2015.2225

frontiers | Frontiers in Medicine

TYPE Original Research
PUBLISHED 13 March 2023
DOI 10.3389/fmed.2023.1107064

OPEN ACCESS

EDITED BY
Leopold Schmetterer,
Medical University of Vienna,
Austria

REVIEWED BY
Berthold Pemp,
Medical University of Vienna,
Austria
Jacqueline Chua,
Singapore National Eye Center,
Singapore

*CORRESPONDENCE
Huiya Fan
✉ fanhy1122@163.com

†These authors have contributed equally to this work and share first authorship

SPECIALTY SECTION
This article was submitted to Ophthalmology, a section of the journal Frontiers in Medicine

RECEIVED 24 November 2022
ACCEPTED 22 February 2023
PUBLISHED 13 March 2023

CITATION
Li Y, Wu K, Chen Z, Xu G, Wang D, Wang J, Bulloch G, Borchert G and Fan H (2023) The association between retinal microvasculature derived from optical coherence tomography angiography and systemic factors in type 2 diabetics.
Front. Med. 10:1107064.
doi: 10.3389/fmed.2023.1107064

The association between retinal microvasculature derived from optical coherence tomography angiography and systemic factors in type 2 diabetics

Yi Li[1,2†], Kunfang Wu[1†], Zilin Chen[1], Guihua Xu[1], Dingding Wang[1], Juanjuan Wang[1], Gabriella Bulloch[3,4], Grace Borchert[3,4] and Huiya Fan[1*]

[1]Department of Ophthalmology, Huizhou Central People's Hospital, Huizhou, China, [2]Shantou University Medical College, Shantou, China, [3]Centre for Eye Research Australia, Melbourne, VIC, Australia, [4]The University of Melbourne, Melbourne, VIC, Australia

Aims: To investigate the correlation between the retinal microvasculature using optical coherence tomography angiography (OCTA) and systemic factors in type 2 diabetes mellitus (T2DM) patients.

Methods: This cross-sectional study obtained OCTA data from patients with T2DM administered at hospital and referred to ophthalmic services. Patient data about demographics, comorbid conditions, and blood biomarkers were extracted from electronic medical records. Data from OCTA scans obtained by CIRRUS HD-OCT Model 5,000 were obtained. Vessel density (VD) and perfusion density (PD) within the superficial capillary plexus, and foveal avascular zone (FAZ) area were automatically segmented. These parameters were tested for their correlations with systemic factors by univariate and multivariable linear regression analyses.

Results: A total of 144 T2DM patients (236 eyes) were available for analysis, with mean age of 53.6 (SD=10.34) and 56.9% were male. Chronic kidney disease, cardiovascular disease, increased serum creatinine (Scr), red blood cell count (RBC), platelets (PLT), apolipoprotein B (APOB), and decreased urine albumin to creatinine ratio (UACR) were significantly associated with lower VD and PD (all $p<0.013$). UACR and triglyceride (TRIG) were significantly correlated with FAZ area (all $p<0.017$). In multivariate analyses, PLT, eGFR, and APOB were independent risk factors for retinal rarefaction, and UACR was a significant predictor of FAZ area.

Conclusion: We found several systemic risk factors, such as PLT, renal function and lipid profiles were associated with PD, VD, and FAZ area among Chinese T2DM patients.

KEYWORDS

OCTA, retinal microvasculature, systemic factors, T2DM, correlation

Introduction

Type 2 diabetes mellitus (T2DM) is a worldwide epidemic that carries considerable morbidity, mortality, and financial burden from its deleterious complications and associations with other comorbid conditions. According to the latest International Diabetes Federation (IDF) diabetes atlas (1), an estimated 537 million people had diabetes in 2021, with this figure projected to reach 643 million by 2030.

Type 2 diabetes mellitus accounts for over 90% of all diabetes worldwide (1, 2) and is characterized by chronic hyperglycemia and insulin resistance resulting from lifestyle and genetic factors. If uncontrolled, T2DM leads to vascular damage of the eyes, kidneys, and heart. (3) Increased vascular permeability, vascular cell apoptosis, and altered blood flow contribute to macrovascular (peripheral vascular disease and coronary heart disease) and microvascular (diabetic retinopathy and diabetic nephropathy) complications (4) which result in morbidity and eventually mortality if unmanaged. Therefore, early identification and risk stratification of T2DM patients who are at risk of vascular complications is an area of growing research for the control and prevention of poor outcomes.

The retina is a structure at the back of the eye that contains a rich network of microvasculature. Growing evidence suggests retinal imaging can detect microstructural changes to vascular networks, (5) and fundoscopy studies (6–8) report concordance between the retinal microvasculature and systemic risk factors such as hypertension, diabetes, and smoking. A recent study also discovered significant retinal microvascular alterations in diabetic patients with subclinical atherosclerosis. (9) These findings have led to the idea that the retina is the window to the cardiovascular system and its suggestion as a screening tool.

Optical coherence tomography angiography (OCTA) is a non-invasive imaging technique that allows for three-dimensional visualization of retinal microvasculature networks with contrast for high-resolution imaging. Unlike fundoscopy, it can detect subtle microvascular abnormalities on retinal layers and choriocapillaris, which has led to its establishment for the early detection of diabetic retinopathy (DR). (10, 11) Additionally, OCTA can quantify the number of perfused vessels in the vascular bed (functional rarefaction) and perfused vessels in the tissue (structural rarefaction) (12), making it a useful tool for evaluating microvascular changes longitudinally in people with T2DM, dyslipidemia, and chronic kidney disease. (13–15)

Despite the widespread use of OCTA for eye diseases, little is known about the impact of systemic risk factors on OCTA parameters in diabetic eyes. Therefore, this study investigated the association between OCTA-derived retinal microvasculature parameters and systemic factors to understand its impact on vascular function in a Chinese diabetic population.

Materials and methods

Study population

This cross-sectional study included T2DM patients who had admitted to and received ophthalmic consultation in Huizhou Central People's Hospital from January 2021 to June 2022. This study was approved by the Institutional Review Board of Huizhou Central People's Hospital (IRB approval number: kyl20210115) and followed the tenets of the Declaration of Helsinki. Written informed consent was obtained from all participants.

This study included patients with T2DM (2) aged >18 years old. Participants were excluded if they had: (1) severe media opacity (e.g., corneal disease, dense cataract, vitreous hemorrhage); (2) any ocular illness that may affect ocular circulation (e.g., glaucoma, retinal vascular occlusion, retinal detachment, exudative aged macular degeneration, pathologic myopia); (3) signal strength of OCTA scans <5/10, or OCTA scans with artifacts or segmentation errors; (4) a history of surgical treatments for eye diseases (except cataract) or laser treatment; (5) uncontrollable high blood pressure (HBP) (≥180/110 mmHg); (6) any severe systemic diseases (e.g., tumor, heart failure, and cerebral infarction);

Obtaining data on systemic factors and blood biomarkers

Systemic factors were retrieved from patient electronic medical records (EMR) and included gender, age, time from diagnosis of T2DM, body mass index (BMI), blood pressure readings, smoking history, cardiovascular disease history, chronic kidney disease history, obesity, and blood biomarkers. These included systolic blood pressure (SBP), diastolic blood pressure (DBP), glucose, hemoglobin A1c (HbA1c), red blood cell count (RBC), hemoglobin (HGB), blood platelet (PLT), serum creatinine (Scr), estimated glomerular filtration rate (eGFR), urine albumin to creatinine ratio (UACR), total cholesterol (CHOL), triglyceride (TRIG), high-density lipoprotein cholesterol (HDL), low-density lipoprotein cholesterol (LDL), lipoprotein a (Lpa), apolipoprotein A (ApoA), apolipoprotein B (ApoB). All patients had their blood drawn at 8 AM after an overnight fast and before taking morning medications. Overnight first-void urine samples were also obtained. The eGFR was calculated based on the Chronic Kidney Disease Epidemiology Collaboration (CKD-EPI) equation (16). Chronic kidney disease was defined as eGFR<60 ml/min/1.73m^2. Body mass index was calculated as weight in kilograms divided by the square of height in meters. Obesity was defined as BMI ≥ 28 kg/m^2.

Ocular examinations and imaging

All patients underwent an ophthalmic examination, which included best-corrected visual acuity, intraocular pressure, silt lamp examination, fundus photographs, fluorescein fundus angiography (FFA), optical coherence tomography (OCT), and OCTA by a single trained technician. The presence of DR was confirmed based on FFA, and was categorized as NDR, mild non-proliferative DR (mild NPDR), moderate non-proliferative DR (moderate NPDR), severe non-proliferative DR (severe NPDR), and proliferative DR (PDR) according to the International Clinical Diabetic Retinopathy Severity Scales. (17) Patients underwent OCTA scanning using CIRRUS HD-OCT Model 5,000 (Carl Zeiss, Germany), which uses a super luminescent diode (SLD) with a central wavelength of 840 nm, and a scanning speed of 68,000 A-scans/s. The macular region was scanned using a 6 mm × 6 mm scan pattern, each consisting of 245 A-scan per B-scan. This was automatically divided into three fields: the foveal area (a central circle with a diameter of 1 mm), the parafoveal area (an annulus centered on the fovea with an inner ring with a diameter

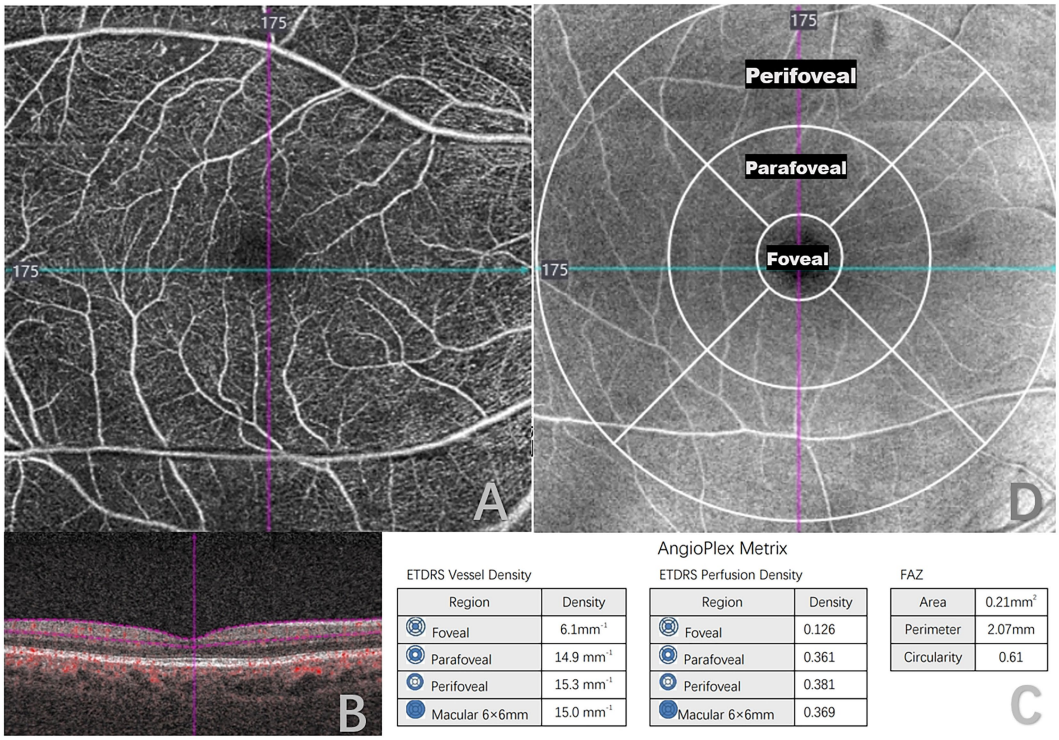

FIGURE 1
Quantitative measurement of optical coherence tomography angiography (OCTA) 6×6-mm scans in a type 2 diabetes mellitus (T2DM) patient. **(A)** 6×6-mm en face image of the superficial capillary plexus (SCP). **(B)** B-scans with flow encoding show the slab segmentation (horizontal purple lines), which included the SCP. **(C)** Angioplex metrics, including vessel density, perfusion density and foveal avascular zone (FAZ) parameters. **(D)** OCT en face image of the superficial layer overlaid with the early treatment of diabetic retinopathy study grid (ETDRS).

of 3 mm), and the perifoveal area (an annulus centered on the fovea with outer ring diameters of 6 mm; Figure 1).Vessel density (VD), perfusion density (PD), and foveal avascular zone (FAZ) parameters were quantitatively analyzed within the superficial capillary plexus (SCP), defined as the area extending from the inner limiting membrane to 110 μm above the retinal pigment epithelium. This was analyzed by built-in angiography software, which calculated the average VD and PD using a grid overlay according to standard ETDRS subfields. VD was defined as the total length of perfused vessels per unit area in the measurement region, and PD was defined as the total area of perfused retinal microvasculature per unit area on binarized vasculature images. FAZ was defined as a region within the foveal at the center of the retina devoid of retinal blood vessels. Area, perimeter, and circularity are FAZ parameters that we used for this study.

Statistical analysis

All data analyses were performed using SPSS version 25.0 (IBM Corp, Armonk, NY, USA). Continuous data were represented as mean ± standard deviations (SD), categorical data were expressed as number (percentage, %). Univariate linear regression models were used to analyze potential associations between systemic risk factors and OCTA-derived metrics, with regression coefficients calculated to estimate the magnitude of microvascular change associated with predictor variables. Bonferroni correction for multiple comparison was performed to assess differences between FAZ parameters and VD, PD at each annulus. Multiple linear regression analyses were subsequently performed to determine independent risk factors of retinal microvascular dysfunction. Generalized estimating equations approach were used to adjust for correlations between paired eyes. A p-value of <0.013 (0.05/4) for VD, PD, and a p-value of <0.017 (0.05/3) for FAZ parameters were considered statistically significant for association.

Results

A total of 191 patients underwent OCTA examinations. Thirty participants were excluded due to a history of reported ocular diseases, surgeries, or laser treatments, and 10 participants were excluded due to a history of severe systemic diseases or having type 1 diabetes. A further seven participants were excluded due to poor quality. 236 eyes of 144 T2DM patients were included for analysis, with a mean (SD) age of 53.61 (10.34) years, and 56.9% males. Characteristics of participants are detailed in Table 1, and prevalence of hypertension (33.3%), chronic kidney disease (12.5%), smoking history (22.2%), obesity (7.6%), and cardiovascular disease (6.3%) were noted amongst study subjects.

Table 2 describes the mean characteristics of vessel density and perfusion density within regions captured by OCTA. Mean SCP-VD in the parafoveal region was 14.97 ± 2.88 and 15.23 ± 2.31 mm^{-1} in the macular region. Mean SCP-PD in the parafoveal region was 0.36 ± 0.07

TABLE 1 Patient demographics and clinical characteristics.

Characteristic	Subjects (*n*=144)
Demographics	
Male, *n* (%)	82 (56.9)
Age (y)	53.61 ± 10.34
DM duration (y)	7.92 ± 5.48
BMI (kg/m^2)	23.51 ± 3.39
SBP (mmHg)	128.36 ± 16.51
DBP (mmHg)	80.19 ± 10.04
Comorbidities	
Hypertension, *n* (%)	48 (33.3)
Chronic kidney disease, *n* (%)	18 (12.5)
Cardiovascular disease, *n* (%)	9 (6.3)
Smoking history, *n* (%)	32 (22.2)
Obesity, *n* (%)	11 (7.6)
DR, *n* (%)	115 (79.9)
DR stage	
Mild NPDR, *n* (%)	54 (20.1)
Moderate NPDR, *n* (%)	16 (11.1)
Severe NPDR, *n* (%)	22 (15.3)
PDR, *n* (%)	23 (16.0)
Lab values	
HbA1c (%)	9.69 ± 2.56
Glucose (mmol/L)	12.13 ± 5.69
HGB (g/L)	133.40 ± 19.30
RBC (10^12/L)	4.59 ± 0.77
PLT (10^9/L)	254.01 ± 73.72
Scr (μmol/L)	72 (IQR 61–88)
eGFR (mL/min/L.73m^2)	89.05 ± 24.84
UACR (mg/g)	19 (IQR 8–89)
CHOL (mmol/L)	4.84 ± 1.23
TRIG (mmol/L)	2.34 ± 1.98
HDL (mmol/L)	1.00 ± 0.30
LDL (mmol/L)	3.05 ± 1.07
Lpa (mg/L)	0.29 ± 0.27
APOA (g/L)	1.19 ± 0.26
APOB (g/L)	1.12 ± 0.57

BMI, body mass index; SBP, systolic blood pressure; DBP, diastolic blood pressure; DM, diabetes mellitus; DR, diabetic retinopathy; NPDR, nonproliferative diabetic retinopathy; PDR, proliferative diabetic retinopathy; RBC, red blood cell count; HGB, hemoglobin; PLT, blood platelet; eGFR, estimated glomerular filtration rate; Scr, serum creatinine; UACR, urine albumin to creatinine ratio; CHOL, total cholesterol; TRIG, triglyceride; HDL, high-density lipoprotein cholesterol; LDL, low-density lipoprotein cholesterol; Lpa, lipoprotein a; ApoA, apolipoprotein A; ApoB, apolipoprotein B.

and 0.37 ± 0.06 in the macular region. The average FAZ area was 0.29 ± 0.12 mm^2.

Table 3 demonstrates the association of various systemic factors with SCP-VD in anatomical regions captured by OCTA. Significant associations with signal strength, sex, cardiovascular disease, DR stage, CKD, RBC, PLT, Scr, UACR, and APOB for VD were apparent

TABLE 2 Vessel density and perfusion density in superficial vascular capillary plexus and foveal avascular zone (FAZ) measurements.

Optical coherence tomography angiography (OCTA) parameters	(*n*=236 eyes)
Signal strength	7.78 ± 1.28
Vessel density (mm^{-1})	
Foveal	5.76 ± 2.91
Parafoveal	14.97 ± 2.88
Perifoveal	15.67 ± 2.26
Macular 6*6 mm	15.23 ± 2.31
Perfusion density	
Foveal	0.13 ± 0.07
Parafoveal	0.36 ± 0.07
Perifoveal	0.39 ± 0.06
Macular 6*6 mm	0.37 ± 0.06
FAZ parameters	
FAZ area (mm^2)	0.29 ± 0.12
FAZ perimeter (mm)	2.25 ± 0.55
FAZ circularity	0.68 ± 0.09

on univariate analysis (all $p < 0.05$). Following multivariable analysis, macular VD correlated positively with signal strength ($\beta = 0.968$, $p < 0.001$), eGFR ($\beta = 0.601$, $p = 0.009$), and APOB ($\beta = 0.290$, $p < 0.001$). Similarly, abnormal renal function was associated with reduced VD as measured by OCTA (Figure 2). Foveal VD was also significantly correlated with signal strength ($\beta = 0.559$, $p = 0.001$), diabetes mellitus (DM) duration ($\beta = 0.576$, $p = 0.011$), and PLT ($\beta = 0.544$, $p = 0.003$).

Table 4 demonstrates associations between systemic factors and SCP-PD. Univariate linear regression analysis showed that sex, signal strength, cardiovascular disease, DR stage, PLT, Scr, and APOB were associated with PD (all $p < 0.013$). Following adjustment for confounding factors, positive associations remained for signal strength ($\beta = 0.027$, $p < 0.001$), DM duration ($\beta = 0.013$, $p = 0.012$), PLT ($\beta = 0.013$, $p = 0.002$), eGFR ($\beta = 0.017$, $p = 0.006$), and APOB ($\beta = 0.007$, $p = 0.002$). The diagrams showing the correlations between OCTA parameters and systemic risk factors such as PLT, APOB and eGFR are shown in Figure 3.

Table 5 shows the association between systemic factors and FAZ parameters in OCTA 6 × 6-mm scans. Univariate linear regression analysis showed that DR stage, UACR, and TRIG were associated with FAZ parameters (all $p < 0.017$). In a multivariable-adjusted model, UACR was negatively associated with FAZ area ($\beta = -0.029$, $p = 0.007$) and FAZ perimeter ($\beta = -0.159$, $p = 0.003$), whilst age and chronic kidney disease positively impacted FAZ area ($\beta = 0.030$, $p = 0.06$; $\beta = 0.128$, $p = 0.016$, respectively), and FAZ perimeter ($\beta = 0.117$, $p = 0.014$; $\beta = 0.688$, $p = 0.007$, respectively).

Discussion

In this study, the retinal microvasculature of a Chinese population with T2DM was examined for its correlation with

TABLE 3 Associations of systemic factors with vessel density in 6×6-mm optical coherence tomography angiography (OCTA) scans.

	(a) Univariate analysis							
	Foveal	*P*-value	Parafoveal	*P*-value	Perifoveal	*P*-value	Macular	*P*-value
Demographics								
Sex	**1.157**	**0.007***	0.394	0.370	0.091	0.798	0.191	0.596
Age	−0.298	0.117	−0.088	0.790	−0.197	0.302	−0.176	0.370
DM duration	0.212	0.420	−0.187	0.298	**−0.337**	**0.045**	−0.289	0.072
BMI	−0.007	0.977	0.391	0.079	0.121	0.543	0.177	0.365
SBP	0.238	0.463	0.026	0.904	−0.294	0.177	−0.211	0.309
DBP	0.379	0.148	0.279	0.209	−0.014	0.947	0.061	0.763
Signal strength	0.285	0.136	**0.931**	**<0.001***	**0.981**	**<0.001***	**0.949**	**<0.001***
Comorbidities								
Hypertension	−0.507	0.293	−0.459	0.358	−0.526	0.174	−0.512	0.200
Cardiovascular disease	0.050	0.950	0.837	0.108	**1.061**	**0.011***	**0.988**	**0.019**
Smoking	0.542	0.384	**0.906**	**0.044**	**0.800**	**0.048**	**0.817**	**0.037**
Chronic kidney disease	0.921	0.452	**−1.234**	**0.046**	**−1.626**	**0.009***	**−1.469**	**0.013**
Obesity	−0.025	0.969	0.764	0.311	0.316	0.660	0.411	0.563
DR stage								
Mild NPDR	0.192	0.702	−0.754	0.115	−0.756	0.037	−0.724	0.053
Moderate NPDR	−0.202	0.708	−0.812	0.162	−0.652	0.138	−0.685	0.132
Severe NPDR	1.304	0.171	**−1.744**	**0.031**	**−2.220**	**<0.001***	**−2.018**	**0.002***
PDR	0.555	0.438	**−1.982**	**0.001***	**−2.229**	**<0.001***	**−2.107**	**<0.001***
Lab values								
Glucose	0.003	0.986	−0.044	0.814	−0.019	0.897	−0.025	0.867
HbA1c	0.077	0.744	0.134	0.524	0.063	0.714	0.082	0.642
HGB	−0.055	0.868	**0.586**	**0.018**	**0.437**	**0.031**	**0.459**	**0.025**
RBC	0.171	0.406	**0.472**	**0.011***	**0.347**	**0.039**	**0.372**	**0.025**
PLT	**0.565**	**0.008***	0.342	0.059	0.263	0.079	0.288	0.057
Scr	**0.872**	**0.011***	−0.017	0.923	−0.221	0.413	−0.145	0.538
eGFR	−0.447	0.187	0.184	0.363	**0.417**	**0.036**	0.343	0.072
UACR	0.641	0.188	−0.468	0.148	**−0.590**	**0.011***	**−0.532**	**0.030**
CHOL	0.411	0.080	0.005	0.981	−0.023	0.889	−0.004	0.981
TRIG	0.006	0.971	−0.188	0.360	−0.211	0.184	−0.200	0.222
HDL	−0.245	0.236	−0.148	0.461	0.095	0.532	0.031	0.842
LDL	0.340	0.231	−0.010	0.957	−0.041	0.819	−0.024	0.892
Lpa	0.256	0.564	−0.037	0.811	−0.071	0.713	−0.057	0.732
APOA	−0.180	0.415	−0.170	0.422	−0.060	0.722	−0.088	0.608
APOB	**0.411**	**0.012***	**0.427**	**<0.001***	**0.312**	**0.001***	**0.341**	**<0.001***
(b) Multivariable analysis								
	Foveal	***P*-value**	**Parafoveal**	***P*-value**	**Perifoveal**	***P*-value**	**Macular**	***P*-value**
Signal strength	**0.559**	**0.001***	**1.008**	**<0.001***	**0.973**	**<0.001***	**0.968**	**<0.001***
DM duration	**0.576**	**0.011***	0.208	0.316	0.082	0.329	0.123	0.404
Hypertension	**−0.911**	**0.033**	−0.023	0.955	−0.043	0.875	−0.059	0.837
DR stage								

(Continued)

TABLE 3 (Continued)

	(b) Multivariable analysis							
	Foveal	*P*-value	Parafoveal	*P*-value	Perifoveal	*P*-value	Macular	*P*-value
Mild NPDR	−0.009	0.993	−0.986	0.152	**−1.283**	**0.017**	**−1.193**	**0.028**
Moderate NPDR	0.727	0.401	−0.628	0.408	−1.045	0.066	−0.904	0.123
Severe NPDR	−0.355	0.487	−0.831	0.118	−0.634	0.090	−0.681	0.077
PDR	0.033	0.947	−0.792	0.084	**−0.768**	**0.015**	**−0.750**	**0.023**
PLT	**0.544**	**0.003***	0.182	0.277	0.095	0.413	0.124	0.313
eGFR	−0.077	0.817	0.547	0.064	**0.637**	**0.005***	**0.601**	**0.009***
CHOL	0.235	0.355	0.433	0.061	**−0.324**	**0.038**	**−0.327**	**0.040**
APOB	0.099	0.449	**0.424**	**0.001***	**0.258**	**0.001***	**0.290**	**<0.001***

Values in bold are results that are statistically significant before Bonferroni correction ($P < 0.05$).
*Statistically significant results ($P < 0.013$).
Multivariable model-adjusted for age, sex, signal strength, DM duration, hypertension, cardiovascular disease, DR stage, chronic kidney disease, RBC, PLT, eGFR, UACR, CHOL, TRIG, and APOB.

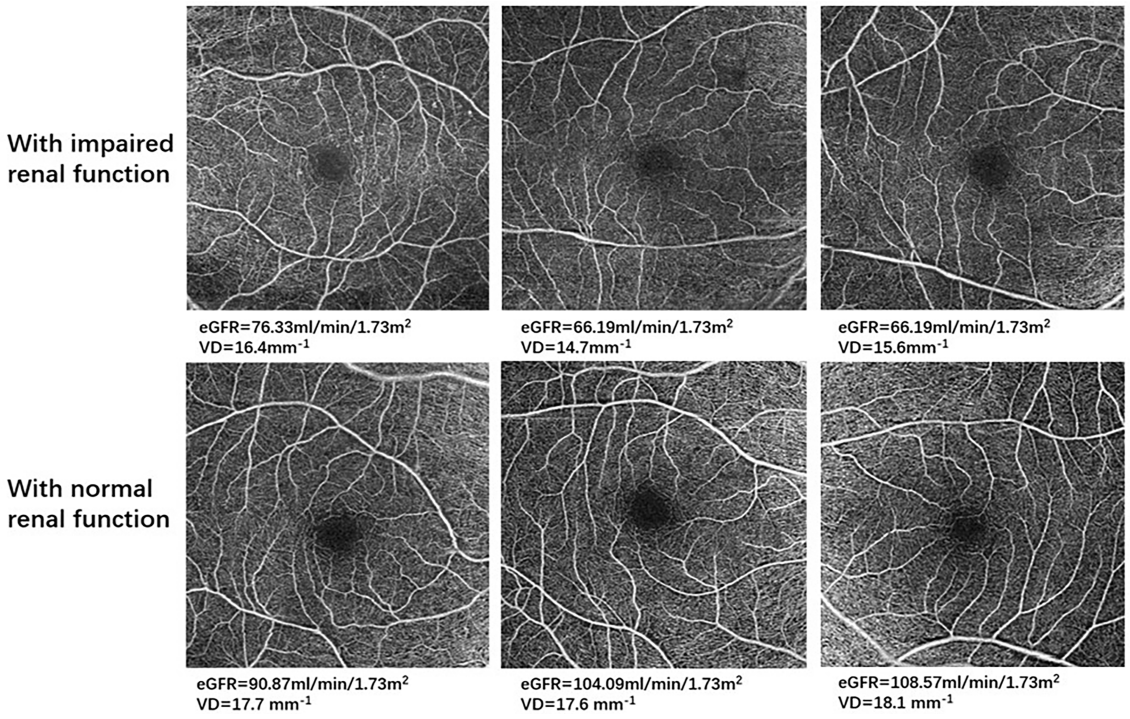

FIGURE 2
Optical coherence tomography angiography (OCTA) images in representative patients with impaired renal function and with normal renal function. For all 6×6-mm OCTA images, the top row demonstrates retinal microvasculature in type 2 diabetes mellitus (T2DM) patients with impaired renal function, and the bottom row shows retinal microvasculature in T2DM patients with normal renal function.

systemic factors. Of note, several blood biomarkers and systemic influences were correlated with VD and PD regions of interest within OCTA scans after adjustment for confounding factors, including signal strength, DM duration, PLT, eGFR, and APOB. After multivariable analysis, age, chronic kidney disease, DR stage, UACR, and APOB correlated with FAZ parameters. Our results suggest the retinal microvasculature may be influenced by the presence of systemic factors.

DM duration correlates with OCTA parameters

DM duration was independently associated with foveal VD and PD in the multivariable-adjusted model, indicating the long-term impact of abnormal blood glucose levels in the microvascular system. Our findings were in concordance with previous research by Czakó et al. (18), who found that DM duration was strongly associated with

TABLE 4 Associations of systemic factors with perfusion density in 6×6-mm optical coherence tomography angiography (OCTA) scans.

	(a) Univariate analysis							
	Foveal	*P*-value	Parafoveal	*P*-value	Perifoveal	*P*-value	Macular	*P*-value
Demographics								
Sex	**0.027**	**0.007***	0.013	0.248	0.006	0.504	0.008	0.371
Age	−0.007	0.133	−0.002	0.700	−0.005	0.281	−0.005	0.350
DM duration	0.005	0.391	−0.004	0.422	**−0.009**	**0.041**	−0.007	0.075
BMI	−0.001	0.843	0.009	0.108	0.003	0.596	0.004	0.419
SBP	0.006	0.453	0.001	0.910	−0.008	0.165	−0.006	0.300
DBP	0.009	0.149	0.007	0.238	−0.001	0.887	0.001	0.823
Signal strength	0.007	0.139	**0.023**	**<0.001***	**0.026**	**<0.001***	**0.025**	**<0.001***
Comorbidities								
Hypertension	−0.011	0.301	−0.011	0.382	−0.013	0.203	−0.013	0.229
Cardiovascular disease	0.001	0.945	0.020	0.152	**0.027**	**0.011***	**0.024**	**0.025**
Smoking	0.013	0.378	0.022	0.056	**0.021**	**0.049**	**0.021**	**0.040**
Chronic kidney disease	0.027	0.374	−0.025	0.117	**−0.037**	**0.027**	**−0.033**	**0.036**
Obesity	−0.004	0.805	0.014	0.461	0.003	0.859	0.006	0.750
DR stage								
Mild NPDR	0.005	0.674	−0.018	0.142	−0.019	0.050	−0.018	0.064
Moderate NPDR	−0.003	0.827	−0.016	0.272	−0.015	0.209	−0.015	0.211
Severe NPDR	0.032	0.157	−0.035	0.089	**−0.051**	**0.003***	**−0.045**	**0.010***
PDR	0.019	0.272	**−0.040**	**0.012***	**−0.047**	**0.001***	**−0.004**	**0.001***
Lab values								
Glucose	0.000	0.989	−0.001	0.765	−0.001	0.865	−0.001	0.835
HbA1c	0.002	0.768	0.002	0.680	0.002	0.675	0.002	0.669
HGB	−0.002	0.797	**0.014**	**0.033**	**0.011**	**0.033**	**0.012**	**0.032**
RBC	0.003	0.542	**0.011**	**0.024**	**0.009**	**0.043**	**0.009**	**0.035**
PLT	**0.013**	**0.008***	0.008	0.067	0.007	0.089	0.007	0.068
Scr	**0.021**	**0.019**	0.001	0.821	−0.005	0.440	−0.003	0.579
eGFR	−0.011	0.170	0.003	0.501	0.010	0.051	0.008	0.100
UACR	0.017	0.160	−0.010	0.243	**−0.014**	**0.030**	−0.012	0.064
CHOL	0.010	0.078	−0.001	0.910	−0.001	0.823	−0.001	0.895
TRIG	0.000	0.969	−0.005	0.323	−0.005	0.224	−0.005	0.248
HDL	−0.005	0.250	−0.004	0.378	0.001	0.705	0.000	0.995
LDL	0.008	0.216	0.000	0.963	−0.001	0.802	−0.001	0.870
Lpa	0.007	0.507	0.000	0.985	−0.001	0.825	−0.001	0.864
APOA	−0.004	0.408	−0.005	0.364	−0.002	0.602	−0.003	0.517
APOB	**0.009**	**0.019**	**0.010**	**0.001***	**0.007**	**0.008***	**0.008**	**0.004***
(b) Multivariable analysis								
	Foveal	***P*-value**	**Parafoveal**	***P*-value**	**Perifoveal**	***P*-value**	**Macular**	***P*-value**
Signal strength	**0.014**	**<0.001***	**0.026**	**<0.001***	**0.027**	**<0.001***	**0.027**	**<0.001***
DM duration	**0.013**	**0.012***	0.005	0.300	0.001	0.801	0.002	0.563
Hypertension	**−0.021**	**0.029**	−0.001	0.911	−0.002	0.782	−0.002	0.748
DR stage								
Mild NPDR	0.005	0.831	−0.018	0.327	−0.021	0.142	−0.020	0.174

(Continued)

TABLE 4 (Continued)

	(b) Multivariable analysis							
	Foveal	*P*-value	Parafoveal	*P*-value	Perifoveal	*P*-value	Macular	*P*-value
Moderate NPDR	0.021	0.201	−0.010	0.606	−0.020	0.192	−0.017	0.283
Severe NPDR	−0.006	0.617	−0.017	0.203	−0.014	0.155	−0.015	0.146
PDR	0.001	0.905	−0.020	0.088	**−0.020**	**0.016**	**−0.019**	**0.023**
PLT	**0.013**	**0.002***	0.004	0.295	0.002	0.557	0.003	0.405
eGFR	−0.001	0.857	0.014	0.052	**0.018**	**0.003***	**0.017**	**0.006***
CHOL	0.006	0.312	−0.012	0.043	**−0.009**	**0.023**	**−0.009**	**0.023**
APOB	0.002	0.535	**0.010**	**0.002***	**0.006**	**0.004***	**0.007**	**0.002***

Values in bold are results that are statistically significant before Bonferroni correction ($P < 0.05$).

*Statistically significant results ($P < 0.013$).

Multivariable model-adjusted for age, sex, signal strength, DM duration, hypertension, cardiovascular disease, DR stage, chronic kidney disease, RBC, PLT, eGFR, UACR, CHOL, TRIG, and APOB.

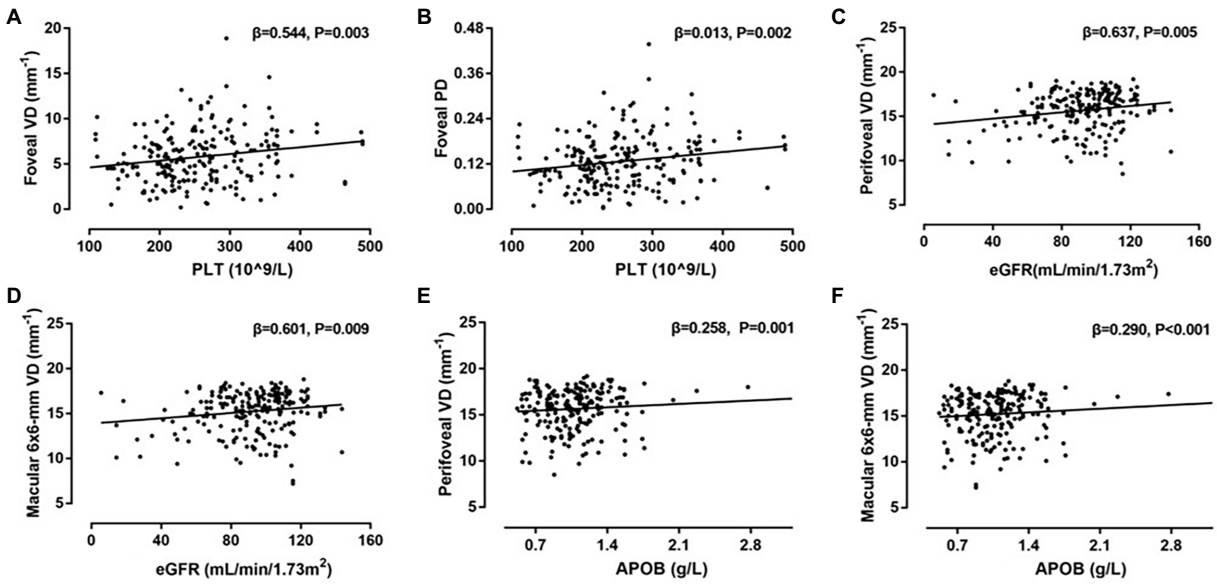

FIGURE 3
Correlations between systemic risk factors and optical coherence tomography angiography (OCTA) parameters. **(A)** Scatter plot between platelets (PLT) and vessel density (VD) in foveal; **(B)** scatter plot between PLT and perfusion density (PD) in foveal; **(C)** scatter plot between eGFR and VD in perifoveal; **(D)** scatter plot between eGFR and VD in macular 6×6-mm; **(E)** scatter plot between APOB and VD in perifoveal; **(F)** Scatter plot between apolipoprotein B (APOB) and VD in macular 6×6-mm.

decreased retinal VD after interaction analysis with the effects of systemic risk factors, and by Qian et al. (11), who reported a negative correlation between DM duration and OCTA metrics such as SCP-VD and SCP-PD in 1118 DM patients. Furthermore, larger FAZ and lower retinal capillary densities in children and adolescents with diabetes were observed in a case–control study (19), and these changes are associated with DM duration and poor glycemic control.

Although DM duration was a significant risk factor for microvascular abnormalities, we found no correlations between OCTA parameters and HbA1c or blood glucose in univariate or multivariable models. In this study, we assessed T2DM patients with a relatively short period of diabetes (71.5%, ≤10 years), and less than half of the patients (43.3%) had poor glycemic control (HbA1c > 10%), which may not be representative of all disease durations, and the results should be interpreted with caution.

Hypertension weakly correlates with OCTA parameters

Hypertension negatively impacted foveal VD and PD after controlling for confounding factors ($p < 0.05$), demonstrating some influence over vessel integrity. However, none of these correlations persist after Bonferroni correction. In spite of several observational studies (20, 21) not finding hypertension or blood pressure to be risk factors for microvascular complication in diabetics, multiple OCTA studies have demonstrated its impacts on retinal microvasculature, including Lee et al. (13) whom reported hypertension correlated with lower SCP-VD ($\beta = -0.239$, $p = 0.039$) in diabetic patients than hypertensive controls, and case-control studies by Sun et al. (22) and Donati et al. (23) demonstrating non-diabetic hypertensive eyes had decreased VD as well as increased FAZ after adjusting for sex, age, and

TABLE 5 Association of systemic factors with FAZ parameters in OCTA 6×6-mm scans.

	Univariate						Multivariable-adjusted					
	FAZ area	*P*-value	FAZ perimeter	*P*-value	FAZ circularity	*P*-value	FAZ area	*P*-value	FAZ perimeter	*P*-value	FAZ circularity	*P*-value
Demographics												
Sex	0.022	0.245	0.053	0.525	0.016	0.186	0.017	0.358	0.037	0.666	0.008	0.520
Age	**0.017**	**0.044**	0.061	0.125	0.006	0.276	**0.030**	**0.006***	**0.117**	**0.014***	−0.003	0.707
DM duration	−0.001	0.932	0.000	0.996	−0.005	0.360	-	-	-	-	-	-
BMI	0.002	0.483	−0.006	0.612	0.001	0.738	-	-	-	-	-	-
SBP	−0.009	0.342	−0.041	0.336	−0.006	0.340	-	-	-	-	-	-
DBP	−0.012	0.180	−0.058	0.107	−0.008	0.230	-	-	-	-	-	-
Signal strength	0.003	0.722	0.009	0.804	0.006	0.232	-	-	-	-	-	-
Comorbidities												
Hypertension	−0.005	0.803	0.001	0.989	−0.003	0.809	0.018	0.399	0.083	0.358	0.004	0.758
Cardiovascular disease	−0.011	0.711	−0.015	0.900	0.019	0.140	-	-	-	-	-	-
Smoking	0.000	0.999	−0.002	0.982	−0.002	0.884	-	-	-	-	-	-
Chronic kidney disease	−0.007	0.854	0.054	0.767	**−0.045**	**0.017**	**0.128**	**0.016***	**0.688**	**0.007***	−0.072	0.018
Obesity	0.031	0.167	−0.130	0.272	0.029	0.234	-	-	-	-	-	-
DR stage												
Mild NPDR	**−0.052**	**0.010***	**−0.211**	**0.011***	−0.017	0.215	**−0.063**	**0.009***	**−0.259**	**0.010***	−0.016	0.282
Moderate NPDR	0.021	0.448	**0.210**	**0.046**	**−0.065**	**0.004***	0.028	0.343	**0.249**	**0.034**	**−0.070**	**0.005***
Severe NPDR	−0.021	0.481	−0.155	0.277	−0.021	0.190	0.017	0.679	−0.067	0.731	−0.002	0.906
PDR	−0.065	0.067	−0.247	0.128	**−0.052**	**0.018**	−0.025	0.514	−0.067	0.674	−0.038	0.187
Lab values												
Glucose	−0.013	0.118	−0.046	0.159	−0.003	0.648	-	-	-	-	-	-
HbA1c	−0.013	0.153	−0.034	0.394	−0.007	0.165	-	-	-	-	-	-
HGB	−0.005	0.670	−0.013	0.773	−0.003	0.617	-	-	-	-	-	-
RBC	−0.005	0.607	−0.010	0.800	0.001	0.822	-	-	-	-	-	-
PLT	−0.016	0.123	−0.063	0.150	−0.004	0.503	-	-	-	-	-	-
Scr	−0.015	0.104	−0.057	0.148	−0.002	0.646	-	-	-	-	-	-
eGFR	0.009	0.371	0.032	0.460	0.001	0.916	0.027	0.059	0.113	0.069	−0.012	0.270

(Continued)

10.3389/fmed.2023.1107064

10.3389/fmed.2023.1107064

TABLE 5 (Continued)

	Univariate						Multivariable-adjusted					
	FAZ area	*P*-value	FAZ perimeter	*P*-value	FAZ circularity	*P*-value	FAZ area	*P*-value	FAZ perimeter	*P*-value	FAZ circularity	*P*-value
UACR	**−0.024**	**<0.001***	**−0.125**	**0.001***	−0.001	0.897	**−0.029**	**0.007***	**−0.159**	**0.003***	0.005	0.375
CHOL	**−0.020**	**0.020**	**−0.083**	**0.026**	0.002	0.699	−0.014	0.074	−0.051	0.128	0.002	0.718
TRIG	**−0.017**	**0.007***	−0.057	0.102	−0.008	0.248	−0.008	0.239	−0.026	0.438	−0.010	0.170
HDL	0.006	0.528	0.007	0.862	0.011	0.119	-	-	-	-	-	-
LDL	−0.013	0.152	−0.057	0.156	−0.001	0.854	-	-	-	-	-	-
Lpa	0.007	0.447	0.029	0.585	−0.004	0.668	-	-	-	-	-	-
APOA	0.004	0.720	−0.008	0.862	0.007	0.351	-	-	-	-	-	-
APOB	−0.007	0.216	−0.033	0.124	**0.008**	**0.026**	-	-	-	-	-	-

Values in bold are results that are statistically significant before Bonferroni correction ($P < 0.05$).
*Statistically significant results ($P < 0.017$).
Multivariable model-adjusted for age, sex, DM duration, hypertension, DR stage, chronic kidney disease, eGFR, UACR, CHOL, and TRIG.

ocular parameters. In addition, a longitudinal analysis of 4,758 T2DM patients with non- or mild DR demonstrated blood pressures conferred to risk of DR progression (24).

Hypertension is thought to contribute to accelerated microvascular impairment in individuals with T2DM. Chronic hyperglycemia results in global microvascular changes like thickening of the vascular basement membrane and increased endothelial permeability, and the presence of hypertension increases pressure along these membranes which accelerate the pathological change and weaken retinal capillary walls. Therefore, a deficit in perfusion density on OCTA should present as a red flag for underlying poor blood pressure control and could be a risk factor if investigated further. More studies with large-scale sample sizes and detailed blood pressure monitoring are required to clarify the impact of hypertension on retinal microvasculature and diabetes management.

Chronic kidney disease and renal function correlate with OCTA parameters

Our results showed that eGFR was positively associated with VD and PD, which was in line with results from previous studies exploring correlations between renal function and retinal microvasculature. Yeung et al. (25) reported that patients with CKD (eGFR<60 mL/min/1.73m^2) had lower parafoveal SCP-VD compared to those of control group ($p < 0.001$), with eGFR strongly related with SCP-VD in multivariate-adjusted models. Observational cross-sectional studies (26, 27) aimed at investigating the relationship between systemic risk factors and OCTA parameters in patients with systemic hypertension found a significant correlation between eGFR and retinal capillary density after adjusting for age, sex, and blood pressure, suggesting impaired renal function could be one of important risk factors in retinal microvascular alterations. Similarly, Zhuang et al. (28) demonstrated that decreased SCP-VD was independently correlated with lower eGFR among T2DM patients, while other investigators (29) found a significant relationship between lower SCP-VD, SCP-PD, and higher UACR in T2DM patients after controlling for systemic and ocular parameters.

In addition, our study showed that chronic kidney disease positively impacted FAZ area and perimeter, while UACR was negatively associated with FAZ area and perimeter after adjusting for multiple variables. Lee et al. (13) reported that lower eGFR was associated with greater FAZ size in diabetic patients, which suggested that abnormal renal function may have an impact on the foveal and adjacent small vessels. However, FAZ morphology can be variable even in healthy individuals (30, 31), this variation must be considered and posed as a challenge when assessing possible pathological FAZ alternations. A relatively low number of chronic kidney disease patients (18/144) in our study population may hinder the interpretation of these findings, larger longitudinal studies will be needed to examine the effects of renal function in OCTA-derived metrics.

Aberrant lipid indices correlate with OCTA parameters

Our study suggested that APOB was positively correlated with parafoveal, perifoveal and macular VD and PD, after controlling for other variables. TRIG was negatively correlated with FAZ area, although this correlation did not persist in multivariable analysis.

Dyslipidemia is an established risk factor for microvascular complications. It is now recognized that elevated CHOL levels induced inflammatory reaction in the microvascular system, which occurs long before events in the large vessels. (32) A randomized placebo-controlled trial by Kaushik et al. (33) proved that cholesterol-reducing medications retards DR progression in diabetic patients with proper glycemic control and hypercholesterolemia. This observation corresponds well with a nested case–control study by Aryan et al. (34) whom indicated a positive association of serum CHOL levels with microvascular complications (OR = 1.1, CI:1.0–2.2, $p = 0.004$) on 444 T2DM cases and 439 controls, although this correlation disappeared after interaction analysis with demographic and systemic factors. A large-scale cohort study (35), on the other hand, found a significant correlation between elevated serum levels of TRIG, decreased HDL levels, and diabetes-related microvascular complications in 72,289 T2DM patients, implying that aberrant lipid indices may reflect retinal microangiopathy in diabetics.

While there is little evidence that LDL has a causal effect on the risk of microvascular disease, growing evidence (36, 37) has shown that compared to traditional lipid indices, ApoB provides incremental information on lipid metabolism and may play a significant role in the development of vascular disease. To date, only a few studies have looked into the relationship between ApoB and retinal vascular system in diabetics. Shi et al. (38) found that foveal SCP-VD measured from OCTA 3 × 3 mm scans were negatively correlated with serum ApoB levels in T2DM patients ($\beta = -0.016$, $p < 0.001$), however, this correlation was not significant after controlling for other risk factors.

PLT correlates with OCTA parameters

Our study found that PLT was significantly associated with increased VD and PD in the foveal region after adjusting for other confounders. The influence of PLT on the microvascular system has so far remained uncertain. Considering the physical proximity of PLT to the vascular endothelium, a relationship between PLT and microvascular alterations is assumed. Yuan et al. (39) implicated that platelet hyperactivity in diabetic individuals may undermine tissue perfusion as well as contribute to microvascular occlusion. Data from 3,009 participants recruited for the Blue Mountains Eye Study (BMES) (40) revealed that higher PLT correlated with narrower arteriolar caliber and wider venular caliber, implying that elevated levels of PLT could have adverse effects on microvasculature. However, the mechanisms that underlie this association are unclear and research on this topic is sparse. Based on OCTA measurement, we speculate that PLT levels may be a marker for microvascular dysfunction in diabetic patients. More studies are required to corroborate this hypothesis.

Limitation

There are several limitations of our present study. The first one is that the study was a single-center study with a relatively small sample size. Second, most participants in this study have mild or moderate diabetic retinopathy (115/140, 79.9%), while the effect of diabetic retinopathy has been taken into account in multivariable models, it may still have confounding effects on OCTA measurement due to the pathological change in DR itself. Thirdly, we did not account for ocular factors, such as axial length and refractive error in the analysis, as subjects with high myopia (axial length > 26 mm) were excluded. However, ocular magnification in OCTA images caused by varying axial lengths may interfere with accurate interpretation of OCTA measures. (10) Finally, VD and PD in the deep capillary plexus (DCP) could not be evaluated due to the limitations of built-in angiography software in the OCTA instrument, which may be more sensitive in detecting retinal microvascular changes in diabetic patients at an early stage.

In conclusion, this study provided evidence that systemic risk factors are associated with retinal microvasculature among T2DM patients in a Chinese population. Further longitudinal and large-scale studies are needed to corroborate our findings.

Data availability statement

The original contributions presented in the study are included in the article/supplementary material, further inquiries can be directed to the corresponding author.

Ethics statement

The studies involving human participants were reviewed and approved by the Institutional Review Board of Huizhou Central People's Hospital. The patients/participants provided their written informed consent to participate in this study.

Author contributions

YL and KW drafted the manuscript and interpreted the results. YL, GX, and KW performed the data analysis. HF, ZC, GX, DW, and JW revised the manuscript for important intellectual content. GBu and GBo were involved in interpreting the results. All authors contributed to the article and approved the submitted version.

Funding

This study was supported by the Science and Technology Plan Project of Huizhou Science and Technology Bureau (grant number: 2021WC0106369).

Conflict of interest

The authors declare that the research was conducted in the absence of any commercial or financial relationships that could be construed as a potential conflict of interest.

Publisher's note

References

1. Sun H, Saeedi P, Karuranga S, Pinkepank M, Ogurtsova K, Duncan BB, et al. Idf diabetes atlas: global, regional and country-level diabetes prevalence estimates for 2021 and projections for 2045. *Diabetes Res Clin Pract*. (2022) 183:109119. doi: 10.1016/j.diabres.2021.109119

2. American DA. 2. Classification and diagnosis of diabetes: standards of medical Care in Diabetes-2018. *Diabetes Care*. (2018) 41:S13–27. doi: 10.2337/dc18-S002

3. Zhang H, Dellsperger KC, Zhang C. The link between metabolic abnormalities and endothelial dysfunction in type 2 diabetes: an update. *Basic Res Cardiol*. (2012) 107:237. doi: 10.1007/s00395-011-0237-1

4. Wright WS, Eshaq RS, Lee M, Kaur G, Harris NR. Retinal physiology and circulation: effect of diabetes. *Compr Physiol*. (2020) 10:933–74. doi: 10.1002/cphy.c190021

5. Farrah TE, Dhillon B, Keane PA, Webb DJ, Dhaun N. The eye, the kidney, and cardiovascular disease: old concepts, better tools, and new horizons. *Kidney Int*. (2020) 98:323–42. doi: 10.1016/j.kint.2020.01.039

6. Cheung CY, Biousse V, Keane PA, Schiffrin EL, Wong TY. Hypertensive eye disease. *Nat Rev Dis Primers*. (2022) 8:14. doi: 10.1038/s41572-022-00342-0

7. Flammer J, Konieczka K, Bruno RM, Virdis A, Flammer AJ, Taddei S. The eye and the heart. *Eur Heart J*. (2013) 34:1270–8. doi: 10.1093/eurheartj/eht023

8. Ojaimi E, Nguyen TT, Klein R, Islam FM, Cotch MF, Klein BE, et al. Retinopathy signs in people without diabetes: the multi-ethnic study of atherosclerosis. *Ophthalmology*. (2011) 118:656–62. doi: 10.1016/j.ophtha.2010.08.007

9. Yoon J, Kang HJ, Lee JY, Kim JG, Yoon YH, Jung CH, et al. Associations between the macular microvasculatures and subclinical atherosclerosis in patients with type 2 diabetes: an optical coherence tomography angiography study. *Front Med (Lausanne)*. (2022) 9:843176. doi: 10.3389/fmed.2022.843176

10. Chua J, Sim R, Tan B, Wong D, Yao X, Liu X, et al. Optical coherence tomography angiography in diabetes and diabetic retinopathy. *J Clin Med*. (2020) 9:1723. doi: 10.3390/jcm9061723

11. Qian J, Haq Z, Yang D, Jin JQ, Stewart JM. Duration of diabetes as a risk factor for retinal microvasculature alterations detected with optical coherence tomography angiography in patients without clinical retinopathy. *Diagnostics (Basel)*. (2022) 12:3020. doi: 10.3390/diagnostics12123020

12. Levy BI, Schiffrin EL, Mourad JJ, Agostini D, Vicaut E, Safar ME, et al. Impaired tissue perfusion: a pathology common to hypertension, obesity, and diabetes mellitus. *Circulation*. (2008) 118:968–76. doi: 10.1161/CIRCULATIONAHA.107.763730

13. Lee DH, Yi HC, Bae SH, Cho JH, Choi SW, Kim H. Risk factors for retinal microvascular impairment in type 2 diabetic patients without diabetic retinopathy. *PLoS One*. (2018) 13:e0202103. doi: 10.1371/journal.pone.0202103

14. Sun MT, Huang S, Chan W, Craig JE, Knight LSW, Sanders P, et al. Impact of Cardiometabolic factors on retinal vasculature: a 3 X 3, 6 X 6 and 8 X 8-mm ocular coherence tomography angiography study. *Clin Exp Ophthalmol*. (2021) 49:260–9. doi: 10.1111/ceo.13913

15. Ting DSW, Tan GSW, Agrawal R, Yanagi Y, Sie NM, Wong CW, et al. Optical coherence tomographic angiography in type 2 diabetes and diabetic retinopathy. *JAMA Ophthalmol*. (2017) 135:306–12. Epub 2017/02/17. doi: 10.1001/jamaophthalmol.2016.5877

16. Levey AS, Stevens LA, Schmid CH, Zhang Y, Castro AF III, Feldman HI, et al. A new equation to estimate glomerular filtration rate. *Ann Intern Med*. (2009) 150:604–12. doi: 10.7326/0003-4819-150-9-200905050-00006

17. Wilkinson CP, Ferris FL 3rd, Klein RE, Lee PP, Agardh CD, Davis M, et al. Proposed international clinical diabetic retinopathy and diabetic macular edema disease severity scales. *Ophthalmology*. (2003) 110:1677–82. doi: 10.1016/S0161-6420(03)00475-5

18. Czakó C, Sándor G, Ecsedy M, Récsán Z, Horváth H, Szepessy Z, et al. Decreased retinal capillary density is associated with a higher risk of diabetic retinopathy in patients with diabetes. *Retina*. (2019) 39:1710–9. doi: 10.1097/IAE.0000000000002232

19. Sherif EM, Matter RM, Salah NY, Abozeid NEH, Atif HM, Tantawy NM. Changes in early optical coherence tomography angiography among children and adolescents with type 1 diabetes: relation to fibroblast growth factor 21. *Diabetes Metab Res Rev*. (2022) 39:e3598. doi: 10.1002/dmrr.3598

20. Klein R, Sharrett AR, Klein BE, Moss SE, Folsom AR, Wong TY, et al. The Association of Atherosclerosis, vascular risk factors, and retinopathy in adults with diabetes: the atherosclerosis risk in communities study. *Ophthalmology*. (2002) 109:1225–34. doi: 10.1016/S0161-6420(02)01074-6

21. Klein R, Klein BE, Moss SE, Davis MD, DeMets DL. Is blood pressure a predictor of the incidence or progression of diabetic retinopathy? *Arch Intern Med*. (1989) 149:2427–32. doi: 10.1001/archinte.1989.00390110033008

22. Sun C, Ladores C, Hong J, Nguyen DQ, Chua J, Ting D, et al. Systemic hypertension associated retinal microvascular changes can be detected with optical coherence tomography angiography. *Sci Rep*. (2020) 10:9580. doi: 10.1038/s41598-020-66736-w

23. Donati S, Maresca AM, Cattaneo J, Grossi A, Mazzola M, Caprani SM, et al. Optical coherence tomography angiography and arterial hypertension: a role in identifying subclinical microvascular damage? *Eur J Ophthalmol*. (2021) 31:158–65. doi: 10.1177/1120672119880390

24. Liu Y, Wang M, Morris AD, Doney AS, Leese GP, Pearson ER, et al. Glycemic exposure and blood pressure influencing progression and remission of diabetic retinopathy: a longitudinal cohort study in Godarts. *Diabetes Care*. (2013) 36:3979–84. doi: 10.2337/dc12-2392

25. Yeung L, Wu IW, Sun CC, Liu CF, Chen SY, Tseng CH, et al. Early retinal microvascular abnormalities in patients with chronic kidney disease. *Microcirculation*. (2019) 26:e12555. doi: 10.1111/micc.12555

26. Chua J, Chin CWL, Hong J, Chee ML, Le TT, Ting DSW, et al. Impact of hypertension on retinal capillary microvasculature using optical coherence tomographic angiography. *J Hypertens*. (2019) 37:572–80. doi: 10.1097/HJH.0000000000001916

27. Chua J, Le TT, Sim YC, Chye HY, Tan B, Yao X, et al. Relationship of quantitative retinal capillary network and myocardial remodeling in systemic hypertension. *J Am Heart Assoc*. (2022) 11:e024226. doi: 10.1161/JAHA.121.024226

28. Zhuang X, Cao D, Zeng Y, Yang D, Yao J, Kuang J, et al. Associations between retinal microvasculature/microstructure and renal function in type 2 diabetes patients with early chronic kidney disease. *Diabetes Res Clin Pract*. (2020) 168:108373. doi: 10.1016/j.diabres.2020.108373

29. Wang Q, Liu L, Jonas JB, Gao B, Wu SL, Chen SH, et al. Albuminuria and retinal vessel density in diabetes without diabetic retinopathy: the Kailuan eye study. *Acta Ophthalmol*. (2021) 99:e669–78. doi: 10.1111/aos.14670

30. Samara WA, Say EA, Khoo CT, Higgins TP, Magrath G, Ferenczy S, et al. Correlation of foveal avascular zone size with foveal morphology in Normal eyes using optical coherence tomography angiography. *Retina*. (2015) 35:2188–95. doi: 10.1097/IAE.0000000000000847

31. Tan CS, Lim LW, Chow VS, Chay IW, Tan S, Cheong KX, et al. Optical coherence tomography angiography evaluation of the Parafoveal vasculature and its relationship with ocular factors. *Invest Ophthalmol Vis Sci*. (2016) 57:OCT224–34. doi: 10.1167/iovs.15-18869

32. Stokes KY. Microvascular responses to hypercholesterolemia: the interactions between innate and adaptive immune responses. *Antioxid Redox Signal*. (2006) 8:1141–51. doi: 10.1089/ars.2006.8.1141

33. Sen K, Misra A, Kumar A, Pandey RM. Simvastatin retards progression of retinopathy in diabetic patients with hypercholesterolemia. *Diabetes Res Clin Pract*. (2002) 56:1–11. doi: 10.1016/S0168-8227(01)00341-2

34. Aryan Z, Afarideh M, Ghajar A, Esteghamati S, Esteghamati A, Nakhjavani M. Conflicting interactions of apolipoprotein a and high density lipoprotein cholesterol with microvascular complications of type 2 diabetes. *Diabetes Res Clin Pract*. (2017) 133:131–41. doi: 10.1016/j.diabres.2017.07.037

35. Toth PP, Simko RJ, Palli SR, Koselleck D, Quimbo RA, Cziraky MJ. The impact of serum lipids on risk for Microangiopathy in patients with type 2 diabetes mellitus. *Cardiovasc Diabetol*. (2012) 11:1–110, 109, doi: 10.1186/1475-2840-11-109

36. Sasongko MB, Wong TY, Nguyen TT, Kawasaki R, Jenkins A, Shaw J, et al. Serum apolipoprotein Ai and B are stronger biomarkers of diabetic retinopathy than traditional lipids. *Diabetes Care*. (2011) 34:474–9. doi: 10.2337/dc10-0793

37. Schmidt C, Bergstrom G. Apolipoprotein B and Apolipopotein a-I in vascular risk prediction—a review. *Curr Pharm Des*. (2014) 20:6289–98. doi: 10.2174/13816128206661406201218 28

38. Shi R, Lu Y, Liu D, Guo Z. Association of Serum Apolipoprotein B with retinal neurovascular structural alterations in patients with type 2 diabetes: an optical coherence tomography angiography study. *Acta Diabetol*. (2021) 58:1673–81. doi: 10.1007/s00592-021-01775-x

39. Yuan Y, Wu M, Alwis I, Maiocchi S, Jackson S. Thromboinflammatory functions of platelets in ischemia–reperfusion injury and its dysregulation in diabetes. *Semin Thromb Hemost*. (2018) 44:102–13. doi: 10.1055/s-0037-1613694

40. Liew G, Wang JJ, Rochtchina E, Wong TY, Mitchell P. Complete blood count and retinal vessel calibers. *PLoS One*. (2014) 9:e102230. doi: 10.1371/journal.pone.0102230

frontiers | Frontiers in Medicine

TYPE Original Research
PUBLISHED 23 March 2023
DOI 10.3389/fmed.2023.1037919

OPEN ACCESS

EDITED BY
Fabrizio Giansanti,
University of Florence, Italy

REVIEWED BY
Bingyao Tan,
Nanyang Technological University, Singapore
Yanjun Hua,
Shanghai Jiao Tong University, China
Mengmeng Wang,
Hebei Eye Hospital, China

*CORRESPONDENCE
Qinmei Wang
✉ wangqm55@126.com
Shihao Chen
✉ chenle@rocketmail.com
Jinhai Huang
✉ vip999vip@163.com

†These authors have contributed equally to this work and share first authorship

SPECIALTY SECTION
This article was submitted to Ophthalmology, a section of the journal Frontiers in Medicine

RECEIVED 06 September 2022
ACCEPTED 27 February 2023
PUBLISHED 23 March 2023

CITATION
Chen R, Liu X, Yao M, Zou Z, Chen X, Li Z, Chen X, Su M, Lian H, Lu W, Yang Y, McAlinden C, Wang Q, Chen S and Huang J (2023) Precision (repeatability and reproducibility) of papillary and peripapillary vascular density measurements using optical coherence tomography angiography in children. *Front. Med.* 10:1037919. doi: 10.3389/fmed.2023.1037919

Precision (repeatability and reproducibility) of papillary and peripapillary vascular density measurements using optical coherence tomography angiography in children

Ruru Chen[1†], Xinyu Liu[1†], Mingyu Yao[1†], Zhilin Zou[1], Xinyi Chen[1], Zheng Li[1], Xin Chen[1], Mengjuan Su[1], Hengli Lian[1], Weiwei Lu[1], Yizhou Yang[1], Colm McAlinden[2,3,4,5], Qinmei Wang[1]*, Shihao Chen[1]* and Jinhai Huang[1,2,3,6]*

[1]School of Ophthalmology and Optometry and Eye Hospital, Wenzhou Medical University, Wenzhou, Zhejiang, China, [2]Department of Ophthalmology, Eye Institute, Eye and ENT Hospital, Fudan University, Shanghai, China, [3]NHC Key Laboratory of Myopia (Fudan University), Key Laboratory of Myopia, Chinese Academy of Medical Sciences, Shanghai, China, [4]Department of Ophthalmology, Singleton Hospital, Swansea Bay University Health Board, Swansea, United Kingdom, [5]Department of Ophthalmology, Royal Gwent Hospital, Aneurin Bevan University Health Board, Newport, United Kingdom, [6]Shanghai Research Center of Ophthalmology and Optometry, Shanghai, China

Importance: Optical coherence tomography angiography (OCTA) has been widely applied into children, however, few studies have assessed the repeatability and reproducibility of papillary and peripapillary VD in healthy children.

Objective: To assess the precision of papillary and peripapillary vascular density (VD) measurements using optical coherence tomography angiography (OCTA) and analyze the effects of the signal strength index (SSI) and axial length (AL) on precision estimates.

Design, setting, and participants: This was a prospective observational study. Seventy-eight children aged 6–16 years underwent 4.5 × 4.5 mm OCTA (RTVue XR Avanti) disc scans: two scans by one examiner (repeatability) and two additional scans by another examiner (reproducibility). Within-subject standard deviation (Sw), test-retest reproducibility (TRT), within-subject coefficient of variation (CoV), intraclass correlation coefficient (ICC), and Bland–Altman analysis were performed.

Main outcomes and measures: In repeatability measurement, the fluctuation ranges (minimum to maximum) of VD between intraexaminer A/B in Sw, TRT, CoV, and ICC were (1.05–2.17)% / (1.16–2.32)%, (2.9–6)% / (3.21–6.44)%, (1.9–4.47)% / (2.08–5)%, and (0.588–0.783)% / (0.633–0.803)%, respectively. In reproducibility measurement, the fluctuation ranges of VD in Sw, TRT, CoV, and ICC were 1.11–2.13%, 3.07–5.91%, 1.99–4.41%, and 0.644–0.777%, respectively. VD was negatively correlated with SSI in most sectors of the peripapillary (e.g., inferior nasal, temporal inferior, temporal superior, superior temporal, and superior nasal). AL was positively correlated with inferior temporal VD and negatively correlated with superior nasal VD.

Conclusion and relevance: Optical coherence tomography angiography showed moderate-to-good repeatability and reproducibility for papillary and peripapillary perfusion measurements in healthy children. The SSI value affects most of the peripapillary VD, while AL affects only the temporal inferior and nasal superior peripapillary VD.

KEYWORDS

vascular density, optical coherence tomography angiography, repeatability, reproducibility, children

Highlights

- To assess the precision of papillary and peripapillary vascular density (VD) measurements using optical coherence tomography angiography (OCTA), 78 children aged 6–16 years underwent 4.5 × 4.5 mm OCTA disc scans.
- OCTA showed moderate-to-good repeatability and reproducibility for papillary and peripapillary perfusion measurements in healthy children.

Introduction

Examination of papillary and peripapillary blood flow in children can help understand the pathological mechanisms of some optic nerve diseases, such as juvenile glaucoma and optic neuritis (1, 2). Consequently, precise estimates of the parameters of the papillary and peripapillary blood flow are imperative.

With the advent of optical coherence tomography angiography (OCTA), it is now possible to non-invasive images and quantify macular, papillary and peripapillary vascular networks through fast scanning and image processing algorithms (3–5). Repeated measurements of blood flow parameters, such as vascular density (VD), will often fluctuate near the true value for the same retinal location of the same individual. It is important to assess the precision of repeated measurements to determine clinical changes in these blood flow parameters; therefore, they are considered when evaluating individual or longitudinal measurements.

Previous studies have shown that OCTA has high repeatability and reproducibility in measuring the area of the foveal avascular zone, superficial and deep retinal VD, and papillary and peripapillary VD in healthy adults (6–11). However, only a few studies have assessed the repeatability and reproducibility of these parameters in healthy children. Zhang et al. (12) reported that OCTA is reliable for evaluating macular perfusion in 8–16 years old children, but the algorithm was not applied to the measurement of papillary and peripapillary VD. Other studies have evaluated the impact of image magnification, associations with ocular biometry, and the effect of patient-specific factors on OCTA measurements (13–15).

In this study, the precision (repeatability and reproducibility) of OCTA was evaluated in measuring papillary and peripapillary VD in 6–16 years old healthy Chinese children in a large sample. Additional objectives were to provide reference values for clinical use and analyze the effects of the signal strength index (SSI) and axial length (AL) on the VD.

Materials and methods

This prospective observational study was conducted at the Eye Hospital of Wenzhou Medical University. The study protocol was approved by the Medical Ethics Committee of the Eye Hospital of Wenzhou Medical University. Written informed consent was obtained from the legal guardian of each child.

Children aged 6–16 years attending the hospital were invited to participate in this study. The inclusion criteria were as follows: (1) monocular best-corrected distance visual acuity 20/20 or better; (2) refractive spheres between −5.00 D and +5.00 D and cylinder within ± 3 D; (3) intraocular pressure between 10 and 21 mmHg; (4) no retinal pathology; (5) no history of systemic disease.

The papillary and peripapillary VDs were generated by OCTA using the RTVue XR Avanti device (software RTVue, version 2018.1.1.63; Optovue Inc., Fremont, CA, USA) with the Angio Disc (4.5 × 4.5 mm) mode. The measurement principle of angiography and flow imaging has been reported in previous studies (6, 16).

Examiner A (WWL) acquired two repeated scans of the right eye for each patient. Examiner B (LHL) acquired two additional scans of the right eye. Two measurements were taken from previous studies to avoid the fatigue effect in children (17, 18). After the baseline scan was used as the reference scan, the follow-up scan option was chosen to automatically track the same location.

The software automatically segmented the papillary and peripapillary VD (**Figure 1**) between the inner limiting membrane and the nerve fiber layer. The VD was defined as the ratio of the area of the large and capillary vessels divided by the total area measured sectors. The capillary VD was the VD, except for the large vessels. According to the Garway-Heath Partition Method, the peripapillary area is subdivided into eight sectors: nasal superior, nasal inferior, inferior nasal, inferior tempo, tempo inferior, tempo superior, superior tempo, and superior nasal. Eyes with poor-quality images with OCTA (quality score < 8), significant motion, or blink artifacts were excluded from the analysis. The AL was measured using an IOLMaster 700 (Zeiss, Germany).

Statistical analysis

Statistical analyses were performed using Statistical Product and Service Solution (SPSS) statistical software V24.0. Only the

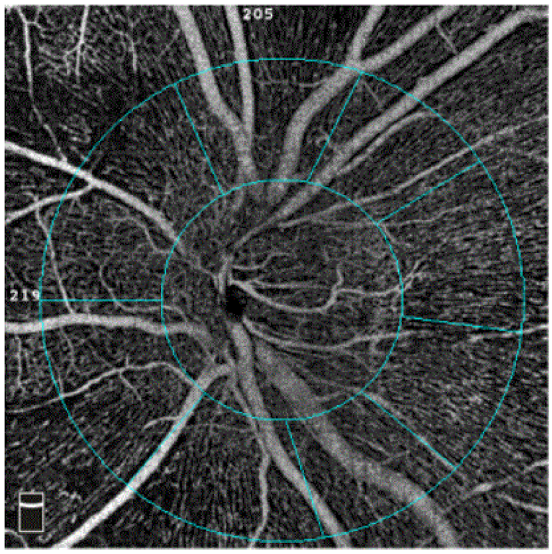

FIGURE 1
Automatic measured images of optic disc by OCTA with a 4.5 × 4.5 scan pattern.

right eye was analyzed. Kolmogorov–Smirnov analysis was used to test the normality of the data distribution. Normally distributed variables were described as mean ± standard deviation (SD). Median and interquartile ranges were used to describe non-normally distributed parameters.

The within-subject standard deviation (Sw) (19), test-retest repeatability (TRT) (20, 21), within-subject coefficient of variation (CoV) (22, 23), and intraclass correlation coefficient (ICC) (23, 24) were used to evaluate repeatability and reproducibility. The Sw value was taken as the square root of the residual mean. The TRT value was equal to the Sw multiplied by 2.77. An ICC value > 0.8 or < 0.4 indicates good or poor reproducibility between every two repeated measurements. The CoV value is Sw divided by the average measurement and is expressed as a percentage. A lower CoV indicates greater repeatability (25).

In addition, the Bland–Altman analysis was used to plot the differences in VD and SSI between interexaminer measurements and their means. The method uses the mean difference and 95% limits of agreement (LoAs) between the two examiner measurements. The significance level was set at $P < 0.05$.

To assess interexaminer reproducibility, the two examiners' mean values between two measurements of each parameter were included in the analysis.

Generalized estimation equations were used to analyze the effects of SSI and AL on precision estimates.

Results

Eighty-five children were enrolled in this study; seven were excluded due to motion and blink artifacts (two children) or poor image quality (five children). Therefore, the study included 78 children with a median age (interquartile range) of 10 (9–12) years (range, 6–16 years). The mean (± SD) of AL was 24.72 ± 1.26 mm. The mean spherical equivalent refraction was −2.72 ± 1.94 D.

For the repeatability of two measurements within intra-examiners A and B, the mean ± SD, Sw, TRT, CoV, and ICC of SSI of the whole images were 73.57 ± 8.03 and 72.46 ± 8.02, 3.91, and 3.49, 10.83, and 9.66, 5.31, and 4.81, 0.788 (0.686–0.859), and 0.827 (0.741–0.886), respectively. Table 1 and Figures 2, 3 show the intraexaminer repeatability in measuring papillary and peripapillary VD. The fluctuation ranges of VD between examiners A and B in Sw, TRT, CoV, and ICC were (1.05–2.17)% / (1.16–2.32)%, (2.9–6)% / (3.21–6.44)%, (1.9–4.47)% / (2.08–5)%, and (0.588–0.783) / (0.633–0.803), respectively.

In the interexaminer reproducibility measurement, the mean ± SD, Sw, TRT, CoV, and ICC of SSI were 73.01 ± 8.02, 4.74, 13.14, 6.50, and 0.652 (0.505–0.763). The fluctuation ranges of VD in Sw, TRT, CoV, and ICC were 1.11–2.13%, 3.07–5.91%, 1.99–4.41%, and 0.644–0.777, respectively, as shown in Table 2 and Figures 2, 3.

In the reproducibility measurement of papillary and peripapillary VD, the interexaminer 95% LoA range for whole, whole capillary, disc, disc capillary, peripapillary, and peripapillary capillary was 6.0, 6.1, 9.9, 11.3, 6.6, and 7.2%, respectively, and other sectors were shown in Figure 4.

The effects of SSI and AL on the repeatability measurements for two examiners of papillary and peripapillary VD are shown in Tables 3, 4. Overall, the disc, disc capillary, and VD increased with increasing SSI. This relationship was the opposite in most sectors of the peripapillary, including the inferior nasal, temporal inferior, temporal superior, superior temporal, and superior nasal. In other sectors, there is no relationship between the two.

Axial length was positively correlated with VD in the temporal inferior sector, while in the nasal superior sector it was the opposite. In most other sectors, the AL did not correlate with the VD. There was no correlation between age and the repeatability of the papillary and peripapillary vascular density measurement (all $P > 0.05$), except for superior temporal sector in measurement of the examiner A, shown in Table 5.

Discussion

Many previous studies have reported that OCTA showed moderate-to-good repeatability and reproducibility in adult measurements with small samples (1, 26–29). Although the OCTA measurement scan is fast, it should also be performed in some patients with poor cooperation, such as children. It is rarely reported in larger samples, particularly in the papillary and peripapillary regions of children. The present study showed moderate-to-good repeatability and reproducibility of the OCTA measurements of papillary and peripapillary VD in healthy Chinese children using comprehensive and systematic evaluation indicators.

In repeatability measurement, Venugopal et al. (26) reported that in 30 normal adult eyes (aged 57 years old), Sw, TRT, CoV, ICC of the papillary and each peripapillary sector were 1.3–2.6%, 3.3–7.0%, 2.4–4.4%, and 0.71–0.85, respectively, for three repeated measurements (1). Manalastas et al. (9) found

TABLE 1 Intra-examiner repeatability of the OCTA in measuring the papillary and peripapillary vascular density.

Parameter	Examiner	Mean ± SD (%)	Sw (%)	TRT (%)	CoV (%)	ICC (95% CI)
Whole	A	56.01 ± 1.82	1.06	2.94	1.9	0.709 (0.579–0.804)
	B	55.70 ± 1.88	1.16	3.21	2.08	0.681 (0.542–0.785)
Whole capillary	A	49.18 ± 1.82	1.05	2.9	2.13	0.714 (0.586–0.808)
	B	48.94 ± 1.93	1.26	3.48	2.57	0.650 (0.501–0.762)
Disc	A	63.33 ± 2.95	1.88	5.2	2.96	0.588 (0.413–0.721)
	B	62.87 ± 3.24	1.73	4.79	2.75	0.665 (0.515–0.775)
Disc capillary	A	54.94 ± 4.00	2.15	5.95	3.91	0.749 (0.633–0.833)
	B	54.47 ± 4.55	2.13	5.89	3.9	0.803 (0.707–0.869)
Peripapillary	A	57.64 ± 2.21	1.19	3.29	2.06	0.739 (0.613–0.829)
	B	57.44 ± 2.18	1.25	3.48	2.18	0.667 (0.515–0.778)
Peripapillary capillary	A	50.72 ± 2.40	1.28	3.54	2.52	0.757 (0.636–0.841)
	B	50.62 ± 2.44	1.51	4.18	2.98	0.691 (0.546–0.795)
-Superior hemi	A	58.02 ± 2.22	1.22	3.39	2.11	0.746 (0.621–0.834)
	B	57.88 ± 2.23	1.25	3.47	2.16	0.737 (0.609–0.828)
-Inferior hemi	A	57.24 ± 2.34	1.35	3.75	2.36	0.713 (0.584–0.807)
	B	56.96 ± 2.30	1.41	3.9	2.47	0.684 (0.545–0.786)
-Superior hemi capillary	A	50.96 ± 2.54	1.33	3.69	2.62	0.746 (0.629–0.831)
	B	51.01 ± 2.62	1.53	4.25	3.01	0.700 (0.566–0.798)
-Inferior hemi capillary	A	50.58 ± 2.62	1.52	4.22	3.01	0.711 (0.580–0.805)
	B	50.39 ± 2.63	1.6	4.44	3.18	0.686 (0.548–0.788)
-Nasal superior	A	46.98 ± 3.41	1.89	5.24	4.03	0.732 (0.610–0.820)
	B	46.57 ± 3.53	1.8	5	3.87	0.768 (0.659–0.846)
-Nasal inferior	A	46.44 ± 3.98	2.06	5.72	4.44	0.763 (0.652–0.842)
	B	45.67 ± 3.84	2.28	6.33	5	0.700 (0.567–0.797)
-Inferior nasal	A	48.17 ± 4.18	2.15	5.96	4.47	0.765 (0.655–0.844)
	B	48.31 ± 4.10	2.04	5.65	4.22	0.779 (0.674–0.853)
-Inferior temporal	A	54.71 ± 3.58	2.17	6	3.96	0.675 (0.531–0.781)
	B	54.97 ± 3.59	2.32	6.44	4.23	0.633 (0.475 to 0.751)
-Temporal inferior	A	54.64 ± 3.03	1.74	4.82	3.19	0.717 (0.590 to 0.810)
	B	54.39 ± 3.31	2	5.54	3.68	0.690 (0.553–0.791)
-Temporal superior	A	56.05 ± 3.29	1.62	4.5	2.9	0.783 (0.680–0.856)
	B	56.01 ± 3.28	1.88	5.21	3.36	0.719 (0.593–0.811)
-Superior temporal	A	53.51 ± 3.59	2.09	5.79	3.9	0.711 (0.580–0.805)
	B	53.55 ± 3.71	2.21	6.12	4.12	0.699 (0.565–0.797)
-Superior nasal	A	48.19 ± 3.58	1.96	5.44	4.08	0.747 (0.623–0.834)
	B	48.70 ± 3.98	2.02	5.6	4.15	0.785 (0.675–0.860)

SD, standard deviation; Sw, within-subject standard deviation; TRT, test-retest repeatability (2.77 Sw); CoV, within-subject coefficient of variation; ICC, intraclass correlation coefficient.

that in two continuous optic nerve head scans of 15 healthy adults aged approximately 70 years old, the Sw, CoV, and ICC of the papillary and each peripapillary sector were 1.58–3.61%, 2.9–5.8%, and 0.42–0.80, respectively. Consistent with this study, Sw, TRT, CoV, and ICC of the papillary and each peripapillary sector in intraexaminer A/B for two repeated measurements were 1.09–2.17% / 1.16–2.32%, 2.94–6.0% / 3.21–6.44%, 1.9–4.47% / 2.08–5.00%, and 0.588–0.783 / 0.633–0.785. Venugopal et al. (26) reported that a TRT < 6% had no clinical significance. The TRT measured for reproducibility and repeatability in this study were lower than this value. Using the same OCTA equipment, the reliability of repeated measurements of papillary and peripapillary VD in children is close to that in adults.

Capillary density (CD) has a potential value in the evaluation of glaucoma (27). Mansoori et al. (28) visualized the radial peripapillary capillary network using OCTA. Repeatability

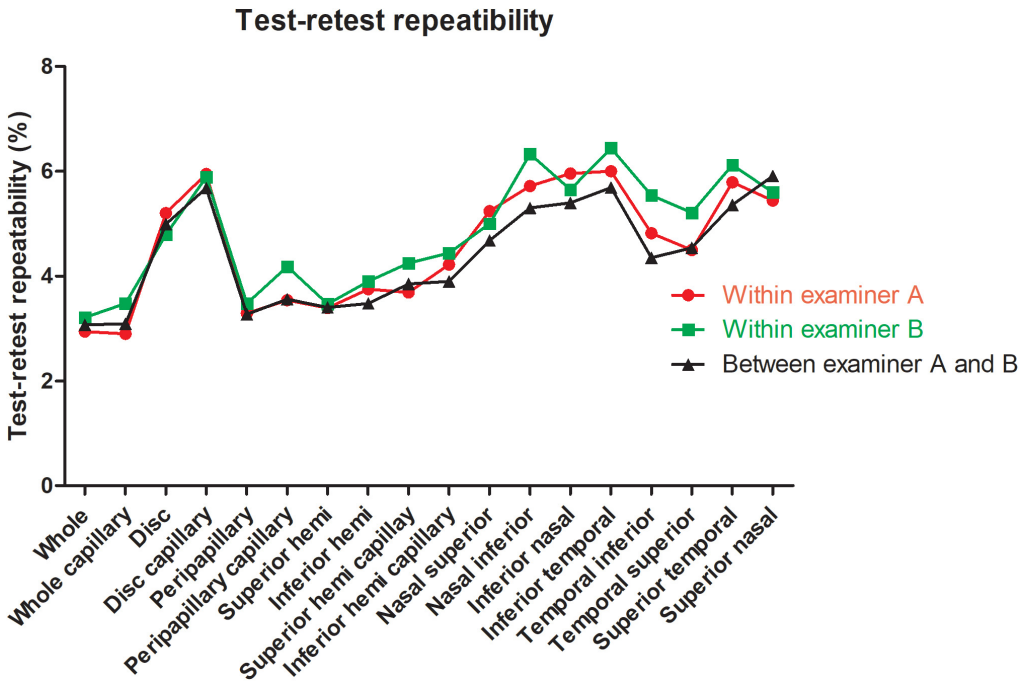

FIGURE 2
Test-retest repeatability of papillary and peripapillary vascular density measurements intraexaminer and interexaminer.

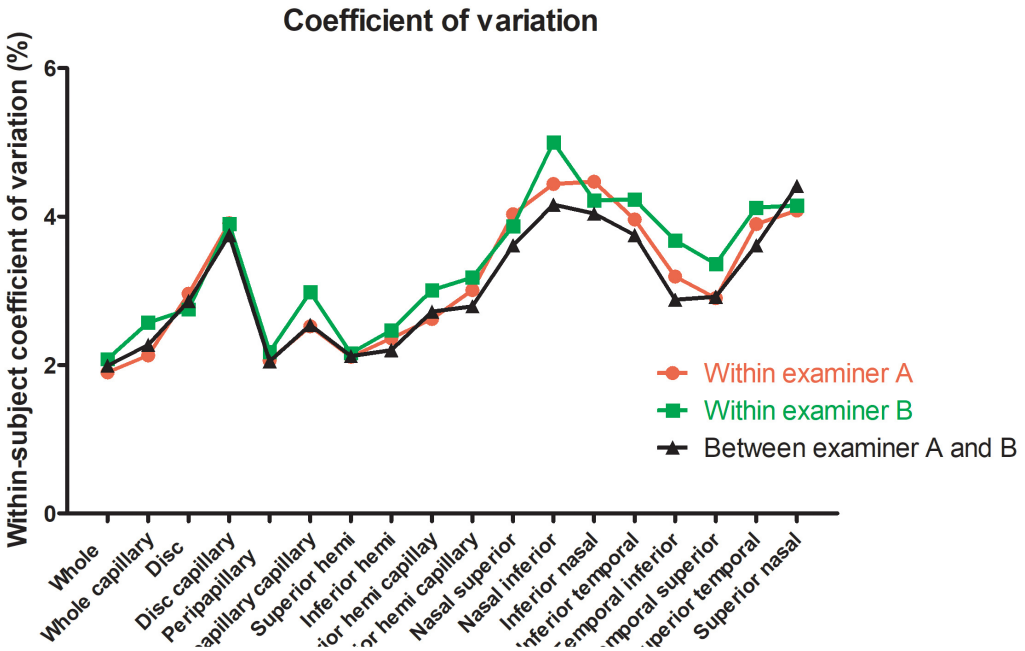

FIGURE 3
Within-subject coefficient of papillary and peripapillary vascular density measurements intraexaminer and interexaminer.

measurements of CD have also been reported in the adult macula (18, 29, 30). Pappelis and Jansonius (17) reported two measurements of pericapillary CD in 30 healthy adult eyes using Canon OCT-HS 100 angiography; the ICC and TRT were 0.79 and 1.8%, respectively. Consistent with this study, the intra-examiner ICC of examiners A/B was 0.757 / 0.691, and the TRT was 3.54% / 4.18%. This shows that as the operational proficiency of the examiner and cooperation of children increases, the repeatability measurement of pericapillary CD in children approaches that of adults.

Rao et al. (31) found that the use of Cirrus HD-OCT (software version 11.0.0.29946) follow-up scans can make repeatability

TABLE 2 Inter-examiner agreement of the OCTA in measuring the papillary and peripapillary vascular density.

Parameter	Mean ± SD (%)	Sw (%)	TRT (%)	CoV (%)	ICC
Whole	55.86 ± 1.85	1.11	3.07	1.99	0.644 (0.494–0.757)
Whole capillary	49.06 ± 1.87	1.11	3.09	2.27	0.648 (0.499–0.760)
Disc	63.10 ± 3.10	1.80	4.99	2.86	0.664 (0.520–0.772)
Disc capillary	54.70 ± 4.28	2.05	5.68	3.75	0.771 (0.663–0.848)
Peripapillary	57.54 ± 2.19	1.18	3.27	2.05	0.711 (0.582–0.805)
Peripapillary capillary	50.67 ± 2.41	1.29	3.56	2.54	0.717 (0.589–0.810)
-Superior hemi	57.95 ± 2.21	1.23	3.40	2.12	0.693 (0.557–0.793)
-Inferior hemi	57.10 ± 2.32	1.26	3.48	2.20	0.708 (0.578–0.803)
-Superior hemi capillary	50.98 ± 2.57	1.39	3.85	2.72	0.709 (0.571–0.808)
-Inferior hemi capillary	50.49 ± 2.62	1.41	3.90	2.79	0.712 (0.583–0.806)
-Nasal superior	46.78 ± 3.46	1.69	4.68	3.61	0.763 (0.653–0.842)
-Nasal inferior	46.05 ± 3.92	1.91	5.30	4.16	0.764 (0.646–0.846)
-Inferior nasal	48.24 ± 4.12	1.95	5.40	4.04	0.777 (0.671–0.852)
-Inferior temporal	54.84 ± 3.58	2.06	5.69	3.75	0.671 (0.529–0.777)
-Temporal inferior	54.51 ± 3.16	1.57	4.35	2.88	0.755 (0.641–0.836)
-Temporal superior	56.03 ± 3.28	1.64	4.54	2.92	0.751 (0.635–0.834)
-Superior temporal	53.53 ± 3.64	1.93	5.36	3.61	0.719 (0.591–0.811)
-Superior nasal	48.45 ± 3.78	2.13	5.91	4.41	0.683 (0.545–0.785)

SD, standard deviation; Sw, within-subject standard deviation; TRT, test-retest reproducibility (2.77 Sw); COV, within-subject coefficient of variation; ICC, intraclass correlation coefficient.

measurements more reliable compared to non-referenced scans in 33 normal adults (48 eyes), and they reported that the nasal, superior, temporal, and inferior peripapillary were 2.2, 2.2, 2.7, and 1.9% for TRT, 1.8, 2.0, 2.1, and 1.8% for CoV, 0.92, 0.92, 0.85, and 0.97, respectively. Venugopal et al. (26) included 46 eyes of 33 healthy adults using non-referenced high-density scans of RTVue-XR SD-OCT (AngioVue, V.2016.2.0.35) and reported that the repeatability estimates of the papillary and peripapillary sections ranged from 1.1 to 1.8% for Sw, 3.0 to 4.9% for TRT, and 2.0 to 3.1% for CoV. Based on follow-up scanning, this study found that the nasal superior, nasal inferior, inferior nasal, inferior temporal, temporal inferior, temporal superior, superior temporal, and superior nasal peripapillaries of intraexaminer A were 1.89, 2.06, 2.15, 2.17, 1.74, 1.62, 2.09, and 1.96% in Sw; 5.24, 5.72, 5.96, 6, 4.82, 4.5, 5.79, and 5.44% in TRT; 4.03, 4.44, 4.47, 3.96, 3.19, 2.9, 3.9, and 4.08% in CoV; and 0.732, 0.763, 0.765, 0.675, 0.717, 0.783, 0.711, and 0.747 in ICC. Differences in the results may be attributed to different sample sizes, including subjects, scanning mode, devices, and algorithms.

In assessing the reproducibility of interexaminer measurements, She et al. (32) reported that CoV was $< 2\%$ and ICC was > 0.8 in different sectors of the peripapillary in normal adults. The Bland–Altman plots showed that the 95% LoA range was 12.2% in the superotemporal, 10.1% in the temporal, 11.3% in the inferotemporal, 12.0% in the inferonasal, 8.0% in the nasal, and 7.4% in the superior peripapillary (32). In our study, CoV and TRT were $< 4.5\%$ and $< 6\%$, respectively, and ICC was > 0.64. The Bland–Altman plots showed that the 95% LoA range was 9.3% in the nasal superior, 10.3% in the nasal inferior, 10.9% in the inferior nasal, 11.5% in the inferior temporal, 8.7% in the temporal superior, 9.1% in the temporal superior, and 10.8% in the superior temporal, 11.8% in the superior nasal regions. This shows that the reproducibility measurement for children is acceptable but remains lower than that for adults. The unstable fixation in children may affect the image quality and reliability of the measurement. She et al. (32) also found that the reproducibility and repeatability of measurements in different sectors were different, and this study also had similar findings. However, the reason for this difference is unknown.

Some studies have reported that SSI is positively correlated with macular and peripapillary VD, and clinicians should consider the effect of SSI on VD during follow-up studies (12, 15). Based on repeated measurements, Venugopal et al. (26) claimed that SSI was positively correlated with papillary and sectoral peripapillary VD. Lim et al. (33) showed that SSI was positively correlated with peripapillary microvascular VD through a 3×3 mm angiography scan. Interestingly, in the sample of children in this study, considering the two examiners repeated measurement factors, SSI was negatively correlated with VD in most peripapillary sectors. Similarly, Rao et al. (31) used Cirrus OCTA and found that SSI was only negatively correlated with peripapillary temporal VD, while there was no correlation in other sectors. Due to differences in scan area, partition algorithm, equipment, and included subjects, further research is needed on the influence of SSI on peripapillary VD measurement. In addition, the influence of physiological factors, such as small fluctuations in perfusion pressure, should also be considered.

Based on repeatability measurements, Lei et al. (34) reported that AL was only positively correlated with peripapillary temporal VD in Optovue and Triton OCTA; this correlation did not exist

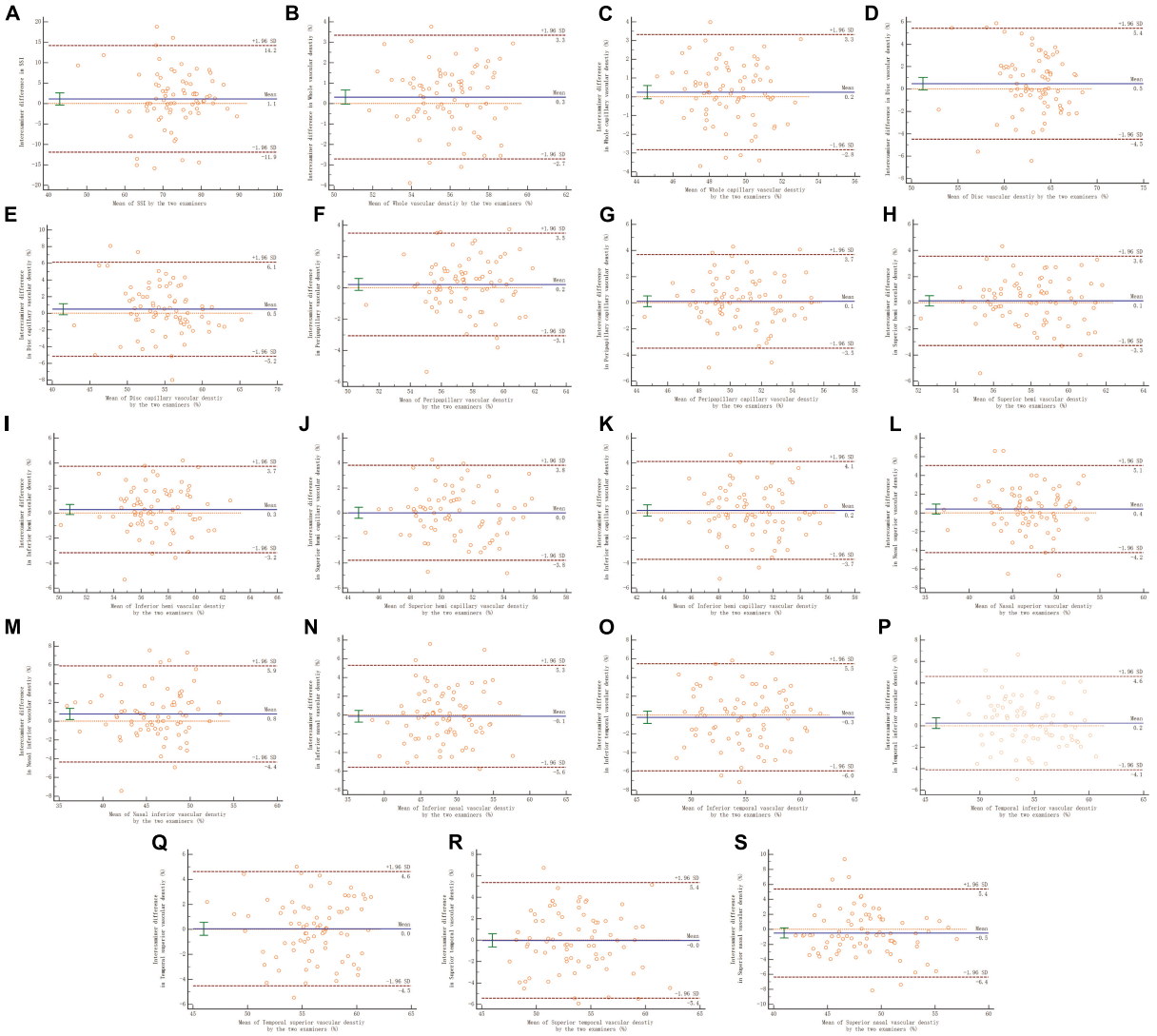

FIGURE 4
Panels **(A–S)** shows the Bland–Altman plots of reproducibility of interexaminer on papillary and peripapillary vascular density measurement. A solid line represents the mean difference. The upper and lower lines represent the 95% limit of agreement.

in other sectors. In the Spectralis and Cirrus OCTA, the positive correlation between AL and VD was reflected in the superior and inferior sectors, and there was no such correlation in other sectors (34). This study also showed that AL was only positively correlated with inferior temporal VD in Optovue OCTA. However, previous studies have demonstrated a negative correlation between peripapillary VD and AL (35, 36), and Sampson et al. (13) suggested that attention should be paid to the correction of AL in VD calculations. This study included healthy children and excluded subjects with high myopia and analyzed them based on repeated measurements by two examiners, which may be the source of differences in the results of the study.

This study has some limitations. First, this study only included Chinese children who used an OCTA device. The reliability of children's measurements of multiple devices, including other ethnic groups, requires further research. Second, this study removed images with low-quality scores or significant motion and blinking artifacts. Previous studies have reported a large number of low quality OCTA images (37, 38). The latest version of the OCTA algorithm reduces image defects using real-time tracking. Finally, the repeatability and reproducibility of OCTA depend on multiple factors, including system parameters, imaging protocols, and subject compliance. System parameters include optical or mechanical stability and algorithm robustness. Imaging protocols include scan location, scan speed, and field of view: wide-field (39) or narrow field. Lastly, young/elderly subjects (26) and ocular disease (40) can lower the OCTA precision. We need to further observe the consistency of the measurements with a long-term follow-up.

This study reports the reliability of papillary and peripapillary VD measurements in healthy Chinese children. Our results demonstrated low intraexaminer and interexaminer variations in papillary and peripapillary perfusion parameters. Considering the factors of repeatability measurement by the two examiners, SSI

TABLE 3 Effect of signal strength index on the repeatability measurement of the papillary and peripapillary vascular density.

Vascular density	Coefficient (SE)	95% CI	*P*-value
Whole	0.053 (0.013)	0.027–0.079	<0.001
Whole capillary	0.010 (0.014)	−0.017 to 0.037	0.471
Disc	0.215 (0.019)	0.178–0.252	<0.001
Disc capillary	0.213 (0.028)	0.158–0.267	<0.001
Peripapillary	0.002 (0.016)	−0.029 to 0.034	0.879
Peripapillary capillary	−0.062 (0.017)	−0.096 to −0.028	<0.001
-Superior hemi	0.003 (0.161)	−0.031 to 0.032	0.985
-Inferior hemi	0.004 (0.017)	−0.029 to 0.037	0.812
-Superior hemi capillary	−0.071 (0.018)	−0.106 to −0.036	<0.001
-Inferior hemi capillary	−0.052 (0.019)	−0.090 to −0.015	0.006
-Nasal superior	0.036 (0.025)	−0.013 to 0.085	0.149
-Nasal inferior	0.005 (0.028)	−0.050 to 0.061	0.857
-Inferior nasal	−0.118 (0.029)	−0.175 to −0.061	<0.001
-Inferior temporal	−0.026 (0.026)	−0.077 to 0.026	0.333
-Temporal inferior	−0.075 (0.023)	−0.119 to −0.030	0.001
-Temporal superior	−0.118 (0.023)	−0.162 to −0.073	<0.001
-Superior temporal	−0.096 (0.026)	−0.147 to −0.045	<0.001
-Superior nasal	−0.156 (0.026)	−0.207 to −0.105	<0.001

TABLE 4 Effect of axial length on the repeatability measurement of the papillary and peripapillary vascular density.

Vascular density	Coefficient (SE)	95% CI	*P*-value
Whole	−0.121 (0.091)	−0.301 to 0.058	0.184
Whole capillary	−0.007 (0.093)	−0.191 to 0.176	0.936
Disc	−0.052 (0.153)	−0.353 to 0.250	0.735
Disc capillary	0.319 (0.205)	−0.085 to 0.723	0.121
Peripapillary	−0.088 (0.108)	−0.300 to 0.124	0.413
Peripapillary capillary	0.042 (0.119)	−0.193 to −0.277	0.727
-Superior hemi	−0.133 (0.108)	−0.346 to 0.080	0.220
-Inferior hemi	−0.045 (0.115)	−0.272 to 0.182	0.698
-Superior hemi capillary	0.021 (0.124)	−0.223 to 0.265	0.867
-Inferior hemi capillary	0.060 (0.131)	−0.197 to 0.317	0.647
-Nasal superior	−0.340 (0.167)	−0.668 to −0.012	0.042
-Nasal inferior	−0.037 (0.192)	−0.416 to 0.341	0.846
-Inferior nasal	−0.160 (0.202)	−0.557 to 0.237	0.429
-Inferior temporal	0.133 (0.180)	−0.220 to 0.488	0.458
-Temporal inferior	0.399 (0.154)	0.095 to 0.702	0.010
-Temporal superior	0.087 (0.161)	−0.230 to −0.403	0.590
-Superior temporal	0.203 (0.181)	−0.153 to 0.560	0.263
-Superior nasal	0.351 (0.185)	−0.013 to 0.714	0.058

affects most of the peripapillary VD, while AL only affects the temporal inferior and nasal peripapillary VD.

TABLE 5 Effect of age on the repeatability measurement of the papillary and peripapillary vascular density.

	Pearson's*r*		
Vascular density	Examiners A	Examiners B	Mean
Whole	−0.164	0.122	−0.104
Whole capillary	−0.16	0.069	−0.101
Disc	−0.117	−0.062	−0.158
Disc capillary	−0.042	−0.098	−0.078
Peripapillary	−0.146	0.06	0.075
Peripapillary capillary	−0.115	−0.003	0.053
-Superior hemi	−0.11	0.036	0.121
-Inferior hemi	−0.163	0.104	0.061
-Superior hemi capillary	−0.116	−0.003	0.15
-Inferior hemi capillary	−0.126	0.034	0.032
-Nasal superior	−0.061	0.183	0.056
-Nasal inferior	−0.038	0.164	0.172
-Inferior nasal	−0.166	0.05	0.018
-Inferior temporal	−0.147	0.186	0.118
-Temporal inferior	−0.175	0.182	0.011
-Temporal superior	0.126	0.043	−0.016
-Superior temporal	−0.277*	−0.11	0.158
-Superior nasal	−0.132	−0.049	−0.091

*$P < 0.05$.

Data availability statement

The original contributions presented in this study are included in the article/supplementary material, further inquiries can be directed to the corresponding authors.

Ethics statement

The studies involving human participants were reviewed and approved by the Eye Hospital of Wenzhou Medical University. Written informed consent to participate in this study was provided by the participants' legal guardian/next of kin. Written informed consent was obtained from the individual(s), and minor(s)' legal guardian/next of kin, for the publication of any potentially identifiable images or data included in this article.

Author contributions

RC, XL, MY, QW, SC, and JH contributed to the conception and design of the study. ZZ, XyC, ZL, XC, and MS organized the database. HL performed the statistical analysis. RC wrote the first draft of the manuscript. WL, YY, CM, QW, SC, and JH wrote sections of the manuscript. All authors contributed to manuscript revision, read, and approved the submitted version.

Funding

This work was supported in part by Science and Technology Planning Project of Zhejiang Province (LGF19H120002); the Eye and ENT Hospital of Fudan University High-level Talents Program (2021318); the Zhejiang National Natural Science Foundation (LQ16B010002); the Wenzhou Bureau of Science and Technology (Y20160061 and Y2020037); the Medical and Health Science and Technology Program of Zhejiang Province (2019KY111); the Program for Professor of Special Appointment (Eastern Scholar) at Shanghai Institutions of Higher Learning; Multidisciplinary innovation team of traditional Chinese medicine for the treatment of myopia and amblyopia in children in Zhejiang Province; and the funders had no role in study design, data collection and analysis, decision to publish, or reparation of the manuscript.

Conflict of interest

The authors declare that the research was conducted in the absence of any commercial or financial relationships that could be construed as a potential conflict of interest.

Publisher's note

All claims expressed in this article are solely those of the authors and do not necessarily represent those of their affiliated organizations, or those of the publisher, the editors and the reviewers. Any product that may be evaluated in this article, or claim that may be made by its manufacturer, is not guaranteed or endorsed by the publisher.

References

1. Werner A, Shen LQ. A review of OCT angiography in glaucoma. *Semin Ophthalmol.* (2019) 34:279–86. doi: 10.1080/08820538.2019.1620807

2. Abdelrahman A, Eltanamly R, Elsanabary Z, Hassan L. Optical coherence tomography angiography in juvenile open angle glaucoma: correlation between structure and perfusion. *Int Ophthalmol.* (2021) 41:883–9. doi: 10.1007/s10792-020-01643-7

3. Spaide RF, Klancnik JM Jr, Cooney MJ. Retinal vascular layers imaged by fluorescein angiography and optical coherence tomography angiography. *JAMA Ophthalmol.* (2015) 133:45–50. doi: 10.1001/jamaophthalmol.2014.3616

4. Jia Y, Bailey S, Hwang T, McClintic S, Gao S, Pennesi M, et al. Quantitative optical coherence tomography angiography of vascular abnormalities in the living human eye. *Proc Natl Acad Sci USA.* (2015) 112:E2395–402. doi: 10.1073/pnas.1500185112

5. Savastano MC, Lumbroso B, Rispoli M. In vivo characterization of retinal vascularization morphology using optical coherence tomography angiography. *Retina.* (2015) 35:2196–203. doi: 10.1097/iae.0000000000000635

6. Coscas F, Sellam A, Glacet-Bernard A, Jung C, Goudot M, Miere A, et al. Normative data for vascular density in superficial and deep capillary plexuses of healthy adults assessed by optical coherence tomography angiography. *Invest Ophthalmol Vis Sci.* (2016) 57:OCT211–23. doi: 10.1167/iovs.15-18793

7. Yu J, Jiang C, Wang X, Zhu L, Gu R, Xu H, et al. Macular perfusion in healthy Chinese: an optical coherence tomography angiogram study. *Invest Ophthalmol Vis Sci.* (2015) 56:3212–7. doi: 10.1167/iovs.14-16270

8. Iafe N, Phasukkijwatana N, Chen X, Sarraf D. Retinal capillary density and foveal avascular zone area are age-dependent: quantitative analysis using optical coherence tomography angiography. *Invest Ophthalmol Vis Sci.* (2016) 57:5780–7. doi: 10.1167/iovs.16-20045

9. Manalastas P, Zangwill L, Saunders L, Mansouri K, Belghith A, Suh M, et al. Reproducibility of optical coherence tomography angiography macular and optic nerve head vascular density in glaucoma and healthy eyes. *J Glaucoma.* (2017) 26:851–9. doi: 10.1097/IJG.0000000000000768

10. You Q, Freeman W, Weinreb R, Zangwill L, Manalastas P, Saunders L, et al. Reproducibility of vessel density measurement with optical coherence tomography angiography in eyes with and without retinopathy. *Retina.* (2017) 37:1475–82. doi: 10.1097/IAE.0000000000001407

11. Shahlaee A, Samara W, Hsu J, Say E, Khan M, Sridhar J, et al. In vivo assessment of macular vascular density in healthy human eyes using optical coherence tomography angiography. *Am J Ophthalmol.* (2016) 165:39–46. doi: 10.1016/j.ajo.2016.02.018

12. Zhang Z, Huang X, Meng X, Chen T, Gu Y, Wu Y, et al. In vivo assessment of macula in eyes of healthy children 8 to 16 years old using optical coherence tomography angiography. *Sci Rep.* (2017) 7:8936. doi: 10.1038/s41598-017-08174-9

13. Sampson D, Gong P, An D, Menghini M, Hansen A, Mackey D, et al. Axial length variation impacts on superficial retinal vessel density and foveal avascular zone area measurements using optical coherence tomography angiography. *Invest Ophthalmol Vis Sci.* (2017) 58:3065–72. doi: 10.1167/iovs.17-21551

14. Tai E, Li L, Wan-Hazabbah W, Wong T, Shatriah I. Effect of axial eye length on retinal vessel parameters in 6 to 12-year-old malay girls. *PLoS One.* (2017) 12:e0170014. doi: 10.1371/journal.pone.0170014

15. Rao H, Pradhan Z, Weinreb R, Reddy H, Riyazuddin M, Sachdeva S, et al. Determinants of peripapillary and macular vessel densities measured by optical coherence tomography angiography in normal eyes. *J Glaucoma.* (2017) 26:491–7. doi: 10.1097/IJG.0000000000000655

16. Bazvand F, Mirshahi R, Fadakar K, Faghihi H, Sabour S, Ghassemi F. The quantitative measurements of vascular density and flow area of optic nerve head using optical coherence tomography angiography. *J Glaucoma.* (2017) 26:735–41. doi: 10.1097/IJG.0000000000000722

17. Pappelis K, Jansonius N. Quantification and repeatability of vessel density and flux as assessed by optical coherence tomography angiography. *Transl Vis Sci Technol.* (2019) 8:3. doi: 10.1167/tvst.8.3.3

18. Al-Sheikh M, Tepelus T, Nazikyan T, Sadda S. Repeatability of automated vessel density measurements using optical coherence tomography angiography. *Br J Ophthalmol.* (2017) 101:449–52. doi: 10.1136/bjophthalmol-2016-308764

19. Maassen G. The two errors of using the within-subject standard deviation (Wsd) as the standard error of a reliable change index. *Arch Clin Neuropsychol.* (2010) 25:451–6. doi: 10.1093/arclin/acq036

20. Huang J, Savini G, Wu F, Yu X, Yang J, Yu A, et al. Repeatability and reproducibility of ocular biometry using a new noncontact optical low-coherence interferometer. *J. Cataract Refract Surg.* (2015) 41:2233–41. doi: 10.1016/j.jcrs.2015.10.062

21. Huang J, Ding X, Savini G, Pan C, Feng Y, Cheng D, et al. A comparison between scheimpflug imaging and optical coherence tomography in measuring corneal thickness. *Ophthalmology.* (2013) 120:1951–8. doi: 10.1016/j.ophtha.2013.02.022

22. Tian L. Inferences on the within-subject coefficient of variation. *Stat Med.* (2006) 25:2008–17. doi: 10.1002/sim.2330

23. Huang J, Savini G, Hu L, Hoffer K, Lu W, Feng Y, et al. Precision of a new scheimpflug and placido-disk analyzer in measuring corneal thickness and agreement with ultrasound pachymetry. *J Cataract Refract Surg.* (2013) 39:219–24. doi: 10.1016/j.jcrs.2012.10.034

24. Xue C, Yuan J, Lo G, Chang A, Poon D, Wong O, et al. Radiomics feature reliability assessed by intraclass correlation coefficient: a systematic review. *Quant Imaging Med Surg.* (2021) 11:4431–60. doi: 10.21037/qims-21-86

25. Wang Q, Ding X, Savini G, Chen H, Feng Y, Pan C, et al. Anterior chamber depth measurements using scheimpflug imaging and optical coherence tomography: repeatability, reproducibility, and agreement. *J Cataract Refract Surg.* (2015) 41:178–85. doi: 10.1016/j.jcrs.2014.04.038

26. Venugopal J, Rao H, Weinreb R, Dasari S, Riyazuddin M, Pradhan Z, et al. Repeatability and comparability of peripapillary vessel density measurements of high-density and non-high-density optical coherence tomography angiography scans in normal and glaucoma eyes. *Br J Ophthalmol.* (2019) 103:949–54. doi: 10.1136/bjophthalmol-2018-312401

27. Rao H, Kadambi S, Weinreb R, Puttaiah N, Pradhan Z, Rao D, et al. Diagnostic ability of peripapillary vessel density measurements of optical coherence tomography angiography in primary open-angle and angle-closure glaucoma. *Br J Ophthalmol.* (2017) 101:1066–70. doi: 10.1136/bjophthalmol-2016-309377

28. Mansoori T, Sivaswamy J, Gamalapati J, Agraharam S, Balakrishna N. Measurement of radial peripapillary capillary density in the normal human retina

using optical coherence tomography angiography. *J Glaucoma.* (2017) 26:241–6. doi: 10.1097/ijg.0000000000000594

29. Lei J, Durbin M, Shi Y, Uji A, Balasubramanian S, Baghdasaryan E, et al. Repeatability and reproducibility of superficial macular retinal vessel density measurements using optical coherence tomography angiography en face images. *JAMA Ophthalmol.* (2017) 135:1092–8. doi: 10.1001/jamaophthalmol.2017.3431

30. Alnawaiseh M, Brand C, Bormann E, Sauerland C, Eter N. Quantification of macular perfusion using optical coherence tomography angiography: repeatability and impact of an eye-tracking system. *BMC Ophthalmol.* (2018) 18:123. doi: 10.1186/s12886-018-0789-z

31. Rao HL, Dasari S, Riyazuddin M, Lavanya R, Nk P, Pradhan ZS, et al. Referenced scans improve the repeatability of optical coherence tomography angiography measurements in normal and glaucoma eyes. *Br J Ophthalmol.* (2020) 105:1542–7. doi: 10.1136/bjophthalmol-2020-316480

32. She X, Guo J, Liu X, Zhu H, Li T, Zhou M, et al. Reliability of vessel density measurements in the peripapillary retina and correlation with retinal nerve fiber layer thickness in healthy subjects using optical coherence tomography angiography. *Ophthalmologica.* (2018) 240:183–90. doi: 10.1159/000485957

33. Lim H, Kim Y, Nam K, Ryu C, Jo Y, Kim J. Signal strength as an important factor in the analysis of peripapillary microvascular density using optical coherence tomography angiography. *Sci Rep.* (2019) 9:16299. doi: 10.1038/s41598-019-52818-x

34. Lei J, Pei C, Wen C, Abdelfattah N. Repeatability and reproducibility of quantification of superficial peri-papillary capillaries by four different optical coherence tomography angiography devices. *Sci Rep.* (2018) 8:17866. doi: 10.1038/s41598-018-36279-2

35. Wang X, Kong X, Jiang C, Li M, Yu J, Sun X. Is the peripapillary retinal perfusion related to myopia in healthy eyes? A prospective comparative study. *BMJ Open.* (2016) 6:e010791. doi: 10.1136/bmjopen-2015-010791

36. Mo J, Duan A, Chan S, Wang X, Wei W. Vascular flow density in pathological myopia: an optical coherence tomography angiography study. *BMJ Open.* (2017) 7:e013571. doi: 10.1136/bmjopen-2016-013571

37. Spaide R, Fujimoto J, Waheed N. Image artifacts in optical coherence tomography angiography. *Retina.* (2015) 35:2163–80. doi: 10.1097/IAE.0000000000000765

38. Suh M, Zangwill L, Manalastas P, Belghith A, Yarmohammadi A, Medeiros F, et al. Optical coherence tomography angiography vessel density in glaucomatous eyes with focal lamina cribrosa defects. *Ophthalmology.* (2016) 123:2309–17. doi: 10.1016/j.ophtha.2016.07.023

39. Hong J, Tan B, Quang N, Gupta P, Lin E, Wong D, et al. Intra-session repeatability of quantitative metrics using widefield optical coherence tomography angiography (OCTA) in elderly subjects. *Acta Ophthalmol.* (2019) 98:e570–8. doi: 10.1111/aos.14327

40. Lee J, Grisafe D, Burkemper B, Chang B, Zhou X, Chu Z, et al. Intrasession repeatability and intersession reproducibility of peripapillary OCTA vessel parameters in non-glaucomatous and glaucomatous eyes. *Br J Ophthalmol.* (2021) 105:1534–41. doi: 10.1136/bjophthalmol-2020-317181

frontiers | Frontiers in Medicine

TYPE Study Protocol
PUBLISHED 29 March 2023
DOI 10.3389/fmed.2023.1089652

OPEN ACCESS

EDITED BY
Eduardo Normando,
Imperial College London,
United Kingdom

REVIEWED BY
Manfred Boehm,
National Heart, Lung,
and Blood Institute (NIH),
United States
Jaroslava Halper,
University of Georgia,
United States
Eric Singman,
University of Maryland Medical System,
United States

*CORRESPONDENCE
Mihaela Oana Romanitan
✉ mihaela.romanitan@sll.se
Ruxandra Pirvulescu
✉ ruxandra.pirvulescu@umfcd.ro;
✉ ruxandrapascu78@gmail.com
Raluca Iancu
✉ ralucavasile2002@yahoo.com

SPECIALTY SECTION
This article was submitted to
Ophthalmology,
a section of the journal
Frontiers in Medicine

RECEIVED 04 November 2022
ACCEPTED 07 March 2023
PUBLISHED 29 March 2023

CITATION
Cherecheanu MP, Romanitan MO, Pirvulescu R, Iancu R, Garhöfer G, Iancu G, Cherecheanu AP, Zemba M, Vasile V, Simonov A and Branisteanu D (2023) Uncommon association between vascular Ehlers–Danlos syndrome and ocular complications.
Front. Med. 10:1089652.
doi: 10.3389/fmed.2023.1089652

Uncommon association between vascular Ehlers–Danlos syndrome and ocular complications

Matei Popa Cherecheanu[1,2], Mihaela Oana Romanitan[3]*, Ruxandra Pirvulescu[1,4]*, Raluca Iancu[1,4]*, Gerhard Garhöfer[5], George Iancu[1,6], Alina Popa Cherecheanu[1,4], Mihail Zemba[1,7], Victor Vasile[1], Andrei Simonov[8] and Daniel Branisteanu[9]

[1]Carol Davila University of Medicine and Pharmacy, Bucharest, Romania, [2]Cardiovascular Surgery Clinic, Prof. Dr. Agrippa Ionescu Emergency Clinical Hospital, Bucharest, Romania, [3]Department for Emergency Internal Medicine and Neurology, Stockholm South General Hospital, Stockholm, Sweden, [4]Department of Ophthalmology, University Emergency Hospital, Bucharest, Romania, [5]Department of Clinical Pharmacology, Medical University of Vienna, Vienna, Austria, [6]Filantropia Clinical Hospital, Bucharest, Romania, [7]Department of Ophthalmology, Clinical Military Emergency Hospital, Bucharest, Romania, [8]Department of Interventional Radiology, University Emergency Hospital, Bucharest, Romania, [9]Department of Ophthalmology, University of Medicine and Pharmacy Grigore T. Popa Iasi, Iasi, Romania

Ehlers–Danlos syndromes (EDS) represent a group of rare inherited disorders that affect connective tissues. There are 13 types of disease, most of them affecting joints or skin; symptoms usually include loose joints, joint pain, stretchy velvety skin, abnormal scar formation. However, the most serious type of disease is vascular EDS (vEDS), or EDS type 4 because patients may suffer vessels dissections or internal organs lesions, followed by bleeding, which endangers patient's life, but also thromboembolic events. We present two clinical cases of vEDS managed in our clinic in 1year distance. In both cases, patients were active young persons (in their thirties, and respectively, twenties), both with multiple non-traumatic vascular dissections, and severe ocular complications: arterio-venous fistula with massive exophthalmia, and central retinal artery occlusion, respectively. Both cases were challenging since the life of the patients were threatened by their condition. However, in both cases, prompt treatment and finding the right trigger of the ocular pathology and vascular injuries helped doctors to provide proper and prompt medical care, in order to prevent future similar events to happen and to preserve a good quality of life for these patients.

KEYWORDS

vascular Ehlers–Danlos syndrome, vascular dissections, retinal artery occlusion, arterio-venous fistula, young persons

Introduction

Ehlers–Danlos Syndromes (EDS) are a group of heritable connective tissue disorders, that are usually characterized by skin hyper elasticity, joint hyperlaxity and tissue fragility (1, 2). These syndromes appear due to abnormalities in biosynthesis and/or structure extracellular matrix proteins (3). Most types of EDS that have a known genetic cause, resulting from pathogenic variants of the genes that encode fibrillar collagen types I, III, and V, modifying or transforming enzymes of these collagens, or enzymes that play a crucial role in the biosynthesis

of glycosaminoglycans (GAG) proteoglycan chains (4). The prevalence of EDS is estimated at 1 in 5000, without any ethnic or sex predilection (1, 2).

These syndromes were first identified in the early twentieth century, by dermatologists Edvard Ehlers and HenriAlexandre Danlos. They described patients with joint hypermobility, excessive skin extensibility, easy bruising and abnormal scar formation after injury (4). Even though patients with similar clinical aspects were previously reported by Russian and Danish dermatologists, Ehlers–Danlos disease had a chaotic history which delayed its identification (5).

Several classification structures have been proposed, but the most recent one was determined during the Ehlers–Danlos Syndrome International Symposium in 2017 (6), and includes 13 subtypes of EDS, divided into 7 pathogenic groups (2, 6). The reason it is so important to distinguish the different types of EDS, is because they do not develop in time the same complications and their prognosis is therefore different (6). Classic EDS (former types I and II) and especially hyper-mobile EDS (former type III) represent almost 85% of patients referred for consultation and vascular EDS type (type IV) about 5%. (1). The other EDS represent a small group of Mendelian genetic disorders whose clinical manifestation and causative genes are increasingly better characterized thanks to advances in genetics (1).

Vascular EDS (vEDS) is one if not the most challenging type of EDS. It is caused by mutations in the *COL3A1* gene (rarely *COL1A1*) (7). Patients often have a suggestive morphotype and thin skin revealing the subcutaneous venous network. They are often exposed to life-threatening complications: arterial complications (dissection, aneurysm, or arteriovenous fistula), spontaneous colonic perforations, pneumothorax and, in women's case, risk of fragility of the uterine wall (particularly during childbirth) (6). Among all the medical problems to which patients with vEDS are exposed, vascular and/or organ rupture are the two most feared and deadly complications (8–10).

Beside the life-threatening complications, vEDS may also include ophthalmic findings such as: high refractive errors (e.g., myopia – 25.3%), irregular astigmatism, steep keratometry values, convergence insufficiency, strabismus, thin pachymetry, increased applanation-related stromal folds. Among the symptoms the patients experience, the most upsetting are blurred vision, difficulty focusing at near, binocular diplopia, dry eye sensation, headaches (2, 10).

Eye examination of EDS patients may identify ptosis (32%), infraorbital creases (29.3%), epicanthal folds (18.6%), hypertelorism (8%), strabismus (8%), blue sclerae, lenticular changes, corneal thinning (11).

However, besides minor ophthalmic signs and symptoms, sometimes major events with direct or indirect ophthalmic implications may occur. Among those, there are retinal artery occlusions or carotid-cavernous fistula (11).

Vascular Ehlers–Danlos syndrome (vEDS) should be considered in individuals with any one of the major diagnostic criteria or several minor diagnostic criteria, particularly in those under 40 years (see Table 1) (11).

Clinical diagnostic criteria established in 2017 the opportunity of genetic testing. The certainty diagnosis of vEDS is determined either by identification of a heterozygous pathogenic variant in *COL3A1* on molecular genetic testing, by abnormalities in synthesis and mobility of type III collagen chains on biochemical analysis of type III procollagen from cultured fibroblasts, or even by histopathological examination of tissue biopsy; the latter one may be challenging, since histopathological findings of vEDS are not widely recognized (12).

TABLE 1 Major and minor diagnostic criteria for vEDS (11).

Major diagnostic criteria	Minor diagnostic criteria
• Arterial aneurysms, dissection, or rupture	• Thin, translucent skin (especially noticeable on the chest/abdomen)
• Intestinal rupture	• Characteristic facial appearance (narrow nose, thin lips, micrognathia, prominent eyes)
• Uterine rupture during pregnancy	•Acrogeria (an aged appearance to the extremities, particularly the hands)
• Family history of vEDS	• Carotid-cavernous sinus arteriovenous fistula
	• Hypermobility of small joints
	• Tendon/muscle rupture
	• Early-onset varicose veins
	• Hemo/pneumothorax
	• Easy bruising (spontaneous or with minimal trauma)
	• Chronic joint subluxations/ dislocations
	• Congenital dislocation of the hips
	• Clubfoot

Studies show that the majority (60%) of individuals with vEDS diagnosed under age of 18 are identified because of a positive family history (13). Death usually occurs in the first two decades of life almost always because of spontaneous artery rupture or dissection. Artery rupture, 60% of which involved the aorta, was responsible for all deaths in young males. Death before age 20 years was seen in a 3:1 ratio of males: females. In adults with a *COL3A1* pathogenic variant, vascular rupture or dissection and gastrointestinal perforation or organ rupture are the presenting signs in 70% of cases (4).

Complications in vEDS patients are dramatic and often unexpected, presenting as sudden death, stroke and its neurologic sequelae, acute abdomen, retroperitoneal bleeding, uterine rupture at pregnancy, and/or shock. Vascular complications include rupture, aneurysm, and/or dissection of major or minor arteries. Arterial rupture may be preceded by aneurysm, arteriovenous fistulae, or dissection, or may occur spontaneously. The sites of arterial rupture are the thorax and abdomen (66%), head and neck (17%), and extremities (17%). Patients may also experience hemothorax and hemopneumothorax, often in association with pulmonary blebs, cystic lesions, and hemorrhagic or fibrous nodules, often followed by hemoptysis can be severe and recurrent, even life threatening (14, 15).

We hereby present two clinical cases of vEDS, each one presented in ER with different severity, one of them with both general life threatening and sight-threatening conditions and the other one with a sudden decrease in visual acuity, without other apparent signs and symptoms. In this latter case, further tests revealed that beyond clinical signs, may lie dangerous disorders and proper care and treatment made the difference between life and death.

Case 1

Carotid cavernous fistula in vEDS

A 28-year-old female patient presented to the ER for binocular diplopia, right axial proptosis, right hemicrania, tinnitus, pronounced vertigo when changing position. The disorders lasted for 2–3 days and were accompanied by nausea and vomiting, for approximately 24 h before the time of admission. The patient did not have any knowledge of an underlying medical condition, such as EDS.

During hospitalization, the patient complains of intense pain in the lumbar area and in the left flank with sudden onset and anterior irradiation. The general condition deteriorated, and the patient became hemodynamically unstable with 70/40 mmHg ABP, cardiac frequency 120/min, signs of hemorrhagic sock. The abdominal CT exam revealed an anatomic anomaly with two left renal arteries, one smaller 2 mm and the other 4 mm diameter, the latter with an aneurismal dilation (8/7 mm in one axis and 4/5 in the other) localized at 21 mm of the origin of the renal artery from the aorta, voluminous retroperitoneal, peripancreatic and peri-renal hematoma as well as left kidney infarction. Emergency surgical intervention was performed, which consisted in left nephrectomy and left adrenalectomy of necessity, restoration of aortic arterial flow by interposition of DACRON 18 prosthesis following aortic abdominal rupture (due to an aortic aneurism which was identified during surgery and explained the massive hematoma). Postoperative, the evolution was difficult with acute kidney failure, need of renal replacement therapy (veno-venous hemodiafiltration CCVHD) because of hyperkalemia and metabolic acidosis.

When the patient was hemodynamically stabile, she was transferred to the Ophthalmology Department of the Emergency Hospital of Bucharest for right carotid cavernous fistula suspicion. The presence of a lumbar suppurative wound at the nephrectomy incision was noted on his arrival at our clinic.

The visual acuity in the right eye was approximately 1/50 without correction. The examination was performed with the patient lying horizontally, due to the recent surgery, so a best corrected visual acuity was not possible. Intraocular pressure was elevated in the right eye (24 mm Hg) and within normal limits in the left eye (12 mm Hg), measured by Perkins applanation tonometer.

Clinical examination in the right eye revealed marked conjunctival hyperemia with massive conjunctival chemosis and prolapse of the conjunctiva over the lower lid, axial proptosis, and internal and external ophthalmoplegia (Figures 1A,B). Cortico-nuclear lens opacities were identified in both eyes. Fundus exam of both eyes showed slightly tortuous vessels, more obvious in the right eye than in the left eye.

Another aspect that caught our attention was the particular appearance of the patient: narrow nose, translucent skin, thin vermilion lips (Figure 2).

The brain Magnetic Resonance Angiography (MRA) examination revealed:

- Right carotid-cavernous fistula (arterialization of the cavernous sinus) (Figure 3)
- Axial proptosis, dilatation of the superior right ophthalmic vein, oedema of the intraconal fat, enlarged eye muscles in diameter on the right side (Figure 4)
- Subacute stage meningeal hemorrhage in the right paratentorial area and left peri- and intergyral fronto-parietal area,
- Subacute hemorrhagic spot intraparenchymal cerebellar hemisphere on the left side,
- Pituitary adenoma,
- Right frontal sinusitis.

The patient was referred to the Interventional Neurology department for cerebral angiography and subsequent embolization of the carotid-cavernous fistula. Cerebral angiography revealed a direct carotid-cavernous fistula (Type D) with discharge through the right ophthalmic vein and subsequently at the level of both facial veins, as well as stenosis at the level of the M1 segment of the left middle cerebral artery (MCA) of approx. 80% with small post-stenotic dilations. Irregular appearance of the medium and small branches of the left anterior cerebral artery (ACA) and MCA can be observed (Figures 5A,B, 6A,B).

Interventional treatment was performed by embolizing the carotid-cavernous fistula through a right femoral vein approach. Multiple embolization coils were deployed at the level of the right cavernous sinus *via* a right facial vein approach and an optimal post-embolization result was obtained with no loading at the level of the fistula, without any peri-procedural neurological incidents (Figures 7A,B, 8A,B). Figures 9A,B show the complete embolization of the carotid cavernous fistula.

One month after the intervention, remission of axial proptosis and chemosis, recovery of external and internal ocular motility can be observed (Figure 10).

Given the nature of the patient's injuries and the clear fulfilment of several major and minor criteria for vEDS (multiple vascular lesions, the clinical general and ophthalmic aspects, and the physical appearance of the patient), we did not consider a skin biopsy as initial diagnosis test, instead, patient underwent specific genetic tests that confirmed the diagnosis of vascular Ehlers–Danlos syndrome, by finding missense mutation in exon 39 of the *COL3A1* gene.

Case 2

Central retinal artery occlusion (CRAO) in vEDS

The second case we present in this paper is a 28-year-old male, from the urban environment, who presented in the ER with sudden, painless decrease of visual acuity in the left eye, 2 weeks before. The general aspect of the patient was similar with the previous case: translucent skin, narrow nose, thin vermilion lips (Figure 11). From the medical history of the patient arouse: premature birth (2 months before term), loss of consciousness after a cranio-cerebral trauma (10 years *a priori*), capillary fragility with easy bruising, and patient's father – known with ischemic heart disease (two stents). Same as the previous clinical case, the patient was not aware of any medical condition such as EDS.

The ophthalmological exam showed best corrected visual acuity in the right eye 50/50, and no central vision in the left eye. Visual field was within normal limits in the right eye, while in the left eye only a small temporal island of vision was identified. Intraocular pressure was within normal limits in both eyes; IOP in both eyes was 15 mmHg.

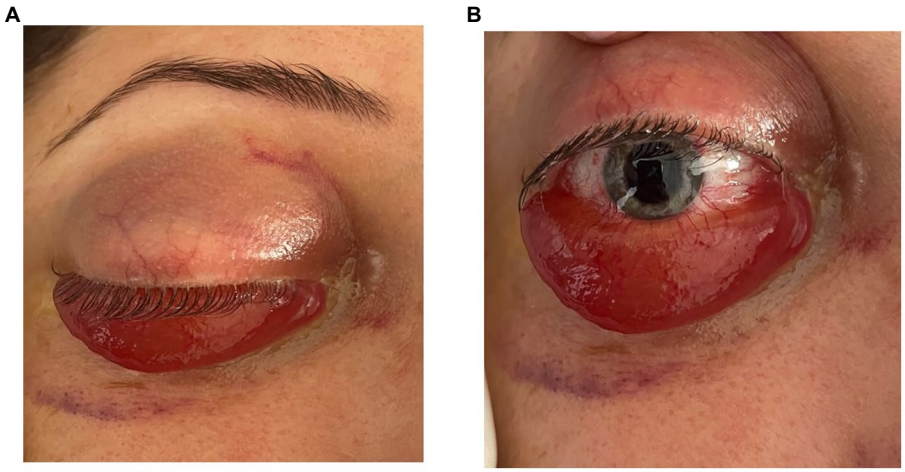

FIGURE 1
(A,B) Frontal view showing axial proptosis, as well the massive chemosis with conjunctival prolapse over the lower eyelid.

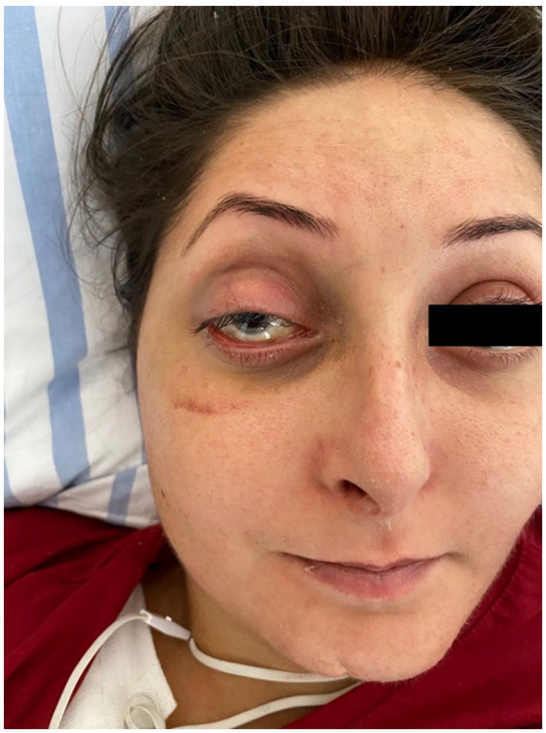

FIGURE 2
Patient's appearance: narrow nose, translucent skin, thin vermilion lips.

Eye fundus in the right eye showed slightly narrowed retinal vessels, while in the left eye it showed an optic disc with discrete blurred margins (superiorly and inferiorly), whitish retinal oedema, small, perfused area between the optic disc and the macula (patent cilioretinal artery), and thin retinal vessels (Figure 12).

The general clinical exam was within normal limits. Blood tests showed a slightly delayed prothrombin time (PT = 18 s) and an international normalized ratio (INR) of 1.65, which is considered a high value for a healthy person.

Further examinations included a transcranial echo-Doppler exam, which revealed decreased velocity flow in the left internal carotid artery (ICA). Following the neurological exam, cerebral angiography was indicated (Figures 13A–E), and it exposed:

- dissection at the left ICA level, image of a pseudoaneurysm adjacent to the dissection,
- significant hemodynamic stenosis
- suggestive aspects of dissection in both vertebral arteries
- an anatomical variant of the right trigeminal artery

Patient was referred to Neurology Clinic and underwent percutaneous transluminal angioplasty with left ICA stenting.

Given the fact that patient had a significant ophthalmic event, sub-clinical non-traumatic vascular dissections, history of capillary fragility with repeated ecchymosis, as well as an appearance with narrow nose, translucent and elastic skin and small stature, a skin biopsy was performed, revealing changes in the elastic fibers and fibrillar collagen suggestive for vEDS. More specifically, the tissue sections revealed knots of elastic fibers in transverse and oblique sections, with marked pathological changes. Some areas showed elastic fibers disintegrated almost completely, while other remnants elastic fibers had an annular, relatively round appearance and other elastic fibers had an irregular, wavy, garlanded, outline; the modifications were present in all analyzed skin samples, in variable size.

Subsequent genetic tests confirmed the diagnosis, by finding a mutation on *COL3A1* gene.

Patient underwent anticoagulant treatment, with favorable results, was advised to avoid any physical effort that might put him at risk for vascular dissections and continues to manage his condition properly and carefully.

Discussion and conclusion

Vascular Ehlers–Danlos syndrome (vEDS) is a particular type of EDS characterized by multiple organ fragility, arterial, intestinal, and/

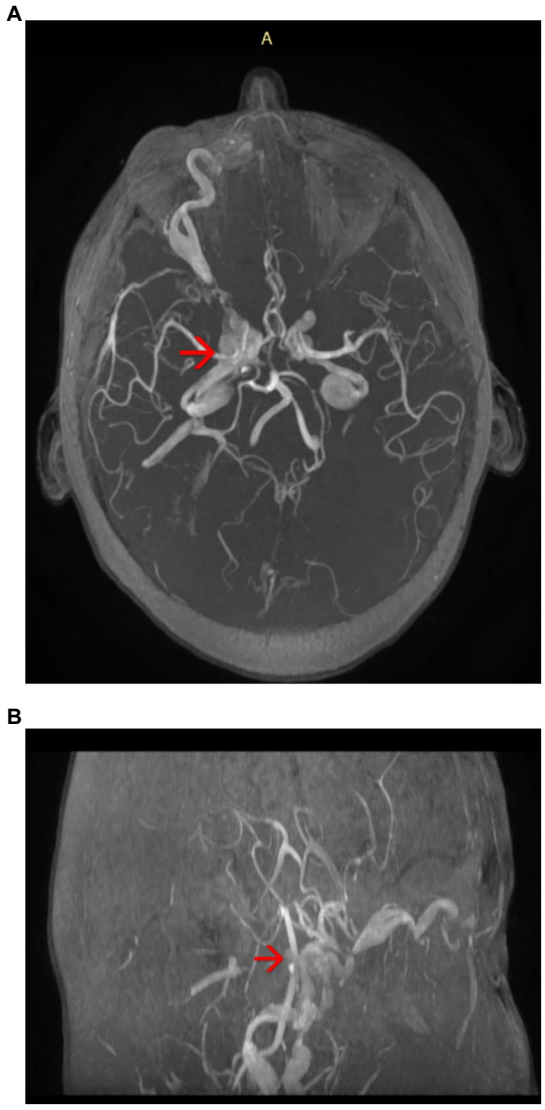

FIGURE 3
(A,B) Magnetic resonance angiography (MRA) of the brain highlighting the arterialization of the cavernous sinus (axial plane) – see red arrows.

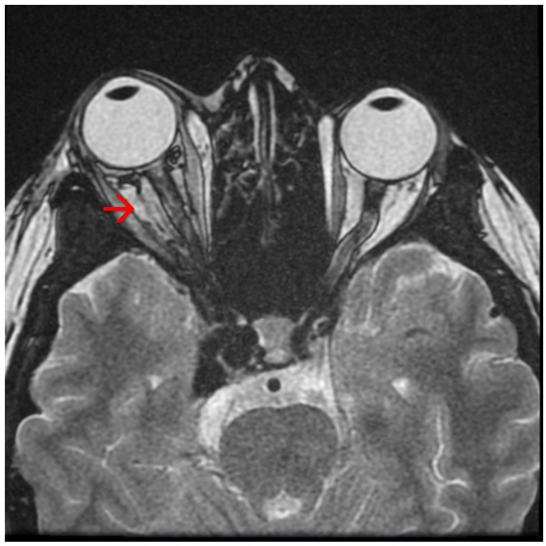

FIGURE 4
Magnetic resonance angiography (MRA) showing axial proptosis and dilation of the superior right ophthalmic vein – see red arrow.

or uterine; patient's skin appears thin and translucent; among the general clinical aspects of the disease, are included easy bruising, characteristic facial appearance (thin vermilion of the lips, micrognathia, narrow nose, prominent eyes), which were present in both our patients' case; extremities of these patients have an aged appearance particularly involving the hands (see Table 1). Individuals with vEDS are unfortunately inclined to vascular dissections or ruptures, gastrointestinal perforations, or even organ ruptures, as pointed out by our clinical cases. Usually, organ/vascular dissections are the presenting signs in most adults with vEDS. In some cases, arterial rupture may be preceded by arteriovenous fistulae, aneurysms, or dissection but it may also occur spontaneously. Most subjects with vEDS (60%), who are diagnosed before 18 years old, are identified because of a positive family history. In our patients' situation, due to circumstantial factors, the family link could not be established. When family inheritance is suspected, specific clinical exams and tests should be performed on neonates as soon as possible, especially when identifying specific morphological and clinical signs.

To better understand the evolution of patients with vEDS, particularly these two clinical cases, we should look back to vEDS from a holistic point of view. The most comprehensive descriptions of clinical features and natural history of vEDS individuals arise from two types of studies: a cross-sectional and retrospective view obtained at the time of diagnostic testing and a nearly 15-year-long cohort study from one group in France (13, 15). A retrospective review of the health history of more than 1,200 individuals with vEDS outlined the natural course of the disorder (13). Most individuals were discovered due to a major complication (70%), at an average age of 30 years. Mean survival in the population was 50 years, with a younger mean survival in males (by 5 years) than in females, partially due to a higher rate of lethal vascular events in males than females before 20 years of age. Similar results were reported in the French cohort of 215 individuals with vEDS, but in this case, a difference in mean survival based on sex was not observed (15).

In our patients' cases, unsuspected young adult patients present to the ER having a vascular potentially life-threatening event (vascular dissection or arterial occlusion), and only careful step by step approach and interdisciplinary clinical management led to correct diagnosis and treatment.

In the first patient we identified a carotid-cavernous fistula (CCF). CCF is an abnormal communication between the cavernous sinus venosus and the carotid artery, and can appear spontaneously or after a head trauma (3).

Barrow et al. proposed in 1985 a classification of carotid-cavernous fistulas into 4 types (4):

Type A: carotid-cavernous fistulas with full channel, high flow (5). Type A fistula is a direct, high-flow fistula between the internal carotid artery and the cavernous sinus. It is the most common type of CCF after head trauma, but it can also occur spontaneously in a predisposing vascular area such as in Ehlers–Danlos syndrome. The etiopathogenic hypothesis of direct fistulas assumes the formation

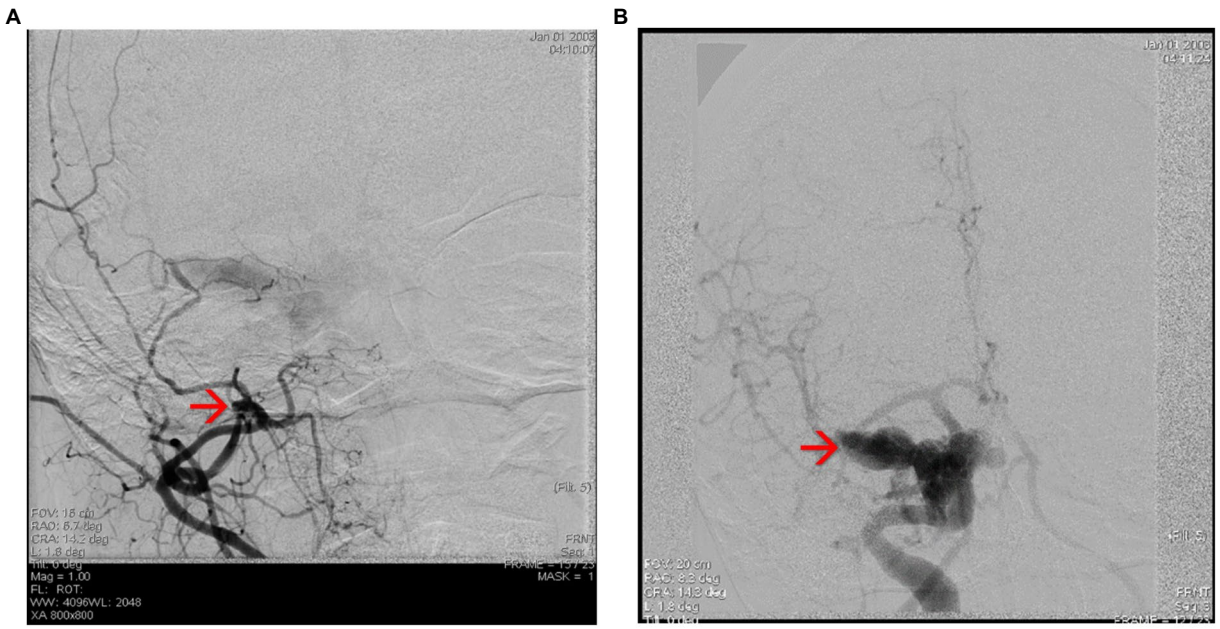

FIGURE 5
(A,B) Cerebral angiography highlighting the Type D carotid-cavernous fistula [according to Barrow classification (4)] on the right side, and dural shunts between both branches from the external carotid artery (ECA) ant the internal carotid artery (ICA).

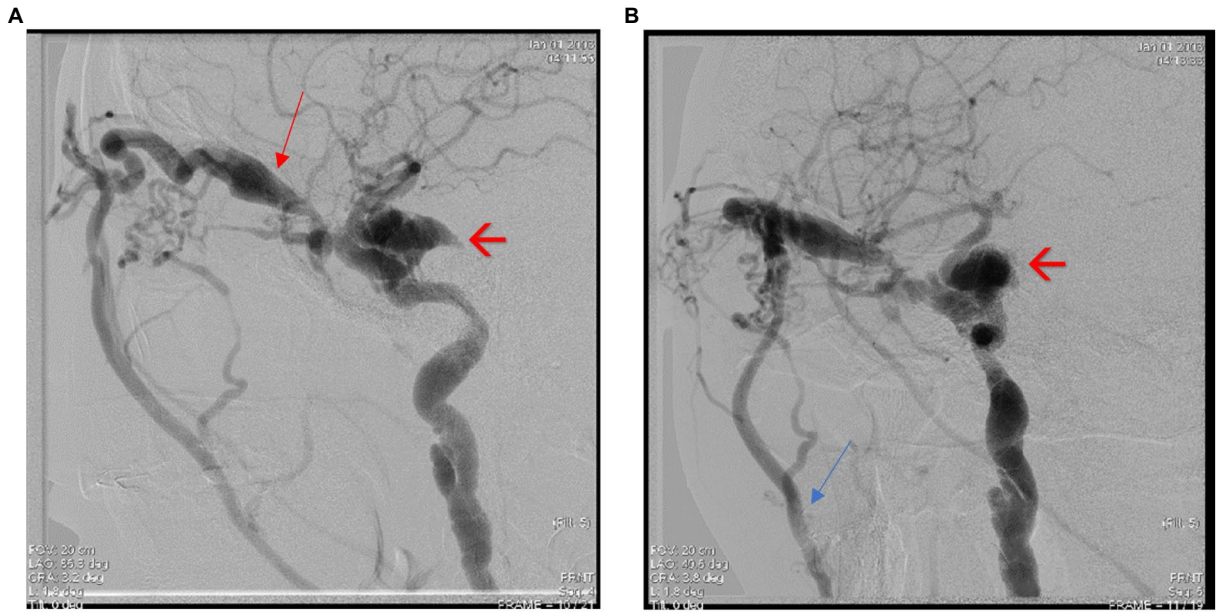

FIGURE 6
(A,B) Cerebral angiography highlighting the direct carotid-cavernous fistula (Type D). Notice the dilated superior ophthalmic vein – see red arrow, and the shunts between ECA and ICA and the facial vein – see blue arrow.

from a traumatic rupture of the wall of the cavernous internal carotid artery or because of the rupture of an aneurysm. Thus, arterial blood with high pressure gains rapid access to the venous system and leads to venous hypertension (6).

Type B: dural fistulas with low flow, fed by the branches of the intra-cavernous internal carotid artery.

Type C: dural fistulas with reduced flow, fed by the cavernous branches of the external carotid.

Type D: low-flow dural fistulas supplied by both internal and external carotid branches (5).

BD types, or indirect fistulas, occur between the meningeal branches of the external or internal carotid artery and the cavernous

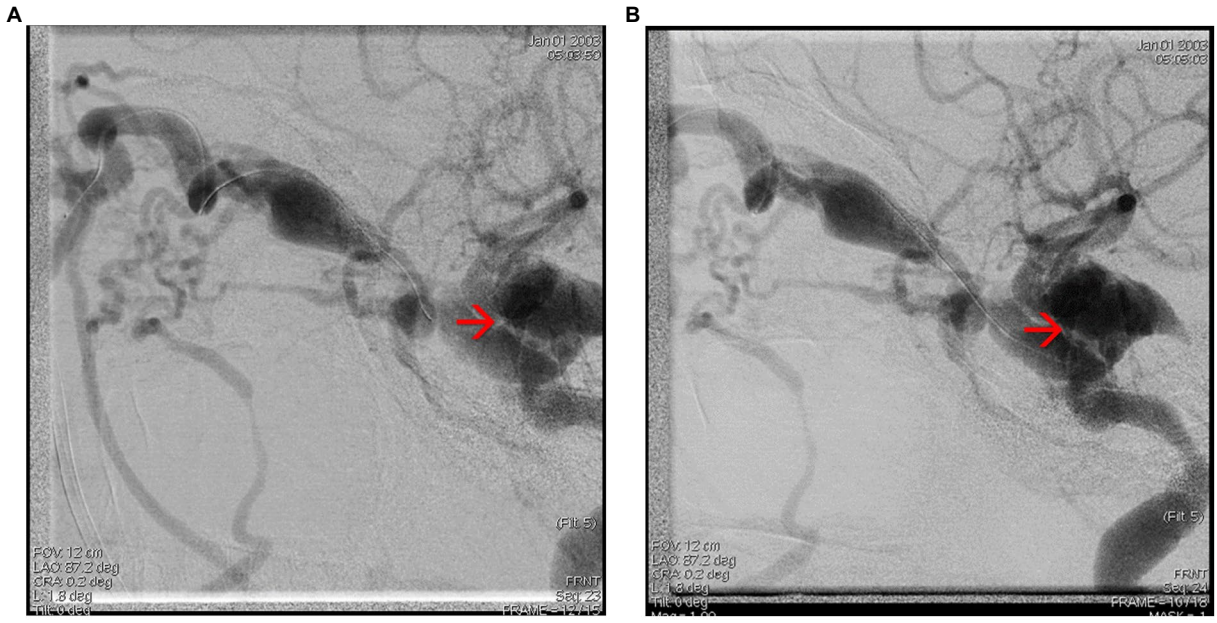

FIGURE 7
(A,B) Cerebral angiography capture showing embolization of the carotid-cavernous fistula through the facial vein – see red arrows.

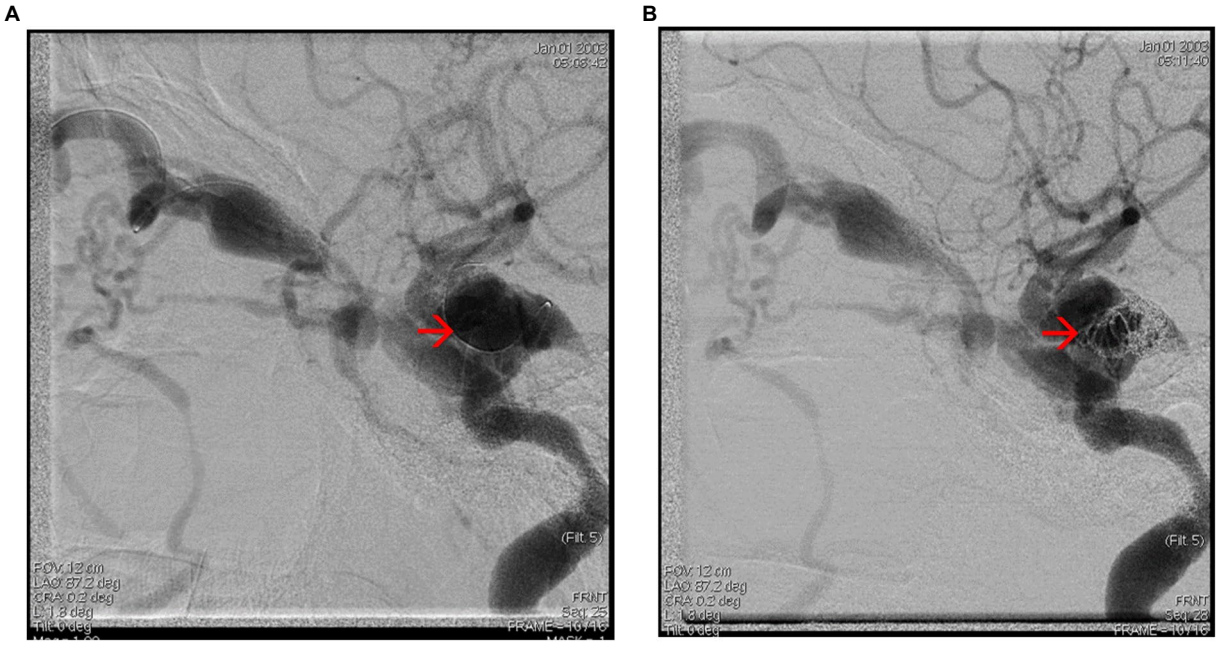

FIGURE 8
(A,B) Cerebral angiography captures showing embolization of the carotid-cavernous fistula – see red arrows.

sinus (7). These are low-flow fistulas. Symptoms are usually milder and may include dilatation of conjunctival and episcleral vessels and proptosis, diplopia (6).

Once the diagnosis of CCF is evoked, it is possible to visualize the carotid-cavernous fistula on dynamic angio-MRI or through an arteriography which remains the reference examination for diagnosis and which makes it possible to plan the therapeutic management (8).

This rare pathology is a therapeutic emergency because it involves a vital and visual prognosis and requires a close collaboration between radiologists, neurosurgeons, and ophthalmologists. Current treatment of CCF is based on interventional neuroradiology (9). Its principle is the occlusion of the fistula by inserting removable intravascular balloons or metal coils, as was the case with our patient, while respecting the patency

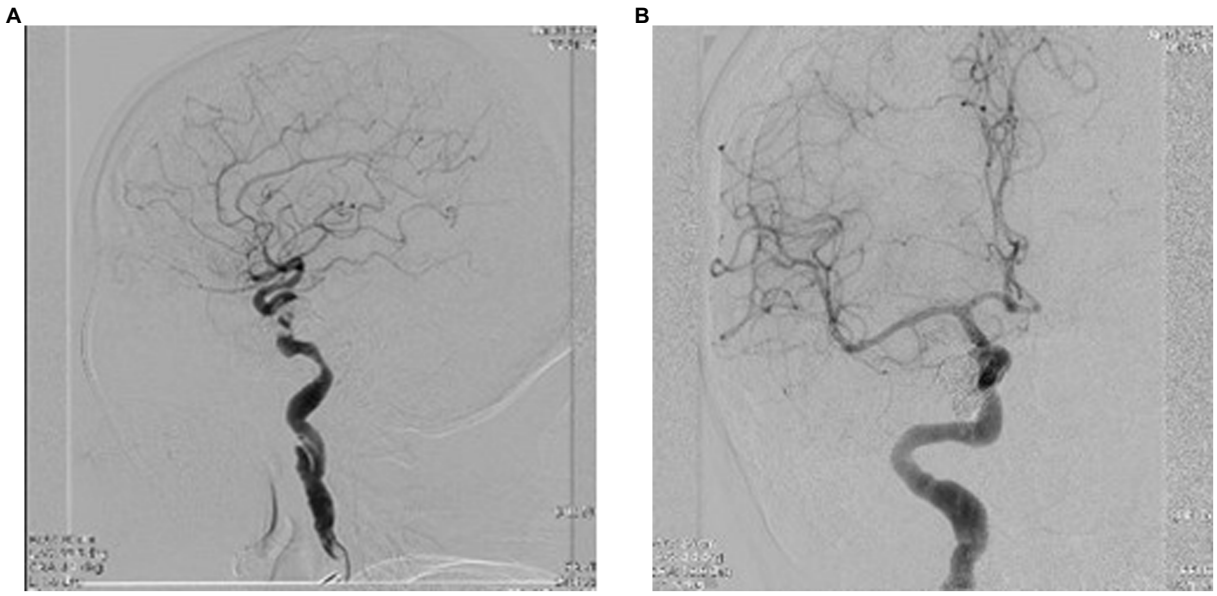

FIGURE 9
(A,B) Final ICA injection showing complete embolization of the carotid cavernous fistula, frontal, and lateral view.

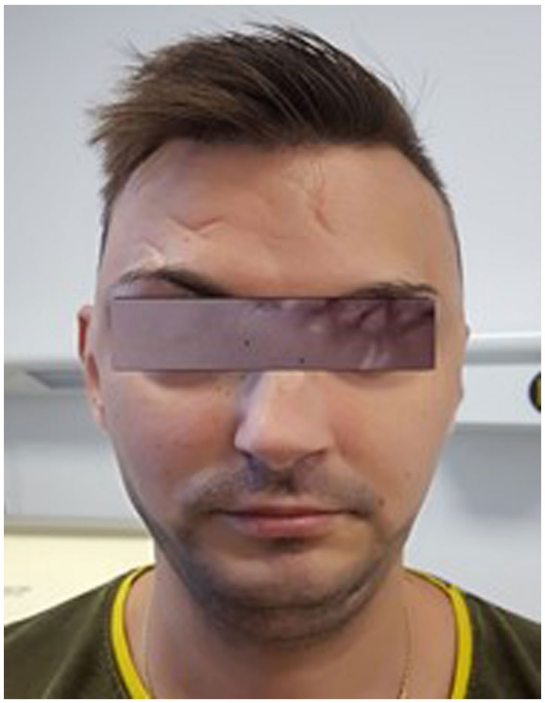

FIGURE 10
Front view of the patient, 1month after the angiographic intervention.

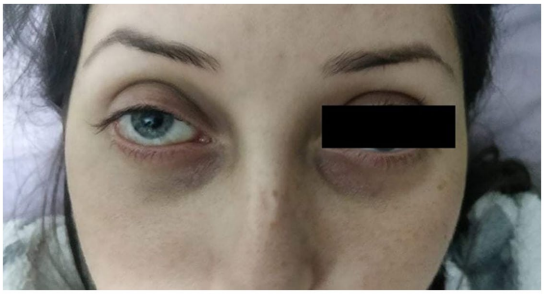

FIGURE 11
Appearance of the 28years old patient presented in the ER with CRAO in the left eye.

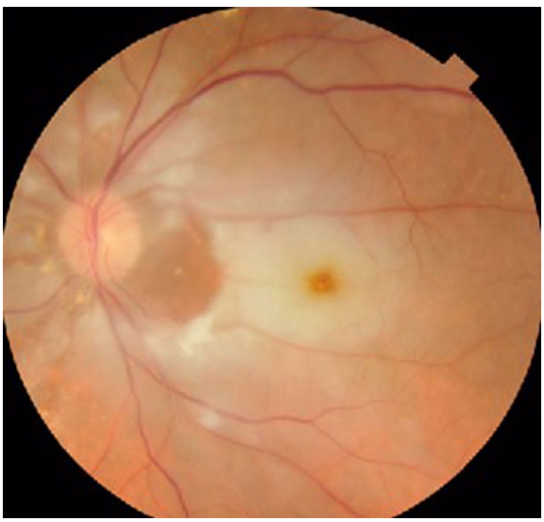

FIGURE 12
Aspect of the left eye fundus showing CRAO with cilioretinal artery sparing.

of the carotid axis. The approach can be done *via* the arterial route (inferior and posterior fistula) or retrograde venous route (superior and anterior fistula) (12). Neurosurgical treatment by arterial ligation retains its place in case of failure of endovascular therapy (5).

In the second patient's case, the presentation diagnosis was CRAO. CRAO is not a frequent diagnosis in a young person; when such an event occurs, it is very important to establish what caused it,

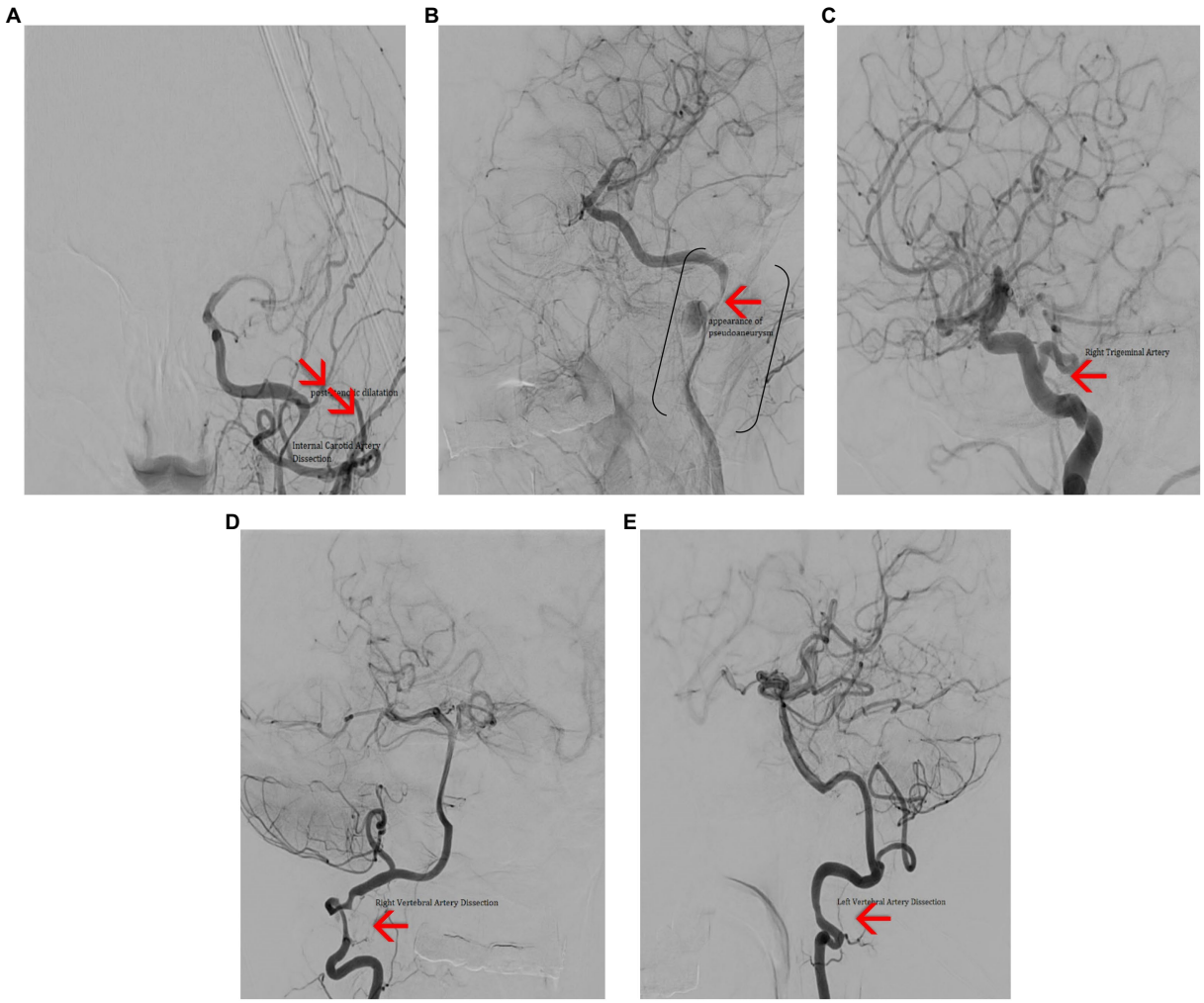

FIGURE 13
Cerebral angiography **(A)** – frontal view showing dissection in the C2–C3 segments of the left ICA, with post stenotic dilatation and poor intracranial filling. **(B)** Left anterior oblique view showing dissection of the C2–C3 segments of the ICA (brackets) and a pseudo-aneurism (red arrow). **(C)** Lateral view showing persistent right trigeminal artery (red arrow). **(D)** Frontal view showing right VA dissection (red arrow). **(E)** Lateral view showing left VA dissection (red arrow).

since it is uncommon at such young age. In this situation, properly investigating the patient and diagnosing the vascular dissections saved patient's life and further led to the underlying cause. At this moment, the patient is aware of his condition, takes proper anti-coagulant medications, avoids any intense physical efforts, and has a good life quality.

Diagnosing vEDS is not an easy task. The genetic tests establish the certainty diagnosis, but sometimes it may become difficult for a patient to acquire these tests, usually for objective reasons. As previously pointed out, diagnosis of vEDS is established in a proband by identification of a heterozygous pathogenic variant in *COL3A1*, or, when molecular genetic testing does not identify a *COL3A1* pathogenic variant, on biochemical analysis of type III procollagen from cultured fibroblasts, or even by histopathological exam of biopsy tissue, which could be difficult but orients the diagnosis in the right track. In the first case, the female patient, the diagnosis was made by genetic analysis, in the latter, the male patient, the strong(er) suspicion was made after the skin biopsy and genetic tests confirmed the suspicion.

Further management of the vEDS cases include proper and prompt treatment of manifestations. Patients with vEDS may face a lot of challenges and unexpected events. As such, affected individuals are instructed to pursue immediate medical attention for sudden, unexplained pain. Patients with vEDS require periodic arterial screening by ultrasound examination, magnetic resonance angiogram, or computed tomography angiogram with and without venous contrast. It is highly recommended blood pressure monitoring on a regular basis, to be able to identify as early as possible any sign of hypertension.

All the manoeuvers that may cause vascular injury to the patient should be carefully considered. Arteriography should be discouraged and used only to identify life-threatening sources of bleeding prior to surgical intervention; routine colonoscopy in the absence of concerning symptoms or a strong family history of colon cancer should be avoided; elective surgery should be considered only if the benefit for the patient is expected to be substantial.

Patients should be instructed to avoid any kind of trauma, including collision sports or weight training with extreme lifting.

When having a female young patient diagnosed with vEDS, it is important to advise the patient regarding pregnancy risk. It is known that affected women have a 5% mortality risk with each pregnancy. Thus, female patients should be informed about the maternal risks and, if pregnant, should receive a careful follow up in a high-risk obstetric program.

Genetic counseling is another issue to be considered when referring to vEDS patients. vEDS is frequently inherited as an autosomal dominant disease, but on some occasions it may have a biallelic inheritance. That means that 50% of affected individuals inherit the *COL3A1* pathogenic variant from an affected parent, and about 50% of affected individuals have a de novo pathogenic variant. Each child of an affected individual has a 50% chance of inheriting the pathogenic variant and developing the disorder. Prenatal testing for a pregnancy at increased risk and preimplantation genetic testing are possible in families in which the pathogenic variant in *COL3A1* has been identified.

Last, but not least, vEDS patients should carry documentation of their genetic diagnosis, such as an emergency letter, MedicAlert®, or vEDS "passport" (4, 12).

Although rare, vEDS is a syndrome that one may encounter in an interdisciplinary emergency hospital (the two cases presented in the ER at 1 year distance); it is important to recognize the signs of such disease, since the right diagnosis, treatment, and prevention of further lesions, may make the difference between life and death. Each patient may have different clinical aspects that require different approaches, so being aware of all sides of this pathology and keeping an open mind as clinicians could make a difference in these cases, regardless of the gravity of their clinical state.

Ethics statement

Written informed consent was obtained from the individual(s) for the publication of any potentially identifiable images or data included in this article No. 15003/13.03.2023.

Author contributions

MC, RP, and DB contributed to the conception and design of the manuscript, the acquisition, analysis, and interpretation of data, the drafting of the work, revision and editing all data to cover all aspects for the proper intellectual content. RI contributed to the acquisition, the analysis and interpretation of data of the study, to the drafting of the work and its critical revision for important intellectual content. GG and AC contributed to the conception and design of the manuscript. MC contributed to the drafting of the work and its critical revision for important intellectual content. MR contributed to the drafting of the work and its critical revision for important intellectual content. MZ, GI, and VV contributed to the drafting of the work. AS contributed to the acquisition and interpretation of data, and final revision of the manuscript. All authors read and approved the final version of the manuscript and agreed to be accountable for all aspects presented in the paper in ensuring that questions related to the accuracy or integrity of any part of the work are appropriately investigated and resolved.

Conflict of interest

The authors declare that the research was conducted in the absence of any commercial or financial relationships that could be construed as a potential conflict of interest.

Publisher's note

References

1. Germain DP. Ehlers-Danlos syndromes. *Ann Dermatol Venereol*. (2017) 144:744–58. doi: 10.1016/j.annder.2017.06.017

2. Engelmann A. Ehlers-Danlos syndrome. *EyeWiki*. (2022). Available at: https://eyewiki.aao.org/Ehlers-Danlos_Syndrome, (Accessed September 2022)

3. Yeowell HN, Pinnell SR. The Ehlers-Danlos syndromes. *Semin Dermatol*. (1993) 12:229–40.

4. Malfait F, Castori M, Francomano CA, Giunta C, Kosho T, Byers PH. The Ehlers–Danlos syndromes. *Nat Rev Dis Prim*. (2020) 6:1–25. doi: 10.1038/s41572-020-0194-9

5. Hamonet C, Amoretti R, Brock I, Fredy D, Baeza-Velasco C, Nourissat G. Hypermobilité, syndrome d'Ehlers-Danlos (SED) et performances sportives. *J Traumatol Sport*. (2016) 33:80–7. doi: 10.1016/j.jts.2016.03.001

6. Bénistan K. Ehlers–Danlos syndromes: classification, treatment and differential diagnosis. *Douleurs*. (2018) 19:161–5. doi: 10.1016/j.douler.2018.07.010

7. Tinkle B, Castori M, Berglund B, Cohen H, Grahame R, Kazkaz H, et al. Hypermobile Ehlers-Danlos syndrome (a.k.a. Ehlers-Danlos syndrome type III and Ehlers-Danlos syndrome hypermobility type): clinical description and natural history. *Am J Med Genet C Semin Med Genet*. (2017) 175:48–69. doi: 10.1002/ajmg.c.31538

8. Symoens S, Syx D, Malfait F, Callewaert B, De Backer J, Vanakker O, et al. Comprehensive molecular analysis demonstrates type V collagen mutations in over 90% of patients with classic EDS and allows to refine diagnostic criteria. *Hum Mutat*. (2012) 33:1485–93. doi: 10.1002/humu.22137

9. Malfait F, Wenstrup RJ, De Paepe A. Clinical and genetic aspects of Ehlers-Danlos syndrome, classic type. *Genet. Med. Off. J. Am. Coll. Med. Genet.* (2010) 12:597–605. doi: 10.1097/GIM.0b013e3181eed412

10. Asanad S, Bayomi M, Brown D, Buzzard J, Lai E, Ling C, et al. Ehlers-Danlos syndromes and their manifestations in the visual system. *Front Med (Lausanne)*. (2022) 9:996458. doi: 10.3389/fmed.2022.996458

11. Byers PH. Vascular Ehlers-Danlos syndrome In: MP Adam, DB Everman and GM Mirzaa et al, editors. *GeneReviews® [Internet]*. Seattle, WA: University of Washington, Seattle (1999).

12. Hwang HS, Song JW, Jang SJ. Vascular Ehlers-Danlos syndrome with distinct histopathologic features. *J Pathol Transl Med*. (2022) 56:167–9. doi: 10.4132/jptm.2021.03.24

13. Pepin MG, Schwarze U, Rice KM, Liu M, Leistritz D, Byers PH. Survival is affected by mutation type and molecular mechanism in vascular Ehlers-Danlos syndrome (EDS type IV). *Genet Med Off J Am Coll Med Genet*. (2014) 16:881–8. doi: 10.1038/gim.2014.72

14. Hatake K, Morimura Y, Kudo R, Kawashima W, Kasuda S, Kuniyasu H. Respiratory complications of Ehlers-Danlos syndrome type IV. *Leg Med (Tokyo)*. (2013) 15:23–7. doi: 10.1016/j.legalmed.2012.07.005.d

15. Frank M, Albuisson J, Ranque B, Golmard L, Mazzella J-M, Bal-Theoleyre L, et al. The type of variants at the COL3A1 gene associates with the phenotype and severity of vascular Ehlers-Danlos syndrome. *Eur J Hum Genet*. (2015) 23:1657–64. doi: 10.1038/ejhg.2015.32

frontiers | Frontiers in Medicine

TYPE Mini Review
PUBLISHED 18 May 2023
DOI 10.3389/fmed.2023.1112996

OPEN ACCESS

EDITED BY
Doina Gherghel,
Aston University, United Kingdom

REVIEWED BY
Xiangmei Kong,
Fudan University, China
Xueqing Wang,
China Medical University, China

*CORRESPONDENCE
Alexandra Benavente-Perez
✉ abenavente@sunyopt.edu

RECEIVED 30 November 2022
ACCEPTED 02 May 2023
PUBLISHED 18 May 2023

CITATION
Benavente-Perez A (2023) Evidence of vascular involvement in myopia: a review.
Front. Med. 10:1112996.
doi: 10.3389/fmed.2023.1112996

Evidence of vascular involvement in myopia: a review

Alexandra Benavente-Perez*

Department of Biological Sciences, State University of New York College of Optometry, New York, NY, United States

The benign public perception of myopia (nearsightedness) as a visual inconvenience masks the severity of its sight-threatening consequences. Myopia is a significant risk factor for posterior pole conditions such as maculopathy, choroidal neovascularization and glaucoma, all of which have a vascular component. These associations strongly suggest that myopic eyes might experience vascular alterations prior to the development of complications. Myopic eyes are out of focus because they are larger in size, which in turn affects their overall structure and function, including those of the vascular beds. By reviewing the vascular changes that characterize myopia, this review aims to provide an understanding of the gross, cellular and molecular alterations identified at the structural and functional levels with the goal to provide an understanding of the latest evidence in the field of experimental and clinical myopia vascular research. From the evidence presented, we hypothesize that the interaction between excessive myopic eye growth and vascular alterations are tipping-points for the development of sight-threatening changes.

KEYWORDS

myopia, vascular, structure, function, evidence

1. Introduction

The blinding consequences of myopia are often overlooked (1–7). Myopic eyes are larger in size, which alters not only their focusing ability, but also their anatomy and physiology (8). All myopes, regardless of degree, are at increased risk of visual impairment (3, 9, 10). This has significant implications due to the predicted global increase in myopia prevalence and the potential public health crisis it represents (8, 11). As we learn about the role that peripheral refraction (12, 13), light intensity (14, 15), time spent outdoors (16, 17), or the on/off pathways play in the development of myopia (18, 19), the controversy is no longer whether myopia is genetic or environmental, but whether we can identify the variables that interact in this multifactorial condition. Currently, there are no preventive markers for myopic degeneration, which is predicted to threaten the eyesight of five billion people by 2050. Myopic eyes have thinner choroids and scleras and, if they progress into high myopia, they can have secondary macular defects in Bruch's membrane along with a complete loss of retinal pigment epithelium, choriocapillaris, and retinal photoreceptors, which confirms the effect of myopia on the ocular vasculature.

The eye's vascular network comprises a complex grid of supply and drainage structures. The retina has a high metabolic rate and oxygen consumption per unit weight in the body (20). In humans, the retina is supplied by the central retinal artery (CRA) - directly in charge of the inner two thirds by diffusion to rods, cones and outer layers - and the choroid, supplying the outer third. The retina is particularly vulnerable to ischemia because of its high oxygen demand and low vascularity of the inner layers (21, 22). The choroid has a high flow rate, low oxygen exchange

and a fenestrated capillary bed. While the choroidal circulation is mainly controlled by sympathetic innervation and thought not to be autoregulated (23), the retinal circulation is ruled by locally controlled autoregulatory mechanisms, including mediators released by endothelial cells (23). A web-like capillary network spreads throughout the retina to provide additional supply (24), connects arteries and veins, and allows direct transport of oxygen, water and lipids to the tissues by diffusion. Capillaries are most abundant in the macula but absent from the fovea (capillary-free zone), which obtains its nutrients from the choriocapillaris (25). The superficial optic nerve head zone is supplied by the central retinal artery, while the short posterior ciliary arteries supply the lamina cribrosa (24, 26).

Until recently, the perfusion features of the human myopic eye had only been studied in human pathological myopia (27, 28) and experimental models of myopia (29–33). This review aims to summarize the latest evidence and controversies in the field of experimental and clinical myopia vascular research by addressing the structural and functional gross, cellular and molecular vascular alterations identified in myopic eyes.

2. Vascular features of the human myopic eye

Most of the techniques used to assess ocular hemodynamics *in vivo* are non-invasive imaging systems that assess retinal blood-flow velocity directly or indirectly (laser doppler velocimetry, LDV) (34), oxygen saturation (oximetry) (35), capillary perfusion (optical coherence tomography angiography, OCTA) (36), microvascular health (adaptive optics scanning light ophthalmoscope fluorescein angiography, AOSLO FA) (37), blood flow (laser speckle contrast imaging LSCI) (38), choroidal pulsatile ocular blood flow (POBF) (39), retrobulbar blood velocity (color doppler imaging, CDI) and retinal blood velocity (laser doppler velocimetry, LDV) (34), amongst others. Until recently, the only method providing a measure of absolute retinal blood flow was the combination of LDV blood velocity with retinal vessel diameter measures from fundus photographs (40, 41). This technique is time-consuming and impractical in the clinic. The recent development of doppler optical coherence tomography (DOCT) provides full quantitative volumetric information of blood flow and vascular/structural anatomy (42). Due to the variety of techniques available, it is imperative to consider the unique technical, anatomical and clinical characteristics of each instrument when interpreting outcomes.

It is hypothesized that the compromised hemodynamics observed in young healthy myopes is an early feature of the decreased ocular blood flow reported in pathological myopia. Such vascular features would increase the susceptibility of the myopic eye for vascular and age-related eye diseases. For instance, impaired retinal blood flow might increase the risk to develop chorioretinal atrophy in high myopia. These changes possibly interact with the known effect of aging on the retinal and choroidal vasculature, including decreased tissue perfusion, deep capillary plexus vessel density, venous, capillary and choroidal blood flow and loss of endothelial cells amongst others (43–50). Below we review experimental and clinical evidence suggesting the existence of vascular alterations in physiological and degenerative myopia (Figure 1).

3. The effect of myopia on the retinal vasculature

The retinal vasculature provides metabolic support to neural and glial cells while minimally interfering with light-sensing mechanisms (51). One of the first pieces of evidence describing an altered retinal circulation in myopic eyes was the discovery of delayed filling times in the arterial, arterial–venous and venous phases of high myopic eyes using fluorescein angiography in the 1970s (52, 53). Subsequently, myopic eyes have been found to exhibit narrower vessel diameters

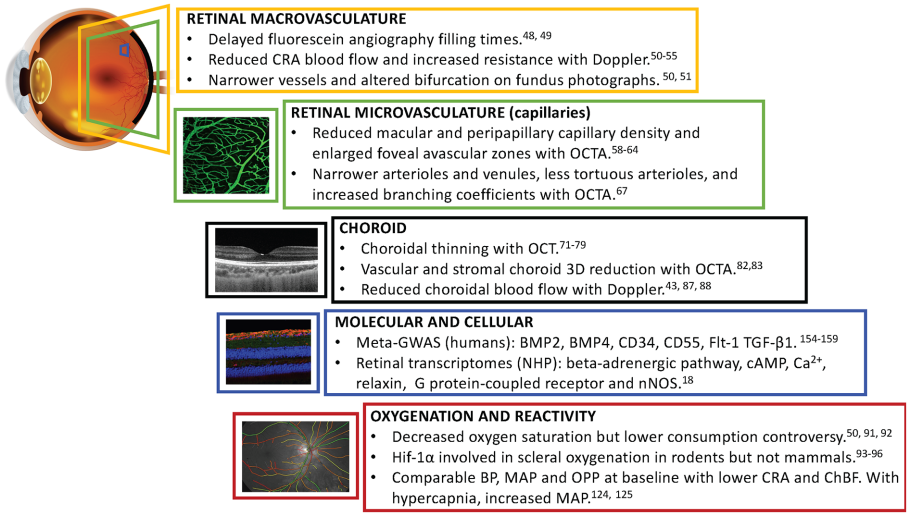

FIGURE 1
Schematic summary describing key vascular findings identified in myopic eyes to date. CRA, central retinal artery; OCTA, optical coherence tomography angiography; BMP2 and BMP4, bone morphogenetic proteins 2 and 4; CD34 and CD55, transmembrane proteins CD34 and CD55; Flt-1, vascular endothelial growth factor receptor-1; TGF-β1, transforming growth factor beta receptor; cAMP, cyclic adenosine monophosphate; Ca^{2+}, calcium; nNOS, neuronal isoform of nitric oxide; Hif-1α, hypoxia-inducible factor 1-alpha; BP, blood pressure; MAP, mean arterial pressure; OPP, ocular perfusion pressure; ChBF, choroidal blood flow.

(54), altered bifurcation (55) and reduced central retinal artery (CRA) diameter and blood flow (56–59). This effect appears localized to the CRA once it branches out of the ophthalmic artery (OA), and therefore affects the inner retina but not structures supplied by the OA such as eyelids, lacrimal gland, conjunctiva, posterior uveal tract or extraocular muscles. In degenerative myopia, both choroidal and retinal blood flow appear reduced, which has been hypothesized to be partly due to increased vascular resistance or adaptive changes the myopic eye experiences to cope with its enlargement (27, 28, 60).

At the retinal microvascular level, healthy myopic eyes show reduced macular superficial, deep and radial peripapillary capillary vessel density, along with increased density inside the disc and enlarged foveal avascular zones (61–67). There is controversy, however, to whether these reductions in capillary densities actually result in altered capillary blood flow (63, 64), since there is evidence that reductions in capillary density are not necessarily associated with choroidal thickness (66) or retinal nerve fiber layer function (68). In terms of anatomy, myopic eyes with greater axial lengths exhibit narrower and less tortuous arterioles and venules, and greater branching coefficients (69). The lower capillary density observed in myopic eyes has been proposed to be a protective mechanism for decreased risk of diabetic retinopathy, but the protective effect has not been confirmed in later studies (70).

The alterations observed in healthy myopic eyes may be precursors of changes seen in pathological myopia and possibly involved in the pathophysiology of myopic degeneration: decreased density of the deep radial capillary plexus and a reduction in OA blood flow that relates to the severity of the retinal degeneration (27).

4. The effect of myopia on the choroidal vasculature

Choroidal thickness is a marker of myopia development first identified in experimental myopia in avian eyes (32, 71). In fact, gross anatomical changes in choroidal appearance from myopic chick eyes led to a series of publications confirming bidirectional choroidal thickness changes in response to defocus (72). These changes have been observed in mammal, non-human and human primate eyes (72–80). In addition, during childhood the choroid thickens with normal eye development, but to a lesser extent in children developing myopia, which confirms the role the choroid may play during myopia development (81, 82). There is also evidence of a three-dimensional reduction in choroidal vascular and stromal components in myopic eyes, mainly in the nasal and subfoveal region (83), although this vascular thinning remains controversial (84). The ocular pulsatile blood flow, thought to be mainly choroidal (85), also appears reduced in myopic eyes (39). This reduction, however, might be an artefact of enlarged eye volume (56, 86), since ocular pulsatile calculations depend on intraocular volume (87). In experimental models of myopia, choroidal flow reductions relate to thickness changes, suggesting an altered choroidal supply and thickness changes that might be responsible for choroidal flow changes or vice versa (88). However, this relationship has not been confirmed in humans - choroidal blood flow might remain constant in eyes with non-pathological myopia (89). There is also evidence that moderate, but not high myopes, exhibit greater ocular perfusion pressure as the choroid thins (90), and choriocapillaris flow deficits are greater in high myopes with no pathology (91). This suggests that early vascular anatomical and functional differences between moderate and high myopes need to be evaluated longitudinally and might represent clinically applicable biomarkers of early pathologic myopia.

A major cause of visual impairment in pathological myopia is loss of photoreceptors, which are nourished by the choroid. Therefore, any choroidal dysfunction can have detrimental consequences in myopic eyes. In fact, eyes with degenerative myopia exhibit lower posterior ciliary artery blood flow, which supply the choroid (27). Choroidal structure measures such as thickness, luminal and stromal area, and choroidal vascularity index are also significantly reduced in pathological myopia. In addition, thickness and vascularity index appear associated with degeneration severity and visual acuity, highlighting the role the choroid represents for degenerative myopia (92, 93).

5. Retinal oxygen saturation in myopia

The retina is characterized by its high metabolic rate and considered one of the tissues with the largest oxygen consumption per unit weight in the body (20). Retinal oximetry performed using commercially available systems like the Oxymap has identified a lower arterio/venous oxygen saturation ratio in myopic eyes that points towards a possibly lower retinal oxygen consumption (94). However, a significantly larger cross-sectional study with 1,461 participants found that when age, gender, body mass index (BMI), intraocular pressure (IOP) and axial length (AL) were corrected for, longer and more myopic eyes did not exhibited a lower, but a greater oxygen and arterio-venous ratio saturation (95). These findings suggest that as eyes grow larger, they might be able to maintain an adequate oxygenation profile for its growing size, until they reach a degenerative state and the oxygenation profile is affected (96). There is also work suggesting that myopic choroidal thinning and reduced choroidal blood flow might affect scleral oxygenation (97). If this is correct, manipulating hypoxia signaling pathways might be a myopia control alternative in the future (98). Recent evidence suggests that, in fact, anti-hypoxia drugs reducing Hif-1α levels can slow axial elongation (99), which points towards a possible relationship between myopia, hypoxia and Hif-1α. This relationship has also been described in genetic analyses revealing a moderate involvement of the Hif-1α signaling pathway in myopia (98, 100), However, tree shrews induced with myopia do not exhibit changes in scleral Hif-1α mRNA expression (101, 102), and guinea pigs with induced myopia show reduced scleral Hif-1α mRNA, highlighting the need for additional work in this field (102).

6. Vascular reactivity in myopia

The presence of structural and hemodynamic changes in the retinal vasculature in myopia suggests that myopic eyes might be suffering from an abnormal vascular function before degenerative changes occur (1, 54, 103–108). However, assessing ocular blood flow under normal conditions is not sufficient to detect vascular dysfunction. Retinal vascular function is assessed using provocation tests, indispensable to evaluate retinal reactivity and autoregulation (109–115). Autoregulation is the inherent local mechanism that ensures sufficient and stable blood flow under changing conditions to preserve adequate function of the surrounding tissues (116). Vascular regulation or vasoreactivity can be assessed by quantifying blood flow or vessel diameter changes that occur in response to flicker light (metabolic autoregulation), variations in the concentration of

breathing oxygen (metabolic), or changes in systemic and intraocular pressure (shear-dependent and myogenic) (113, 117–120). Both the ocular and cerebral circulation exhibit an autoregulatory capacity (110, 117, 121–124). Three studies have evaluated the vascular reactivity profile of myopic eyes to date, and they used hypercapnia (increased pCO_2) and hyperoxia (increased $p0_2$) as provocation tests to assess the response from the retinal vasculature under stress conditions (125–127). Under room-air conditions prior to the provocation test, myopic and non-myopic eyes exhibited comparable systemic and ocular perfusion pressures –myopes exhibiting lower central retinal artery and choroidal blood flow. After inducing hypercapnia, myopic but not emmetropic eyes showed an increase in mean arterial pressure, along with a greater choroidal blood flow response, suggesting that myopes had a significantly lower resting choroidal flow that was highly responsive to CO_2 (125, 126). These results insinuate an altered autoregulation ability in myopic eyes that, due to the increase mean arterial pressure observed, may lie in an autonomic dysregulation. Interestingly, there is evidence that eyes with pathological myopia eyes have comparable retinal vascular reactivity, suggesting that the retinal oxygen consumption, but not the choroidal, is altered in high-myopic eyes (128).

7. Molecular and cellular evidence of vascular changes in myopia

In order to understand the nature of the architectural and functional vascular described in myopia, it is important to comprehend the molecular and cellular changes taking place. The most extensive genetic myopia pathway analyses to date are clinical studies (meta-GWAS from 23andMe and the Consortium of Refractive Error And Myopia, CREAM) (129–134) and studies in common marmosets (*Callithrix jacchus*), a well-established non-human primate model of myopia (18).

Genetic meta-GWAS studies using human specimens have identified several signaling pathways involved in myopia, many of which were previously known, such as the extracellular matrix and ion channel pathways, while others were new, like those involved in angiogenesis. The following genes have been recently identified in meta-GWAS studies and found to have a role in vascular homeostasis: BMP2 and BMP4, CD34, CD55, Flt-1 and TGF-β receptor 1. BMP2 and BMP4 bone morphogenetic proteins (BMPs), named for their bone and cartilage formation ability (135, 136), are increasingly recognized as multifunctional regulators of angiogenesis. BMP2 has a pathological role in the development of vascular inflammation (137, 138), and induces retinal endothelial cell barrier dysfunction in diabetic macular edema and pathological retinal neovascularization (135). Over-expression of BMP4 inhibits experimental choroidal neovascularization by modulating VEGF and MMP-9 (139). CD34 is a transmembrane protein expressed in endothelial cells that promotes the formation of invasive vessels during neovascularization (140). The membrane-bound complement regulator CD55 is highly expressed in the retinal vascular endothelium (141), and significantly decreased in hyperoxic retinas (142). VEGF receptor–1 (also known as Flt-1) is needed for adequate blood vessel patterning on retinal astrocytes and can modulate VEGF-A activation of endothelial cells (143, 144). Flt-1 has unique and important roles in coordinating endothelial sprouting (145, 146), blood vessel anastomosis (147), and genetic loss of *flt-1* leading to vascular overgrowth and reduced network complexity (148). TGF-β receptor 1 inhibits and deep vascular plexus formation (149, 150), and its endothelial loss leads to aberrant contractile pericyte differentiation and hemorrhagic vascular malformations, and is essential for maintaining the integrity of mature vessels (151).

The analysis of retinal transcriptomes in marmosets induced with myopia has identified major molecular pathways activated during myopic eye growth (18). Some of the key pathways described are involved in vascular signaling and include the beta-adrenergic pathway, cyclic adenosine monophosphate (cAMP), Ca^{2+}, relaxin (152), G protein-coupled receptor and nNOS. Beta-adrenergic signaling, for instance, is involved in hypoxia (153); there is a 90% increase in noradrenaline levels during hypoxia (154, 155), and beta-adrenorceptor activation is followed by an upregulation of hypoxia-inducible factor-1α (HIF-1α) and vascular endothelial growth factor (VEGF), both involved in neovascularization (156, 157). The cAMP pathway regulates neuronal, vascular, and inflammatory components of diabetic retinopathy (158). Calcium signaling is involved in capillary - but not arteriole - retinal blood flow as seen by the active dilation observed following astroglial Ca^{2+} signaling (159, 160). Relaxin, a peptide found at high concentrations during pregnancy, is found in endothelial and smooth muscle cells in arteries and veins, supporting its vasodilating role (161–163). G protein-coupled receptors 91 and 81 (GPR91and GPR81), localized in ganglion cells and Muller cells respectively, are involved in the pathogenesis of diabetic retinopathy (DR) and hypoxic retinal diseases such as retinopathy of prematurity (ROP), inner vascular network development and restoration of the vasculature in response to injury (152, 164). The neuronal isoform of nitric oxide (nNOS) is present in the vascular endothelium and contributes to the maintenance of homeostasis in the cardiovascular system. NO contributes to both retinal and choroidal neovascularization (165).

In terms of vascular cellular anatomy, the neurovascular interplay between neuronal, vascular, and glial cells, which is crucial for retinal structural and nutritional support and ion and neurotransmitter homeostasis, appears to be affected by myopia. Marmosets with induced myopia show a lower astrocyte density, increased GFAP-immunopositive staining, lower peripheral capillary branching, and increased numbers of string vessels compared to controls. These changes suggest an activation and reorganization of the astrocyte and vascular templates during myopia development and progression (166). Whether or not these adaptations are beneficial or harmful to the developing retina remains to be investigated.

8. Myopia-associated conditions showing vascular alterations

Myopic macular degeneration, glaucoma, choroidal neovascularization, retinal detachment, posterior staphyloma and cataract amongst the most prevalent myopia complications (167). In this section we review the vascular features of these myopia-associated conditions to help understand the vascular nature of myopia.

8.1. Myopic macular degeneration

Myopic maculopathy is the most common cause of vision loss in myopic eyes (5, 168), but its etiology remains unclear. The distinctive elongation and deformation of the myopic eye, along with its characteristic neovascularization, suggest that vascular pathways likely contribute to the degenerative process. Evidence for a vascular etiology

of myopic maculopathy include a significant choroid thinning, enlarged foveal avascular zone, smaller choriocapillaris flow area, vascular dropout, lower fractal dimension, and a more profound decrease in deep but not superficial retinal capillary plexus density, suggesting that microvascular alterations appear crucial for myopic maculopathy (169–171). In addition, choroidal watershed zones, which are areas situated at the edge of end-arteries usually exhibiting a delayed choroidal filling, have been proposed to play a vascular role in the etiology of myopic maculopathy (172).

8.2. Glaucoma

Glaucoma is a complex neuropathy that preferentially affects the ganglion cell complex (GCC) (173) and exhibits features of vascular etiology and dysfunction (174). The relationship between myopia and glaucoma has been confirmed by several large population-based studies (175–180). Yet, the nature of the myopia-glaucoma relationship remains unknown. Low ocular perfusion has been identified as a risk factor for glaucoma progression independent of intraocular pressure (181–183). Both glaucomatous and myopic eyes show parallel vascular changes: retinal microvasculature attenuation (184), decreased capillary density (63, 66, 184–186), and reduced retinal and ONH blood flow and vascular dysregulation (56, 57, 65, 68, 89, 91, 187–189). In fact, the longer the axial eye length and the thinner the ocular wall in glaucoma patients, the greater the retinal microcirculation reduction (190). In addition, when the vascular features of glaucomatous patients with and without myopia were compared, myopic glaucomatous eyes exhibited greater vascular changes than non-myopic glaucomatous eyes: larger reductions in choroidal blood flow and velocity (191), lower macular and peripapillary capillary density (184, 192), and impaired peripapillary vasoreactivity (127). Therefore, it has been hypothesized that the relationship between myopia and glaucoma might partly be vascular in nature, specifically microvascular, and may be present before the glaucomatous degeneration is evident. In addition, the study of vascular reactivity in glaucomatous patients with and without high myopia has confirmed that the retinal vasoreactivity of the peripapillary capillaries is compromised in glaucomatous eyes with high myopia (127).

8.3. Choroidal neovascularization

Choroidal neovascularization (CNV) is characterized by an atypical choroidal vasculature growth into the retinal pigment epithelium potentially leading to fluid and blood accumulation in the macula (50). Eyes with lower foveolar choroidal blood volume and flow have been identified to be at a higher risk of developing CNV. This reduced choroidal blood supply appears greater than any changes observed in eyes without CNV, suggesting that alterations in the foveal choroidal circulation might precede be part of CNV etiology (193). In addition, the choroidal thinning and capillary density reduction observed in degenerative pathological myopia is believed to trigger RPE and glial cells hypoxia, resulting in an upregulation of VEGF expression (194).

8.4. Retinal detachment

The most prevalent form of neurosensory retina separation from the retinal pigment epithelium (RPE) is the rhegmatogenous retinal detachment. This type of detachment disrupts the retinal vasculature leading to smaller vascular diameters, tortuosity, and vascular density (195). Capillary dilatation, hyperpermeability and fluorescein leakage have also been observed with fluorescein angiography on the detached retina, and have been proposed to originate from tissue hypoxia (196, 197).

8.5. Posterior staphyloma

Peripapillary posterior staphyloma (PPS) is one of six types of posterior staphylomas identified in degenerative myopia (198). Eyes with PPS have an increased macular vessel density in the deep plexus, reduced macular choriocapillaris and radial peripapillary capillary density, and thinner choroids (199). In addition, a retrospective study also identified reduced choriocapillaris flow and thinner subfoveal choroidal thickness, confirming that eyes with posterior staphyloma have thinner choroids and lower perfusion (200).

8.6. Cataract

A relationship between lens opacity and hypertension was identified in the initial cross-sectional phase of the Beaver Dam Eye Study (201). However, this relationship was not confirmed once the longitudinal 5-year Beaver Dam Eye Study was completed (202). There is, however, evidence of lower ocular blood velocity in cataract patients that requires further evaluation to understand the nature of the changes (203).

9. Conclusion

Adequate blood flow is fundamental for tissue homeostasis (204). In view of the findings described in the literature and discussed in this review, studying the haemodynamics and vascular autoregulation features of healthy myopic eyes may be crucial to identify early markers of associated degeneration and help develop novel vascular interventions to preserve the health of myopic eyes.

Author contributions

AB-P conceived, designed, wrote and reviewed the manuscript.

Acknowledgments

The author would like to acknowledge William Bourassa for his invaluable assistance with graphics and manuscript editing.

Conflict of interest

The author declares that the research was conducted in the absence of any commercial or financial relationships that could be construed as a potential conflict of interest.

Publisher's note

References

1. Ohno-Matsui K, Akiba M, Ishibashi T, Moriyama M. Observations of vascular structures within and posterior to sclera in eyes with pathologic myopia by swept-source optical coherence tomography. *Invest Ophthalmol Vis Sci*. (2012) 53:7290–8. doi: 10.1167/iovs.12-10371

2. Vongphanit J, Mitchell P, Wang JJ. Prevalence and progression of myopic retinopathy in an older population. *Ophthalmology*. (2002) 109:704–11. doi: 10.1016/S0161-6420(01)01024-7

3. Saw SM. How blinding is pathological myopia? *Br J Ophthalmol*. (2006) 90:525–6. doi: 10.1136/bjo.2005.087999

4. Ruiz-Moreno JM, Arias L, Montero JA, Carneiro A, Silva R. Intravitreal anti-Vegf therapy for choroidal neovascularisation secondary to pathological myopia: 4-year outcome. *Br J Ophthalmol*. (2013) 97:1447–50. doi: 10.1136/bjophthalmol-2012-302973

5. Neelam K, Cheung CM, Ohno-Matsui K, Lai TY, Wong TY. Choroidal neovascularization in pathological myopia. *Prog Retin Eye Res*. (2012) 31:495–525. doi: 10.1016/j.preteyeres.2012.04.001

6. Mutti DO, Semina E, Marazita M, Cooper M, Murray JC, Zadnik K. Genetic loci for pathological myopia are not associated with juvenile myopia. *Am J Med Genet*. (2002) 112:355–60. doi: 10.1002/ajmg.10683

7. Morgan IG, Ohno-Matsui K, Saw SM. Myopia. *Lancet*. (2012) 379:1739–48. doi: 10.1016/s0140-6736(12)60272-4

8. Ohno-Matsui K, Kawasaki R, Jonas JB, Cheung CMG, Saw S-M, Verhoeven VJM, et al. International photographic classification and grading system for myopic maculopathy. *Am J Ophthalmol*. (2015) 159:877–83.e7. doi: 10.1016/j.ajo.2015.01.022

9. Curtin BJ. *The Myopias: Basic Science and Clinical Management*. Philadelphia: Harper and Row (1985).

10. Vutipongsatorn K, Yokoi T, Ohno-Matsui K. Current and emerging pharmaceutical interventions for myopia. *Br J Ophthalmol*. (2019) 103:1539. doi: 10.1136/bjophthalmol-2018-313798

11. Holden BA, Fricke TR, Wilson DA, Jong M, Naidoo KS, Sankaridurg P, et al. Global prevalence of myopia and high myopia and temporal trends from 2000 through 2050. *Ophthalmology*. (2016) 123:1036–42. doi: 10.1016/j.ophtha.2016.01.006

12. Smith EL III. Prentice award lecture 2010: a case for peripheral optical treatment strategies for myopia. *Optom Vis Sci*. (2011) 88:1029–44. doi: 10.1097/OPX.0b013e3182279cfa

13. Faria-Ribeiro M, Queirós A, Lopes-Ferreira D, Jorge J, González-Méijome JM. Peripheral refraction and retinal contour in stable and progressive myopia. *Optom Vis Sci*. (2013) 90:9–15. doi: 10.1097/OPX.0b013e318278153c

14. Ashby RS, Schaeffel F. The effect of ambient illuminance on the development of deprivation myopia in chicks. *Invest Ophthalmol Vis Sci*. (2009) 50:5348–54. doi: 10.1167/iovs.09-3419

15. Smith EL III, Hung LF, Huang J. Effects of high ambient lighting on the development of form-deprivation myopia in infant Rhesus monkeys. *Invest Ophthalmol Vis Sci*. (2012) 53:421–8. doi: 10.1167/iovs.11-8652

16. Rose KA, Morgan IG, Ip J, Kifley A, Huynh S, Smith W, et al. Outdoor activity reduces the prevalence of myopia in children. *Ophthalmol*. (2008) 115:1279–85. doi: 10.1016/j.ophtha.2007.12.019

17. Dirani M, Tong L, Gazzard G, Zhang X, Chia A, Young TL, et al. Outdoor activity and myopia in Singapore teenage children. *Br J Ophthalmol*. (2009) 93:997–1000. doi: 10.1136/bjo.2008.150979

18. Tkatchenko TV, Troilo D, Benavente-Perez A, Tkatchenko AV. Gene expression in response to optical defocus of opposite signs reveals bidirectional mechanism of visually guided eye growth. *PLoS Biol*. (2018) 16:e2006021. doi: 10.1371/journal.pbio.2006021

19. Chakraborty R, Park HN, Hanif AM, Sidhu CS, Iuvone PM, Pardue MT. On pathway mutations increase susceptibility to form-deprivation myopia. *Exp Eye Res*. (2015) 137:79–83. doi: 10.1016/j.exer.2015.06.009

20. Forrester JV, Dick AD, McMenamin PG, Roberts F, Pearlman E. *The Eye: Basic Sciences in Practice*. Edinburgh, United Kingdom: Elsevier (2001).

21. Yu DY, Cringle SJ. Oxygen distribution and consumption within the retina in vascularised and avascular retinas and in animal models of retinal disease. *Prog Retin Eye Res*. (2001) 20:175–208. doi: 10.1016/S1350-9462(00)00027-6

22. Hayreh SS In: D Dartt, editor. *Encyclopedia of the Eye*. United States: Academic Press (2010). 43:1–8.

23. Delaey C, Van de Voorde J. Regulatory mechanisms in the retinal and choroidal circulation. *Ophthalmic Res*. (2000) 32:249–56. doi: 10.1159/000055622

24. Flammer J, Orgüla S, Costab V, Orzalesic N, Krieglsteind G, Metzner Serrae K, et al. The impact of ocular blood flow in glaucoma. *Prog Retin Eye Res*. (2002) 21:359–93. doi: 10.1016/S1350-9462(02)00008-3

25. Bron A, Tripathi R, Tripathi B. *Wolff's Anatomy of the Eye and Orbit. 8th* ed. London: Chapman & Hall Medical (1997).

26. Hayreh SS. Blood flow in the optic nerve head and factors that may influence it. *Prog Retin Eye Res*. (2001) 20:595–624. doi: 10.1016/S1350-9462(01)00005-2

27. Akyol N, Kukner A, Ozdemir T, Esmerligil S. Choroidal and retinal blood flow changes in degenerative myopia. *Can J Ophthalmol*. (1996) 31:113–9.

28. Dimitrova G, Tamaki Y, Kato S, Nagahara M. Retrobulbar circulation in myopic patients with or without myopic choroidal neovascularisation. *Br J Ophthalmol*. (2002) 86:771–3. doi: 10.1136/bjo.86.7.771

29. Wu H, Seet B, Yap E, Saw S, Lim T, Chia K. Does education explain ethnic differences in myopia prevalence? A population-based study of Young adult males in Singapore. *Optom Vis Sci*. (2001) 78:234–9. doi: 10.1097/00006324-200104000-00012

30. Fitzgerald M, Wildsoe C, Anton R. Temporal relationship of choroidal blood flow and thickness changes during recovery from form deprivation myopia in chicks. *Exp Eye Res*. (2001) 74:561–70. doi: 10.1006/exer.2002.1142

31. Fitzgerald MEC, Tolley E, Jackson B, Zagvazdin YS, Cuthbertson SL, Hodos W, et al. Anatomical and functional evidence for progressive age-related decline in parasympathetic control of choroidal blood flow in pigeons. *Exp Eye Res*. (2005) 81:478–91. doi: 10.1016/j.exer.2005.03.008

32. Wildsoet C, Wallman J. Choroidal and scleral mechanisms of compensation for spectacle lenses in chicks. *Vis Res*. (1995) 35:1175–94. doi: 10.1016/0042-6989(94)00233-C

33. Jin N, Stjernschantz J. Regional blood flow in the myopic Chick eye during and after form deprivation: a study with radioactively-labelled microspheres. *Exp Eye Res*. (2000) 71:233–8. doi: 10.1006/exer.2000.0871

34. Riva C, Ross B, Benedek GB. Laser Doppler measurements of blood flow in capillary tubes and retinal arteries. *Investig Ophthalmol*. (1972) 11:936–44.

35. Olafsdottir OB, Eliasdottir TS, Kristjansdottir JV, Hardarson SH, Stefánsson E. Retinal vessel oxygen saturation during 100% oxygen breathing in healthy individuals. *PLoS One*. (2015) 10:e0128780. doi: 10.1371/journal.pone.0128780

36. de Carlo TE, Romano A, Waheed NK, Duker JS. A review of optical coherence tomography angiography (Octa). *Int J Retina Vitreous*. (2015) 1:5. doi: 10.1186/s40942-015-0005-8

37. Mo S, Krawitz B, Efstathiadis E, Geyman L, Weitz R, Chui TY, et al. Imaging foveal microvasculature: optical coherence tomography angiography versus adaptive optics scanning light ophthalmoscope fluorescein angiography. *Invest Ophthalmol Vis Sci*. (2016) 57:130–40. doi: 10.1167/iovs.15-18932

38. Senarathna J, Rege A, Li N, Thakor NV. Laser speckle contrast imaging: theory, instrumentation and applications. *IEEE Rev Biomed Eng*. (2013) 6:99–110. doi: 10.1109/RBME.2013.2243140

39. Zion IB, Harris A, Siesky B, Shulman S, McCranor L, Garzozi HJ. Pulsatile ocular blood flow: relationship with flow velocities in vessels supplying the retina and choroid. *Br J Ophthalmol*. (2007) 91:882–4. doi: 10.1136/bjo.2006.108340

40. Garhofer G, Werkmeister R, Dragostinoff N, Schmetterer L. Retinal blood flow in healthy Young subjects. *Invest Ophthalmol Vis Sci*. (2012) 53:698–703. doi: 10.1167/iovs.11-8624

41. Riva CE, Grunwald JE, Sinclair SH, Petrig BL. Blood velocity and volumetric flow rate in human retinal vessels. *Invest Ophthalmol Vis Sci*. (1985) 26:1124–32.

42. Leitgeb RA, Werkmeister RM, Blatter C, Schmetterer L. Doppler optical coherence tomography. *Prog Retin Eye Res*. (2014) 41:26–43. doi: 10.1016/j.preteyeres.2014.03.004

43. Emeterio Nateras OS, Harrison JM, Muir ER, Zhang Y, Peng Q, Chalfin S, et al. Choroidal blood flow decreases with age: an Mri study. *Curr Eye Res*. (2014) 39:1059–67. doi: 10.3109/02713683.2014.892997

44. Burgansky-Eliash Z, Lowenstein A, Neuderfer M, Kesler A, Barash H, Nelson DA, et al. The correlation between retinal blood flow velocity measured by the retinal function imager and various physiological parameters. *Ophthalmic Surg Lasers Imaging Retina*. (2013) 44:51–8. doi: 10.3928/23258160-20121221-13

45. Yu J, Jiang C, Wang X, Zhu L, Gu R, Xu H, et al. Macular perfusion in healthy Chinese: an optical coherence tomography angiogram study. *Invest Ophthalmol Vis Sci*. (2015) 56:3212–7. doi: 10.1167/iovs.14-16270

46. Yu J, Gu R, Zong Y, Xu H, Wang X, Sun X, et al. Relationship between retinal perfusion and retinal thickness in healthy subjects: an optical coherence tomography angiography study. *Invest Ophthalmol Vis Sci*. (2016) 57:204–10. doi: 10.1167/iovs.15-18630

47. Lin Y, Jiang H, Liu Y, Rosa Gameiro G, Gregori G, Dong C, et al. Age-related alterations in retinal tissue perfusion and volumetric vessel density. *Invest Ophthalmol Vis Sci*. (2019) 60:685–93. doi: 10.1167/iovs.18-25864

48. Wei Y, Jiang H, Shi Y, Qu D, Gregori G, Zheng F, et al. Age-related alterations in the retinal microvasculature, microcirculation, and microstructure. *Invest Ophthalmol Vis Sci*. (2017) 58:3804–17. doi: 10.1167/iovs.17-21460

49. Fitzgerald MEC, Tolley E, Frase S, Zagvazdin Y, Miller RF, Hodos W, et al. Functional and morphological assessment of age-related changes in the choroid and outer retina in pigeons. *Vis Neurosci*. (2001) 18:299–317. doi: 10.1017/S0952523801182143

50. Chirco KR, Sohn EH, Stone EM, Tucker BA, Mullins RF. Structural and molecular changes in the aging choroid: implications for age-related macular degeneration. *Eye (Lond)*. (2017) 31:10–25. doi: 10.1038/eye.2016.216

51. Kur J, Newman EA, Chan-Ling T. Cellular and physiological mechanisms underlying blood flow regulation in the retina and choroid in health and disease. *Prog Retin Eye Res*. (2012) 31:377–406. doi: 10.1016/j.preteyeres.2012.04.004

52. Avetisov ES, Savitskaya NF. Some features of ocular microcirculation in myopia. *Ann Ophthalmol*. (1977) 9:1261–4.

53. Bal'zhanova AB. Fluorescence angiography in assessing choroidal circulation in highly progressive myopia. *Vestn oftalmol*. (1978) 1:25–30.

54. Lim LS, Cheung CY, Lin X, Mitchell P, Wong TY, Mei-Saw S. Influence of refractive error and axial length on retinal vessel geometric characteristic. *Invest Ophthalmol Vis Sci*. (2011) 52:669–78s. doi: 10.1167/iovs.10-6184

55. Sun C, Chen T, Cong J, Wu X, Wang J, Yuan Y. Changes in retinal vascular bifurcation in eyes with myopia. *BMC Ophthalmol*. (2022) 22:408. doi: 10.1186/s12886-022-02629-y

56. Benavente-Perez A, Hosking SL, Logan NS, Broadway DC. Ocular blood flow measurements in healthy human myopic eyes. *Graefes Arch Clin Exp Ophthalmol*. (2010) 248:1587–94. doi: 10.1007/s00417-010-1407-9

57. Shimada N, Ohno-Matsui K, Harino S, Yoshida T, Yasuzumi K, Kojima A, et al. Reduction of retinal blood flow in high myopia. *Graefes Arch Clin Exp Ophthalmol*. (2004) 242:284–8. doi: 10.1007/s00417-003-0836-0

58. Karczewicz D, Modrzejewska M. Blood flow in eye arteries assessed by Doppler ultrasound in patients with myopia. *Klin Ocz*. (2004) 106:211–3.

59. Mamikonian VR, Shmeleva-Demir OA, Kharlap SI, Andzhelova DV, Kazarian EE, Makashova NV, et al. Hemodynamic changes in myopia of different degrees. *Vestn oftalmol*. (2013) 129:24–7.

60. Mo J, Duan A, Chan S, Wang X, Wei W. Vascular flow density in pathological myopia: an optical coherence tomography angiography study. *BMJ Open*. (2017) 7:e013571. doi: 10.1136/bmjopen-2016-013571

61. Yang Y, Wang J, Jiang H, Yang X, Feng L, Hu L, et al. Retinal microvasculature alteration in high myopia. *Invest Ophthalmol Vis Sci*. (2016) 57:6020–30. doi: 10.1167/iovs.16-19542

62. Li Y, Miara H, Ouyang P, Jiang B. The comparison of regional Rnfl and fundus vasculature by Octa in Chinese myopia population. *J Ophthalmol*. (2018) 2018:10. doi: 10.1155/2018/3490962

63. Su L, Ji YS, Tong N, Sarraf D, He X, Sun X, et al. Quantitative assessment of the retinal microvasculature and Choriocapillaris in myopic patients using swept-source optical coherence tomography angiography. *Graefes Arch Clin Exp Ophthalmol*. (2020) 258:1173–80. doi: 10.1007/s00417-020-04639-2

64. Min CH, Al-Qattan HM, Lee JY, Kim J-G, Yoon YH, Kim YJ. Macular microvasculature in high myopia without pathologic changes: an optical coherence tomography angiography study. *Korean J Ophthalmol*. (2020) 34:106–12. doi: 10.3341/kjo.2019.0113

65. Wang X, Kong X, Jiang C, Li M, Yu J, Sun X. Is the Peripapillary retinal perfusion related to myopia in healthy eyes? A prospective comparative study. *BMJ Open*. (2016) 6:e010791. doi: 10.1136/bmjopen-2015-010791

66. Al-Sheikh M, Phasukkijwatana N, Dolz-Marco R, Rahimi M, Iafe NA, Freund KB, et al. Quantitative Oct angiography of the retinal microvasculature and the Choriocapillaris in myopic eyes. *Invest Ophthalmol Vis Sci*. (2017) 58:2063–9. doi: 10.1167/iovs.16-21289

67. Wang T, Li H, Zhang R, Yu Y, Xiao X, Wu C. Evaluation of retinal vascular density and related factors in youth myopia without maculopathy using Octa. *Sci Rep*. (2021) 11:15361. doi: 10.1038/s41598-021-94909-8

68. Qu D, Lin Y, Jiang H, Shao Y, Shi Y, Airen S, et al. Retinal nerve Fiber layer (Rnfl) integrity and its relations to retinal microvasculature and microcirculation in myopic eyes. *Eye Vis*. (2018) 5:25. doi: 10.1186/s40662-018-0120-3

69. Lim LS, Cheung CY, Lin X, Mitchell P, Wong TY, Mei-Saw S. Influence of refractive error and axial length on retinal vessel geometric characteristics. *Invest Ophthalmol Vis Sci*. (2011) 52:669–78. doi: 10.1167/iovs.10-6184

70. Man RE, Sasongko MB, Xie J, Best WJ, Noonan JE, Lo TC, et al. Decreased retinal capillary flow is not a mediator of the protective myopia-diabetic retinopathy relationship. *Invest Ophthalmol Vis Sci*. (2014) 55:6901–7. doi: 10.1167/iovs.14-15137

71. Wallman J, Wildsoet C, Xu A, Gottlieb MD, Nickla D, Marran L, et al. Moving the retina: choroidal modulation of refractive state. *VR*. (1995) 35:37–70.

72. Hirata A, Negi A. Morphological changes of Choriocapillaris in experimentally induced Chick Myopa. *Graefes Arch Clin Exp Ophthalmol*. (1998) 236:132–7.

73. Fitzgerald MEC, Wildsoet CF, Reiner A. Choroidal blood flow and thickness changes during recovery from form deprivation myopia in chicks – are they causally related? *ARVO*. (1998) 39:S868.

74. Troilo D, Nickla DL, Wildsoet CW. Choroidal thickness changes during altered eye growth and refractive state in a primate. *Investig Ophthalmol Vis Sci*. (2000) 41:1249–58.

75. Shih YF, Fitzgerald MEC, Norton TT, Gamlin PDR, Hodos W, Reiner A. Reduction in choroidal blood flow occurs in chicks wearing goggles that induce eye growth toward myopia. *Curr Eye Res*. (1993) 12:219–27.

76. Hirata A, Negi A. Lacquer crack lesions in experimental Chick myopia. *Graefes Arch Clin Exp Ophthalmol*. (1998) 236:138–45.

77. Fitzgerald MEC, Wildsoet CF, Reiner A. Temporal relationship of choroidal blood flow and thickness changes during recovery from form deprivation myopia in chicks. *Exp Eye Res*. (2002) 74:561–70. doi: 10.1006/exer.2002.1142

78. Harb E, Hyman L, Gwiazda J, Marsh-Tootle W, Zhang Q, Hou W, et al. Choroidal thickness profiles in myopic eyes of Young adults in the correction of myopia evaluation trial cohort. *Am J Ophthalmol*. (2015) 160:62–71.e2. doi: 10.1016/j.ajo.2015.04.018

79. Hung LF, Wallman J, Smith EL. Vision-dependent changes in the choroidal thickness of macaque monkeys. *Invest Ophthalmol Vis Sci*. (2000) 41:1259–69.

80. Howlett MH, McFadden SA. Spectacle Lens compensation in the pigmented Guinea pig. *Vis Res*. (2009) 49:219–27. doi: 10.1016/j.visres.2008.10.008

81. Read SA, Alonso-Caneiro D, Vincent SJ, Collins MJ. Longitudinal changes in choroidal thickness and eye growth in childhood. *Invest Ophthalmol Vis Sci*. (2015) 56:3103–12. doi: 10.1167/iovs.15-16446

82. Read SA, Alonso-Caneiro D, Vincent SJ, Collins MJ. Peripapillary choroidal thickness in childhood. *Exp Eye Res*. (2015) 135:164–73. doi: 10.1016/j.exer.2015.03.002

83. Liu L, Zhu C, Yuan Y, Hu X, Chen C, Zhu H, et al. Three-dimensional choroidal vascularity index in high myopia using swept-source optical coherence tomography. *Curr Eye Res*. (2022) 47:484–92. doi: 10.1080/02713683.2021.2006236

84. Alshareef RA, Khuthaila MK, Goud A, Vupparaboina KK, Jana S, Chhablani J. Subfoveal choroidal vascularity in myopia: evidence from spectral-domain optical coherence tomography. *Ophthalmic Surg Lasers Imaging Retina*. (2017) 48:202–7. doi: 10.3928/23258160-20170301-02

85. Hitchings R. The ocular pulse. *Br J Ophthalmol*. (1991) 75:65. doi: 10.1136/bjo.75.2.65

86. Berisha F, Findl O, Lasta M, Kiss B, Schmetterer L. A study comparing ocular pressure pulse and ocular fundus pulse in dependence of axial eye length and ocular volume. *Acta Ophthalmol*. (2010) 88:766–72. doi: 10.1111/j.1755-3768.2009.01577.x

87. James CB, Trew DR, Clark K, Smith SE. Factors influencing the ocular pulse – axial length. *Graefes Arch Clin Exp Ophthalmol*. (1991) 229:341–4. doi: 10.1007/bf00170692

88. Zhang S, Zhang G, Zhou X, Xu R, Wang S, Guan Z, et al. Changes in choroidal thickness and choroidal blood perfusion in Guinea pig myopia. *Invest Ophthalmol Vis Sci*. (2019) 60:3074–83. doi: 10.1167/iovs.18-26397

89. Scherm P, Pettenkofer M, Maier M, Lohmann CP, Feucht N. Choriocapillary blood flow in myopic patients measured with Oct angiography. *Invest Ophthalmol Vis Sci*. (2018) 59:2821.

90. Ning J, Joshi N, Franchi-Pereira R, Benavente-Perez A. Longitudinal evaluation of choroidal thickness and ocular perfusion pressure in progressing Myopes, baseline data. *Invest Ophthalmol Vis Sci*. (2017) 58:1106.

91. Cheng W, Song Y, Gao X, Lin F, Li F, Wang P, et al. Axial length and Choriocapillaris flow deficits in non-pathological high myopia. *Am J Ophthalmol*. (2022) 244:68–78. doi: 10.1016/j.ajo.2022.08.005

92. Wang Y, Chen S, Lin J, Chen W, Huang H, Fan X, et al. Vascular changes of the choroid and their correlations with visual acuity in pathological myopia. *Invest Ophthalmol Vis Sci*. (2022) 63:20. doi: 10.1167/iovs.63.12.20

93. Zhang Z, Qi Y, Wei W, Jin Z-B, Wang W, Duan A, et al. Investigation of macular choroidal thickness and blood flow change by optical coherence tomography angiography after posterior scleral reinforcement. *Front Med*. (2021):8. doi: 10.3389/fmed.2021.658259

94. Lim LS, Lim XH, Tan L. Retinal vascular oxygen saturation and its variation with refractive error and axial length. *Transl Vis Sci Technol*. (2019) 8:22. doi: 10.1167/tvst.8.4.22

95. Liu X, He X, Yin Y, Zhang B, Sun S, Zhu J, et al. Retinal oxygen saturation in 1461 healthy children aged 7-19 and its associated factors. *Acta Ophthalmol*. (2019) 97:287–95. doi: 10.1111/aos.14043

96. Zheng Q, Zong Y, Li L, Huang X, Lin L, Yang W, et al. Retinal vessel oxygen saturation and vessel diameter in high myopia. *Ophthalmic Physiol Opt*. (2015) 35:562–9. doi: 10.1111/opo.12223

97. Liu Y, Wang L, Xu Y, Pang Z, Mu G. The influence of the choroid on the onset and development of myopia: from perspectives of choroidal thickness and blood flow. *Acta Ophthalmol*. (2021) 99:730–8. doi: 10.1111/aos.14773

98. Brown DM, Mazade R, Clarkson-Townsend D, Hogan K, Datta Roy PM, Pardue MT. Candidate pathways for retina to scleral signaling in refractive eye growth. *Exp Eye Res*. (2022) 219:109071. doi: 10.1016/j.exer.2022.109071

99. Wu H, Chen W, Zhao F, Zhou Q, Reinach PS, Deng L, et al. Scleral hypoxia is a target for myopia control. *Proc Natl Acad Sci*. (2018) 115:E7091–100. doi: 10.1073/pnas.1721443115

100. Zhao F, Zhang D, Zhou Q, Zhao F, He M, Yang Z, et al. Scleral Hif-1α is a prominent regulatory candidate for genetic and environmental interactions in human myopia pathogenesis. *EBioMedicine*. (2020) 57:102878. doi: 10.1016/j.ebiom.2020.102878

101. Guo L, Frost MR, Siegwart JT Jr, Norton TT. Gene expression signatures in tree shrew sclera during recovery from minus-Lens Wear and during plus-Lens Wear. *Mol Vis*. (2019) 25:311–28.

102. Guo L, Frost MR, He L, Siegwart JT Jr, Norton TT. Gene expression signatures in tree shrew sclera in response to three Myopiagenic conditions. *Invest Ophthalmol Vis Sci*. (2013) 54:6806–19. doi: 10.1167/iovs.13-12551

103. Benavente-Perez A, Hosking SL, Logan NS, Bansal D. Reproducibility-repeatability of choroidal thickness calculation using Oct. *Optom Vis Sci*. (2010) 87:867–72. doi: 10.1097/OPX.0b013e3181f3eced

104. Goldenberg D, Moisseiev E, Goldstein M, Loewenstein A, Barak A. Enhanced depth imaging optical coherence tomography: choroidal thickness and correlations with age, refractive error, and axial length. *Ophthalmic Surg Lasers Imaging*. (2012) 43:296–301. doi: 10.3928/15428877-20120426-02

105. Li XQ, Larsen M, Munch IC. Subfoveal choroidal thickness in relation to sex and axial length in 93 Danish university students. *Invest Ophthalmol Vis Sci*. (2011) 52:8438–41. doi: 10.1167/iovs.11-8108

106. Agawa T, Miura M, Ikuno Y, Makita S, Fabritius T, Iwasaki T, et al. Choroidal thickness measurement in healthy Japanese subjects by three-dimensional high-penetration optical coherence tomography. *Graefes Arch Clin Exp Ophthalmol*. (2011) 249:1485–92.

107. Ohno-Matsui K, Akiba M, Modegi T, Tomita M, Ishibashi T, Tokoro T, et al. Association between shape of sclera and myopic Retinochoroidal lesions in patients with pathologic myopia. *Invest Ophthalmol Vis Sci*. (2012) 53:6046–61. doi: 10.1167/iovs.12-10161

108. Ohno-Matsui K, Akiba M, Moriyama M, Ishibashi T, Tokoro T, Spaide RF. Imaging Retrobulbar subarachnoid space around optic nerve by swept-source optical coherence tomography in eyes with pathologic myopia. *Invest Ophthalmol Vis Sci*. (2011) 52:9644–50. doi: 10.1167/iovs.11-8597

109. Riva C. Rhythmic changes in velocity, volume and blood flow in the optic nerve head tissue. *Microvasc Res*. (1990) 40:36–45. doi: 10.1016/0026-2862(90)90005-C

110. Hafez A, Bizzarro R, Rivard M, Trabut I, Lovasik J, Kergoat H, et al. Reproducibility of retinal and optic nerve head perfusion measurements using scanning laser Doppler Flowmetry. *Ophthalmic Surg Lasers Imaging*. (2003) 34:422–32. doi: 10.3928/1542-8877-20030901-18

111. Schemetterer L, Lexer F, Findl LO, Graselli U, Eichler H, Woltz M. The effect of inhalation of different mixtures of O2and Co2on ocular fundus pulsations. *Exp Eye Res*. (1996) 63:351–5. doi: 10.1006/exer.1996.0125

112. Schmetterer L. Noninvasive investigations of the Normal ocular circulation in humans. *Invest Ophthalmol Vis Sci*. (1998) 39:1210.

113. Hosking SL, Harris A, Chung HS, Jonescu-Cuypers CP, Kagemann L, Roff Hilton EJ, et al. Ocular Haemodynamic responses to induced hypercapnia and Hyperoxia in Glaucoma. *Br J Ophthalmol*. (2004) 88:406–11. doi: 10.1136/bjo.2002.008995

114. Embleton S, Hosking S, Roff Hilton E, Cunliffe I. Effect of senescence on ocular blood flow in the retina, neuroretinal rim and lamina cribrosa, using scanning laser Doppler flowmetry. *Eye (Lond)*. (2002) 16:156–62. doi: 10.1038/sj.eye.6700100

115. Logan N, Gilmartin B, Cox W. Ocular Volume and Blood Flow in Human Anisomyopia. *Invest Ophthalmol Vis Sci*. (2002) 43:199.

116. Guyton AC. Evidence for tissue oxygen demand as the major factor causing autoregulation. *Circ Res*. (1964) 15:60–9.

117. Riva CE, Grunwald JE, Petrig BL. Autoregulation of human retinal blood flow. An investigation with laser Doppler velocimetry. *Invest Ophthalmol Vis Sci*. (1986) 27:1706–12.

118. Michelson G, Groh M, Gründler A. Regulation of ocular blood flow during increases of arterial blood pressure. *Br J Ophthalmol*. (1994) 78:461–5. doi: 10.1136/bjo.78.6.461

119. Kergoat H, Faucher C. Effects of oxygen and Carbogen breathing on choroidal hemodynamics in humans. *Invest Ophthalmol Vis Sci*. (1999) 40:2906–11.

120. Schumann J, Orgül S, Gugleta K, Dubler B, Flammer J. Interocular difference in progression of Glaucoma correlates with Interocular differences in Retrobulbar circulation. *Am J Ophthalmol*. (2000) 129:728–33. doi: 10.1016/S0002-9394(99)00481-X

121. Aaslid R, Lindegaard KF, Sorteberg W, Nornes H. Cerebral autoregulation dynamics in humans. *Stroke*. (1989) 20:45–52. doi: 10.1161/01.STR.20.1.45

122. Riva C, Hero M, Titze P, Petrig B. Autoregulation of human optic nerve head blood flow in response to acute changes in ocular perfusion pressure. *Graefes Arch Clin Exp Ophthalmol*. (1997) 235:618–26. doi: 10.1007/BF00946937

123. Longo A, Geiser M, Riva C. Posture changes and subfoveal choroidal blood flow. *Investig Ophthalmol Vis Sci*. (2004) 45:546–51. doi: 10.1167/iovs.03-0757

124. Riva CE, Logean E, Falsini B. Visually evoked Hemodynamical response and assessment of neurovascular coupling in the optic nerve and retina. *Prog Retin Eye Res*. (2005) 24:183–215. doi: 10.1016/j.preteyeres.2004.07.002

125. Benavente-Perez A, Hosking SL, Logan NS. Defective haemodynamic autoregulation associated with autonomic dysregulation in human myopia. *Invest Ophthalmol Vis Sci*. (2007) 48:1041.

126. Benavente-Perez A, Hosking SL, Logan NS. Myopes exhibit reduced choroidal blood velocity which is highly responsive to hypercapnia. *Invest Ophthalmol Vis Sci*. (2008) 49:3581.

127. Fan X, Xu H, Zhai R, Sheng Q, Sun Y, Shao T, et al. Peripapillary vascular reactivity in primary open-angle Glaucoma with high myopia by using optical coherence tomography angiography. *Front Med*. (2022) 9:850483. doi: 10.3389/fmed.2022.850483

128. La Spina C, Corvi F, Bandello F, Querques G. Static characteristics and dynamic functionality of retinal vessels in longer eyes with or without pathologic myopia. *Graefes Arch Clin Exp Ophthalmol*. (2016) 254:827–34. doi: 10.1007/s00417-015-3122-z

129. Tedja MS, Wojciechowski R, Hysi PG, Eriksson N, Furlotte NA, Verhoeven VJM, et al. Genome-wide association Meta-analysis highlights light-induced signaling as a driver for refractive error. *Nat Genet*. (2018) 50:834–48. doi: 10.1038/s41588-018-0127-7

130. Tedja MS, Haarman AEG, Meester-Smoor MA, Kaprio J, Mackey DA, Guggenheim JA, et al. Imi–myopia genetics report. *Invest Ophthalmol Vis Sci*. (2019) 60:M89–M105. doi: 10.1167/iovs.18-25965

131. Verhoeven VJ, Hysi PG, Wojciechowski R, Fan Q, Kiefer AK, Klaver CCW, et al. Genome-wide mega-analysis on myopia and refractive error in Cream and 23andme. *Invest Ophthalmol Vis Sci*. (2014) 55:839.

132. Verhoeven VJM, Hysi PG, Wojciechowski R, Fan Q, Guggenheim JA, Höhn R, et al. Genome-wide Meta-analyses of multiancestry cohorts identify multiple new susceptibility loci for refractive error and myopia. *Nat Genet*. (2013) 45:314–8. doi: 10.1038/ng.2554

133. Kiefer AK, Tung JY, Do CB, Hinds DA, Mountain JL, Francke U, et al. Genome-wide analysis points to roles for extracellular matrix remodeling, the visual cycle, and neuronal development in myopia. *PLoS Genet*. (2013) 9:e1003299. doi: 10.1371/journal.pgen.1003299

134. Haarman AEG, Tedja MS, Meester-Smoor MA, Kaprio J, Mackey DA, Guggenheim JA, et al. Consortium for refractive error and myopia (Cream): vision, Mission, and accomplishments In: G Prakash and T Iwata, editors. *Advances in Vision Research, Volume III: Genetic Eye Research Around the Globe*. Singapore: Springer Singapore (2021). 381–407.

135. Al-Shabrawey M, Hussein K, Wang F, Wan M, Elmasry K, Elsherbiny N, et al. Bone morphogenetic Protein-2 induces non-canonical inflammatory and oxidative pathways in human retinal endothelial cells. *Front Immunol*. (2021):11. doi: 10.3389/fimmu.2020.568795

136. Nasrabadi D, Rezaeiani S, Eslaminejad MB, Shabani A. Improved protocol for Chondrogenic differentiation of bone marrow derived mesenchymal stem cells-effect of Pthrp and Fgf-2 on Tgfβ1/Bmp2-induced chondrocytes hypertrophy. *Stem Cell Rev Rep*. (2018) 14:755–66. doi: 10.1007/s12015-018-9816-y

137. Simões Sato AY, Bub GL, Campos AH. Bmp-2 and-4 produced by vascular smooth muscle cells from atherosclerotic lesions induce monocyte chemotaxis through direct Bmprii activation. *Atherosclerosis*. (2014) 235:45–55. doi: 10.1016/j.atherosclerosis.2014.03.030

138. Helbing T, Rothweiler R, Ketterer E, Goetz L, Heinke J, Grundmann S, et al. Bmp activity controlled by Bmper regulates the Proinflammatory phenotype of endothelium. *Blood*. (2011) 118:5040–9. doi: 10.1182/blood-2011-03-339762

139. Xu J, Zhu D, Sonoda S, He S, Spee C, Ryan SJ, et al. Over-expression of Bmp4 inhibits experimental choroidal neovascularization by modulating Vegf and Mmp-9. *Angiogenesis*. (2012) 15:213–27. doi: 10.1007/s10456-012-9254-4

140. Siemerink MJ, Hughes MR, Dallinga MG, Gora T, Cait J, Vogels IM, et al. Cd34 promotes pathological epi-retinal neovascularization in a mouse model of oxygen-induced retinopathy. *PLoS One*. (2016) 11:e0157902. doi: 10.1371/journal.pone.0157902

141. Zauhar R, Biber J, Jabri Y, Kim M, Hu J, Kaplan L, et al. As in real estate, location matters: cellular expression of complement varies between macular and peripheral regions of the retina and supporting tissues. *Front Immunol*. (2022):13. doi: 10.3389/fimmu.2022.895519

142. Kim C, Smith KE, Castillejos A, Diaz-Aguilar D, Saint-Geniez M, Connor KM. The alternative complement pathway aids in vascular regression during the early stages of a murine model of proliferative retinopathy. *FASEB J*. (2016) 30:1300–5. doi: 10.1096/fj.15-280834

143. Suchting S, Freitas C, le Noble F, Benedito R, Bréant C, Duarte A, et al. The notch Ligand Delta-like 4 negatively regulates endothelial tip cell formation and vessel branching. *Proc Natl Acad Sci U S A*. (2007) 104:3225–30. doi: 10.1073/pnas.0611177104

144. Lobov IB, Renard RA, Papadopoulos N, Gale NW, Thurston G, Yancopoulos GD, et al. Delta-like ligand 4 (Dll4) is induced by Vegf as a negative regulator of Angiogenic sprouting. *Proc Natl Acad Sci U S A*. (2007) 104:3219–24. doi: 10.1073/pnas.0611206104

145. Kappas NC, Zeng G, Chappell JC, Kearney JB, Hazarika S, Kallianos KG, et al. The Vegf receptor Flt-1 spatially modulates Flk-1 signaling and blood vessel branching. *J Cell Biol*. (2008) 181:847–58. doi: 10.1083/jcb.200709114

146. Chappell JC, Cluceru JG, Nesmith JE, Mouillesseaux KP, Bradley VB, Hartland CM, et al. Flt-1 (Vegfr-1) coordinates discrete stages of blood vessel formation. *Cardiovasc Res*. (2016) 111:84–93. doi: 10.1093/cvr/cvw091

147. Nesmith JE, Chappell JC, Cluceru JG, Bautch VL. Blood vessel anastomosis is spatially regulated by Flt1 during angiogenesis. *Development*. (2017) 144:889–96. doi: 10.1242/dev.145672

148. Chappell JC, Mouillesseaux KP, Bautch VL. Flt-1 (vascular endothelial growth factor receptor-1) is essential for the vascular endothelial growth factor-notch feedback loop during angiogenesis. *Arterioscler Thromb Vasc Biol*. (2013) 33:1952–9. doi: 10.1161/ATVBAHA.113.301805

149. Tosi GM, Orlandini M, Galvagni F. The controversial role of Tgf-B in Neovascular age-related macular degeneration pathogenesis. *Int J Mol Sci*. (2018) 19:3363. doi: 10.3390/ijms19113363

150. Zarkada G, Howard JP, Xiao X, Park H, Bizou M, Leclerc S, et al. Specialized endothelial tip cells guide Neuroretina vascularization and blood-retina-barrier formation. *Dev Cell*. (2021) 56:2237–2251.e6. doi: 10.1016/j.devcel.2021.06.021

151. Goumans MJ, Valdimarsdottir G, Itoh S, Rosendahl A, Sideras P, ten Dijke P. Balancing the activation state of the endothelium via two distinct Tgf-Beta type I receptors. *EMBO J*. (2002) 21:1743–53. doi: 10.1093/emboj/21.7.1743

152. Hu J, Li T, Du X, Wu Q, Le YZ. G protein-coupled receptor 91 signaling in diabetic retinopathy and hypoxic retinal diseases. *Vis Res*. (2017) 139:59–64. doi: 10.1016/j.visres.2017.05.001

153. DeGraff AC, Frieden J, Ahlquist RP. Present state of alpha-and Beta-adrenergic drugs I. *Adrenerg Recept Am Heart J*. (1976) 92:661–4. doi: 10.1016/S0002-8703(76)80086-5

154. Dal Monte M, Martini D, Latina V, Pavan B, Filippi L, Bagnoli P. Beta-Adrenoreceptor Agonism influences retinal responses to hypoxia in a model of retinopathy of prematurity. *Invest Ophthalmol Vis Sci*. (2012) 53:2181–92. doi: 10.1167/iovs.11-9408

155. Lindgren I, Altimiras J. Chronic prenatal hypoxia sensitizes Beta-adrenoceptors in the embryonic heart but causes postnatal desensitization. *Am J Physiol Regul Integr Comp Physiol*. (2009) 297:R258–64. doi: 10.1152/ajpregu.00167.2009

156. Casini G, Dal Monte M, Fornaciari I, Filippi L, Bagnoli P. The B-adrenergic system as a possible new target for pharmacologic treatment of Neovascular retinal diseases. *Prog Retin Eye Res*. (2014) 42:103–29. doi: 10.1016/j.preteyeres.2014.06.001

157. Martinez-Camarillo JC, Spee CK, Trujillo-Sanchez GP, Rodriguez A, Hinton DR, Giarola A, et al. Blocking ocular sympathetic activity inhibits choroidal neovascularization. *Front Neurosci*. (2021) 15:780841. doi: 10.3389/fnins.2021.780841

158. Steinle JJ. Review: role of camp signaling in diabetic retinopathy. *Mol Vis*. (2020) 26:355–8.

159. Biesecker KR, Srienc AI, Shimoda AM, Agarwal A, Bergles DE, Kofuji P, et al. Glial cell calcium signaling mediates capillary regulation of blood flow in the retina. *J Neurosci*. (2016) 36:9435–45. doi: 10.1523/JNEUROSCI.1782-16.2016

160. Newman EA. Functional hyperemia and mechanisms of neurovascular coupling in the retinal vasculature. *J Cereb Blood Flow Metab*. (2013) 33:1685–95. doi: 10.1038/jcbfm.2013.145

161. Novak J, Parry LJ, Matthews JE, Kerchner LJ, Indovina K, Hanley-Yanez K, et al. Evidence for local Relaxin ligand-receptor expression and function in arteries. *FASEB J*. (2006) 20:2352–62. doi: 10.1096/fj.06-6263com

162. Jelinic M, Leo CH, Post Uiterweer ED, Sandow SL, Gooi JH, Wlodek ME, et al. Localization of Relaxin receptors in arteries and veins, and region-specific increases in compliance and bradykinin-mediated relaxation after in vivo Serelaxin treatment. *FASEB J*. (2014) 28:275–87. doi: 10.1096/fj.13-233429

163. Ng HH, Jelinic M, Parry LJ, Leo CH. Increased superoxide production and altered nitric oxide-mediated relaxation in the aorta of Young but not old male Relaxin-deficient mice. *Am J Phys Heart Circ Phys*. (2015) 309:H285–96. doi: 10.1152/ajpheart.00786.2014

164. Madaan A, Chaudhari P, Nadeau-Vallée M, Hamel D, Zhu T, Mitchell G, et al. Müller cell-localized G-protein-coupled receptor 81 (Hydroxycarboxylic acid receptor 1) regulates inner retinal vasculature via Norrin/Wnt pathways. *Am J Pathol*. (2019) 189:1878–96. doi: 10.1016/j.ajpath.2019.05.016

165. Ando A, Yang A, Mori K, Yamada H, Yamada E, Takahashi K, et al. Nitric oxide is proangiogenic in the retina and choroid*. *J Cell Physiol*. (2002) 191:116–24. doi: 10.1002/jcp.10083

166. Lin C, Toychiev A, Ablordeppey R, Slavi N, Srinivas M, Benavente-Perez A. Myopia alters the structural Organization of the Retinal Vasculature, Gfap-positive glia and ganglion cell layer thickness. *Int J Mol Sci*. (2022) 23:6202. doi: 10.3390/ijms23116202

167. Haarman AEG, Enthoven CA, Tideman JWL, Tedja MS, Verhoeven VJM, Klaver CCW. The complications of myopia: a review and Meta-analysis. *Invest Ophthalmol Vis Sci*. (2020) 61:49. doi: 10.1167/iovs.61.4.49

168. Sun J, Wang Y, Wang J. Choroidal arterial watershed zone topography and its relationship with maculopathy in highly myopic eyes. *Eye*. (2021) 35:2624–30. doi: 10.1038/s41433-021-01427-y

169. Wong CW, Phua V, Lee SY, Wong TY, Cheung CMG. Is choroidal or scleral thickness related to myopic macular degeneration? *Invest Ophthalmol Vis Sci*. (2017) 58:907–13. doi: 10.1167/iovs.16-20742

170. Hsia Y, Wang S-W, Huang C-J, Hung K-C, Chen M-S, Ho T-C. Clinical characteristics of highly myopic patients with asymmetric myopic atrophic maculopathy–analysis using multimodal imaging. *Invest Ophthalmol Vis Sci*. (2021) 62:21. doi: 10.1167/iovs.62.3.21

171. Li J, Zhou H, Feinstein M, Wong J, Wang RK, Chan L, et al. Choriocapillaris changes in myopic macular degeneration. *Transl Vis Sci Technol*. (2022) 11:37. doi: 10.1167/tvst.11.2.37

172. Ohno-Matsui K, Lai TY, Lai CC, Cheung CM. Updates of pathologic myopia. *Prog Retin Eye Res*. (2016) 52:156–87. doi: 10.1016/j.preteyeres.2015.12.001

173. Weinreb RN, Aung T, Medeiros FA. The pathophysiology and treatment of Glaucoma: a review. *JAMA*. (2014) 311:1901–11. doi: 10.1001/jama.2014.3192

174. Chan KKW, Tang F, Tham CCY, Young AL, Cheung CY. Retinal vasculature in Glaucoma: a review. *BMJ Open Ophthalmol*. (2017) 1:e000032. doi: 10.1136/bmjophth-2016-000032

175. Mitchell P, Hourihan F, Sandbach J, Wang JJ. The relationship between Glaucoma and myopia - the Blue Mountains eye study. *Ophthalmology*. (1999) 106:2010–5. doi: 10.1016/S0161-6420(99)90416-5

176. Cedrone C, Mancino R, Ricci F, Cerulli A, Culasso F, Nucci C. The 12-year incidence of Glaucoma and Glaucoma-related visual field loss in Italy: the Ponza eye study. *J Glaucoma*. (2012) 21:1–6. doi: 10.1097/IJG.0b013e3182027796

177. Czudowska MA, Ramdas WD, Wolfs RCW, Hofman A, De Jong PTVM, Vingerling JR, et al. Incidence of glaucomatous visual field loss: a ten-year follow-up from the Rotterdam study. *Ophthalmology*. (2010) 117:1705–12. doi: 10.1016/j.ophtha.2010.01.034

178. Kuzin AA, Varma R, Reddy HS, Torres M, Azen SPLos Angeles Latino Eye Study G. Ocular biometry and open-angle Glaucoma: the Los Angeles Latino eye study. *Ophthalmology*. (2010) 117:1713–9. doi: 10.1016/j.ophtha.2010.01.035

179. Marcus MW, de Vries MM, Montolio FGJ, Jansonius NM. Myopia as a risk factor for open-angle Glaucoma: a systematic review and Meta-analysis. *Ophthalmology*. (2011) 118:1989–94.e2. doi: 10.1016/j.ophtha.2011.03.012

180. Xu L, Wang Y, Wang S, Wang Y, Jonas JB. High myopia and Glaucoma susceptibility: the Beijing eye study. *Ophthalmology*. (2007) 114:216–20. doi: 10.1016/j.ophtha.2006.06.050

181. Memarzadeh F, Ying-Lai M, Chung J, Azen SP, Varma R. Blood pressure, perfusion pressure, and open-angle Glaucoma: the Los Angeles Latino eye study. *Invest Ophthalmol Vis Sci*. (2010) 51:2872–7. doi: 10.1167/iovs.08-2956

182. Leske MC, Wu SY, Hennis A, Honkanen R, Nemesure B. Risk factors for incident open-angle Glaucoma: the Barbados eye studies. *Ophthalmology*. (2008) 115:85–93. doi: 10.1016/j.ophtha.2007.03.017

183. Fuchsjäger-Mayrl G, Wally B, Georgopoulos M, Rainer G, Kircher K, Buehl W, et al. Ocular blood flow and systemic blood pressure in patients with primary open-angle Glaucoma and ocular hypertension. *Invest Ophthalmol Vis Sci*. (2004) 45:834–9. doi: 10.1167/iovs.03-0461

184. Suwan Y, Fard MA, Geyman LS, Tantraworasin A, Chui TY, Rosen RB, et al. Association of Myopia with Peripapillary perfused capillary density in patients with Glaucoma: an optical coherence tomography angiography study. *JAMA Ophthalmol*. (2018) 136:507–13. doi: 10.1001/jamaophthalmol.2018.0776

185. Mammo Z, Heisler M, Balaratnasingam C, Lee S, Yu DY, Mackenzie P, et al. Quantitative optical coherence tomography angiography of radial Peripapillary capillaries in Glaucoma, Glaucoma suspect, and Normal eyes. *Am J Ophthalmol*. (2016) 170:41–9. doi: 10.1016/j.ajo.2016.07.015

186. Ye J, Lin J, Shen M, Chen W, Zhang R, Lu F, et al. Reduced radial Peripapillary capillary in pathological myopia is correlated with visual acuity. *Front Neurosci*. (2022) 16:818530. doi: 10.3389/fnins.2022.818530

187. Yamazaki Y, Drance SM. The relationship between progression of visual field defects and retrobulbar circulation in patients with Glaucoma. *Am J Ophthalmol*. (1997) 124:287–95. doi: 10.1016/S0002-9394(14)70820-7

188. Findl O, Rainer G, Dallinger S, Dorner G, Polak K, Kiss B, et al. Assessment of optic disk blood flow in patients with open-angle Glaucoma. *Am J Ophthalmol*. (2000) 130:589–96. doi: 10.1016/S0002-9394(00)00636-X

189. Venkataraman ST, Flanagan JG, Hudson C. Vascular reactivity of optic nerve head and retinal blood vessels in glaucoma – a review. *Microcirculation*. (2010) 17:568–81. doi: 10.1111/j.1549-8719.2010.00045.x

190. Németh J, Michelson G, Harazny J. Retinal microcirculation correlates with Ocular Wall thickness, axial eye length, and refraction in Glaucoma patients. *J Glaucoma*. (2001) 10:390–5. doi: 10.1097/00061198-200110000-00005

191. Samra WA, Pournaras C, Riva C, Emarah M. Choroidal hemodynamic in myopic patients with and without primary open-angle Glaucoma. *Acta Ophthalmol*. (2013) 91:371–5. doi: 10.1111/j.1755-3768.2012.02386.x

192. Lin F, Li F, Gao K, He W, Zeng J, Chen Y, et al. Longitudinal changes in macular optical coherence tomography angiography metrics in primary open-angle Glaucoma with high myopia: a prospective study. *Invest Ophthalmol Vis Sci.* (2021) 62:30. doi: 10.1167/iovs.62.1.30

193. Metelitsina TI, Grunwald JE, DuPont JC, Ying GS, Brucker AJ, Dunaief JL. Foveolar choroidal circulation and choroidal neovascularization in age-related macular degeneration. *Invest Ophthalmol Vis Sci*. (2008) 49:358–63. doi: 10.1167/iovs.07-0526

194. Wakabayashi T, Ikuno Y, Oshima Y, Hamasaki T, Nishida K. Aqueous concentrations of vascular endothelial growth factor in eyes with high myopia with and without choroidal neovascularization. *J Ophthalmol.* (2013) 2013:257381. doi: 10.1155/2013/257381

195. Feng B, Su W, Chen Q, Gan R, Wang M, Wang J, et al. Quantitative analysis of retinal vasculature in rhegmatogenous retinal detachment based on ultra-Widefield fundus imaging. *Front Med*. (2021) 8:797479. doi: 10.3389/fmed.2021.797479

196. Tolentino FI, Lapus JV, Novalis G, Trempe CL, Gutow GS, Ahmad A. Fluorescein angiography of degenerative lesions of the peripheral fundus and Rhegmatogenous retinal detachment. *Int Ophthalmol Clin*. (1976) 16:13–29. doi: 10.1097/00004397-197601610-00005

197. Cardillo PF. Vascular changes in Rhegmatogenous retinal detachment. *Ophthalmologica*. (1983) 186:17–24. doi: 10.1159/000309255

198. Ohno-Matsui K. Proposed classification of posterior staphylomas based on analyses of eye shape by three-dimensional magnetic resonance imaging and wide-field fundus imaging. *Ophthalmology*. (2014) 121:1798–809. doi: 10.1016/j.ophtha.2014.03.035

199. Nie F, Zhang L, Cao M, Zhou D, Liu K, Ouyang J, et al. Impact of Peripapillary staphylomas on the vascular and structural characteristics in myopic eyes: a propensity score matching analysis. *Graefes Arch Clin Exp Ophthalmol*. (2023) 2013:257381. doi: 10.1007/s00417-022-05966-2

200. Nie F, Ouyang J, Tang W, Luo L, Cao M, Zhang L, et al. Posterior staphyloma is associated with the microvasculature and microstructure of myopic eyes. *Graefes Arch Clin Exp Ophthalmol*. (2021) 259:2119–30. doi: 10.1007/s00417-020-05057-0

201. Klein BE, Klein R, Jensen SC, Linton KL. Hypertension and Lens opacities from the beaver dam eye study. *Am J Ophthalmol*. (1995) 119:640–6. doi: 10.1016/S0002-9394(14)70223-5

202. Klein BE, Klein R, Lee KE. Diabetes, cardiovascular disease, selected cardiovascular disease risk factors, and the 5-year incidence of age-related cataract and progression of Lens opacities: the beaver dam eye study. *Am J Ophthalmol*. (1998) 126:782–90. doi: 10.1016/S0002-9394(98)00280-3

203. Grieshaber MC, Koçak I, Dubler B, Flammer J, Orgül S. Retrobulbar blood flow in patients with cataract. *Br J Ophthalmol*. (2006) 90:1512–5. doi: 10.1136/bjo.2006.101261

204. Jakobsson L, Bentley K, Gerhardt H. Vegfrs and notch: a dynamic collaboration in vascular patterning. *Biochem Soc Trans*. (2009) 37:1233–6. doi: 10.1042/BST0371233

frontiers | Frontiers in Medicine

TYPE Review
PUBLISHED 08 June 2023
DOI 10.3389/fmed.2023.1110166

OPEN ACCESS

EDITED BY
Georgios D. Panos,
Nottingham University Hospitals NHS Trust, United Kingdom

REVIEWED BY
Veena Rao Raiji,
Rush University, United States
Francesco Maria D'Alterio,
Imperial College Healthcare NHS Trust, United Kingdom

*CORRESPONDENCE
Kelvin Yi Chong Teo
✉ kelvin.teo.y.c@singhealth.com.sg

RECEIVED 28 November 2022
ACCEPTED 23 May 2023
PUBLISHED 08 June 2023

CITATION
Tan TE, Ibrahim F, Chandrasekaran PR and Teo KYC (2023) Clinical utility of ultra-widefield fluorescein angiography and optical coherence tomography angiography for retinal vein occlusions.
Front. Med. 10:1110166.
doi: 10.3389/fmed.2023.1110166

Clinical utility of ultra-widefield fluorescein angiography and optical coherence tomography angiography for retinal vein occlusions

Tien-En Tan[1,2], Farah Ibrahim[1], Priya R. Chandrasekaran[1] and Kelvin Yi Chong Teo[1,2]*

[1]Singapore Eye Research Institute, Singapore National Eye Centre, Singapore, Singapore, [2]Duke-NUS Medical School, Singapore, Singapore

Retinal vein occlusions (RVOs) are the second most common retinal vascular disease after diabetic retinopathy, and are a significant cause of visual impairment, especially in the elderly population. RVOs result in visual loss due to macular ischemia, cystoid macular edema (CME), and complications related to neovascularization. Vascular assessment in RVOs traditionally relies on standard fluorescein angiography (FA) for assessment of macular and retinal ischemia, which aids in prognostication and guides intervention. Standard FA has significant limitations—it is time-consuming, requires invasive dye administration, allows for limited assessment of the peripheral retina, and is usually evaluated semi-qualitatively, by ophthalmologists with tertiary expertise. More recently, the introduction of ultra-widefield FA (UWF FA) and optical coherence tomography angiography (OCTA) into clinical practice has changed the tools available for vascular evaluation in RVOs. UWF FA allows for evaluation of peripheral retinal perfusion, and OCTA is non-invasive, rapidly-acquired, and provides more information on capillary perfusion. Both modalities can be used to provide more quantitative parameters related to retinal perfusion. In this article, we review the clinical utility and impact of UWF FA and OCTA in the evaluation and management of patients with RVOs.

KEYWORDS

branch retinal vein occlusion (BRVO), central retinal vein occlusion (CRVO), ultra-widefield (UWF), optical coherence tomography angiography (OCTA), fluorescein angiography (FA), retinal imaging, imaging modality

1. Introduction

Retinal vein occlusions (RVOs) are the second most common retinal vascular disease after diabetic retinopathy (DR), and are a significant cause of visual impairment, especially in the elderly population. Globally, it was estimated in 2015 that RVO affects 28 million individuals, with 0.77% prevalence among individuals aged 30–89 years (1). Broadly, there are two main types of RVOs: central retinal vein occlusion (CRVO) occurs due to an occlusion (usually thrombotic) of the central retinal vein at or posterior to the lamina cribrosa, while a branch retinal vein occlusion (BRVO) occurs at the level of a retinal venule, usually at the site of an arteriovenous crossing (2). BRVOs are about 5 times more common than CRVOs, but both of

these subtypes share common major risk factors (1–3). The factors leading to thrombosis and RVO follow that of Virchow's triad, namely vascular wall or endothelial damage, venous stasis, and hypercoagulability. Accordingly, the major risk factors for most RVOs, which are older age, hypertension, hyperlipidemia, diabetes mellitus and cigarette smoking, are all related to vascular endothelial damage, and therefore intricately linked to systemic vascular disease as well (2). Consequently, upon diagnosis of an RVO, systemic screening and management of these underlying systemic vascular diseases is crucial to prevent an RVO recurrence, as well as other related atherosclerotic diseases such as coronary artery disease or cerebrovascular accidents.

From an ocular perspective, visual loss in RVOs usually occurs due to macular ischemia, cystoid macular edema (CME), or complications of neovascularization such as vitreous hemorrhage, tractional retinal detachment and neovascular glaucoma (NVG). Various forms of retinal imaging play a crucial role in detecting and guiding management of these ocular complications. Optical coherence tomography (OCT) is the modality of choice for diagnosis of CME, and CME can be treated with intravitreal anti-vascular endothelial growth factor (anti-VEGF) injections, intravitreal corticosteroid injections, or macular grid laser photocoagulation in select cases (4–7). Fluorescein angiography (FA) is the traditional standard of care imaging modality for determining risk of neovascularization after RVOs, and areas of retinal non-perfusion quantified by standard FA are the basis for classification of RVOs as "ischemic" or "non-ischemic." Specifically, the landmark Branch Vein Occlusion Study (BVOS) defined "ischemic" BRVOs as those with at least five disc areas of retinal non-perfusion, and demonstrated that such eyes had a 40% risk of developing retinal neovascularization at 3 years (8). Similarly, the Central Vein Occlusion Study (CVOS) defined "ischemic" CRVOs as those with at least 10 disc areas of retinal non-perfusion. "Ischemic" or indeterminate CRVOs had a 35% risk of developing iris neovascularization at 3 years, compared to "non-ischemic" eyes that had only a 10% risk (9). Scatter laser photocoagulation is effective in preventing neovascularization and vitreous hemorrhage in BRVOs, and in inducing regression of iris neovascularization in CRVOs, and therefore, FA is crucial in clinical practice for prognostication of RVOs, and for guiding clinical management (8, 10). However, FA has some important limitations. First, FA requires the administration of fluorescein dye, which is invasive, time-consuming, and carries some systemic risk, including allergy, anaphylaxis, and cardiac events (11). Second, "standard" FA is typically performed with fundus cameras capable of 30°–55° fields of view. Even with montage of steered images, this provides assessment of the posterior pole and up to the mid-periphery only, with limited assessment of the retinal far periphery (12). Third, evaluation and assessment of standard FA is typically performed qualitatively or semi-quantitatively, and requires tertiary retinal specialist expertise.

New imaging technologies have been introduced recently, that significantly improve our ability to evaluate the retinal vasculature, and can overcome many of the challenges associated with standard FA imaging. Ultra-widefield (UWF) imaging technology allows for a much wider field of view and reproducible, objective assessment of the retinal far periphery (12). Optical coherence tomography angiography (OCTA) now allows for non-invasive evaluation of the retinal vasculature, including evaluation of the retinal capillary microvasculature, without the need for invasive dye (13). These imaging technologies are commercially available and increasingly accessible, and they have transformed how we clinically assess the retinal vasculature in RVOs, as well as other retinal vascular diseases. In this paper, we review the utility and impact of UWF FA and OCTA in the clinical assessment, evaluation, and management of RVOs.

2. Ultra-widefield fluorescein angiography

2.1. Ultra-widefield imaging

Imaging techniques for assessment of retinal vascular disease have evolved significantly over the years. For example, in DR severity grading and assessment, the established gold standard for the past three decades has been the Early Treatment of Diabetic Retinopathy Study (ETDRS) fundus photography protocol, which originally captured seven standardized 30° fields of the posterior retina with film-based cameras (14). These standard photographic fields represented the area of the retina that could be reliably and reproducibly imaged at the time. However, in total, these seven fields only cover about 30% of the retinal surface area (15, 16). We have since transitioned to digital photographs and larger fields of view, but standard fundus cameras still generally have fields of view between 45° and 55°, which limits assessment of the retinal far periphery. More recent advances in UWF fundus imaging technology have enabled reliable imaging of the retinal far periphery, with commercial UWF imaging platforms such as the Optos (Optos PLC, Dunfermline, United Kingdom) able to capture up to 200° in a single image, which corresponds to about 80% of the retina (Figure 1) (15). Montage of steered images increases the field of view to 220°, covering more than 95% of the retina. Terminology for such imaging capability has been variable, but a recent consensus statement amongst retinal imaging experts has defined UWF imaging as having a field of view of 110°–220°, and providing visualization of at least the anterior edge of the vortex vein ampullae and beyond (12).

The more extensive view of the peripheral retina that is provided by UWF imaging allows for detection of additional peripheral lesions, which have important implications for diagnosis, prognostication, and management of various retinal vascular diseases (Figure 1). For example, in DR, the use of UWF imaging detects a more severe level of DR compared to standard ETDRS 7-field photographs in 10%–19% of eyes (17–20). Furthermore, the presence of predominantly peripheral lesions (PPLs) and areas of non-perfusion on UWF FA in DR have been identified as significant independent risk factors for DR progression, above and beyond the risk stratification provided by the ETDRS severity scale grading (21, 22). Clearly, there is valuable information in the retinal periphery that can help to inform our clinical management in patients with retinal vascular disease.

2.2. UWF FA and risk of neovascularization

Similarly, UWF FA imaging can provide important information from the retinal periphery in the clinical assessment of eyes with RVO. The disease process in RVOs affects the peripheral retina as well as the posterior retina. Retinal non-perfusion and ischemia in RVOs is not confined to the posterior pole, and frequently extends out to the far periphery, based on the area of retina drained by the occluded

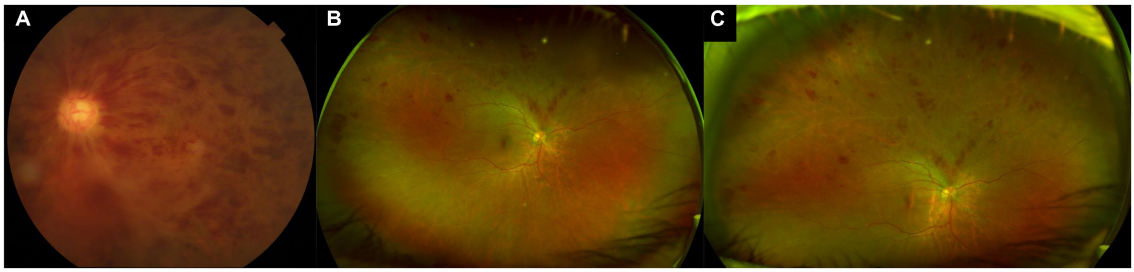

FIGURE 1
Standard color and ultra-widefield (UWF) photographs of retinal vein occlusions. **(A)** Standard 50° color photograph of a central retinal vein occlusion, allowing for visualization just beyond the posterior pole. **(B)** Ultra-widefield (UWF) pseudocolor photograph of a superior branch retinal vein occlusion, showing a much wider field of view, including much of the retinal periphery. **(C)** Steered UWF pseudocolor photograph of the same eye as in **(B)**, but taken in upgaze, to provide a better view of pathology in the superior far periphery.

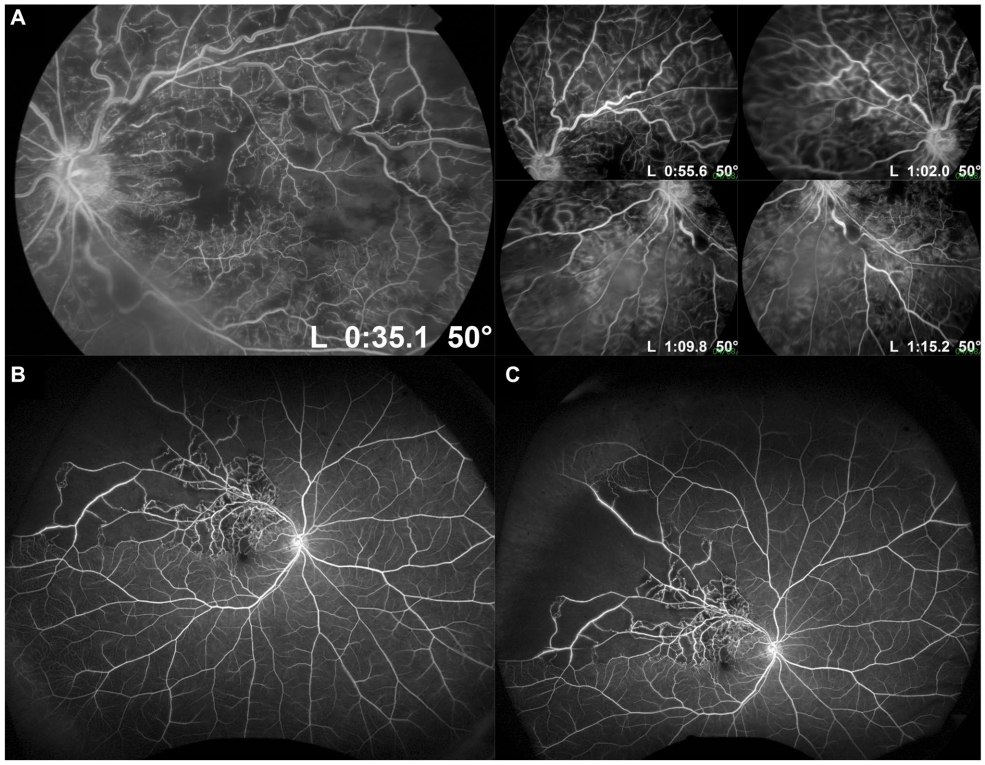

FIGURE 2
Standard and ultra-widefield (UWF) fluorescein angiography (FA) of retinal vein occlusions. **(A)** Standard 50° FA images of a central retinal vein occlusion in primary gaze showing the posterior pole, and steered in different directions of gaze to increase the field of view up to the mid-periphery. **(B)** UWF FA image of a superotemporal branch retinal vein occlusion, showing a much wider field of view, including much of the retinal periphery. **(C)** Steered UWF FA image of the same eye as in **(B)**, but taken in upgaze to provide a better view of pathology in the superior far periphery. This image shows extensive peripheral retinal non-perfusion out to the superotemporal far periphery, which would not have been appreciated on standard FA.

venule (Figure 2). Turczyńska et al. demonstrated in 102 eyes with RVO that 59.8% had zones of peripheral ischemia (23). Such areas of retinal non-perfusion are a significant risk factor for iris and retinal neovascularization, which can lead to visual loss (8, 9, 24). Standard FA frequently underestimates the amount of retinal non-perfusion that is present, and in some cases can completely miss areas of peripheral non-perfusion. For example, in a retrospective series of 42 CRVO cases imaged with UWF FA, Nicholson et al. found that 31.0% of eyes had significant peripheral non-perfusion, despite a completely perfused posterior pole (25). Similarly, in the series by Turczyńska et al., 20.6% of eyes showed only peripheral ischemia, with no detectable ischemia in the posterior pole. Such peripheral ischemia was only visualized on UWF FA, and this was significant as it required a change in treatment decision with scatter laser photocoagulation in their series (23). In clinical practice, with only standard FA, such eyes may be mis-labelled as "non-ischemic," and may return with visual loss from neovascular complications that could otherwise have been prevented.

By imaging a much larger area of the retina, UWF FA reveals larger absolute areas of non-perfusion and ischemia in RVOs than standard FA (Figure 2). Therefore, our traditional cut-off values of 5 and 10 disc areas for BRVOs and CRVOs, respectively, to be considered "ischemic" need to be re-evaluated (8, 9). Tsui et al. attempted to develop a cut-off value based on an ischemic index (ISI) on UWF FA images (26). ISI was measured by delineating the area of retinal non-perfusion, and dividing it by the total retinal area in pixels, as seen in the arteriovenous phase of a UWF FA image. They suggested an ISI of more than 45% was associated with greater risk of neovascularization. Thomas et al. similarly measured ISI on UWF FA images in a retrospective cohort of 60 eyes, and suggested that an ISI of 35% or more was highly sensitive and specific for ischemic CRVOs (27). However, both these studies did not account for peripheral image magnification on UWF images and distortion correction. Nicholson et al. subsequently addressed this issue of image distortion on UWF FA in their series of 42 eyes with CRVO, and also attempted to develop a clinically-useful cut-off value (25). They found that when considering total retinal non-perfusion on UWF FA, 30 disc areas was probably a more useful cut-off than 10 disc areas: risk of neovascularization was only 5.3% in eyes with less than 30 disc areas of non-perfusion, but increased to 52.2% when this threshold was exceeded. However, their findings also suggested that the distribution of non-perfusion made a difference as well. More than 10 disc areas of non-perfusion in the posterior pole conferred a significantly higher risk of neovascularization than 10 disc areas of non-perfusion in the periphery, if the posterior pole remained perfused. More studies, with longitudinal design, are required to address this question, and to validate clinically-relevant thresholds of non-perfusion on UWF FA for intervention in both CRVOs and BRVOs. Table 1 summarizes the key advantages and disadvantages of UWF FA for detection of retinal non-perfusion and neovascularization in RVOs.

2.3. UWF FA and cystoid macular edema

Besides neovascularization, UWF FA abnormalities are also associated with other important complications of RVOs, such as CME. CME is a common complication, and a major cause of visual impairment in RVOs. It has long been postulated that the extent and location of retinal ischemia may be causally related to the development and persistence of CME, due to the upregulation of VEGF and other vasogenic and inflammatory cytokines from areas of non-perfusion (28, 29). These cytokines and mediators result in breakdown of the inner blood-retinal barrier and increased vascular permeability, which lead to the development of CME. Several cross-sectional studies have linked areas of retinal non-perfusion on UWF FA to CME. In a few studies, greater areas of ischemia (quantified by ISI) have been correlated with increasing severity of CME and central macular thickness (30, 31). Prasad et al. examined UWF FA images in 76 eyes with BRVO, and found that areas of untreated non-perfusion were associated with CME. Interestingly, in this study, it was particularly areas of peripheral non-perfusion (anterior to the equator) that were strongly associated with CME, whereas the same association was not evident with posterior non-perfusion (29). It has also been suggested that areas of *partial* retinal ischemia are more likely to be associated with CME than areas of *complete* ischemia (28, 32). It is postulated that in partial ischemia, viable cells are still capable of producing cytokines in response to ischemia, whereas in complete ischemia there is cellular loss, reduced oxygen demand, and hence less cytokine-driven CME. Besides areas of non-perfusion, leakage evident on UWF FA has also been linked to CME. Wang et al. quantified leakage in various retinal zones on UWF FA in eyes with CRVO, and showed that greater leakage indices were significantly associated with the presence of CME. Furthermore, increased central macular thickness was correlated with pan-retinal leakage, peri-macular leakage, near-peripheral leakage, and mid-peripheral leakage, with the strongest correlation for peri-macular leakage (33).

Greater areas of retinal non-perfusion have been linked to RVOs with recalcitrant CME (31). Accordingly, greater areas of retinal non-perfusion on UWF FA are associated with higher anti-VEGF treatment burden for CME (34). Abri Aghdam et al. quantified non-perfusion on UWF FA in treatment-naïve CRVOs with CME, and found that cases with greater non-perfusion at baseline subsequently required significantly more ranibizumab injections (34). Following the hypothesis that recalcitrant CME is driven by persistent areas of untreated retinal non-perfusion, various groups have attempted to use UWF FA to guide targeted scatter laser photocoagulation as an adjunct treatment for CME, with conflicting results. Tomomatsu et al. reported results from a randomized clinical trial comparing intravitreal bevacizumab and targeted laser photocoagulation versus bevacizumab alone for CME in patients with ischemic BRVOs, showing that the addition of laser photocoagulation reduced the burden of bevacizumab retreatments (35). Similarly, Goel et al. showed in another randomized clinical trial for BRVOs with CME that the addition of UWF FA-guided targeted laser photocoagulation reduced the number of intravitreal ranibizumab treatments required (36).

In contrast, the WAVE trial did not demonstrate a significant reduction in ranibizumab injections with targeted laser photocoagulation in RVO patients with CME. This may have been due to the relatively modest sample size in the study ($n = 30$), but they also postulated that the lack of treatment effect could have been due to persistent areas of posterior retinal non-perfusion, even in the laser group, as these areas were too posterior to be safely lasered (37). The RELATE trial is the largest clinical trial to date ($n = 81$) investigating the role of targeted scatter laser photocoagulation for CME in RVOs. This study also did not show any significant reduction in ranibizumab injections with the addition of targeted laser photocoagulation (38). Comparison of all these studies is limited by differences in terms of study population, and laser treatment timing and protocol. As such, the role of targeted scatter laser in RVOs with recalcitrant CME is still unclear. Nevertheless, UWF FA is still clearly useful for assessment and prognostication in these eyes.

2.4. Accurate quantification of non-perfusion and ischemia on UWF FA

Much of the research and potential clinical utility of UWF FA in RVOs centers around the accurate quantification of areas of non-perfusion or retinal ischemia. As outlined above, such quantification has been done with different methods, with some approaches focusing on ISI, while others quantify areas of non-perfusion in absolute surface area or disc areas (25–27). The reliability of ISI grading on UWF FA images in terms of intergrader and intragrader agreement has been shown to be acceptable (39).

TABLE 1 Advantages and disadvantages of ultra-widefield fluorescein angiography and optical coherence tomography angiography for detection of retinal non-perfusion and neovascularization in retinal vein occlusions.

		UWF FA	OCTA
Detection of retinal non-perfusion	Advantages	Greater field of view, ability to detect much larger areas of non-perfusion, including up to the far periphery, which would be missed on standard FA or OCTA	Non-perfusion areas correlate/agree well with FA, and may be more accurate (no issues with choroidal background fluorescence)
		Peripheral non-perfusion areas linked to risk of neovascularization (but needs further validation)	Non-perfusion areas linked to risk of neovascularization (but needs further validation)
		Greater focus on objective, quantitative parameters (compared to standard FA), such as ISI	Provides automated, objective, quantitative parameters and metrics in relation to perfusion
			No dye leakage to interfere with measurement/ quantification of non-perfusion
			Non-invasive, with no systemic risk, and faster, more convenient acquisition of images
	Disadvantages	Clinically-useful cut-offs for non-perfusion have yet to be determined and validated—current evidence mostly cross-sectional, and need for more longitudinal studies	Clinically-useful cut-offs for non-perfusion have yet to be determined and validated—current evidence mostly cross-sectional, and need for more longitudinal studies
		Variability of total area of imaged/gradable peripheral retina can result in changes to ISI and other quantitative metrics	Limited field of view with current technology compared to UWF FA, even with montage of multiple steered images
		Potential inaccuracies related to peripheral image distortion and warp	Heterogeneity and lack of standardization in commercial devices and metrics
		Potential inaccuracies related to changes in choroidal background fluorescence	Image artefacts, quality and gradability
		Potential inaccuracies related to dye leakage, which can obscure areas of non-perfusion	
		Quantitative metrics currently derived manually, which is time-consuming and ill-suited to clinical application	
		Fundamentally similar to standard FA—still requires invasive dye administration, with associated systemic risk, and takes time to acquire	
Detection of neovascularization	Advantages	Greater field of view, allows for detection of neovascularization in retinal periphery, which would be missed on standard FA or OCTA	Better differentiation of collaterals from neovascularization—cross-sectional scans can detect flow/ vascular structures anterior to ILM
		Image interpretation potentially easier—no need for segmentation, and greater familiarity for ophthalmologists and retinal specialists	Potentially more sensitive for detection of neovascularization within the same area as FA
			Better structural characterization of neovascular lesions
			Non-invasive, with no systemic risk, and faster, more convenient acquisition of images
	Disadvantages	Detection of neovascularization dependent on leakage, which can be variable or minimal in some cases—can lead to neovascularization being missed	Limited field of view with current technology compared to UWF FA, even with montage of multiple steered images
		Fundamentally similar to standard FA—still requires invasive dye administration, with associated systemic risk, and takes time to acquire	Technically more difficult to interpret, with need for segmentation and scrolling through cross-sectional scans

UWF, ultra-widefield; FA, fluorescein angiography; OCTA, optical coherence tomography angiography; ISI, ischemic index; ILM, internal limiting membrane.

However, one major limitation of UWF images in this regard that has to be acknowledged is the phenomenon of peripheral image distortion and warp. The retina is a three-dimensional (3D) structure that is being imaged, and UWF imaging platforms are able produce a two-dimensional (2D) image of this 3D structure via a mathematical transformation known as stereographic projection (40). This technique produces 2D images where the relative directions and locations of anatomic structures are preserved, but results in unequal magnification and distances, particularly in the periphery. Objects in the peripheral retina appear larger than they are, and the same number of pixels on the 2D image represent a much smaller area in the peripheral retina than in the central/posterior retina (40). This is potentially problematic for approaches that rely on quantifying pixels on an UWF image, such as the ISI, which is defined as the ratio of the number of pixels in non-perfused areas to the number of pixels in the total gradable area of the retina (26, 39).

To address this issue, some groups have used stereographic projection software to compensate for the image distortion, and to

provide anatomically accurate estimates of retinal surface area from UWF images in mm^2 units (40, 41). Interestingly, when uncorrected ISI values and corrected perfusion percentages (based on surface area corrected with stereographic projection) were compared in the same eyes, both measures showed a very high degree of correlation (Spearman correlation $R = 0.978$), and the mean difference between the two measures was low, at 1.4%. However, the authors did point out that the absolute difference could be as high as 14.8% in some cases (40). The accuracy of these corrected measurements has been verified with UWF images of patients with retinal prosthesis implants *in situ*, using the known dimensions of these implants as "ground truth" measurements (42). This stereographic projection software has been incorporated into commercially available UWF devices such as the Optos (Optos PLC) for clinical and research use (43).

2.5. Other drawbacks of UWF FA

In spite of the tremendous improvements in imaging technology, UWF imaging and UWF FA in particular still have major drawbacks that need to be acknowledged (Table 1). First, UWF FA is an improvement over standard FA in terms of field of view and the retinal surface area that can be imaged, but it is still fundamentally similar in requiring the administration of intravenous fluorescein dye. This is invasive and time-consuming in clinical practice, and carries small but not insignificant systemic risk. Second, even though more of the periphery can be imaged, the amount of peripheral retina that is imaged varies between eyes, and even between captures of the same eye. Some of this may be due to eyelid or lash artefacts. For qualitative evaluation this may not be so crucial, but it can be a major challenge for assessing quantitative metrics such as ISI over time, which rely on the area of imaged/gradable retina (26, 44). If the area of gradable retina varies in the same eye over time, it can be difficult to differentiate changes in ISI due to changes in actual areas of non-perfusion, versus changes in areas of gradable retina. Third, there have been some discrepancies reported in the assessment of ischemic areas between UWF FA and OCTA, and it is thought that changes in choroidal background fluorescence on UWF FA may account for some of these inaccuracies (45). Fourth, though there have been many attempts to provide greater objectivity and quantification in the evaluation of UWF FA metrics, most of these methods are still very manual and time-consuming, and at the moment are ill-suited to direct clinical application. There has been some preliminary work in automating the identification and quantification of areas of non-perfusion on UWF FA images in DR with artificial intelligence and deep learning, but these will need further validation, particularly if they are to be translated for use in RVOs and other retinal vascular diseases (46, 47). Finally, much of the work on UWF FA and RVOs, particularly efforts to identify clinically-useful thresholds for "ischemic" RVOs has been on retrospective datasets (25–27). Other work linking UWF FA abnormalities to CME and other related outcomes has been largely cross-sectional (29–31). There is a pressing need for more prospective, longitudinal natural history studies with UWF FA in RVO, so that clinically-useful thresholds and cut-offs can be determined and robustly validated.

3. Optical coherence tomography angiography

OCTA is a non-invasive imaging modality that allows for evaluation of the retinal microvasculature without the need for invasive dye administration. Based on OCT technology, OCTA infers red blood cell flow by detecting OCT signal changes across multiple, rapidly-acquired, successive OCT scans, and then uses algorithms to derive depth-resolved images of the retinal microvasculature (13, 48). OCTA has a number of key advantages over traditional dye-based angiography techniques. It does not require intravenous dye administration and therefore has no risk of systemic adverse events, it is faster to acquire, it allows superior visualization of the capillary microvasculature, and it provides depth-resolved angiographic images that can be separately segmented to isolate different vascular plexuses in different retinal layers (13, 48). Unlike FA, OCTA technology cannot currently provide information on vascular leakage, though in certain situations this is an advantage, as dye leakage will not obscure vascular or capillary details. Commercial OCTA platforms are based either on spectral domain OCT (SDOCT) or swept source OCT (SSOCT) technology, and currently provide fields of view ranging from 3×3 mm to 12×12 mm, with larger views possible through image montage. For example, the PLEX Elite 9000 device (Carl Zeiss Meditec, Inc., Dublin, CA, United States) is able to montage five steered 12×12 mm OCTA scans into a "panoramic" OCTA image, which has been estimated to cover about 37% of the total retinal surface area, or about half that of an UWF FA image (49).

3.1. Qualitative and quantitative vascular abnormalities in RVO

Many qualitative vascular abnormalities are evident on OCTA in RVOs. Most of these abnormalities are also ophthalmoscopically visible, such as vascular tortuosity and dilatation, collateral vessels, neovascularization and microaneurysms, but they are often more easily appreciated on OCTA. Other abnormalities are only visible with angiographic techniques, such as capillary non-perfusion and FAZ abnormalities (Figure 3). Multiple observational studies have shown that the qualitative vascular abnormalities demonstrated on OCTA correlate well with the "gold standard" FA (50–52).

Qualitative vascular abnormalities that can be appreciated on OCTA include:

1. Capillary non-perfusion: Seen as areas devoid of visible perfused capillaries. Capillary non-perfusion in RVO is typically more extensive in the deep capillary plexus (DCP) than the superficial capillary plexus (SCP) (13, 53–55).
2. Vascular tortuosity, dilatation and telangiectasias: Affects both the venules and capillaries.
3. Collateral or shunt vessels: These can be either a large vessel traversing an area of non-perfusion, or a group of tortuous vessels near the edge of an area of non-perfusion.
4. FAZ enlargement and irregularity.
5. Microaneurysms.
6. Intraretinal hemorrhages.

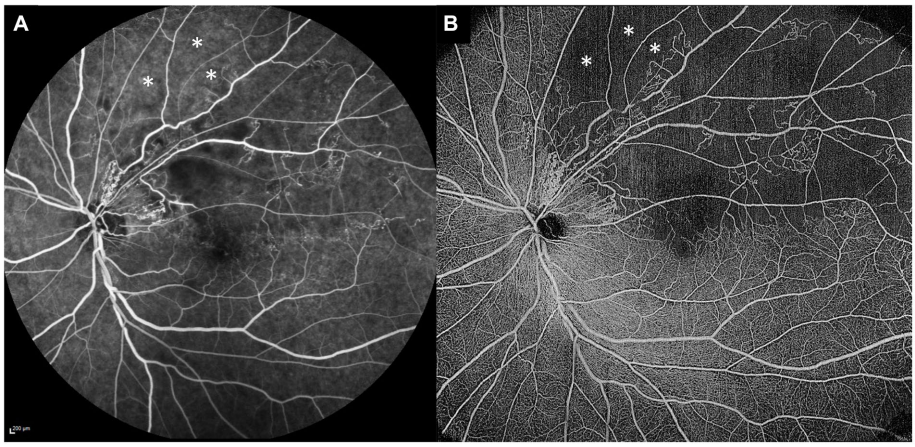

FIGURE 3
Comparison of standard fluorescein angiography (FA) and optical coherence tomography angiography (OCTA) in the same eye. **(A)** Standard 55° FA image of a superotemporal branch retinal vein occlusion. **(B)** 15×15mm montaged OCTA image of the same eye, demonstrating more extensive areas of retinal non-perfusion than the FA image. The OCTA image clearly demonstrates some areas of retinal non-perfusion just beyond the superotemporal arcade (white asterisks), whereas the same areas on the FA image (white asterisks) are not so well-appreciated as non-perfused, due to the underlying increased choroidal background fluorescence.

7. Cystoid spaces/CME.
8. Retinal neovascularization.
9. Optic disc collaterals.
10. Optic disc neovascularization.

Besides qualitative vascular evaluation, commercial OCTA devices also provide a variety of quantitative vascular metrics related to vessel density, fractal dimension (FD), and foveal avascular zone (FAZ) characteristics such as size, diameter and circularity. Most of these quantitative metrics are provided automatically by commercial devices. Multiple cross-sectional studies have demonstrated that eyes with RVO have significant reductions in capillary vessel density in both the SCP and the DCP (56–60). FD is a quantitative metric that reflects complexity of a branching network, and Koulisis showed reductions in FD in both BRVO and CRVO eyes (60). FAZ changes are also clearly evident in eyes with RVO. Adhi et al. showed that eyes with CRVO had larger FAZ areas compared to BRVO, and both CRVO and BRVO had larger FAZ areas than control eyes (53). Other cross-sectional studies have consistently demonstrated increased FAZ areas and diameters in eyes with RVO compared to healthy controls (57–59, 61, 62). FAZ circularity indices have also been found to be reduced in RVO eyes (56).

Although these quantitative parameters are automated and can be easily obtained from commercial devices, one major drawback that limits their clinical utility is that there are multiple commercial OCTA devices available, and these quantitative metrics are not directly comparable across devices. Furthermore, while significant reductions in RVO eyes can be demonstrated, these are typically not necessary for diagnostic purposes. In the future, they may be useful for prognostication of clinical outcomes such as visual acuity or CME, but with the large majority of studies being cross-sectional in nature, clinically useful cut-off values have yet to be determined and validated.

3.2. OCTA and visual acuity

In the absence of neovascularization causing vitreous hemorrhage, tractional retinal detachment or neovascular glaucoma, the major causes of decreased visual acuity in RVOs are related to CME and macular ischemia. CME is readily detected by OCT, and can be treated with intravitreal anti-VEGF agents or corticosteroids. However, visual prognosis after treatment quite frequently depends on the presence and severity of macular ischemia, as well as photoreceptor loss or atrophy. Macular ischemia can only be confirmed with angiography—traditionally with FA, but now with OCTA as well. Typically in OCTA this is seen as an enlarged, irregular FAZ. In fact, OCTA may be the preferred modality for FAZ assessment, as there is no obscuration of detail from dye leakage, which occurs in FA.

A number of studies have looked more closely at the relationship between quantitative metrics and visual acuity in RVOs. Some have shown that poorer visual acuity is correlated with decreased vessel density, decreased FD, and increased FAZ diameter in the DCP, as well as vessel density and FAZ size in the SCP (58, 59, 63, 64). However, many of these studies included a significant proportion of eyes with concurrent CME, and so it is possible that this confounds the analysis and associations (58, 59, 63, 64). Nevertheless, there have been a few studies that excluded eyes with CME, and examined the relationship between OCTA metrics and visual acuity in the absence of this potential confounder. These studies have still found significant correlations between visual acuity and OCTA parameters such as FAZ diameter in the DCP, and FAZ size in the SCP (62, 65) This suggests that OCTA metrics can be useful biomarkers for identifying and monitoring macular ischemia, and can be informative for visual prognostication in RVOs.

3.3. OCTA and cystoid macular edema

As with UWF FA, various OCTA metrics have also been associated with the presence of persistent CME in RVOs. Given the greater field of view and advantages of UWF FA, these studies have concentrated mainly on the overall extent and location (peripheral vs. posterior) of non-perfusion areas and CME (29–31). In contrast, while OCTA provides a more limited field of view, this modality has the key advantage of providing depth-resolved analysis of the different

vascular plexuses, including the SCP and DCP. This has allowed for analysis of relative differences between perfusion areas in the SCP and DCP, and their relation to CME.

OCTA studies have observed that RVOs with CME demonstrate areas of decreased or absent flow in the DCP, and that CME tends to recur in these regions (54, 66). It has been postulated that these areas of absent flow or "perfusion gaps" in the DCP affect intraretinal fluid management, and may therefore contribute to the occurrence or persistence of CME (66). A few studies have examined this question retrospectively. Tsuboi et al. identified areas with "gap vessels" where there was selective DCP loss, by subtracting DCP vessel images from the corresponding SCP vessel images (67). In 20 eyes with BRVO, they showed that areas with gap vessels were significantly larger in eyes that had persistent CME, compared to those without. In a similar vein, Bae et al. evaluated perfusion gaps in 19 eyes with BRVO and CME, and also concluded that larger perfusion gaps (on 12×12 mm OCTA scans) were associated with greater anti-VEGF treatment burden for CME (68). Yeung et al. used a slightly different metric, by quantifying deep-superficial flow ratio (DSFR), which was calculated by dividing DCP vessel density by SCP vessel density (69). They showed in 30 eyes with BRVO that DSFR was significantly lower in eyes with refractory CME, compared to those with a better treatment response. One potential concern with this approach is that the temporal and causative relationships between DCP perfusion gaps and areas of CME have not been definitively established. It is currently not clear whether perfusion gaps occur first and lead to CME, or whether areas of CME develop first (e.g., due to vascular leakage or other mechanisms) and result in displacement of DCP vessels forming "gaps." This highlights the need for longitudinal studies in this area.

3.4. Non-perfusion on OCTA

As outlined above, detection of significant areas of retinal non-perfusion is one of the main clinical indications for performing FA or UWF FA in RVOs. As with FA, areas of retinal non-perfusion can also be detected and quantified on OCTA. Table 1 summarizes the advantages and disadvantages of using OCTA for the detection of retinal non-perfusion. FA has been the gold standard for determination of retinal non-perfusion, and it has been important to establish that areas of non-perfusion on OCTA match those on FA. Most studies examining this question in retinal vascular diseases have shown that there is good and substantial agreement between FA and OCTA (70–73). Firstly, in DR, Sawada et al. showed that OCTA (12×12 mm scans) could detect areas of non-perfusion qualitatively as well as UWF FA (70). Similarly, in a cohort of eyes with DR, Hirano et al. also showed very high levels of agreement for non-perfusion between 12×12 mm OCTA scans and FA (72). In that study, OCTA detected areas of non-perfusion with 95% sensitivity and 100% specificity, and when they compared the quantified areas of non-perfusion between the two modalities, they were highly concordant (72). There is also good evidence to support that this correlation is true in RVO eyes as well. Kadomoto et al. showed that areas of non-perfusion correlated well between OCTA and UWF FA in BRVO (73). Shiraki et al. also examined a cohort of eyes with BRVO who had both OCTA and UWF FA performed. Within the same areas that were imaged on both modalities, they found excellent correlation in non-perfusion areas quantified by the two modalities ($R^2 = 0.9429$, $p < 0.0001$) (71). To our knowledge, there has been one report of significant discrepancies between OCTA and UWF FA in non-perfusion areas in DR (45). In this study, the authors examined both OCTA and UWF FA images before and after intravitreal anti-VEGF treatment, to see if there were significant changes in retinal perfusion. There were apparent areas of re-perfusion on UWF FA, but OCTA in the same areas demonstrated clearly that this was not the case. The authors attributed this spurious re-perfusion on UWF FA as likely due to changes in choroidal background fluorescence, and suggested therefore that OCTA may be a more accurate modality for quantifying retinal non-perfusion than FA (45). Figure 3 shows paired standard FA and OCTA images from the same eye with a BRVO, demonstrating this phenomenon, where clear areas of non-perfusion on the OCTA image are easily missed on FA, due to increased underlying choroidal background fluorescence.

While OCTA may be more convenient, faster, and potentially more accurate for quantification of retinal non-perfusion in comparison to FA, the limitation of current OCTA technology is in field of view. Current commercial OCTA platforms are able to image up to 12×12 mm scans, and can cover larger areas with image montage, but this field of view is still much less than UWF FA is able to achieve (Figure 4). Nevertheless, many groups have attempted to see if OCTA of the posterior retina is able to infer peripheral retinal non-perfusion as well. These studies have generally shown that OCTA metrics and non-perfusion from the posterior retina correlate well with peripheral non-perfusion as revealed by UWF FA (64, 74–77). Huang et al. showed that non-perfusion areas on a 3×3 mm OCTA scan correlated well with non-perfusion area ($R = 0.688$, $p < 0.01$) and ISI ($R = 0.680$, $p < 0.01$) on UWF FA (75). Cavalleri et al. similarly showed that OCTA FAZ area ($R = 0.63$, $p = 0.019$), and vessel density in the SCP ($R = -0.62$, $p = 0.022$) and DCP ($R = -0.66$, $p = 0.011$), all correlated significantly with ISI on UWF FA (77). Ryu et al. looked at multiple OCTA parameters such as vessel density and FD from the SCP and DCP on 6×6 mm OCTA scans and demonstrated that they all correlated with ISI on UWF FA. When attempting to use OCTA parameters to detect "severe retinal ischemia" (defined as ISI > 10%), all the OCTA parameters achieved an area under the receiver operating characteristic curve (AUC) of >0.9, with FD in the DCP showing the greatest classification performance (AUC = 0.948). Based on their series, they were also able to suggest a cut-off of 5.39% for FD, which would perform well in detection of "severe retinal ischemia" (74). Glacet-Bernard et al. showed that vessel density in the SCP and DCP on 12×12 mm OCTA scans correlated significantly with ISI on UWF FA, and that OCTA had 100% sensitivity and 64% specificity for detection of "marked nonperfusion" (defined as ISI ≥ 25%) on UWF FA (76).

The evidence from these studies suggests that although the extent of peripheral retina that can be assessed with OCTA is currently limited, OCTA of the posterior/central retina can still reliably infer areas of non-perfusion in the retinal periphery. Most of these authors suggest therefore, that OCTA can be used as a non-invasive, convenient "screening tool," to identify those eyes who are at risk of having significant peripheral non-perfusion, which would then benefit from an UWF FA procedure.

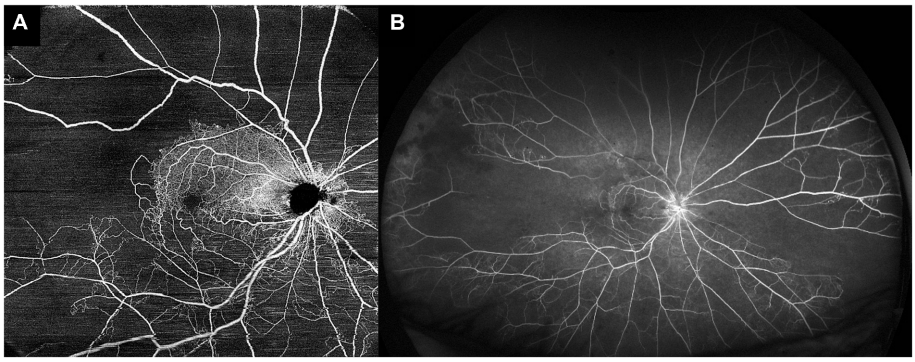

FIGURE 4
Comparison of optical coherence tomography angiography (OCTA) and ultra-widefield fluorescein angiography (UWF FA) in the same eye. **(A)** 15×15mm montaged OCTA image of a central retinal vein occlusion, allowing for visualization of the posterior pole and some of the mid-peripheral retina. **(B)** UWF FA image of the same eye, showing a much wider field of view, and demonstrating significant areas of peripheral retinal non-perfusion that were not detectable with the field of view of the OCTA image.

3.5. OCTA and neovascularization

Similar to how the definition of an "ischemic" RVO needs to be re-examined in UWF FA, some groups have attempted to try and re-define "ischemic" RVOs using OCTA, though this work is still in its initial stages. An et al. performed a cross-sectional study on eyes with CRVO, where they classified them into ischemic or non-ischemic based on areas of non-perfusion on FA (78). They then showed that ischemic CRVOs had lower SCP and DCP vessel densities and larger FAZ area on 3 × 3 mm OCTA scans. They suggested that DCP vessel density was the best parameter for classification, with an AUC of 0.962, and with a threshold of ≤38.4%, DCP vessel density achieved 100% sensitivity and 92.3% specificity for classifying ischemic CRVOs. Khodabandeh et al. used OCT 3 × 3 mm and 8 × 8 mm OCTA scans to classify CRVOs as ischemic, based on the presence of a relative afferent pupillary defect and visual acuity worse than 20/200. Ischemic CRVOs by this definition had lower SCP and DCP vessel densities, and their best-performing classification model had an AUC of 0.84, with 100% sensitivity and 64% specificity (79). The major drawback to both these studies is that their definitions of "ischemic" CRVOs were cross-sectional, and based on imperfect ground truth classifications. Ideally, this question should be investigated with a longitudinal natural history study, with baseline OCTA metrics, and longitudinal observation for neovascularization and associated complications. Kadomoto et al. undertook a small longitudinal cohort study of 26 patients with treatment-naïve BRVOs, performed "baseline" OCTA after 3 monthly anti-VEGF injections, and followed them prospectively for the development of neovascularization over another 9 months (73). They reported that larger non-perfusion areas on OCTA were associated with the development of neovascularization. Similar longitudinal studies, on a larger scale, will be necessary to re-define "ischemic" RVOs using baseline OCTA metrics. Nevertheless, this remains a promising approach. More recently, an international expert consensus group on OCTA imaging published a report recommending that OCTA can be used to define an "ischemic" CRVO, and suggested that because OCTA fields of view vary among different devices, that such definitions should be based on a percentage of the absolute imaged area in which there is "no flow" or non-perfusion (80). They further suggested that ≥30% of "no-flow area" be used to define an ischemic CRVO, though this was a recommendation, and not based on actual cross-sectional or longitudinal data defining risk of neovascularization. This definition will need to be validated in future studies.

OCTA can also be very useful for diagnosis of retinal neovascularization in select cases. Retinal neovascularization is defined as a vascular structure with demonstrable flow anterior to the internal limiting membrane (ILM), and it has been shown that OCTA is very useful for diagnosis of neovascularization and differentiating them from intraretinal microvascular abnormalities (IRMAs) in DR (81). Arya et al. reported that OCTA had 92% sensitivity and 99% specificity for differentiating neovascularization from IRMAs in DR (81). Similarly in RVOs, there may be some suspicious collateral vessels (which by definition are intraretinal, and do not cross the ILM), that can be clinically difficult to differentiate from neovascularization, and OCTA can be an effective, convenient and non-invasive tool in this scenario. Sakimoto et al. reported a case where OCTA effectively clinched the diagnosis of neovascularization after a BRVO (82). In their case, OCTA demonstrated definite retinal neovascularization from about 6 months after presentation, which was not evident on FA. On FA there was some diffuse hyperfluorescence that looked like apparent retinal re-perfusion, without significant leakage. This is an example of a case where OCTA was the better imaging modality for diagnosing neovascularization.

In cases of established retinal neovascularization, OCTA provides much better cross-sectional detail and structural characterization than FA. Sogawa et al. published an example of this, where OCTA demonstrated a retinal neovascular membrane after a BRVO more clearly than FA, and could provide detailed structural information (83). They were able to show with OCTA that the outer border of the neovascularization consisted of looping radial peripapillary capillaries, and that the posterior hyaloid was firmly adherent to the neovascularization, which may have further prognostic and management implications. Huemer et al. looked at a larger series of retinal neovascularization after ischemic RVOs, and could on the basis of OCTA structure, classify the neovascular tufts into different phenotypic types, such as sea-fan or nodular types (84). They found in their series of ischemic RVOs that OCTA had a much higher detection rate for neovascularization than clinical examination, and even detected one case that was missed on UWF FA. That lesion was of the nodular type, which the authors suggest can be easily mistaken for hemorrhage on clinical examination, and which is difficult to detect on FA because

they may not leak significantly. Though classification of neovascularization is now possible with OCTA into different structural phenotypes, the clinical implications and outcomes of these different phenotypes are as yet unclear. OCTA could also be used to follow longitudinal changes in neovascular tufts after treatment to determine regression or the presence of persistent flow, though the clinical implications of these would need to be similarly validated (84, 85). Table 1 summarizes the main advantages of using OCTA to detect neovascularization.

3.6. Drawbacks of OCTA

OCTA technology is clearly promising, and has the potential to provide important angiographic information in a non-invasive manner, to inform prognosis and management of retinal vascular diseases. Nevertheless, this technology has important limitations and drawbacks, some of which have been discussed above (Table 1). The first, and arguably most important limitation, is the heterogeneity and lack of standardization in the field (80, 86). There are multiple different commercial OCTA platforms, using different proprietary algorithms, and providing different quantitative metrics, which are not interchangeable. There are currently no well-established, standardized guidelines for studies reporting OCTA metrics or outcomes. These factors significantly limit the reproducibility and quality of the evidence available for OCTA, which in turn limits the incorporation of OCTA into daily clinical practice and decision-making. There are ongoing efforts among international expert consensus groups to address this issue, and we can expect that more standardized guidelines and nomenclature will be forthcoming soon (80, 86). Second, it is evident from this review that the large majority of evidence for the use of OCTA in RVOs is based on cross-sectional studies. Prospective, longitudinal studies in this area are few, but they are needed for robust validation of OCTA metrics and cut-offs for clinical use. Third, there are still technological limitations, such as issues with image artefacts, quality and gradability issues, and limited field of view. However, OCTA technology is improving rapidly, and we expect that the impact of these technological limitations can be minimized with time.

4. Conclusion

Imaging technology such as UWF FA and OCTA clearly provide a wealth of new information over standard FA imaging techniques, that has the potential to improve clinical management in patients with RVO. Certain key characteristics of these imaging platforms are important advantages for clinical utility—such as the evaluation of a much larger area of the retinal periphery for UWF FA, and the non-invasive, quantitative nature of OCTA. Consequently, by providing more information on perfusion in the peripheral retina, UWF FA in clinical practice has the potential to improve risk stratification and prognostication for neovascularization and CME in RVOs, without any major added drawbacks over standard FA technology. OCTA provides non-invasive information on retinal perfusion, which can inform the need for more invasive dye-based angiography, and also has the potential to provide effective prognostication of important clinical outcomes, such as neovascularization, CME, and eventual visual acuity. Major unmet needs in the field are that of standardization and validation of clinically useful cut-offs with prospective, longitudinal data. These imaging tools have already proved useful in clinical practice for management of RVOs, and as more evidence becomes available to guide our management, they will continue to further improve clinical outcomes for patients with RVO.

Author contributions

T-ET and KT contributed to conception of the study. T-ET, FI, PC, and KT contributed to drafting and revising the manuscript. All authors contributed to the article and approved the submitted version.

Conflict of interest

The authors declare that the research was conducted in the absence of any commercial or financial relationships that could be construed as a potential conflict of interest.

Publisher's note

References

1. Song P, Xu Y, Zha M, Zhang Y, Rudan I. Global epidemiology of retinal vein occlusion: a systematic review and meta-analysis of prevalence, incidence, and risk factors. *J Glob Health*. (2019) 9:010427. doi: 10.7189/jogh.09.010427

2. Wong TY, Scott IU. Clinical practice. Retinal-vein occlusion. *N Engl J Med*. (2010) 363:2135–44. doi: 10.1056/NEJMcp1003934

3. Rogers S, McIntosh RL, Cheung N, Lim L, Wang JJ, Mitchell P, et al. The prevalence of retinal vein occlusion: pooled data from population studies from the United States, Europe, Asia, and Australia. *Ophthalmology*. (2010) 117:313–319.e1. doi: 10.1016/j.ophtha.2009.07.017

4. Campochiaro PA, Heier JS, Feiner L, Gray S, Saroj N, Rundle AC, et al. Ranibizumab for macular edema following branch retinal vein occlusion: six-month primary end point results of a phase III study. *Ophthalmology*. (2010) 117:1102–1112.e1. doi: 10.1016/j.ophtha.2010.02.021

5. Brown DM, Campochiaro PA, Singh RP, Li Z, Gray S, Saroj N, et al. Ranibizumab for macular edema following central retinal vein occlusion: six-month primary end point results of a phase III study. *Ophthalmology*. (2010) 117:1124–1133.e1. doi: 10.1016/j.ophtha.2010.02.022

6. Haller JA, Bandello F, Belfort R Jr, Blumenkranz MS, Gillies M, Heier J, et al. Randomized, sham-controlled trial of dexamethasone intravitreal implant in patients with macular edema due to retinal vein occlusion. *Ophthalmology*. (2010) 117:1134–1146.e3. doi: 10.1016/j.ophtha.2010.03.032

7. The Branch Vein Occlusion Study Group. Argon laser photocoagulation for macular edema in branch vein occlusion. *Am J Ophthalmol*. (1984) 98:271–82. doi: 10.1016/0002-9394(84)90316-7

8. Branch Vein Occlusion Study Group. Argon laser scatter photocoagulation for prevention of neovascularization and vitreous hemorrhage in branch vein occlusion. A

randomized clinical trial. *Arch Ophthalmol*. (1986) 104:34–41. doi: 10.1001/archopht.1986.01050130044017

9. The Central Vein Occlusion Study Group. Natural history and clinical management of central retinal vein occlusion. *Arch Ophthalmol*. (1997) 115:486–91. doi: 10.1001/archopht.1997.01100150488006

10. The Central Vein Occlusion Study Group N Report. A randomized clinical trial of early panretinal photocoagulation for ischemic central vein occlusion. *Ophthalmology*. (1995) 102:1434–44. doi: 10.1016/S0161-6420(95)30848-2

11. Yannuzzi LA, Rohrer KT, Tindel LJ, Sobel RS, Costanza MA, Shields W, et al. Fluorescein angiography complication survey. *Ophthalmology*. (1986) 93:611–7. doi: 10.1016/s0161-6420(86)33697-2

12. Choudhry N, Duker JS, Freund KB, Kiss S, Querques G, Rosen R, et al. Classification and guidelines for widefield imaging: recommendations from the international Widefield imaging study group. *Ophthalmol Retina*. (2019) 3:843–9. doi: 10.1016/j.oret.2019.05.007

13. Spaide RF, Fujimoto JG, Waheed NK, Sadda SR, Staurenghi G. Optical coherence tomography angiography. *Prog Retin Eye Res*. (2018) 64:1–55. doi: 10.1016/j.preteyeres.2017.11.003

14. Early Treatment Diabetic Retinopathy Study Research Group. Grading diabetic retinopathy from stereoscopic color fundus photographs--an extension of the modified Airlie house classification. ETDRS Report Number 10. *Ophthalmology*. (1991) 98:786–806. doi: 10.1016/S0161-6420(13)38012-9

15. Byberg S, Vistisen D, Diaz L, Charles MH, Hajari JN, Valerius M, et al. Optos wide-field imaging versus conventional camera imaging in Danish patients with type 2 diabetes. *Acta Ophthalmol*. (2019) 97:815–20. doi: 10.1111/aos.14118

16. Silva PS, Cavallerano JD, Haddad NMN, Kwak H, Dyer KH, Omar AF, et al. Peripheral lesions identified on ultrawide field imaging predict increased risk of diabetic retinopathy progression over 4 years. *Ophthalmology*. (2015) 122:949–56. doi: 10.1016/j.ophtha.2015.01.008

17. Silva PS, Cavallerano JD, Sun JK, Soliman AZ, Aiello LM, Aiello LP. Peripheral lesions identified by mydriatic ultrawide field imaging: distribution and potential impact on diabetic retinopathy severity. *Ophthalmology*. (2013) 120:2587–95. doi: 10.1016/j.ophtha.2013.05.004

18. Price LD, Au S, Chong NV. Optomap ultrawide field imaging identifies additional retinal abnormalities in patients with diabetic retinopathy. *Clin Ophthalmol*. (2015) 9:527–31. doi: 10.2147/OPTH.S79448

19. Silva PS, El-Rami H, Barham R, Gupta A, Fleming A, van Hemert J, et al. Hemorrhage and/or microaneurysm severity and count in ultrawide field images and early treatment diabetic retinopathy study photography. *Ophthalmology*. (2017) 124:970–6. doi: 10.1016/j.ophtha.2017.02.012

20. Aiello LP, Odia I, Glassman AR, Melia M, Jampol LM, Bressler NM, et al. Comparison of early treatment diabetic retinopathy study standard 7-field imaging with Ultrawide-field imaging for determining severity of diabetic retinopathy. *JAMA Ophthalmol*. (2019) 137:65–73. doi: 10.1001/jamaophthalmol.2018.4982

21. Marcus DM, Silva PS, Liu D, Aiello LP, Antoszyk A, Elman M, et al. Association of predominantly peripheral lesions on ultra-widefield imaging and the risk of diabetic retinopathy worsening over time. *JAMA Ophthalmol*. (2022) 140:946–54. doi: 10.1001/jamaophthalmol.2022.3131

22. Silva PS, Marcus DM, Liu D, Aiello LP, Antoszyk A, Elman M, et al. Association of ultra-widefield fluorescein angiography-identified retinal nonperfusion and the risk of diabetic retinopathy worsening over time. *JAMA Ophthalmol*. (2022) 140:936–45. doi: 10.1001/jamaophthalmol.2022.3130

23. Turczyńska MJ, Krajewski P, Brydak-Godowska JE. Wide-field fluorescein angiography in the diagnosis and management of retinal vein occlusion: a retrospective single-center study. *Med Sci Monit*. (2021) 27:e927782. doi: 10.12659/MSM.927782

24. Hayreh SS, Zimmerman MB. Ocular neovascularization associated with central and hemicentral retinal vein occlusion. *Retina (Philadelphia, PA)*. (2012) 32:1553–65. doi: 10.1097/IAE.0b013e318246912c

25. Nicholson L, Vazquez-Alfageme C, Patrao NV, Triantafyllopolou I, Bainbridge JW, Hykin PG, et al. Retinal nonperfusion in the posterior pole is associated with increased risk of neovascularization in central retinal vein occlusion. *Am J Ophthalmol*. (2017) 182:118–25. doi: 10.1016/j.ajo.2017.07.015

26. Tsui I, Kaines A, Havunjian MA, Hubschman S, Heilweil G, Prasad PS, et al. Ischemic index and neovascularization in central retinal vein occlusion. *Retina*. (2011) 31:105–10. doi: 10.1097/IAE.0b013e3181e36c6d

27. Thomas AS, Thomas MK, Finn AP, Fekrat S. Use of the ischemic index on WIDEFIELD fluorescein angiography to characterize a central retinal vein occlusion as ischemic or nonischemic. *Retina*. (2019) 39:1033–8. doi: 10.1097/IAE.0000000000002126

28. Ryu G, Noh D, van Hemert J, Sadda SR, Sagong M. Relationship between distribution and severity of non-perfusion and cytokine levels and macular thickness in branch retinal vein occlusion. *Sci Rep*. (2021) 11:271. doi: 10.1038/s41598-020-79522-5

29. Prasad PS, Oliver SCN, Coffee RE, Hubschman J-P, Schwartz SD. Ultra wide-field angiographic characteristics of branch retinal and hemicentral retinal vein occlusion. *Ophthalmology*. (2010) 117:780–4. doi: 10.1016/j.ophtha.2009.09.019

30. Singer M, Tan CS, Bell D, Sadda SR. Area of peripheral retinal nonperfusion and treatment response in branch and central retinal vein occlusion. *Retina*. (2014) 34:1736–42. doi: 10.1097/IAE.0000000000000148

31. Kwon S, Wykoff CC, Brown DM, van Hemert J, Fan W, Sadda SR. Changes in retinal ischaemic index correlate with recalcitrant macular oedema in retinal vein occlusion: wave study. *Br J Ophthalmol*. (2018) 102:1066–71. doi: 10.1136/bjophthalmol-2017-311475

32. Sakimoto S, Kamei M, Suzuki M, Yano S, Matsumura N, Sakaguchi H, et al. Relationship between grades of macular perfusion and foveal thickness in branch retinal vein occlusion. *Clin Ophthalmol*. (2013) 7:39–45. doi: 10.2147/OPTH.S37185

33. Wang X, Sun G, Yi Z, Xu A, He L, Jiang J, et al. Leakage index on ultra-widefield fluorescence angiography in different regions of retina and its correlation with cystoid macular edema in central retinal vein occlusion eyes. *Graefes Arch Clin Exp Ophthalmol*. (2021) 259:2149–56. doi: 10.1007/s00417-021-05126-y

34. Abri Aghdam K, Reznicek L, Soltan Sanjari M, Klingenstein A, Kernt M, Seidensticker F. Anti-VEGF treatment and peripheral retinal nonperfusion in patients with central retinal vein occlusion. *Clin Ophthalmol*. (2017) 11:331–6. doi: 10.2147/OPTH.S125486

35. Tomomatsu Y, Tomomatsu T, Takamura Y, Gozawa M, Arimura S, Takihara Y, et al. Comparative study of combined bevacizumab/targeted photocoagulation vs bevacizumab alone for macular oedema in ischaemic branch retinal vein occlusions. *Acta Ophthalmol*. (2016) 94:e225–30. doi: 10.1111/aos.12721

36. Goel S, Kumar A, Ravani RD, Chandra P, Chandra M, Kumar V. Comparison of ranibizumab alone versus ranibizumab with targeted retinal laser for branch retinal vein occlusion with macular edema. *Indian J Ophthalmol*. (2019) 67:1105–8. doi: 10.4103/ijo.IJO_1364_18

37. Wykoff CC, Ou WC, Wang R, Brown DM, Cone C, Zamora D, et al. Peripheral laser for recalcitrant macular edema owing to retinal vein occlusion: the WAVE trial. *Ophthalmology*. (2017) 124:919–21. doi: 10.1016/j.ophtha.2017.01.049

38. Campochiaro PA, Hafiz G, Mir TA, Scott AW, Solomon S, Zimmer-Galler I, et al. Scatter photocoagulation does not reduce macular edema or treatment burden in patients with retinal vein occlusion: the RELATE trial. *Ophthalmology*. (2015) 122:1426–37. doi: 10.1016/j.ophtha.2015.04.006

39. Tsui I, Williams BK, Kok YO, Heilweil G, Schwartz SD. Reliability of ischemic index grading in common retinal vascular diseases. *Ophthalmic Surg Lasers Imaging Retina*. (2015) 46:618–25. doi: 10.3928/23258160-20150610-04

40. Tan CS, Chew MC, van Hemert J, Singer MA, Bell D, Sadda SR. Measuring the precise area of peripheral retinal non-perfusion using ultra-widefield imaging and its correlation with the ischaemic index. *Br J Ophthalmol*. (2016) 100:235–9. doi: 10.1136/bjophthalmol-2015-306652

41. Fan W, Fleming A, Hemert JV, Wykoff CC, Brown DM, Robertson G, et al. Retinal vascular bed area in eyes with retinal vein occlusion on ultra-widefield fluorescein angiography: WAVE study. *Retina*. (2022) 42:1883–8. doi: 10.1097/IAE.0000000000003549

42. Sagong M, van Hemert J, Olmos de Koo LC, Barnett C, Sadda SR. Assessment of accuracy and precision of quantification of ultra-widefield images. *Ophthalmology*. (2015) 122:864–6. doi: 10.1016/j.ophtha.2014.11.016

43. Nagiel A, Lalane RA, Sadda SR, Schwartz SD. Ultra-widefield fundus imaging: a review of clinical applications and future trends. *Retina (Philadelphia, PA)*. (2016) 36:660–78. doi: 10.1097/IAE.0000000000000937

44. Tan CS, Li KZ, Sadda SR. Wide-field angiography in retinal vein occlusions. *Int J Retina Vitreous*. (2019) 5:18. doi: 10.1186/s40942-019-0163-1

45. Couturier A, Rey P-A, Erginay A, Lavia C, Bonnin S, Dupas B, et al. Widefield OCT-angiography and fluorescein angiography assessments of nonperfusion in diabetic retinopathy and edema treated with anti-vascular endothelial growth factor. *Ophthalmology*. (2019) 126:1685–94. doi: 10.1016/j.ophtha.2019.06.022

46. Wang X, Ji Z, Ma X, Zhang Z, Yi Z, Zheng H, et al. Automated grading of diabetic retinopathy with ultra-widefield fluorescein angiography and deep learning. *J Diabetes Res*. (2021) 2021:2611250–9. doi: 10.1155/2021/2611250

47. Lee P-K, Ra H, Baek J. Automated segmentation of ultra-widefield fluorescein angiography of diabetic retinopathy using deep learning. *Br J Ophthalmol*. (2022):bjophthalmol-2022-321063. doi: 10.1136/bjo-2022-321063

48. Chen C-L, Wang RK. Optical coherence tomography based angiography [invited]. *Biomed Opt Express*. (2017) 8:1056–82. doi: 10.1364/BOE.8.001056

49. Kadomoto S, Uji A, Muraoka Y, Akagi T, Miyata M, Tsujikawa A. A novel strategy for quantification of panoramic en face optical coherence tomography angiography scan field. *Graefes Arch Clin Exp Ophthalmol*. (2019) 257:1199–206. doi: 10.1007/s00417-019-04310-5

50. Suzuki N, Hirano Y, Yoshida M, Tomiyasu T, Uemura A, Yasukawa T, et al. Microvascular abnormalities on optical coherence tomography angiography in macular edema associated with branch retinal vein occlusion. *Am J Ophthalmol*. (2016) 161:126–132.e1. doi: 10.1016/j.ajo.2015.09.038

51. Kashani AH, Lee SY, Moshfeghi A, Durbin MK, Puliafito CA. Optical coherence tomography angiography of retinal venous occlusion. *Retina*. (2015) 35:2323–31. doi: 10.1097/IAE.0000000000000811

52. Nobre Cardoso J, Keane PA, Sim DA, Bradley P, Agrawal R, Addison PK, et al. Systematic evaluation of optical coherence tomography angiography in retinal vein occlusion. *Am J Ophthalmol*. (2016) 163:93–107.e6. doi: 10.1016/j.ajo.2015.11.025

53. Adhi M, Filho MAB, Louzada RN, Kuehlewein L, de Carlo TE, Baumal CR, et al. Retinal capillary network and Foveal avascular zone in eyes with vein occlusion and fellow eyes analyzed with optical coherence tomography angiography. *Invest Ophthalmol Vis Sci*. (2016) 57:OCT486–94. doi: 10.1167/iovs.15-18907

54. Coscas F, Glacet-Bernard A, Miere A, Caillaux V, Uzzan J, Lupidi M, et al. Optical coherence tomography angiography in retinal vein occlusion: evaluation of superficial and deep capillary Plexa. *Am J Ophthalmol*. (2016) 161:160–171.e1-2. doi: 10.1016/j.ajo.2015.10.008

55. Tsai G, Banaee T, Conti FF, Singh RP. Optical coherence tomography angiography in eyes with retinal vein occlusion. *J Ophthalmic Vis Res*. (2018) 13:315–32. doi: 10.4103/jovr.jovr_264_17

56. Fan L, Zhu Y, Liao R. Evaluation of macular microvasculature and foveal avascular zone in patients with retinal vein occlusion using optical coherence tomography angiography. *Int Ophthalmol*. (2022) 42:211–8. doi: 10.1007/s10792-021-02015-5

57. Rispoli M, Savastano MC, Lumbroso B. Capillary network anomalies in branch retinal vein occlusion on optical coherence tomography angiography. *Retina*. (2015) 35:2332–8. doi: 10.1097/IAE.0000000000000845

58. Ouederni M, Khalifa MBH, Sassi H, Nefaa F, Ayed O, Cheour M. Quantitative analysis of microvascular network with optical coherence tomography angiography and its correlation with visual acuity in retinal vein occlusion. *J Curr Ophthalmol*. (2021) 33:453–60. doi: 10.4103/joco.joco_163_21

59. Kang J-W, Yoo R, Jo YH, Kim HC. Correlation of microvascular structures on optical coherence tomography angiography with visual acuity in retinal vein occlusion. *Retina*. (2017) 37:1700–9. doi: 10.1097/IAE.0000000000001403

60. Koulisis N, Kim AY, Chu Z, Shahidzadeh A, Burkemper B, Olmos de Koo LC, et al. Quantitative microvascular analysis of retinal venous occlusions by spectral domain optical coherence tomography angiography. *PLoS One*. (2017) 12:e0176404. doi: 10.1371/journal.pone.0176404

61. Suzuki N, Hirano Y, Tomiyasu T, Esaki Y, Uemura A, Yasukawa T, et al. Retinal hemodynamics seen on optical coherence tomography angiography before and after treatment of retinal vein occlusion. *Invest Ophthalmol Vis Sci*. (2016) 57:5681–7. doi: 10.1167/iovs-16-20648

62. Wons J, Pfau M, Wirth MA, Freiberg FJ, Becker MD, Michels S. Optical coherence tomography angiography of the foveal avascular zone in retinal vein occlusion. *Ophthalmologica*. (2016) 235:195–202. doi: 10.1159/000445482

63. Chung CY, Tang HHY, Li SH, Li KKW. Differential microvascular assessment of retinal vein occlusion with coherence tomography angiography and fluorescein angiography: a blinded comparative study. *Int Ophthalmol*. (2018) 38:1119–28. doi: 10.1007/s10792-017-0570-y

64. Seknazi D, Coscas F, Sellam A, Rouimi F, Coscas G, Souied EH, et al. Optical coherence tomography angiography in retinal vein occlusion: correlations between macular vascular density, visual acuity, and peripheral nonperfusion area on fluorescein angiography. *Retina*. (2018) 38:1562–70. doi: 10.1097/IAE.0000000000001737

65. Casselholmde Salles M, Kvanta A, Amrén U, Epstein D. Optical coherence tomography angiography in central retinal vein occlusion: correlation between the foveal avascular zone and visual acuity. *Invest Ophthalmol Vis Sci*. (2016) 57:OCT242–6. doi: 10.1167/iovs.15-18819

66. Spaide RF. Retinal vascular cystoid macular edema: review and new theory. *Retina*. (2016) 36:1823–42. doi: 10.1097/IAE.0000000000001158

67. Tsuboi K, Ishida Y, Kamei M. Gap in capillary perfusion on optical coherence tomography angiography associated with persistent macular edema in branch retinal vein occlusion. *Invest Ophthalmol Vis Sci*. (2017) 58:2038–43. doi: 10.1167/iovs.17-21447

68. Bae K, Bang S-K, Kang SW, Kim ES, Yu S-Y. Gap in capillary perfusion and burden of treatment in branch retinal vein occlusion: a wide-field optical coherence tomography angiography study. *Retina*. (2021) 41:1227–35. doi: 10.1097/IAE.0000000000003006

69. Yeung L, Wu W-C, Chuang L-H, Wang N-K, Lai C-C. Novel optical coherence tomography angiography biomarker in branch retinal vein occlusion macular edema. *Retina*. (2019) 39:1906–16. doi: 10.1097/IAE.0000000000002264

70. Sawada O, Ichiyama Y, Obata S, Ito Y, Kakinoki M, Sawada T, et al. Comparison between wide-angle OCT angiography and ultra-wide field fluorescein angiography for detecting non-perfusion areas and retinal neovascularization in eyes with diabetic retinopathy. *Graefes Arch Clin Exp Ophthalmol*. (2018) 256:1275–80. doi: 10.1007/s00417-018-3992-y

71. Shiraki A, Sakimoto S, Tsuboi K, Wakabayashi T, Hara C, Fukushima Y, et al. Evaluation of retinal nonperfusion in branch retinal vein occlusion using wide-field optical coherence tomography angiography. *Acta Ophthalmol*. (2019) 97:e913–8. doi: 10.1111/aos.14087

72. Hirano T, Kakihara S, Toriyama Y, Nittala MG, Murata T, Sadda S. Wide-field en face swept-source optical coherence tomography angiography using extended field imaging in diabetic retinopathy. *Br J Ophthalmol*. (2018) 102:1199–203. doi: 10.1136/bjophthalmol-2017-311358

73. Kadomoto S, Muraoka Y, Uji A, Tamiya R, Oritani Y, Kawai K, et al. Nonperfusion area quantification in branch retinal vein occlusion: a widefield optical coherence tomography angiography study. *Retina*. (2021) 41:1210–8. doi: 10.1097/IAE.0000000000002999

74. Ryu G, Park D, Lim J, van Hemert J, Sagong M. Macular microvascular changes and their correlation with peripheral nonperfusion in branch retinal vein occlusion. *Am J Ophthalmol*. (2021) 225:57–68. doi: 10.1016/j.ajo.2020.12.026

75. Huang J, Lu Y, Gu X, Zheng B, Chen T. Correlation between the nonperfusion area on ultra-widefield fluorescein angiography and nonflow area on optical coherence tomographic angiography in retinal vein occlusion. *J Ophthalmol*. (2021) 2021:5581319. doi: 10.1155/2021/5581319

76. Glacet-Bernard A, Miere A, Houmane B, Tilleul J, Souied E. Nonperfusion assessment in retinal vein occlusion: comparison between ultra-widefield fluorescein angiography and widefield optical coherence tomography angiography. *Retina*. (2021) 41:1202–9. doi: 10.1097/IAE.0000000000002993

77. Cavalleri M, Sacconi R, Parravano M, Costanzo E, Pezzella M, Bandello F, et al. Optical coherence tomography angiography in central retinal vein occlusion: macular changes and their correlation with peripheral nonperfusion at ultra-widefield fluorescein angiography. *Ophthalmologica*. (2022) 245:275–84. doi: 10.1159/000522503

78. An W, Zhao Q, Yu R, Han J. The role of optical coherence tomography angiography in distinguishing ischemic versus non-ischemic central retinal vein occlusion. *BMC Ophthalmol*. (2022) 22:413. doi: 10.1186/s12886-022-02637-y

79. Khodabandeh A, Shahraki K, Roohipoor R, Riazi-Esfahani H, Yaseri M, Faghihi H, et al. Quantitative measurement of vascular density and flow using optical coherence tomography angiography (OCTA) in patients with central retinal vein occlusion: can OCTA help in distinguishing ischemic from non-ischemic type? *Int J Retina Vitreous*. (2018) 4:47. doi: 10.1186/s40942-018-0152-9

80. Munk MR, Kashani AH, Tadayoni R, Korobelnik J-F, Wolf S, Pichi F, et al. Recommendations for OCT angiography reporting in retinal vascular disease: A Delphi approach by international experts. *Ophthalmol Retina*. (2022) 6:753–61. doi: 10.1016/j.oret.2022.02.007

81. Arya M, Sorour O, Chaudhri J, Alibhai Y, Waheed NK, Duker JS, et al. Distinguishing intraretinal microvascular abnormalities from retinal neovascularization using optical coherence tomography angiography. *Retina*. (2020) 40:1686–95. doi: 10.1097/IAE.0000000000002671

82. Sakimoto S, Kawasaki R, Nishida K. Retinal neovascularization-simulating retinal capillary reperfusion in branch retinal vein occlusion, imaged by wide-field optical coherence tomography angiography. *JAMA Ophthalmol*. (2020) 138:216–8. doi: 10.1001/jamaophthalmol.2019.5018

83. Sogawa K, Nagaoka T, Ishibazawa A, Takahashi A, Tani T, Yoshida A. En-face optical coherence tomography angiography of neovascularization elsewhere in hemicentral retinal vein occlusion. *Int Med Case Rep J*. (2015) 8:263–6. doi: 10.2147/IMCRJ.S93702

84. Huemer J, Khalid H, Wagner SK, Nicholson L, Fu DJ, Sim DA, et al. Phenotyping of retinal neovascularization in ischemic retinal vein occlusion using wide field OCT angiography. *Eye (Lond)*. (2021) 35:2812–9. doi: 10.1038/s41433-020-01317-9

85. Brar M, Grewal DS, Sharma M, Grewal SPS. Rapid regression of retinal neovascularization following intravitreal bevacizumab in branch retinal vein occlusion imaged by optical coherence tomography angiography. *Indian J Ophthalmol*. (2018) 66:572. doi: 10.4103/ijo.IJO_868_17

86. Munk MR, Kashani AH, Tadayoni R, Korobelnik J-F, Wolf S, Pichi F, et al. Standardization of OCT angiography nomenclature in retinal vascular diseases: first survey results. *Ophthalmol Retina*. (2021) 5:981–90. doi: 10.1016/j.oret.2020.12.022

frontiers | Frontiers in Medicine

TYPE Original Research
PUBLISHED 04 August 2023
DOI 10.3389/fmed.2023.1112396

OPEN ACCESS

EDITED BY
Doina Gherghel,
Aston University, United Kingdom

REVIEWED BY
Christine Cheung,
Nanyang Technological University, Singapore
Pablo De Gracia,
University of Detroit Mercy, United States

*CORRESPONDENCE
Alexandra Benavente-Perez
✉ abenavente@sunyopt.edu

RECEIVED 30 November 2022
ACCEPTED 18 July 2023
PUBLISHED 04 August 2023

CITATION
Lin CR, Toychiev A, Ablordeppey RK, Srinivas M and Benavente-Perez A (2023) Age exacerbates the effect of myopia on retinal capillaries and string vessels.
Front. Med. 10:1112396.
doi: 10.3389/fmed.2023.1112396

Age exacerbates the effect of myopia on retinal capillaries and string vessels

Carol Ren Lin, Abduqodir Toychiev, Reynolds Kwame Ablordeppey, Miduturu Srinivas and Alexandra Benavente-Perez*

Department of Biological Sciences, SUNY College of Optometry, New York, NY, United States

The retinal vasculature supplies oxygen and nutrition to the cells and is crucial for an adequate retinal function. In myopia, excessive eye growth is associated with various anatomical changes that can lead to myopia-related complications. However, how myopia-induced ocular growth affects the integrity of the aged retinal microvasculature at the cellular level is not well understood. Here, we studied how aging interacts with myopia-induced alteration of the retinal microvasculature in fourteen marmoset retinas (*Callithrix jacchus*). String vessel and capillary branchpoint were imaged and quantified in all four capillary plexi of the retinal vasculature. As marmosets with lens-induced myopia aged, they developed increasing numbers of string vessels in all four vascular plexi, with increased vessel branchpoints in the parafoveal and peripapillary retina and decreased vessel branchpoints in the peripheral retina. These myopia-induced changes to the retinal microvasculature suggest an adaptive reorganization of the retinal microvascular cellular structure template with aging and during myopia development and progression.

KEYWORDS

myopia, string vessels, vasculature, marmoset, branchpoints, retina

Introduction

Myopia (nearsightedness) is a refractive error that increases the risk of visual impairment (1–4). It has incurred significant public health implications and is projected to affect 4,758 million people by 2050 (5). Although the increase in myopia prevalence and predicted public health crisis are recognized, the mechanisms that make myopia a significant risk factor for visual impairment remain unknown (1, 2). To date, there are not any available strategies available to prevent myopic degeneration (5).

Myopic eyes experience blur in part due to being larger in size, which can result in compromised vascular support to the inner retina (6). Alterations in the ocular vasculature have been reported in human and experimental models of myopia. Choroidal thinning has been described in human eyes as well as marmosets, mice, and chick models of myopia (7–14). The common marmoset is an established non-human primate (NHP) model that has high predictive value for changes that may occur in human diseases both systemic and ocular (7, 15–19). Both human and primate eyes with no myopic degeneration show larger foveal avascular zones (20), decreased capillary density (5, 21), narrowing of retinal vessel diameters (22), decreased peripheral vessel branching (23), increased parafoveal string vessels (23), and lower central retinal artery blood velocities (22, 24). High myopes with significantly larger eye sizes exhibit

decreased ocular perfusion pressure (OPP) as the subfoveal and peripheral choroid thins (13, 25). In marmosets, the OPP is stable during the first year of life but appears to increase with myopia development, possibly related to the changes in metabolic demand that occur as myopic eyes grow larger (26).

Retinal health relies on the interplay between the vasculature, retinal neurons, glial cells, and the extracellular matrix (27). Together, these cells support normal neuronal function and work to provide nutrition (27), metabolic and homeostatic regulation (27–29), and debris phagocytosis (28). During both normal and abnormal development, the blood vessels, glial cells, and ganglion cells work together in a reciprocal feedback loop (30). With the onset of systemic pathology, the neurovascular unit exerts a biphasic influence, experiencing a remodeling reaction that might be harmful in the acute phase and beneficial in the chronic phase (31). Due to the tight relationship between the components of the neurovascular unit, the vascular changes observed in myopic eyes might in turn impair normal vascular and neuronal function, becoming a part of the series of events preceding overt retinal complications associated with myopia (32, 33). However, despite recent progress in the field, the cumulative effects of myopia development and age on the retinal microvasculature cellular structure remain unexplored.

Here, we describe changes to the retinal microvasculature cellular structure in marmosets of different ages with induced myopia. The assessment of the retinal vasculature in all four capillary plexi during myopia development revealed an increase in string-like formation between vascular capillaries and altered blood vessel branching, which are markers observed in vascular pathologies (34–37).

Methods

Marmoset model of myopia

Seventeen marmoset eyes were studied: five 6-month-old untreated controls, six 6-month-old myopes, three 12-month-old controls, and three 12-month-old myopes. Both cohorts of myopic eyes were induced with myopia by imposing hyperopic defocus using full-field negative single-vision soft contact lenses (−5D and −10D) (23, 27). The normal lifespan of a common marmoset is 7–8 years in captivity and maximum lifespan of 16–21 years (38–41). In summary, animals initiated treatment at 10 weeks of age, and were treated with either −5D or −10D contact lenses for 16 weeks (6-month-old marmosets), or 42 weeks (12-month-old marmosets). Earlier studies and statistical power analysis of the principle methods used indicated that 3 animals per experimental group provided 80% power for our statistical analysis ($n = 3$ younger control, $n = 3$ younger myope, $n = 3$ older control, $n = 3$ older myope). All animal care, treatment, and experimental protocols were approved by the SUNY College of Optometry Institutional Animal Care and Use Committee (IACUC), the ARVO statement for the use of animals in ophthalmic and vision research, the US National Research Council's Guide for the Care and Use of Laboratory Animals, the US Public Health Service's Policy on Humane Care and Use of Laboratory Animals, and the Guide for the Care and Use of Laboratory animals.

At baseline and at end of treatment, cycloplegic refractive error (Rx) and ocular axial length (AL) were measured using the Nidek ARK-700A autorefractor (Nidek Co., LTD, Aichi, Japan) and an ultrasound biometer (Panametrics, NDT Ltd., Waltham, MA, United States) prior to tissue collection under anesthesia (alphaxalone, 15 mg/kg, IM).

Tissue collection

At the end of treatment, eyes were enucleated and placed in phosphate-buffered saline (PBS; ThermoFisher, Waltham, MA, United States). Dissected retinas were fixed in Para-Formaldehyde (PFA) 4% in PBS (Santa Cruz Biotechnology, Dallas, TX, United States) for 40 min, washed five times for 30 min each with PBS, and incubated with 5% normal goat serum (ThermoFisher) and 0.5% TritonX (Sigma Aldrich, St. Louis, MO, United States) blocking buffer to avoid non-specific antibody binding. Following blocking, the retina was incubated with antibodies diluted in blocking buffer at 4°C for 3 days. The antibody used in this study was isolectin–Alexa 488 (1:100; ThermoFisher). After the incubation period, the retinas were washed five times for 30 min each with PBS. SuperFrost slides (ThermoFisher) were cleaned with ethanol prior to plating. Retinas were inspected for any signs of debris, and consistent tissue thickness achieved by pinching and cutting vitreal remains. Retinas were plated and cover slips were placed on objectives with DAPI mounting medium (Vector Laboratories, Newark, CA, United States), were permitted to self-seal, and stored at −20°C.

Confocal microscopy and image acquisition

The immunohistochemical samples were imaged using the Olympus FV1200 MPE confocal microscope. The images were gathered, and the analyses were performed in a randomized manner by one blind investigator. Sixteen images (317 μm × 317 μm along the horizontal plane, and 10 μm along the vertical plane) were taken from each of the fourteen retinas imaged. Multi-plane z-series were collected using a 40× objective, with each section spaced 1 μm apart. These 10 sections were processed by the confocal microscope to form a single z-stack of images subtending the whole specimen. The number of string vessels per mm^2 and vessel branch points per mm^2 were assessed by imaging all four retinal quadrants (temporal, nasal, superior, and inferior) in the periphery, peripapillary, parafoveal, and foveal retina (Figure 1A). After enucleation, right and left eyes were kept separately, and denotation of the temporal region was marked by the presence of the foveal pit (yellow circle, Figure 1A). Nasal is directly opposite of the temporal region, and depending on the eye, superior and inferior retina was categorized. This regional analysis was performed with the goal to identify local changes that might occur in myopic eyes due to their asymmetric eye growth pattern.

Image and statistical analysis

Blood vessel branchpoints and number of string vessels per mm^2 were manually counted for each frame on the branches of all orders and converted to number of branch points/mm^2 and number of string vessels/mm^2, respectively. The branch points and string vessels were

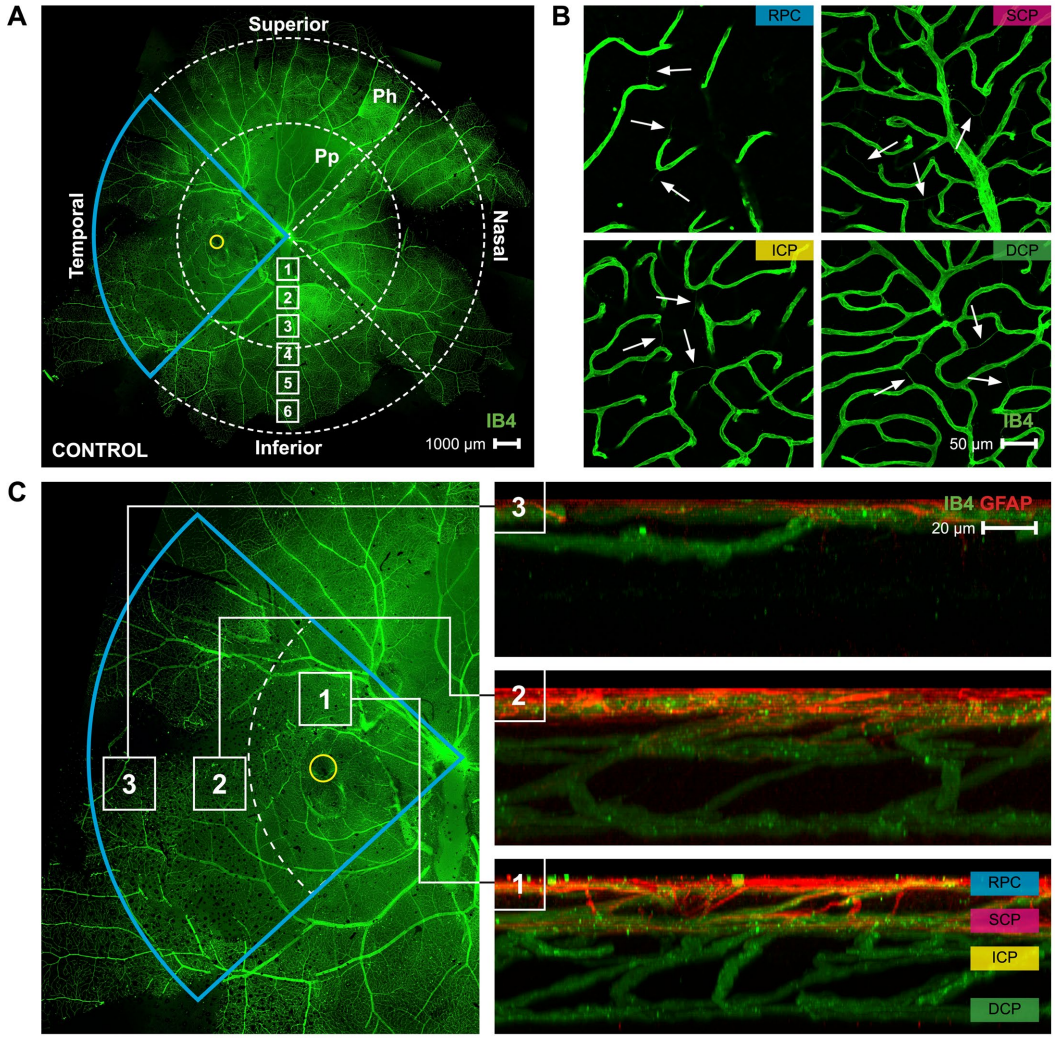

FIGURE 1
A map of the superficial vasculature of a whole mount marmoset retina, and images of the four different vascular plexi. **(A)** A complete of control marmoset retinal vasculature [green (ID: C16 Left)]. The temporal region of the eye is outlined in blue, and the position of the fovea is indicated by the yellow circle. The retinal vasculature was visualized with conjugated IB4-488. Images were acquired at 4× magnification and stitched in Photoshop. Location of peripapillary region (Pp) and peripheral region (Ph) described in this study is shown. White boxes represent focal areas away from the optic disc to periphery. Boxes labeled "Pp" represent locations where peripapillary location images were taken, while boxes labeled "Ph" represent locations where peripheral location images were taken. Superior, inferior, nasal, and temporal quadrants of the retina are shown. Scale, 1,000 µm. **(B)** Representative images of the retinal vasculature (green) acquired from the parafoveal area which show all vascular layers. Scale, 50 µm. White arrows point to string vessels found in the marmoset retinas. **(C)** The blue insert from 1A is highlighted here, with areas 1, 2, and 3 marked with white boxes indicating the (1) parafoveal region, (2) peripapillary region, and (3) peripheral region. Reconstructed images of areas 1, 2, and 3 can be seen in 1C right, showing the distribution of the retinal vasculature (green) and co-localized astrocytes (red) in those areas. The four vascular plexi are the radial peripapillary capillary (RPC), superficial (SCP), intermediate (ICP), and deep (DCP) plexi. Scale, 20 µm. Figure modified from Lin et al. (23).

quantified in the radial peripapillary capillary plexus (RPC, most superficial), superficial capillary plexus (SCP), intermediate capillary plexus (ICP), and deep capillary plexus (DCP). Images were processed using Fiji software. A simple geometric correction for magnification along the two-dimensional plane was performed to account for myopic retinal stretch. Data were assessed for normality and analyzed using student t-test, and one-way analysis of variance (ANOVA) and post-hoc analysis using Tukey tests at the level of $\alpha = 0.05$ were used to examine the differences between treatment and control groups. Pearson's linear correlation was used to explore the relationship between effective age, axial length, and refractive error and compensatory string vessel and branchpoint measurements. Figures were made using OriginPro 2023 software (OriginLab, Northampton, United States) and assembled in Adobe Indesign (Adobe, San Jose, United States).

Results

Retinal vascular plexi in the common marmoset

Marmoset retinas exhibit four vascular plexi in the parafoveal region (Figures 1B,C, area 1): the RPC, SCP, ICP, and DCP. String vessels, thin non-functional connective tissue strands that are remnants of capillaries, are identified in the different plexi of

marmoset retinas as white arrows in Figure 1B. In the parafoveal region, there are four vascular plexi [modified from Lin et al. (23); Figure 1C, area 1]. In the peripapillary region, marmosets have three vascular plexi (Figure 1C, area 2): the SCP, ICP, and DCP. The peripheral region (Figure 1C, area 3) only contains two vascular plexi: the SCP and the DCP. In all four groups of marmosets studied, the vasculature by the optic nerve head contained vessels of varying diameters, while the peripheral vasculature appeared to be smaller and uniform in width. Specifically, the average vein vessel width in focal regions 1–3 of the 6-month-old (6 m) marmosets was 18.06 ± 2.9 μm, while the average artery width in the same regions of the 6 m marmosets was 15.74 ± 3.1 μm ($p > 0.05$). The average vein vessel width in focal regions 4–6 of the 6 m marmosets was 12.25 ± 3.4 μm, while the average artery width was 9.95 ± 2.2 μm ($p > 0.05$). Identification, age, axial length, and refractive error of control and myopic marmosets are listed in Table 1.

The older myopic retinas show increased number of string vessels pan-retinally in all four layers of the retinal vasculature compared to younger myopic, younger control, and older control retinas (Figures 2B, 3B, 4B, 5B), as well as increased capillary branchpoint numbers in the central retina, and decreased capillary branchpoint numbers in the periphery (Figures 2C, 3C, 4C, 5C). Capillary branchpoints/mm^2 was also greater in the innermost vascular layers of the older myopic marmosets, and lower in the outermost vascular layers in all retinal locations (Figures 2C, 3C, 4C, 5C). In the 12-month-old (12 m) marmosets, the average vein and artery vessel widths in focal regions 1–3 were 16.12 ± 1.8 μm and 11.87 ± 2.7 μm, respectively ($p > 0.05$), and 12.04 ± 2.2 μm and 9.49 ± 2.0 μm in focal regions 4–6 ($p > 0.05$). These data suggest that vascular changes are taking place in aging myopic primate retina compared to young myopic retinas.

Vascular changes in the parafoveal radial peripapillary capillary plexus of the myopic marmosets

The radial peripapillary capillary plexus (RPC) was present in all animals and all quadrants of the parafoveal region imaged (Figure 2A). The RPC is located in the retinal nerve fiber layer, limited to the posterior pole and normally located on the temporal side of the retina. We found that in this plexus 6 m myopic retinas had greater string vessel numbers/mm^2 compared to controls (Figure 2B; 6 m control 23.5 ± 8.6 string vessels/mm^2; 6 m myope 61.04 ± 13.8; $p < 0.001$). The 12 m myopic retinas also exhibited greater string vessel numbers/mm^2 compared to 12 m controls (Figure 2B; 12 m control 22.71 ± 4.2 string vessels/mm^2; 12 m myopes 182.22 ± 23.6 string vessels/mm^2; $p < 0.001$). The string vessel density in 6 m controls was not significantly different to that of 12 m controls ($p > 0.05$).

The number of capillary branchpoints/mm^2 in the RPC was also significantly greater in 6 m myopic retinas compared to 6 m controls, and these differences were greater in the older 12 m myopic retinas compared to 12 m controls (Figure 2C: 6 m control 106.79 ± 13.3 branchpoints/mm^2, 6 m myope 156.34 ± 39.8, $p < 0.05$; 12 m control 114.91 ± 14.0, 12 m myope 172.22 ± 15.8; $p < 0.01$). Overall the parafoveal RPC of myopic marmosets had greater string vessels and vessel branchpoints numbers than controls. The number of string vessels increased by 150/mm^2 in 12 m myopic marmosets relative to 12 m control marmosets, and by 40/mm^2 in 6 m myopic marmosets relative to 6 m control marmosets. The number of branchpoints/mm^2 increased by 50/mm^2 in 6 m myopic marmosets relative to 6 m control marmosets, and by 60/mm^2 in 12 m myopic marmosets relative to 12 m control marmosets.

TABLE 1 Treatment started at 10 weeks of age (72.0 ± 5.5 days) following our established protocol [30–32].

6 m control ID, eye	Age (days)	Gender	Axial length (mm)	Refractive error (D)	6 m myope ID, eye	Age (days)	Gender	Axial length (mm)	Refractive error (D)
C16, right	268	Female	10.259	−0.66	B17, right	214	Female	10.900	−7.93
C16, left	268	Female	10.241	−0.13	B17, left	214	Female	10.894	−7.97
G16, left	215	Male	10.279	−1.15	O17, right	204	Male	10.492	−7.28
H16, right	205	Female	10.286	−0.63	O17, left	204	Male	10.212	−3.91
H16, left	205	Female	10.307	−1.12	P17, right	183	Female	10.554	−7.96
					P17, left	183	Female	10.464	−3.08
AVG ± SD	232.2 ± 32.9		10.27 ± 0.03	−0.74 ± 0.4	AVG ± SD	200.3 ± 14.2		10.61 ± 0.3	−7.01 ± 1.8
	$p > 0.05$		$p < 0.05$	$p < 0.01$					
12m control ID, eye	**Age (days)**	**Gender**	**Axial length (mm)**	**Refractive error (D)**	**12m myope ID, eye**	**Age (days)**	**Gender**	**Axial length (mm)**	**Refractive error (D)**
X15, right	381	Female	10.216	−1.12	I19, right	388	Male	10.936	−7.34
X15, left	381	Female	10.2202	−1.04	J19, right	388	Male	10.791	−3.48
S15, right	396	Female	10.181	−1.22	J19, left	388	Male	10.766	−3.82
AVG ± SD	386 ± 8.7		10.20 ± 0.02	−1.12 ± 0.1	AVG ± SD	388 ± 0.0		10.83 ± 0.1	−4.08 ± 2.1
	$p > 0.05$		$p < 0.05$	$p < 0.01$					

Lenses were inserted daily in the morning between 8 and 10 a.m. when lights were turned on in the animal room (700 lux) and removed 9 h later at lights off each day (9 h light/15 h dark) (28, 30). Contact lenses had 6.5 mm diameter, 3.6/3.8 mm base curve, were made of methafilcon A (55% water content, DK, 17), fit 0.10 mm flatter than the flattest keratometry measurement, and were assessed using an ophthalmoscope. No corneal complications were observed in any of the animals treated in this or any earlier studies with marmosets (28, 30).

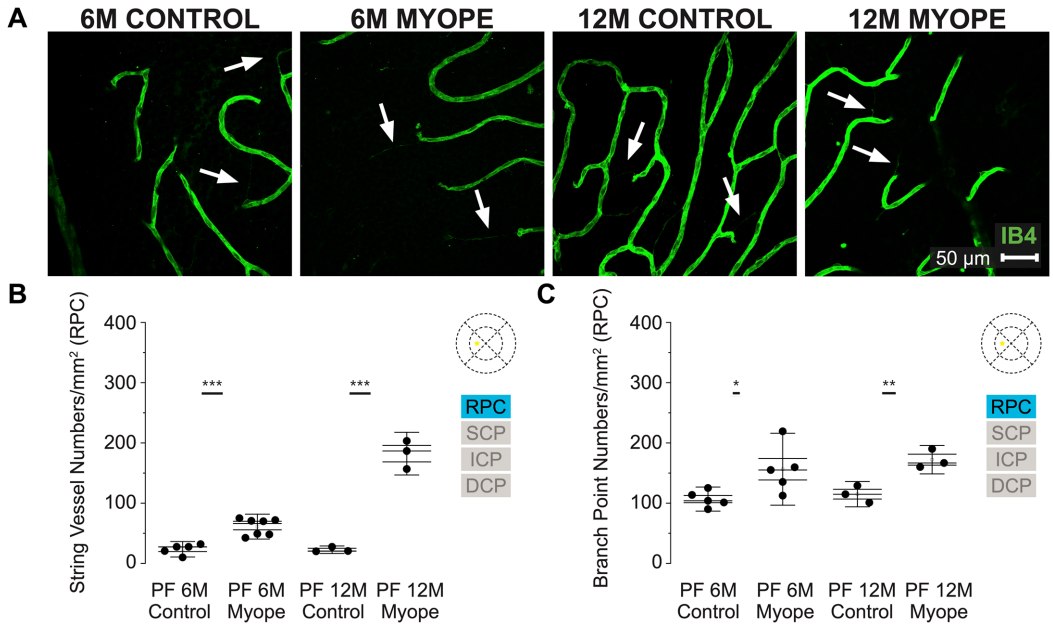

FIGURE 2
Vascular alterations of the myopic marmoset retina, shown with representative images of the parafoveal RPC plexus in six-month-old (6 m) controls, 6 m myopes, twelve-month-old (12 m) controls, and 12 m myopic marmoset retinas and subsequent analysis of the number of string vessels per mm^2 and branchpoints per mm^2 within the RPC of the parafovea. **(A)** Representative images of radial peripapillary capillary plexus vessel structure in the parafoveal region of a 6 m control (ID tag: C16 Right), 6 m myope (ID tag: P17 Right), 12 m control (ID tag: X15 Right) and 12 m myope (ID tag: I19 Right) taken at 40× magnification. Vasculature is labeled with IB4 (green). Scale, 50 µm. White arrows point to string vessels found in the marmoset retinas. *$p < 0.05$, **$p < 0.01$, ***$p < 0.001$. **(B)** Analysis of the number of string vessels per mm^2 in the parafoveal's RPC layer of the superior, inferior, and nasal retina. Data is shown in as a I-graph box plot for 6 m control ($n = 5$), 6 m myopic ($n = 5$), 12 m control ($n = 3$), and 12 m myopic ($n = 3$) marmoset retinas. Inner box lines represent standard error (SE), and outer lines/whiskers represent standard deviation (SD). A significant increase in string vessels in the 6 m myopic parafoveal RPC was noted ($p < 0.001$) and even more significant increase in the 12 m myopic parafoveal RPC ($p < 0.001$). **(C)** Analysis of the RPC vessel branch points in the parafovea region (6 m control $n = 5$, 6 m myope $n = 6$, 12 m control $n = 3$, 12 m myope $n = 3$). A significant increase in branching was seen in the 6 m myopic parafoveal RPC, with more significant increase noted in the 12 m myopic parafoveal RPC ($p < 0.05$; $p < 0.01$).

Vascular changes in the superficial capillary plexus of the myopic marmosets

The superficial capillary plexus (SCP) was present in all animals, all quadrants and areas imaged (Figure 3A). The string vessels/mm^2 densities was greater in 6 m myopic marmoset retinas, and even greater in 12 m myopic retinas compared to that of 6 m or 12 control retinas pan-retinally, respectively (Figure 3B: parafovea 6 m control 35.2 ± 8.4 string vessels/mm^2, 6 m myope 85.42 ± 25.7, $p = 0.001$; 12 m control 54.62 ± 6.9; 12 m myope 198.89 ± 49.1, $p < 0.01$. Peripapillary 6 m control 36.63 ± 14.6 string vessels/mm^2, peripapillary 6 m myope 73.96 ± 17.7, $p < 0.01$; peripapillary 12 m control 54.36 ± 6.3, 12 m myope 155.0 ± 37.2; $p < 0.01$. Periphery 6 m control 44.88 ± 25.0 string vessels/mm^2, periphery 6 m myope 73.23 ± 24.4, $p = 0.09$; periphery 12 m control 65.03 ± 11.5, 12 m myope 114.44 ± 8.4, $p < 0.05$).

In this plexus, the number of capillary branchpoints/mm^2 was unchanged in the 12 and 6 m myopic marmoset retinas compared to 12 and 6 m controls in the parafovea and peripapillary regions (Figure 3C: parafovea 6 m control 147.83 ± 24.1 branchpoints/mm^2, 6 m myope 121.5 ± 27.6, $p = 0.14$; 12 m control 222 ± 19.3, 12 m myope 271.11 ± 38.6, $p = 0.12$; Peripapillary 6 m control 157.5 ± 43.22 branchpoints/mm^2, 6 m myope 111.81 ± 27.4, $p = 0.06$; 12 m control 196.6 ± 22.5, 12 m myope 227.22 ± 67.8, $p = 0.22$). There was a significant decrease in capillary branchpoint density in the retinal periphery of 12 m myopic marmoset retinas compared to 12 m controls (Figure 3C right: Periphery 6 m control 133.0 ± 36.4 branchpoints/mm^2, peripheral 6 m myope 91.11 ± 29.3, $p = 0.06$; peripheral 12 m control 163.33 ± 22.5, 12 m myope 84.44 ± 22.2, $p < 0.05$). The SCP of 12 m myopic marmosets contained more string vessels than 12 m controls, 6 m myopes and 6 m controls did. The SCP vascular branchpoint density was greater in the peripheral retina of 12 m control marmosets. Across the retina, string vessel density increased by 100/mm^2 in 12 m myopic marmosets relative to 12 m control marmosets, and by 40/mm^2 in 6 m myopic marmosets relative to 6 m control marmosets. Similarly, capillary branchpoint density decreased in the peripheral retina by 80/mm^2 in 12 m myopic marmosets relative to 12 m control marmosets, and by 40/mm^2 in 6 m myopic marmosets relative to 6 m controls.

Vascular changes in the intermediate capillary plexus of the myopic marmosets

The intermediate capillary plexus (ICP) was present in the peripapillary and parafoveal regions of all animals, in all quadrants evaluated (Figure 4A). The ICP was not present in the periphery. In the parafovea, the number of string vessels/mm^2 was not significantly different in 6 m or 12 myopic marmoset retinas (Figure 4B: parafovea 6 m control 24.33 ± 5.1 string vessels/mm^2, 6 m myope 28.75 ± 8.5, $p = 0.30$; 12 m control 88.58 ± 12.8, 12 m myope 100 ± 18.1, $p = 0.71$.

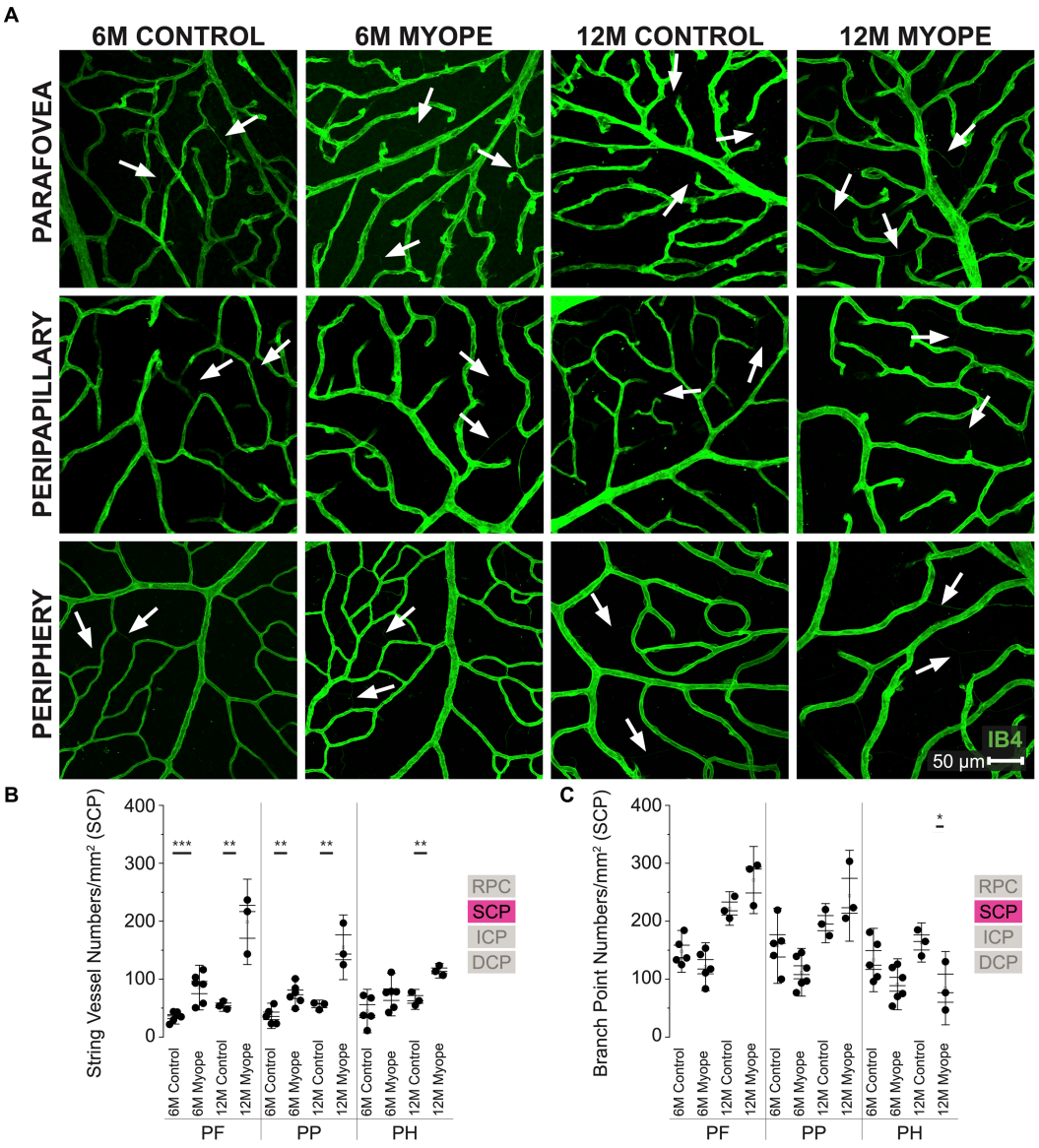

FIGURE 3
Vascular alterations of the myopic marmoset retina, shown with representative images of pan-retinal SCP plexus in 6 m controls, 6 m myopes, 12 m controls, and 12 m myopic marmoset retinas and subsequent analysis of the number of string vessels per mm^2 and branchpoints per mm^2 within the SCP. **(A)** Representative images of superficial capillary plexus vessel structure in the parafoveal, peripapillary, and peripheral region of a 6 m control (ID tag: C16 Right), 6 m myope (ID tag: P17 Right), 12 m control (ID tag: X15 Right), and 12 m myope (ID tag: I19 Right) taken at 40× magnification. Vasculature is labeled with IB4 (green). Scale, 50 µm. White arrows point to string vessels found in the marmoset retinas. *$p < 0.05$, **$p < 0.01$, ***$p < 0.001$. **(B)** Analysis of the number of string vessels per mm^2 in the SCP of the superior, inferior, and nasal retina (6 m control $n = 5$, 6 m myope $n = 6$, 12 m control $n = 3$, 12 m myope $n = 3$). A significant increase in string vessels in the 6 m myopic parafoveal SCP was noted ($p < 0.001$) and an even more significant increase in the 12 m myopic parafoveal SCP ($p < 0.01$). A significant increase in string vessels in the 6 m myopic peripapillary SCP was noted ($p < 0.01$) and an even more significant increase in the 12 m myopic parafoveal SCP ($p < 0.01$). No significant difference was found in string vessels in the 6 m myopic peripheral SCP was noted ($p = 0.09$) with a significant increase in the 12 m myopic peripheral SCP ($p < 0.01$). **(C)** Analysis of the number of vessel branch points in the SCP of the superior, inferior, and nasal retina (6 m control $n = 5$, 6 m myope $n = 6$, 12 m control $n = 3$, 12 m myope $n = 3$). No significant difference was found in SCP branch points of the parafovea or peripapillary myopic eyes, however a significant decrease in peripheral SCP branchpoints per mm^2 in the 12 m myopic SCP was noted ($p < 0.05$).

Peripapillary 6 m control 45.83 ± 18.1 string vessels/mm^2, 6 m myope 32.38 ± 2.8, $p = 0.19$; 12 m control 61.46 ± 9.1, 12 m myope 81.11 ± 25.9; $p = 0.28$).

In the parafovea and peripapillary, the capillary branchpoint density was higher in 12 m myopic parafovea retina compared to 12 m controls, but lower in both 6 m and 12 m myopic peripapillary retinas compared to 6 and 12 m controls, respectively (Figure 4C: parafovea 6 m control 222.76 ± 46.4 branchpoints/mm^2, 6 m myope 173.33 ± 33.3, $p = 0.09$; 12 m control 206.0 ± 16.5, 12 m myope 271.11 ± 38.6, $p < 0.05$. Peripapillary 6 m control 143.18 ± 39.3 branchpoints/mm^2, 6 m myope 79.86 ± 19.6, $p < 0.01$; 12 m control 160.0 ± 15.0, 12 m myope 77.78 ± 10.7; $p < 0.001$).

Overall the ICP in 12 m myopic marmosets contained similar amounts of string vessels/mm^2 than 12 m controls, 6 m controls or 6 m

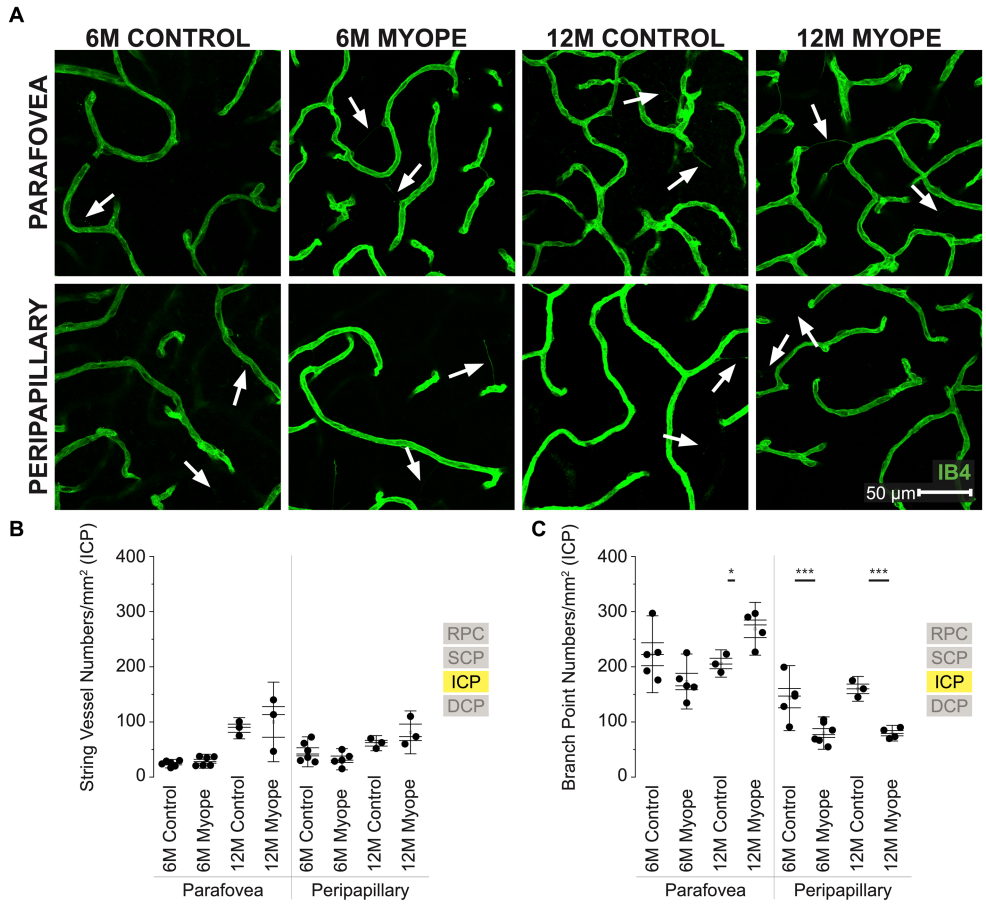

FIGURE 4
Vascular alterations of the myopic marmoset retina, shown with representative images of parafoveal and peripapillary ICP plexus in 6m controls, 6m myopes, 12m controls, and 12m myopic marmoset retinas and subsequent analysis of the number of string vessels per mm² and branchpoints per mm² within the ICP. **(A)** Representative images of intermediate capillary plexus vessel structure in the parafoveal and peripapillary region of a 6m control (ID tag: C16 Right), 6m myope (ID tag: P17 Right), 12m control (ID tag: X15 Right), and 12m myope (ID tag: I19 Right) taken at 60× magnification. Vasculature is labeled with IB4 (green). Scale, 50µm. White arrows point to string vessels found in the marmoset retinas. *p<0.05, **p<0.01, ***p<0.001. **(B)** Analysis of the number of string vessels per mm² in the ICP of the superior, inferior, and nasal retina (6 m control n = 5, 6 m myope n = 6, 12 m control n = 3, 12 m myope n = 3). No significant difference in string vessels in the myopic parafoveal or peripapillary ICP was noted (p > 0.05). **(C)** Analysis of the number of vessel branchpoints per mm² in the ICP of the superior, inferior, and nasal retina (6m control n=5, 6m myope n=6, 12m control n=3, 12m myope n=3). A significant increase in parafoveal ICP branchpoints per mm² in the 12m myopic parafoveal ICP was noted (p<0.05) and significant decrease in parafoveal ICP branchpoints per mm² in the 6m myope ($p \leq$ 0.01). A significant decrease in peripapillary ICP branchpoints per mm² in the 6m myopic ICP was noted (p<0.001) as well as in the 12m myope peripapillary ICP (p<0.001).

myopes across the retina. ICP vascular branchpoints increased in the parafoveal retina of 12 m myopic marmosets and decreased in the peripapillary retina of 6 and 12 m myopic marmosets. The number of branchpoints/mm² increased by 70/mm² in the parafovea of 12 m myopic marmosets relative to 12 m control marmosets, and decreased by 50/mm² in peripapillary of 6 m myopic marmosets relative to 6 m controls. Similarly, the number of branchpoints per mm² in the parafovea decreased by 80/mm² in 12 m myopic marmosets relative to 12 m control marmosets.

Vascular changes in the deep capillary plexus of the myopic marmosets

The DCP was present in all animals and all quadrants imaged (Figure 5A). In the parafovea and peripapillary, the number of string vessels/mm² was greater in 6 m myopic marmoset retinas compared to 6 m controls, and even greater in 12 m myopic retinas compared to 12 m control retinas (Figure 5B: parafovea 6 m control 43.75 ± 22.6 string vessels/mm², 6 m myope 120.89 ± 55.2, p < 0.01; parafovea 12 m control 109.33 ± 18.2, 12 m myope 276.67 ± 59.0, p < 0.01. Peripapillary 6 m control 67.19 ± 44.9 string vessels/mm², 6 m myope 136.77 ± 41.1, p = 0.01; peripapillary 12 m control 131 ± 19.3, 12 m myope 184.44 ± 61.9, p = 0.22). The number of string vessels/mm² was greater in the periphery of 12 m myopic retinas compared to 12 m controls (Periphery 6 m control 45.52 ± 29.5 string vessels/mm², 6 m myope 51.11 ± 25.9, p = 0.69; 12 m control 84.67 ± 9.3, 12 m myope 148.3 ± 20.2; p < 0.01).

The number of parafoveal DCP vessel branchpoints/mm² in 6 m and 12 m myopes was not different from that of 6 or 12 m controls, respectively (Figure 5C: parafovea 6 m control 164.26 ± 26.8 branchpoints/mm², 6 m myope 173.57 ± 39.4, p = 0.67; 12 m control

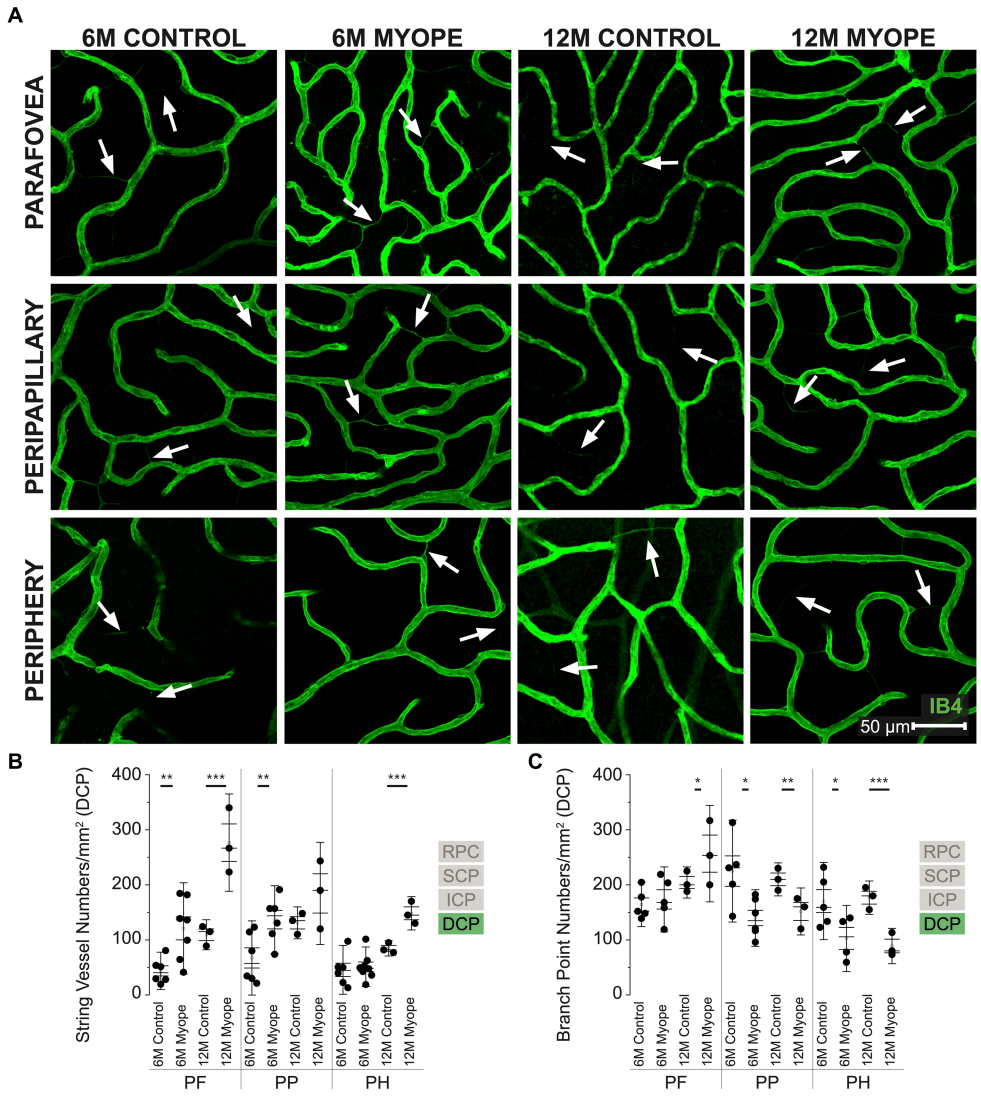

FIGURE 5
Vascular alterations of the myopic marmoset retina, shown with representative images of pan-retinal DCP plexus in 6 m controls, 6 m myopes, 12 m controls, and 12 m myopic marmoset retinas and subsequent analysis of the number of string vessels per mm^2 and branchpoints per mm^2 within the DCP. **(A)** Representative images of deep capillary plexus vessel structure in the parafoveal, peripapillary, and peripheral region of a 6 m control (ID tag: C16 Right), 6 m myope (ID tag: P17 Right), 12 m control (ID tag: X15 Right), and 12 m myope (ID tag: I19 Right) taken at 60× magnification. Vasculature is labeled with IB4 (green). Scale, 50 µm. White arrows point to string vessels found in the marmoset retinas. *p < 0.05, **p < 0.01, ***p < 0.001. **(B)** Analysis of the number of string vessels per mm^2 in the DCP of the superior, inferior, and nasal retina (6 m control n = 5, 6 m myope n = 6, 12 m control n = 3, 12 m myope n = 3). A significant increase in string vessels in the 6 m myopic parafoveal DCP was noted (p < 0.01) and even more significant increase in the 12 m myopic parafoveal DCP (p < 0.001). A significant increase in string vessels in the 6 m myopic peripapillary DCP was noted (p < 0.01) but no difference was noted in the 12 m myopic peripheral DCP (p =0.22). No significant difference was noted in string vessels in the 6m myopic peripheral DCP (p = 0.69) and a significant increase in 12 m myopic peripheral DCP string vessels per mm^2 was noted (p < 0.001). **(C)** Analysis of the number of vessel branch points in the DCP of the superior, inferior, and nasal retina (6 m control n = 5, 6 m myope n = 6, 12 m control n = 3, 12 m myope n = 3). No significant difference in parafoveal DCP branchpoints per mm^2 in the 6mmyopic parafoveal DCP was noted (p = 0.6), with a significant increase in 12 m myopic parafoveal DCP branchpoints per mm^2 was seen (p < 0.05). A significant decrease in both 6 m myopic peripapillary DCP (p < 0.05) and 12 m myopic peripapillary DCP branchpoints per mm^2 (p < 0.01) was noted. A significant decrease in peripheral DCP branchpoints per mm^2 in the 6 m myope (p < 0.05) and 12 m myope (p < 0.001) was noted.

204.33 ± 18.9, 12 m myope 256.67 ± 58.4, p = 0.21). In the peripapillary and peripheral retina, the number of capillary branchpoints/mm^2 was lower in 6 m and 12 myopic retinas compared to that of 6 m control or 12 m control retinas, respectively (Figure 5C: peripapillary 6 m control 225.0 ± 61.8 branchpoints/mm^2, 6 m myope 139.76 ± 34.3, p = 0.01; peripapillary 12 m control 210.0 ± 20.0, 12 m myope 151.67 ± 28.4, p < 0.05. Periphery 6 m control 170.51 ± 46.7 branchpoints/mm^2, 6 m myope 102.55 ± 40.1, p < 0.05; periphery 12 m control 176.67 ± 20.27, 12 m myope 88.89 ± 21.4; p < 0.01).

The DCP of 12 m myopic marmosets contain had greater string vessel density than 12 m controls, 6 m controls or 6 m myopes pan-retinally. DCP vascular branchpoints/mm^2 decreased in the peripapillary and periphery retina of 12 m myopic marmosets. Across

the retina, the number of string vessels per mm^2 increased by 50/mm^2 in 12 m myopic marmosets relative to 6 m myopic marmosets, and by 100/mm^2 relative to 12 m control marmosets. Similarly, the number of branchpoints per mm^2 across the retina decreased by 60/mm^2 in 12 m myopic marmosets relative to 6 m myopic marmosets, and by 110/mm^2 relative to 12 m control marmosets.

Regression analysis

Stepwise multiple regression models were used to evaluate whether the numbers of string vessel/and branchpoints observed would be predicted by the age, axial length, or refractive error of the animals. In these models, age, axial length, or refractive error were the independent variables, and the string vessel and branchpoint measures in each ETDRS region and layer were the dependent variables. As myopic eyes aged, they grew longer and had relatively higher numbers of string vessels and decreased branchpoints in the SCP (multiple regression, $R^2 = 0.16$, $p < 0.001$), ICP (multiple regression: $R^2 = 0.272$, $p < 0.001$) and DCP (multiple regression; $R^2 = 0.321$, $p < 0.001$). Decreasing branchpoints/mm^2 of the SCP were negatively correlated with increasing axial length ($R^2 = 0.83$, $p < 0.001$) and higher refractive error ($R^2 = 0.69$, $p < 0.001$).

Discussion

This study provides evidence of significant changes in all four capillary plexi of the retinal vasculature in marmosets induced with myopia, a NHP model successfully used in vision research due to the similarities in structure and function to the human eye. Compared to 6-month myopic and 6-month old controls, 12-month old myopic marmosets had greater numbers of string vessels in all capillary plexi, and increased branchpoint density in the parafoveal and peripapillary retina. The confocal images obtained confirm the presence of four vascular plexi in the marmoset retina, and the presence of string vessels, similar to human retinas (35–37, 42). These plexi, from inner to outer retina, are the radial peripapillary capillaries (RPC), superficial capillary plexus (SCP), intermediate capillary plexus (ICP), and deep capillary plexus (DCP) (43).

The retina is one of the most energy demanding tissues in the body (44, 45). Several studies suggest that microvasculature changes can be markers of neurological and ocular diseases (35, 46–51), contribute to abnormal blood flow changes (24, 32, 52–54), and compromise vascular integrity resulting in reduced metabolic support (27, 51, 55, 56). In this study, vascular remodeling and plasticity was observed in marmoset retinas with induced myopia, and the changes observed were exacerbated by age. The marmoset (*Callithrix jacchus*) has been established as an excellent non-human primate model in vision and neuroscience research due to its fast development, small size, diurnal foveated retinas, ease in breeding and handling, and high optical quality eye (7, 16, 19). NHP are critically important for the development of human treatments (15, 17, 18).

Age-related conditions such as Alzheimer's disease, dementia and hypertension have been associated with changes in ocular microvasculature (35–37, 51, 57, 58). In this study, retinal microvasculature alterations were observed in marmosets induced with myopia. Specifically, an increase in string vessels and branchpoint densities in all capillary plexi at the parafovea and peripapillary retina were observed as myopic marmosets aged. These findings are in line with others seen in the human retina (35–37); string vessels are present in diabetic retinopathy before microvascular changes occur (34), making the identification of string vessels a vital part of vascular disease management. The RPC is considered highly vulnerable to insult and damage due to high metabolic demand of retinal ganglion cells (RGC) (59–61). There is evidence that structural changes to the RPCs are associated with the pathogenesis of age-related RGC axonal loss in humans (62). RPC loss and glaucomatous nerve fiber layer damage has also been identified in patients with chronic glaucoma (63). The increased string vessel and branchpoint density observed in the parafoveal RPC of marmosets induced with myopia suggests that the myopic retinal microvasculature might be experiencing capillary regression and string vessel formation, similarly to that described in several vascular diseases (51, 64–66). There is also evidence of an increase in string vessel formation as a consequence of ganglion cell injury (67), and related to an induced apoptotic phenomenon associated with endothelial cell destruction, attached by macrophages (6).

String vessels are thin connective tissue strands, non-functional remnants of capillaries that do not carry blood flow (36). The presence of string vessels suggests an originally normal-functioning vessel that gradually disappeared after abrupt or chronic ischemia (68), diabetes (34), aging (35), or neurodegenerative disorders (37), among others. While capillary branchpoint density was significantly greater in the RCP of myopic eyes, its density in the SCP, ICP and DCP layers was lower compared to controls. Reduced vessel branching has been associated with decreased retinal blood supply in mice eyes (46, 69), and an aberrant blood vessel development results in decreased density and branching of the capillary network (70). After three weeks of sustained whole-body hypoxia in ten-week-old mice, increased blood vessel branchpoint density have also been shown to be significantly increased (68).

Despite the branchpoint reduction observed in 6 m marmosets, 12 m myopic marmosets showed an increase in retinal string vessels and decrease in peripheral branchpoints. Increased string vessel formation and decreasing number of microvasculature branches have been noted in the normal aging of human cerebral white matter (42, 71–75), and are likely to occur even in the absence of significant neuron loss (37, 71, 73, 76). In the cortical vasculature of 76–81 years old humans with no vascular dementia, there is a decline in capillary surface area and density compared to those of a younger population under 50 years old (77, 78). This indicates the presence of age-related pathology in the cortical microvasculature, that possibly precedes the pathophysiology of vascular disease. Certain microvascular abnormalities may occur prior to development of disease (76), The retina is part of the blood–brain-barrier, and exhibits similar pathological processes as does the cerebrum. Retinal ischemia has been shown to increase the number of string vessels (79), with decreased vascular density in aging animals (33, 70) shown as well.

We also observed an increase in retinal branchpoint density in all four parafoveal vascular layers, and decrease in retinal branchpoint density of the same layers with increasing distance from the optic nerve head, in the 12 m myopic marmosets compared to the values of 6 m myopic marmosets. This is in line with other studies in primate research. Four different capillary networks (the RPC, SCP, ICP, and DCP) with distinct vascular patterns can

be found in the control primate and non-primate retina (80), specifically in the macula and peripapillary region (81). In humans, the SCP is highest in the macular regions, and decreases in the periphery (82). The peak vessel density of normal, control SCP of humans is higher than the ICP and DCP in the parafoveal region as well, with the density of the ICP and DCP higher in the periphery than in the SCP (82). All retinal vascular layers in the human eye are densest in the macular/peripapillary region, and reduces in thickness and density with increasing eccentricity (43, 59, 83). During the disease onset of diabetes in human eyes, the density of the SCP, ICP, and DCP progressively decreases toward the periphery, increasing disease severity, and with ganglion cell density decrease (84). In a model of human retinal vascular occlusion, decreased vascular density has been shown in both the superficial and deep vascular networks (85).

In our study, increased age, refractive error, and axial length were associated with increased string vessel density across the SCP, ICP, and DCP retinal vascular layers, and decreased SCP branchpoint density in myopic marmosets. Age appears to exacerbate the effect of myopia on the retinal vasculature, specifically by increasing string vessel density and decreasing branchpoint density with increasing retinal eccentricity. The retinas of older myopes appear to be compensating for increased duration of stress to the vasculature due to the sustained effect of increased myopic growth on the vasculature, and the results shown are in line with previous studies. One study in human myopes showed decreased SCP and DCP vessel densities with age and decreased SCP density with high myopia and longer axial length (22). Another study showed decreased deep vascular plexus density in a human model of high myopia was most associated with high myopia (86). In pathological myopia, alterations to inner retinal microvascular density occur, specifically a decrease in the DCP (87).

Conclusion

The results from this study indicate that aging exacerbates the effects of myopic eye growth on the architectural template of the retinal vasculature at the cellular level, in all four vascular plexi in a NHP model of lens-induced myopia. The restructuring and reorganization found reflects what might be an adaptation to the sustained mechanical stress of myopic eye growth. Collectively, this may be a part of a beneficial adaptive chronic response to maintain the adequate functioning of retinal neurons during ocular growth (31). Alternatively, the changes to the vasculature seen could represent the opposite, a detrimental response indicating the onset of compromised structural and functional support to the retinal neurons that preserve vision (31). The vascular changes seen in this study may precede pathological myopic changes to the retina like myopic neovascularization, further emphasizing the importance of this work.

Our study confirms the feasibility of the marmoset in studying the retinal vasculature. The aim of the study was to evaluate how aging interacts with the effect of myopic eye growth on the structure and distribution of the retinal vasculature. The findings of this study confirm that myopic eyes without pathology exhibit changes to the numbers of string vessels and branchpoint in all four vascular plexi, suggesting that the vasculature is indeed affected by the mechanical stretch induced by myopia. Whether these changes noted are beneficial or harmful, and whether their function diminishes with disease progression, remains to be seen. Future studies will aim to evaluate quantitatively the functional changes to the vasculature with increasing myopia and increasing age.

Data availability statement

The raw data supporting the conclusions of this article will be made available by the authors, without undue reservation.

Ethics statement

The animal study was reviewed and approved by IACUC Ethics Committee of SUNY College of Optometry.

Author contributions

CL and AB-P contributed to the conception and design of the study. CL, AT, RA, MS, and AB-P contributed to methodology and data curation. AB-P acquired resources and funding for this study. CL performed the statistical analysis and wrote the original draft of the manuscript. All authors contributed to the article and approved the submitted version.

Funding

This work was supported by the American Academy of Optometry Career Development Award to ABenavente, National Institute of Health's National Eye Institute T35 grant to CL.

Acknowledgments

The authors would like to thank to Stefanie Wohl for her advice on immunohistochemical techniques, Andrew Koo for his help with figure conceptualization, Hardy Zhou, Brian Song, and Gulnoza Azieva, for their help to treat myopic marmosets, and Ana Nour, Rossy Angel, Xiomara Santiago, and Mirella Camargo for their attention and care to the marmosets included in our study.

Conflict of interest

The authors declare that the research was conducted in the absence of any commercial or financial relationships that could be construed as a potential conflict of interest.

Publisher's note

References

1. Curtin BJ. *The myopias: basic science and clinical management*, vol. *xv*. Philadelphia: Harper & Row (1985). 495 p.

2. Saw SM, Gazzard G, Shih-Yen EC, Chua WH. Myopia and associated pathological complications. *Ophthalmic Physiol Opt*. (2005) 25:381–91. doi: 10.1111/j.1475-1313.2005.00298.x

3. Foster PJ, Jiang Y. Epidemiology of myopia. *Eye*. (2014) 28:202–8. doi: 10.1038/eye.2013.280

4. Flitcroft DI, He M, Jonas JB, Jong M, Naidoo K, Ohno-Matsui K, et al. IMI-Defining and Classifying Myopia: A Proposed Set of Standards for Clinical and Epidemiologic Studies. *Invest Ophthalmol Vis Sci*. (2019) 60:M20–30. doi: 10.1167/iovs.18-25957

5. Holden BA, Fricke TR, Wilson DA, Jong M, Naidoo KS, Sankaridurg P, et al. Global Prevalence of Myopia and High Myopia and Temporal Trends from 2000 through 2050. *Ophthalmology*. (2016) 123:1036–42. doi: 10.1016/j.ophtha.2016.01.006

6. Khan MH, Lam AKC, Armitage JA, Hanna LTo CH, Gentle A. Impact of Axial Eye Size on Retinal Microvasculature Density in the Macular Region. *J Clin Med*. (2020) 9:2539. doi: 10.3390/jcm9082539

7. Nickla DL, Wildsoet CF, Troilo D. Diurnal rhythms in intraocular pressure, axial length, and choroidal thickness in a primate model of eye growth, the common marmoset. *Invest Ophthalmol Vis Sci*. (2002) 43:2519–28.

8. Troilo D, Nickla DL, Wildsoet CF. Choroidal thickness changes during altered eye growth and refractive state in a primate. *Invest Ophthalmol Vis Sci*. (2000) 41:1249–58.

9. El-Shazly AA, Farweez YA, ElSebaay ME, El-Zawahry WMA. Correlation between choroidal thickness and degree of myopia assessed with enhanced depth imaging optical coherence tomography. *Eur J Ophthalmol*. (2017) 27:577–84. doi: 10.5301/ejo.5000936

10. Schaeffel F, Feldkaemper M. Animal models in myopia research. *Clin Exp Optom*. (2015) 98:507–17. doi: 10.1111/cxo.12312

11. Edwards MH. Animal models of myopia. A review. *Acta Ophthalmol Scand*. (1996) 74:213–9. doi: 10.1111/j.1600-0420.1996.tb00078.x

12. Chiang ST, Phillips JR, Backhouse S. Effect of retinal image defocus on the thickness of the human choroid. *Ophthalmic Physiol Opt*. (2015) 35:405–13. doi: 10.1111/opo.12218

13. Ulaganathan S, Read SA, Collins MJ, Vincent SJ. Daily axial length and choroidal thickness variations in young adults: Associations with light exposure and longitudinal axial length and choroid changes. *Exp Eye Res*. (2019) 189:107850. doi: 10.1016/j.exer.2019.107850

14. Chakraborty R, Read SA, Collins MJ. Monocular myopic defocus and daily changes in axial length and choroidal thickness of human eyes. *Exp Eye Res*. (2012) 103:47–54. doi: 10.1016/j.exer.2012.08.002

15. Kishi N, Sato K, Sasaki E, Okano H. Common marmoset as a new model animal for neuroscience research and genome editing technology. *Develop Growth Differ*. (2014) 56:53–62. doi: 10.1111/dgd.12109

16. Benavente-Perez A, Nour A, Troilo D. Axial eye growth and refractive error development can be modified by exposing the peripheral retina to relative myopic or hyperopic defocus. *Invest Ophthalmol Vis Sci*. (2014) 55:6765–73. doi: 10.1167/iovs.14-14524

17. Okano H, Hikishima K, Iriki A, Sasaki E. The common marmoset as a novel animal model system for biomedical and neuroscience research applications. *Semin Fetal Neonatal Med*. (2012) 17:336–40. doi: 10.1016/j.siny.2012.07.002

18. Mansfield K. Marmoset models commonly used in biomedical research. *Comp Med*. (2003) 53:383–92.

19. Troilo D, Judge SJ. Ocular development and visual deprivation myopia in the common marmoset (*Callithrix jacchus*). *Vis Res*. (1993) 33:1311–24. doi: 10.1016/0042-6989(93)90039-Y

20. Golebiewska J, Biala-Gosek K, Czeszyk A, Hautz W. Optical coherence tomography angiography of superficial retinal vessel density and foveal avascular zone in myopic children. *PLoS One*. (2019) 14:e0219785. doi: 10.1371/journal.pone.0219785

21. Coscas F, Sellam A, Glacet-Bernard A, Jung C, Goudot M, Miere A, et al. Normative Data for Vascular Density in Superficial and Deep Capillary Plexuses of Healthy Adults Assessed by Optical Coherence Tomography Angiography. *Invest Ophthalmol Vis Sci*. (2016) 57:OCT211-23. doi: 10.1167/iovs.15-18793

22. Leng Y, Tam EK, Falavarjani KG, Tsui I. Effect of Age and Myopia on Retinal Microvasculature. *Ophthalmic Surg Lasers Imaging Retina*. (2018) 49:925–31. doi: 10.3928/23258160-20181203-03

23. Lin C, Toychiev A, Ablordeppey R, Slavi N, Srinivas M, Benavente-Perez A. Myopia Alters the Structural Organization of the Retinal Vasculature, GFAP-Positive Glia, and Ganglion Cell Layer Thickness. *Int J Mol Sci*. (2022) 23:6202. doi: 10.3390/ijms23116202

24. Benavente-Perez A, Hosking SL, Logan NS, Broadway DC. Ocular blood flow measurements in healthy human myopic eyes. *Graefes Arch Clin Exp Ophthalmol*. (2010) 248:1587–94. doi: 10.1007/s00417-010-1407-9

25. Ning J, Joshi N, Franchi-Pereira R, Benavente-Perez A. Longitudinal Evaluation of Choroidal Thickness and Ocular Perfusion Pressure in Progressing Myopes, Baseline Data. *Invest Ophthalmol Vis Sci*. (2017) 58:1106.

26. Ansel T, Nour A, Benavente-Perez A. Non-invasive Measurements of Ocular Perfusion Pressure in Marmosets and its Relationship with Myopia Development and Progression. *Invest Ophthalmol Vis Sci*. (2016) 57:5513.

27. Hawkins BT, Davis TP. The blood-brain barrier/neurovascular unit in health and disease. *Pharmacol Rev*. (2005) 57:173–85. doi: 10.1124/pr.57.2.4

28. Vecino E, Rodriguez FD, Ruzafa N, Pereiro X, Sharma SC. Glia-neuron interactions in the mammalian retina. *Prog Retin Eye Res*. (2016) 51:1–40. doi: 10.1016/j.preteyeres.2015.06.003

29. Sapieha P. Eyeing central neurons in vascular growth and reparative angiogenesis. *Blood*. (2012) 120:2182–94. doi: 10.1182/blood-2012-04-396846

30. Ramirez JM, Trivino A, Ramirez AI, Salazar JJ, Garcia-Sanchez J. Structural specializations of human retinal glial cells. *Vis Res*. (1996) 36:2029–36. doi: 10.1016/0042-6989(95)00322-3

31. Maki T, Hayakawa K, Pham LD, Xing C, Lo EH, Arai K. Biphasic mechanisms of neurovascular unit injury and protection in CNS diseases. *CNS Neurol Disord Drug Targets*. (2013) 12:302–15. doi: 10.2174/18715273113120300004

32. Al-Sheikh M, Phasukkijwatana N, Dolz-Marco R, Rahimi M, Iafe NA, Freund KB, et al. Quantitative OCT Angiography of the Retinal Microvasculature and the Choriocapillaris in Myopic Eyes. *Invest Ophthalmol Vis Sci*. (2017) 58:2063–9. doi: 10.1167/iovs.16-21289

33. Zhu Q, Xing X, Wang M, Zhu M, Ma L, Yuan Y, et al. Characterization of the Three Distinct Retinal Capillary Plexuses Using Optical Coherence Tomography Angiography in Myopic Eyes. *Transl Vis Sci Technol*. (2020) 9:8. doi: 10.1167/tvst.9.4.8

34. Lim RR, Grant DG, Olver TD, Padilla J, Czajkowski AM, Schnurbusch TR, et al. Young Ossabaw Pigs Fed a Western Diet Exhibit Early Signs of Diabetic Retinopathy. *Invest Ophthalmol Vis Sci*. (2018) 59:2325–38. doi: 10.1167/iovs.17-23616

35. Hunter JM, Kwan J, Malek-Ahmadi M, Maarouf CL, Kokjohn TA, Belden C, et al. Morphological and pathological evolution of the brain microcirculation in aging and Alzheimer's disease. *PLoS One*. (2012) 7:e36893. doi: 10.1371/journal.pone.0036893

36. Brown WR, Moody DM, Thore CR, Anstrom JA, Challa VR. Microvascular changes in the white mater in dementia. *J Neurol Sci*. (2009) 283:28–31. doi: 10.1016/j.jns.2009.02.328

37. Challa VR, Thore CR, Moody DM, Anstrom JA, Brown WR. Increase of white matter string vessels in Alzheimer's disease. *J Alzheimers Dis*. (2004) 6:379–83. doi: 10.3233/JAD-2004-6404

38. Salmon AB. Moving toward 'common' use of the marmoset as a non-human primate aging model. *Pathobiol Aging Age Relat Dis*. (2016) 6:32758. doi: 10.3402/pba.v6.32758

39. Nishijima K, Saitoh R, Tanaka S, Ohsato-Suzuki M, Ohno T, Kitajima S. Life span of common marmoset (*Callithrix jacchus*) at CLEA Japan breeding colony. *Biogerontology*. (2012) 13:439–43. doi: 10.1007/s10522-012-9388-1

40. Ross CN, Davis K, Dobek G, Tardif SD. Aging Phenotypes of Common Marmosets (*Callithrix jacchus*). *J Aging Res*. (2012) 2012:567143. doi: 10.1155/2012/567143

41. Tardif SD, Mansfield KG, Ratnam R, Ross CN, Ziegler TE. The marmoset as a model of aging and age-related diseases. *ILAR J*. (2011) 52:54–65. doi: 10.1093/ilar.52.1.54

42. Brown WR. A review of string vessels or collapsed, empty basement membrane tubes. *J Alzheimers Dis*. (2010) 21:725–39. doi: 10.3233/JAD-2010-100219

43. Snodderly DM, Weinhaus RS, Choi JC. Neural-vascular relationships in central retina of macaque monkeys (*Macaca fascicularis*). *J Neurosci*. (1992) 12:1169–93. doi: 10.1523/JNEUROSCI.12-04-01169.1992

44. Joyal JS, Gantner ML, Smith LEH. Retinal energy demands control vascular supply of the retina in development and disease: The role of neuronal lipid and glucose metabolism. *Prog Retin Eye Res*. (2018) 64:131–56. doi: 10.1016/j.preteyeres.2017.11.002

45. Country MW. Retinal metabolism: A comparative look at energetics in the retina. *Brain Res*. (2017) 1672:50–7. doi: 10.1016/j.brainres.2017.07.025

46. Cheng KKW, Tan BL, Brown L, Gray C, Bianchi E, Dhillon B, et al. Macular vessel density, branching complexity and foveal avascular zone size in normal tension glaucoma. *Sci Rep*. (2021) 11:1056. doi: 10.1038/s41598-020-80080-z

47. Jonas JB, Wang YX, Dong L, Panda-Jonas S. High Myopia and Glaucoma-Like Optic Neuropathy. *Asia Pac J Ophthalmol*. (2020) 9:234–8. doi: 10.1097/APO.0000000000000288

48. Suwan Y, Fard MA, Geyman LS, Tantraworasin A, Chui TY, Rosen RB, et al. Association of Myopia With Peripapillary Perfused Capillary Density in Patients With Glaucoma: An Optical Coherence Tomography Angiography Study. *JAMA Ophthalmol*. (2018) 136:507–13. doi: 10.1001/jamaophthalmol.2018.0776

49. Resch H, Garhofer G, Fuchsjager-Mayrl G, Hommer A, Schmetterer L. Endothelial dysfunction in glaucoma. *Acta Ophthalmol*. (2009) 87:4–12. doi: 10.1111/j.1755-3768.2007.01167.x

50. Flammer J, Orgul S. Optic nerve blood-flow abnormalities in glaucoma. *Prog Retin Eye Res*. (1998) 17:267–89. doi: 10.1016/S1350-9462(97)00006-2

51. Buee L, Hof PR, Bouras C, Delacourte A, Perl DP, Morrison JH, et al. Pathological alterations of the cerebral microvasculature in Alzheimer's disease and related dementing disorders. *Acta Neuropathol*. (1994) 87:469–80. doi: 10.1007/BF00294173

52. Trinh M, Kalloniatis M, Nivison-Smith L. Vascular Changes in Intermediate Age-Related Macular Degeneration Quantified Using Optical Coherence Tomography Angiography. *Transl Vis Sci Technol*. (2019) 8:20. doi: 10.1167/tvst.8.4.20

53. Powner MB, Sim DA, Zhu M, Nobre-Cardoso J, Jones R, Syed A, et al. Evaluation of Nonperfused Retinal Vessels in Ischemic Retinopathy. *Invest Ophthalmol Vis Sci*. (2016) 57:5031–7. doi: 10.1167/iovs.16-20007

54. Yu DY, Cringle SJ. Oxygen distribution and consumption within the retina in vascularised and avascular retinas and in animal models of retinal disease. *Prog Retin Eye Res*. (2001) 20:175–208. doi: 10.1016/S1350-9462(00)00027-6

55. Castellani RJ, Smith MA, Perry G, Friedland RP. Cerebral amyloid angiopathy: major contributor or decorative response to Alzheimer's disease pathogenesis. *Neurobiol Aging*. (2004) 25:599–602. doi: 10.1016/j.neurobiolaging.2003.12.019

56. Atwood CS, Bowen RL, Smith MA, Perry G. Cerebrovascular requirement for sealant, anti-coagulant and remodeling molecules that allow for the maintenance of vascular integrity and blood supply. *Brain Res Brain Res Rev*. (2003) 43:164–78. doi: 10.1016/S0165-0173(03)00206-6

57. Cheung CY, Ikram MK, Sabanayagam C, Wong TY. Retinal microvasculature as a model to study the manifestations of hypertension. *Hypertension*. (2012) 60:1094–103. doi: 10.1161/HYPERTENSIONAHA.111.189142

58. Mroczkowska S, Benavente-Perez A, Patel S, Qin L, Bentham P, Gherghel D. Retinal vascular dysfunction relates to cognitive impairment in Alzheimer disease. *Alzheimer Dis Assoc Disord*. (2014) 28:366–7. doi: 10.1097/WAD.0b013e3182a2e221

59. Henkind P. Symposium on glaucoma: joint meeting with the National Society for the Prevention of Blindness. New observations on the radial peripapillary capillaries. *Investig Ophthalmol*. (1967) 6:103–8.

60. Yu PK, Balaratnasingam C, Xu J, Morgan WH, Mammo Z, Han S, et al. Label-Free Density Measurements of Radial Peripapillary Capillaries in the Human Retina. *PLoS One*. (2015) 10:e0135151. doi: 10.1371/journal.pone.0135151

61. Yu PK, Cringle SJ, Yu DY. Quantitative study of age-related endothelial phenotype change in the human vortex vein system. *Microvasc Res*. (2014) 94:64–72. doi: 10.1016/j.mvr.2014.05.004

62. Mammo Z, Heisler M, Balaratnasingam C, Lee S, Yu DY, Mackenzie P, et al. Quantitative Optical Coherence Tomography Angiography of Radial Peripapillary Capillaries in Glaucoma, Glaucoma Suspect, and Normal Eyes. *Am J Ophthalmol*. (2016) 170:41–9. doi: 10.1016/j.ajo.2016.07.015

63. Kornzweig AL, Eliasoph I, Feldstein M. Selective atrophy of the radial peripapillary capillaries in chronic glaucoma. *Arch Ophthalmol*. (1968) 80:696–702. doi: 10.1001/archopht.1968.00980050698002

64. Tilton RG, Miller EJ, Kilo C, Williamson JR. Pericyte form and distribution in rat retinal and uveal capillaries. *Invest Ophthalmol Vis Sci*. (1985) 26:68–73.

65. Tilton RG, Hoffmann PL, Kilo C, Williamson JR. Pericyte degeneration and basement membrane thickening in skeletal muscle capillaries of human diabetics. *Diabetes*. (1981) 30:326–34. doi: 10.2337/diab.30.4.326

66. Kuwabara T, Carroll JM, Cogan DG. Retinal vascular patterns. III. Age, hypertension, absolute glaucoma, injury. *Arch Ophthalmol*. (1961) 65:708–16. doi: 10.1001/archopht.1961.01840020710019

67. Schluter A, Aksan B, Diem R, Fairless R, Mauceri D. VEGFD Protects Retinal Ganglion Cells and, consequently, Capillaries against Excitotoxic Injury. *Mol Ther Methods Clin Dev*. (2020) 17:281–99. doi: 10.1016/j.omtm.2019.12.009

68. Taylor AC, Seltz LM, Yates PA, Peirce SM. Chronic whole-body hypoxia induces intussusceptive angiogenesis and microvascular remodeling in the mouse retina. *Microvasc Res*. (2010) 79:93–101. doi: 10.1016/j.mvr.2010.01.006

69. Bucher F, Stahl A, Agostini HT, Martin G. Hyperoxia causes reduced density of retinal astrocytes in the central avascular zone in the mouse model of oxygen-induced retinopathy. *Mol Cell Neurosci*. (2013) 56:225–33. doi: 10.1016/j.mcn.2013.06.001

70. Ehling M, Adams S, Benedito R, Adams RH. Notch controls retinal blood vessel maturation and quiescence. *Development*. (2013) 140:3051–61. doi: 10.1242/dev.093351

71. Brown WR, Thore CR. Review: cerebral microvascular pathology in ageing and neurodegeneration. *Neuropathol Appl Neurobiol*. (2011) 37:56–74. doi: 10.1111/j.1365-2990.2010.01139.x

72. Challa VR, Thore CR, Moody DM, Brown WR, Anstrom JA. A three-dimensional study of brain string vessels using celloidin sections stained with anti-collagen antibodies. *J Neurol Sci*. (2002) 203-204:165–7. doi: 10.1016/s0022-510x(02)00284-8

73. Hassler O. Vascular changes in senile brains. A micro-angiographic study. *Acta Neuropathol*. (1965) 5:40–53. doi: 10.1007/BF00689161

74. Ravens JR. Vascular changes in the human senile brain. *Adv Neurol*. (1978) 20:487–501.

75. Bell MA, Ball MJ. Morphometric comparison of hippocampal microvasculature in ageing and demented people: diameters and densities. *Acta Neuropathol*. (1981) 53:299–318. doi: 10.1007/BF00690372

76. Bailey TL, Rivara CB, Rocher AB, Hof PR. The nature and effects of cortical microvascular pathology in aging and Alzheimer's disease. *Neurol Res*. (2004) 26:573–8. doi: 10.1179/016164104225016272

77. Bussiere T, Gold G, Kovari E, Giannakopoulos P, Bouras C, Perl DP, et al. Stereologic analysis of neurofibrillary tangle formation in prefrontal cortex area 9 in aging and Alzheimer's disease. *Neuroscience*. (2003) 117:577–92. doi: 10.1016/S0306-4522(02)00942-9

78. Hof PR, Bussiere T, Gold G, Kovari E, Giannakopoulos P, Bouras C, et al. Stereologic evidence for persistence of viable neurons in layer II of the entorhinal cortex and the CA1 field in Alzheimer disease. *J Neuropathol Exp Neurol*. (2003) 62:55–67. doi: 10.1093/jnen/62.1.55

79. Reinecke RD, Kuwabara T, Cogan DG, Weis DR. Retinal vascular patterns. V. Experimental ischemia of the cat eye. *Arch Ophthalmol*. (1962) 67:470–5. doi: 10.1001/archopht.1962.00960020470015

80. Provis JM. Development of the primate retinal vasculature. *Prog Retin Eye Res*. (2001) 20:799–821. doi: 10.1016/S1350-9462(01)00012-X

81. Stone J, van Driel D, Valter K, Rees S, Provis J. The locations of mitochondria in mammalian photoreceptors: relation to retinal vasculature. *Brain Res*. (2008) 1189:58–69. doi: 10.1016/j.brainres.2007.10.083

82. Campbell JP, Zhang M, Hwang TS, Bailey ST, Wilson DJ, Jia Y, et al. Detailed Vascular Anatomy of the Human Retina by Projection-Resolved Optical Coherence Tomography Angiography. *Sci Rep*. (2017) 7:42201. doi: 10.1038/srep42201

83. Alterman M, Henkind P. Radial peripapillary capillaries of the retina. II. Possible role in Bjerrum scotoma. *Br J Ophthalmol*. (1968) 52:26–31. doi: 10.1136/bjo.52.1.26

84. Lavia C, Mece P, Nassisi M, Bonnin S, Marie-Louise J, Couturier A, et al. Retinal Capillary Plexus Pattern and Density from Fovea to Periphery Measured in Healthy Eyes with Swept-Source Optical Coherence Tomography Angiography. *Sci Rep*. (2020) 10:1474. doi: 10.1038/s41598-020-58359-y

85. Samara WA, Shahlaee A, Sridhar J, Khan MA, Ho AC, Hsu J. Quantitative Optical Coherence Tomography Angiography Features and Visual Function in Eyes With Branch Retinal Vein Occlusion. *Am J Ophthalmol*. (2016) 166:76–83. doi: 10.1016/j.ajo.2016.03.033

86. Cheng D, Chen Q, Wu Y, Yu X, Shen M, Zhuang X, et al. Deep perifoveal vessel density as an indicator of capillary loss in high myopia. *Eye*. (2019) 33:1961–8. doi: 10.1038/s41433-019-0573-1

87. Ye J, Wang M, Shen M, Huang S, Xue A, Lin J, et al. Deep Retinal Capillary Plexus Decreasing Correlated With the Outer Retinal Layer Alteration and Visual Acuity Impairment in Pathological Myopia. *Invest Ophthalmol Vis Sci*. (2020) 61:45. doi: 10.1167/iovs.61.4.45

Frontiers in Medicine

Translating medical research and innovation into improved patient care

A multidisciplinary journal which advances our medical knowledge. It supports the translation of scientific advances into new therapies and diagnostic tools that will improve patient care.

Discover the latest Research Topics

See more →

Frontiers

Avenue du Tribunal-Fédéral 34
1005 Lausanne, Switzerland
frontiersin.org

Contact us

+41 (0)21 510 17 00
frontiersin.org/about/contact